The use of a recombinant single chain antibody in the investigation of liver fibrosis.

Helen Marshall, BSc

Thesis submitted in partial fulfilment of the requirements
for the degree of Doctor of Philosophy

Newcastle University

Institute of Cellular Medicine

December 2010

Declaration

I hereby declare that this thesis has been composed by myself and has not been accepted in any previous application for a degree. The work has been carried out by myself unless otherwise stated. All sources of information have been acknowledged accordingly by means of reference.

Helen Marshall

Abstract

Liver fibrosis is one of the leading causes of morbidity and mortality in the western world and represents a significant burden to the health system. The continued elucidation of the mechanisms governing liver fibrosis has identified the hepatic myofibroblast, derived from quiescent hepatic stellate cells, as the principle cell type involved in disease progression with several studies demonstrating that hepatic myofibroblast apoptosis correlated with attenuated fibrosis severity.

A recombinant single chain antibody (scAb), termed C1-3, has been developed and shown to actively target hepatic myofibroblasts expressing synaptophysin both *in vitro* and *in vivo*. The aim of this thesis was to use C1-3 (conjugated to an appropriate agent) as an imaging agent; to examine the effect of hepatic myofibroblast depletion on regeneration following two thirds partial hepatectomy (PHx) and to examine if hepatic myofibroblast depletion in a cirrhosis model promotes fibrosis regression.

The data in this thesis show that conjugation of C1-3 to a fluorophore provides a novel non invasive method for differentiating between the different stages of carbon tetrachloride induced liver fibrosis in animal models, with increasing hepatic myofibroblast number (determined by αSMA staining) correlating with disease progression.

Hepatic myofibroblast depletion prior to and during PHx revealed a complex role for these cells during liver regeneration through the provision of factors that both stimulated and reduced parenchymal cell proliferation.

C1-3 mediated-depletion of hepatic myofibroblasts in a sustained model of liver injury revealed that removal of these cells was not sufficient to stimulate fibrosis regression since no difference in collagen deposition was observed.

The data in this thesis demonstrate the complex role of hepatic myofibroblasts during liver regeneration and sustained injury and suggest that further studies are required to elucidate the exact mechanisms involved before depletion of hepatic myofibroblasts can be a viable therapeutic option.

In loving memory of my dad, Robert George Marshall. The inspiration and motivation behind my work. Miss you, always.

Acknowledgements

I would like to thank Dr. Matthew Wright for his supervision, enthusiasm and motivation throughout this project. I would also like to thank team Wright for their help and support, particularly when I was convinced that all my work was doomed.

Special thanks go to Julia Spielhofer, Hannah Walden and Graeme O'Boyle who are great friends and provided a lot of moral support over the years. Thanks for listening so patiently on those bad days! Thanks to both Helen Robertson and Trevor Booth for their help and advice with immunohistochemistry and microscopy.

Thank you to my best friend Jo Kilford, you have helped me through both my degree and PhD and for that I am eternally grateful.

I would also like to thank my family, particularly my mum and sister for their endless support, without you I don't think this would have been possible. Finally I would like to thank Lewis, you've stuck by me though the good times and the bad and without your constant encouragement, support, motivation and excellent tea making skills I think I would have given up on this months ago.

The work presented in this thesis was supported by the Hunter Memorial Fund.

Index of Figures

Index of Tables

Abbreviations

3D	Three dimensional
ACTH	Adrenocorticotropic hormone
ADRP	Adipose differentiation related protein
AF	Alexa fluorophore
ALF	Acute liver failure
ALP	Alkaline phosphatase
ALT	Alanine aminotransferase
ANT	Adenine nucleotide transporter
AST	Aspartate aminotransferase
BABB	Benzyl alcohol:Benzyl benzoate
BM	Bone marrow
BrDU	Bromodeoxyuridine
BSA	Bovine serum albumin
CCl_4	Carbon tetrachloride
CD4	Cluster of differentiation 4
CD8	Cluster of differentiation 8
CDK	Cyclin dependent kinase
cDNA	Complementary deoxyribonucleic acid
CLV	Centrilobular vein
Col1a1	Collagen 1a1
Cre	Cyclization recombination
CrH	Corticotrophin releasing hormone
CTGF	Connective tissue growth factor
CXCR3	Chemokine receptor three
CYP	Cytochrome
dH_2O	Deionised water
DMEM	Dulbecco’s modification of Eagle’s medium

DMF	Dimethylformamide
DMSO	Dimethyl sulfoxide
DNA	Deoxyribonucleic acid
DS	Downstream
DTT	DL-Dithiothreitol
ECL	Enhanced chemiluminescence
ECM	Extracellular matrix
EDTA	Ethylenediaminetetraacetic acid
EGF	Epidermal growth factor
EGFR1	Epidermal growth factor receptor 1
ELISA	Enzyme linked immunosorbant assay
ELF	Enhanced liver fibrosis
EMT	Epithelial to mesenchymal transition
ERB	Electrophoresis running buffer
ETx	Endotoxin
FCS	Foetal calf serum
FITC	Fluorescein isothiocyanate
GFAP	Glial fibrillary acidic protein
GFP	Green fluorescent protein
GP130	Glycoprotein 130
GT	Gliotoxin
H&E	Haematoxylin and eosin
H_2SO_4	Sulfuric acid
HB-EGF	Heparin binding epidermal like growth factor
HBSS	Hank’s balanced salt solution
HBV	Hepatitis B virus
HCV	Hepatitis C virus
HGF	Hepatocyte growth factor

HRP	Horseradish peroxidase
HSA	Human serum albumin
HSC	Hepatic stellate cell
i.p.	Intraperitoneal
i.v.	Intravenous
ICAM-1	Inter-cellular adhesion protein 1
ICC	Immunocytochemistry
IGF	Insulin like growth factor
IgG	Immunoglobulin G
IHC	Immunohistochemistry
IL-1β	Interleukin 1 beta
IL-6	Interleukin 6
IL-6R	Interleukin 6 receptor
IMAC	Immobilised metal ion affinity chromatography
INFγ	Interferon gamma
IPTG	Isopropyl β-D-1-thiogalactopyranoside
IVIS	*In vivo* imaging system
IκBα	Nuclear factor of kappa light polypeptide gene enhancer in B-cells inhibitor, alpha
LB	Luria-Bertanni
Lox P	Locus of X over P1
M6P	Mannose 6 phosphate
MBS	m-maleimidobenzoyl-N-hydroxysuccinimide ester
MCP-1	Monocyte chemotactic protein 1
MMLV	Moloney murine leukaemia virus
MMPs	Matrix metalloproteinases
mRNA	Messenger ribonucleic acid
NaCO	Sodium carbonate

NAFLD	Non alcoholic fatty liver disease
NaOH	Sodium Hydroxide
NASH	Non alcoholic steatohepatitis
ND	Not determined
NFκB	Nuclear factor kappa light chain enhancer of activated B cells
NK	Natural killer
NPC	Non parenchymal cell
OPT	Optical projection tomography
$p75^{NTR}$	P75 neurotrophin receptor
PA	Portal artery
PAGE	Polyacrylamide gel electrophoresis
PBC	Primary biliary cirrhosis
PBS	Phosphate buffered saline
PBS-T	Phosphate buffered saline containing tween
PCNA	Proliferating cell nuclear antigen
PCR	Polymerase chain reaction
PDGF	Platelet derived growth factor
PHx	Partial hepatectomy
PIIINP	Type 3 procollagen N terminal propeptide
PMPI	N-p-maleimidophenyl isocyanate
PPARγ	Peroxisome proliferator activated receptor gamma
PSC	Primary sclerosing cholangitis
PT	Portal tract
PV	Portal vein
RNA	Ribonucleic acid
ROS	Reactive oxygen species
RT-PCR	Real time polymerase chain reaction

SATA	S-Acetylthioglycolic acid N-hydroxysuccinimide ester
scAb	Single chain antibody
SD	Standard deviation
SDS	Sodium dodecyl sulphate
SET	Small electrotranslucent vesicles
siRNA	Small interfering ribonucleic acid
SOCS-3	Suppressor of cytokine signalling 3
STAT-3	Signal transducer and activator of transcription 3
STAT-3-P	Phosphorylated signal transducer and activator of transcription factor three
TAE	Tris-acetate-ethylenediaminetetraacetic acid
TB	Terrific broth
TBS	Tris buffered saline
TEMED	*N*,*N*,*N*′,*N*′-Tetramethylethylenediamine
Tgfbr2	Transforming growth factor beta receptor 2
TGFα	Transforming growth factor alpha
TGFβ	Transforming growth factor beta
TIMP	Tissue inhibitors of matrix metalloproteinases
TKMS	Tris, potassium chloride, magnesium chloride and sucrose
Tm	Temperature of melting
TMB	3,3′,5,5′-Tetramethylbenzidine
TNFR1	Tumour necrosis factor receptor 1
TNFα	Tumour necrosis factor alpha
TPH1	Tryptophan hydroxylase 1
TRAIL	Tumour necrosis factor related apoptosis inducing ligand
TUNEL	Terminal deoxynucleotidyl transferase dUTP nick end labelling
TVB	Tail vein bleed
UPA	Urokinase plasminogen activator

US	Upstream
UV	Ultraviolet
VCAM-1	Vascular cell adhesion protein one
VEGF	Vascular endothelial growth factor
WRT	With respect to
α2-globulin	Alpha 2 globulin
α2-macroglobulin	Alpha 2 macroglobulin
αSMA	Alpha smooth muscle actin
γ-globulin	Gamma globulin
γGT	Gamma glutamyltransferase

Chapter 1. Introduction

1.1 The Liver

The liver is the largest organ in the human body weighing approximately 1.5kg and is located in the upper right-hand side of the abdominal cavity, resting just below the diaphragm. Apart from a patch where it connects to the diaphragm, the liver is entirely covered by a visceral peritoneum, a double layered membrane encasing the liver, hepatic blood vessels and bile duct in order to reduce friction against other organs. The peritoneum folds back upon itself to form the falciform ligament which divides the liver into four lobes: left, right, quadrate and caudate.

The liver has a unique dual blood supply with the hepatic artery delivering oxygenated blood to provide cellular energy via aerobic respiration and the hepatic portal vein taking all the blood from the intestines to the liver. Blood from the two supplies mixes at the edge of the portal tract and passes through the liver's extensive vascular bed, the sinusoids emptying into the central vein where it returns to the circulatory supply via the inferior vena cava. The space between the endothelial cell and hepatocytes is known as the space of Dissé which drains lymph into the lymphatics.

Bile, generated by the liver to aid digestion of lipids, is secreted by hepatocytes into the bile canaliculi and eventually drains into the left and right hepatic ducts which merge to form the common bile duct. The bile can then either drain into the duodenum via the common bile duct to be excreted, or be stored in the gall bladder via the cystic duct. Each lobe is made up of many functional hepatic units which describes the organisation of hepatocytes with regard to blood supply and bile drainage. Although different models have been proposed, the liver lobule (proposed by Kiernan) and the liver acinus of Rappaport are most favoured. The liver lobule is typically described as a hexagonal structure with portal triads, consisting of a portal vein, hepatic artery and bile duct, at each corner (Figure 1-1A). Hepatocytes, arranged in rows, radiate from a central vein with their basolateral surface lined with fenestrated endothelial forming the sinusoids. The apical surfaces form the bile canaliculus which allows the bile secreted by the hepatocytes to drain into the bile ducts.

The acinus of Rappaport is a smaller functional unit which describes the microcirculatory and secretory function of the liver. The central vein is located at the periphery of each liver acinus, composed of three or more liver acini. Each acinus relates to the terminal branches of the portal triad allowing blood to flow centrifugally and bile flow centripetally (Figure 1-1B). Blood flow within the acinus is divided into three zones, zone 1 has the highest oxygen and substrate supply due to its location nearest the portal triad whereas zone 3 has the poorest oxygen supply as it is located at the end of microcirculatory system, i.e. next to the central vein. This model is highly favoured by pathologists as it explains many pathological lesions.

Both arrangements provide evidence for metabolic zonation of hepatocytes [1, 2], meaning hepatocyte function differs depending upon location within the hepatic unit. Hepatocytes adjacent to the portal triad (periportal) are responsible for catabolism of amino acids and urea synthesis whereas those near the central vein (pericentral or perivenous) utilise ammonia to generate glutamine [1, 3].

Hepatocytes account for 70-80% of the total liver cell population and under a normal light microscope, appear to be undistinguished and unspecialised rows of cells. Upon closer examination under an electron microscope specialised microvilli are revealed (on the membrane in contact with the sinusoids) which increase the area available for uptake of substances from the blood. Hepatocytes perform the majority of functions in the liver:

1. Synthesis of bile salts, cholesterol and phospholipids
2. Protein synthesis including the formation of serum albumin, fibrinogen, clotting factors, enzymes, lipoproteins and many others
3. Carbohydrate metabolism and synthesis
4. Urea cycle
5. Lipid metabolism
6. Hormone & cytokine catabolism
7. Drug and xenobiotic metabolism

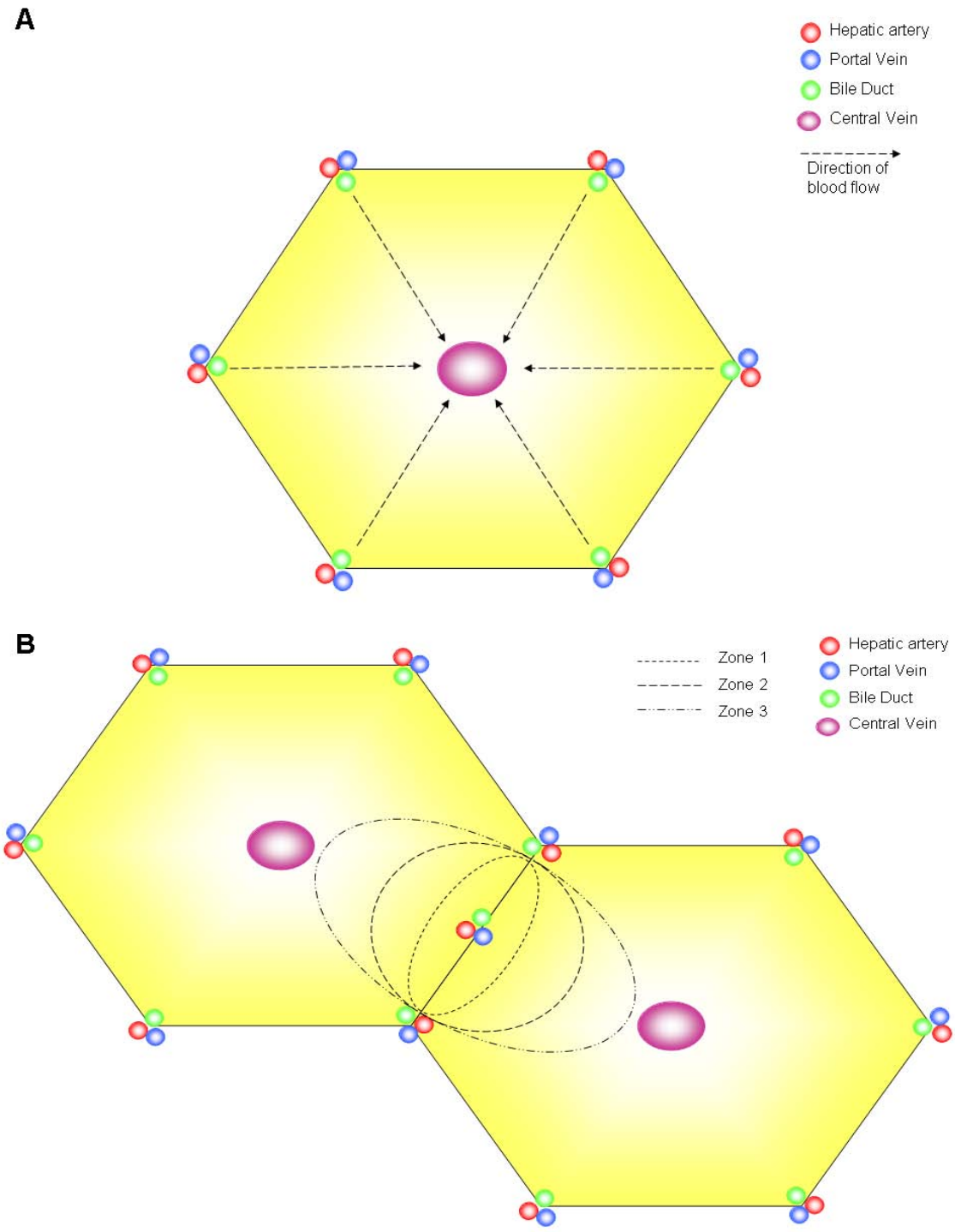

Figure 1-1 Proposed models of functional hepatic units. A: The hepatic lobule is a hexagonal unit with portal triads at each corner and a central vein at the centre. Hepatocytes, arranged in rows, radiate out from the central vein towards to portal triads. B: Acinus of Rappaport is a smaller functional unit which describes the microcirculatory and secretory function of the liver. Blood flows from the terminal branches of the portal triad toward the central vein located at the periphery. Blood oxygenation levels categorised into zones which account for hepatocyte metabolic zonation.

The remaining cellular population is composed of hepatic stellate cells (HSC), kupffer cells, biliary epithelial cells, oval cells and endothelial cells. As mentioned earlier, the endothelial cells form the sinusoids of the liver, however they are

unlike normal vascular endothelial cells as their basement membrane is replaced with pores known as fenestrae to allow the exchange of nutrients and oxygen [4]. Furthermore, the endothelial cells play a key role in the recruitment of immune cells during liver injury by regulating the expression of adhesion molecules. Kupffer cells are specialised liver macrophages and reside in the sinusoids. They act as scavengers and are responsible for the phagocytosis of old erythrocytes, tissue debris, bacteria and foreign proteins. They also play an essential role in the innate immune response through the secretion of soluble inflammatory mediators [5]. HSC reside in the space of Dissé and are the primary site of retinoid (vitamin A) storage in the body. Their dendritic like processes project into the sinusoids between the endothelial cells and hepatocytes, with each spindle containing numerous microprojections (spines) allowing the cell to sense and respond to chemotactic signals [6]. Oval cells are the livers progenitor cells and are capable of differentiating into both hepatocytes and biliary epithelial cells. Cellular organisation within the liver is shown in figure 1-2.

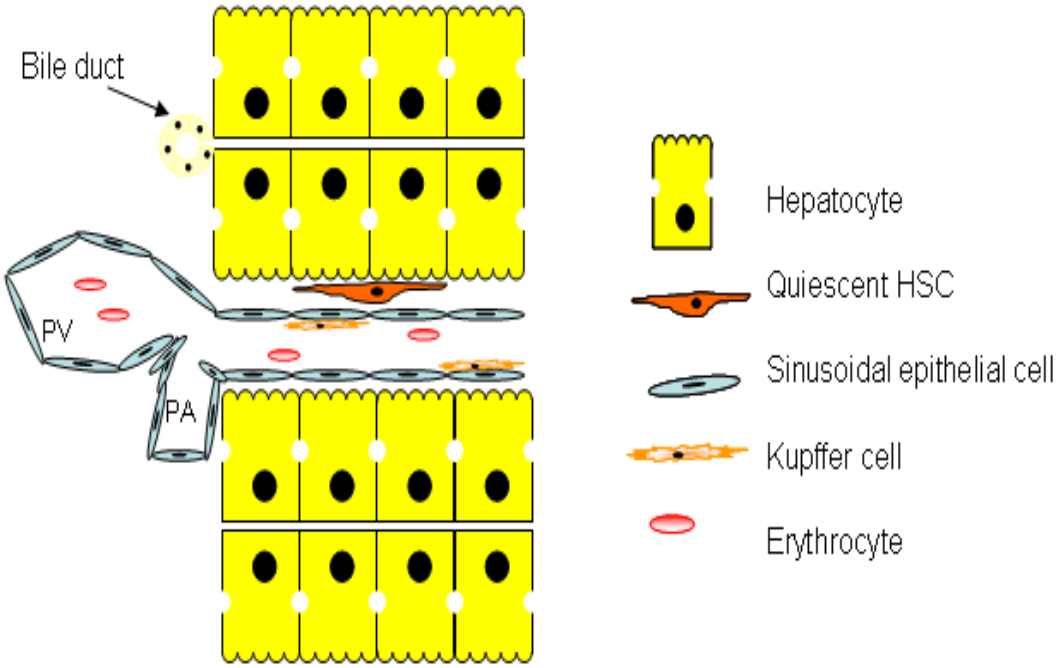

Figure 1-2 Cellular organisation within the liver. Hepatocytes are arranged in rows with their specialised microvilli in contact with the sinusoidal basement membrane allowing for increased uptake of components from the blood delivered by the portal triad. Quiescent HSCs reside in the space between the hepatocytes and sinusoidal basement membrane, termed the space of Dissé, allowing them to monitor and respond to the microenvironment. Kupffer cells patrol the sinusoids providing the first line of defence against injury. PV – Portal vein, PA – portal artery.

1.2 Liver Disease

1.2.1 Clinical perspective

Liver disease is one of the most common causes of morbidity and mortality in the western world and represents a significant burden to the healthcare system. Liver failure can present either with an acute onset or after years of long term liver disease. Acute liver failure (ALF) is defined by the appearance of severe liver complications shortly after the initial symptoms (e.g. jaundice) and implies severe impairment in liver function due to widespread cellular necrosis. It is typically caused by overdose of paracetamol.

Due to the huge compensatory ability of the liver, liver failure is typically diagnosed at its end stages after years of prolonged illness. Currently the major global cause of chronic liver disease is due to viral infection, particularly with the hepatitis C virus, which results in inflammation (hepatitis) [7]. However, in the western world alone, there is an increasing rate of excessive alcohol consumption and high fat diets (Non-alcoholic fatty liver disease (NAFLD) and non alcoholic steato-hepatitis (NASH)) which are now accounting for a high percentage of deaths per annum. Disease can also result from autoimmune disorders where the immune system is triggered into attacking cellular components in the liver, such as autoimmune hepatitis [8] or primary biliary cirrhosis (PBC) [9]. In rare cases, liver disease may arise from genetic conditions caused by the body absorbing and storing too much iron (hereditary haemachromatosis [10]) or copper (Wilson's disease [11]) resulting in toxicity. Finally liver disease may also result from the impairment of bile flow, termed cholestasis, caused by mechanical blockage by gallstones or the progressive loss of bile ducts due to inflammation, cause unknown, termed primary schlerosing cholangitis [12].

1.2.2 Fibrogenesis

Hepatic fibrosis is a classical wound healing or scarring process in response to chronic injury. During acute injury, apoptosis and necrosis of hepatocytes stimulates kupffer and hepatic myofibroblasts to release a vast array of chemokines and cytokines to recruit both local and circulating lymphocytes [13]. This triggers an inflammatory response and upon removal of the insult, the liver

will regenerate via hepatocyte mitosis. Unlike other organs, the liver has a remarkable ability to regenerate even after 70% of the parenchyma is lost. The cellular changes associated with liver injury are illustrated in figure 1-3.

However, in response to chronic injury, the regeneration process becomes overwhelmed and tries to encapsulate the injury [14] but in doing so distorts the normal tissue architecture resulting in functional impairment. Even at this stage, if the insult is removed there is a possibility that regeneration can occur. Nevertheless, the progression to cirrhosis, or end staged liver disease, results after long term liver damage and is characterised by extensive fibrosis with nodule formation and severe disruption in tissue architecture and vasculature.

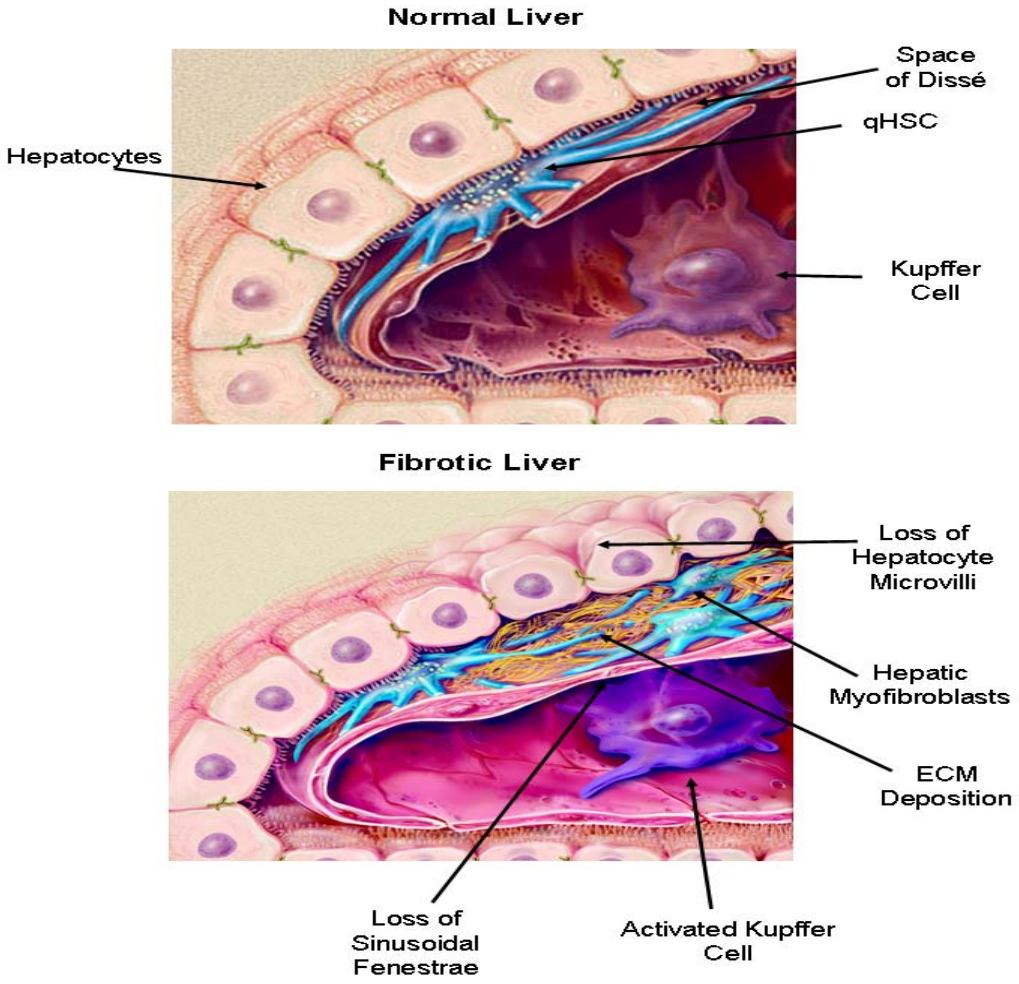

Figure 1-3 Cellular changes in response to liver injury. Adapted from [15]. Hepatocyte necrosis and apoptosis following liver injury results in the activation of kupffer cell. Kupffer cells release proinflammatory cytokines that stimulate the activation and transdifferentiation of quiescent HSC into hepatic myofibroblasts. These cells are responsible for the secretion of the major components of the ECM as well as a vast array of cytokines/chemokines which cause loss of hepatocyte microvilli and sinusoidal fenestrae ultimately affecting liver function.

1.2.3 The Extracellular Matrix

The extracellular matrix (ECM) is thought to have a significant influence on the cellular response during injury. It is comprised of macromolecules belonging to three main families: collagens, proteoglycans and glycoproteins. In the normal liver the ECM is restricted to the central veins, portal tracts and sinusoid walls [16] forming a vital barrier between the blood flow and parenchyma. This scaffold is not only important in providing tensile strength and resistance, it also regulates cell movement and modulates diffusion and vascular flow [17] by allowing continuous signalling between the cells within the liver. This signalling can be enhanced by the stimulated release of growth factors, enzymes, hormones and cytokines, which are stored in their inactive forms in the ECM, to modify the cellular microenvironment [16].

ECM composition differs depending upon its localisation, for example the matrix forming the basement membrane like structure in the space of Dissé is composed of non fibril forming collagens (types IV, VI and XIV), glycoproteins and proteoglycans. However the matrix surrounding the portal regions and large vessel is referred to as an interstitial matrix due to it consisting of fibril forming collagens (types I and III), cellular fibronectin and other glycoconjugates [14].

Different compositions of ECM are essential for maintaining the differentiated functions of the resident liver cells. During fibrosis, the ECM in the liver can increase 3-5 fold [16] with significant changes initially observed in the perisinusoidal space ECM. Nevertheless, the increased ECM deposition results in the basement membrane-like matrix representing the interstitial ECM due to the presence of fibrillar collagens. This influences a change in sinusoidal phenotype resulting in loss of fenestrae inhibiting the exchange in nutrients etc between the blood and hepatocytes [16, 18] which impacts on liver function.

The changing ECM has been shown to affect cellular function due to the changes in microenvironment [14], for example proliferation of hepatocytes and their function *in vitro* has been shown to be dependent on the matrix that they are cultured on [19]. Additionally, Gaça *et al* [20] reported that hepatic myofibroblasts replated on Matrigel rather than on plastic or collagen matrix, reduced their proliferation by up to 30%. After 3-7 days of culture there was a progressive reduction in the levels of mRNA for collagen type I and alpha smooth muscle

actin, both associated with the hepatic myofibroblast phenotype. Furthermore, Zhou *et al* [21] have demonstrated that interaction with the ECM also regulates the proliferation and apoptosis of HSCs.

Whilst it is widely known that the primary producer of ECM under both normal and fibrotic conditions is the hepatic myofibroblast, recent evidence implicates portal myofibroblasts [22, 23], bone marrow derived cells [24] and fibroblasts derived from epithelial-to-mesenchymal transition [25, 26] in ECM deposition during the fibrogenesis process. Determining the contribution of each cell type to ECM deposition is essential in understanding fibrosis and identifying targets for therapeutics.

1.2.4 Role of Myofibroblasts in Fibrosis

Myofibroblasts are a morphological and functional intermediate between fibroblasts and smooth muscle cells and contain cytoplasmic bundles of microfilaments [27]. Myofibroblasts are found in many organs and are known to be the principle cell type involved in both matrix deposition and the production of enzymes involved in matrix degradation, tissue remodelling and scar formation.

Research to date has focused on the hepatic myofibroblast as the main contributor of fibroblasts in the liver. These cells are typically characterised by their transformation to a fibroblast phenotype upon activation and their expression of αSMA [28].

1.2.4.1 The Hepatic Stellate Cell

Historical Perspective

As mentioned previously, the HSC resides in the subendothelial space between the sinusoidal epithelial cells and the hepatocytes. In its quiescent state it is the primary storage site for retinoids (vitamin A) in the body. It was this function which led to its discovery by von Kupffer in 1876 when he used a gold chloride method to detect vitamin A containing droplets in liver tissue. This was the first non-parenchymal cell described in the liver, however its function was unknown. In 1980, Wake suggested that the name of the cell should reflect its morphology until its functions were fully discovered, thus proposed the terms ‘perisinusoidal stellate cell’ or ‘stellate cell’ [29].

Interest in this cell began to grow and it was not long before the functional significance of HSCs was realised. Immunofluorescence studies by Kent *et al* [30] demonstrated that vitamin A storing cells accumulated in necrotic regions in livers from rats treated with carbon tetrachloride (CCl_4). Furthermore, Friedman *et al* [31] used immunofluorescence of HSCs in culture to demonstrate that they are the principal collagen-producing cells in the liver and were capable of producing large amounts of collagen type I with lower levels of collagen type III and IV also detected [32].

The development of reproducible techniques for isolating HSCs has been essential in defining their role in fibrosis [33, 34]. The quiescent HSC undergoes a process of activation, transforming into a proliferating, fibrogenic and contractile hepatic myofibroblast [14, 35]. It can be defined as a two stage process, initiation followed by perpetuation [14, 36].

Initiation is defined by early changes in gene expression and phenotype which occur as a result of paracrine stimulation and render the cells responsive to further stimuli e.g. cytokines [36, 37]. Typically, damage to the liver by toxins, e.g. CCl_4, results in hepatocyte necrosis and apoptosis which in turn causes the release of reactive oxygen species (ROS) and apoptotic fragments into the microenvironment that are fibrogenic for HSCs [38]. These fragments are also engulfed by Kupffer cells which induces expression of Fas and Death ligands further promoting hepatocyte apoptosis in a ‘feed-forward’ loop favouring fibrosis [39]. Kupffer cells also stimulate HSC activation, proliferation and matrix synthesis through cytokine secretion, particularly TNFα and ROS [36]. Endothelial cells and platelets have also been implicated in the activation process though conversion of latent TGFβ to its active form and the provision of PDGF, EGF and TGFβ [40].

HSC activation can also be influenced by the microenvironment through subtle changes in matrix interactions [16], for example i*n vitro* co-culture of HSCs with freshly isolated differentiated sinusoidal epithelial cells promoted HSC quiescence. However, co-culture with capillarized sinusoidal epithelial cells promoted HSC activation into hepatic myofibroblasts [41]. This may be explained by the expression of a splice variant of fibronectin, EIIIA, which is synthesised by sinusoidal epithelial cells following injury [42].

Following initiation, the continued activation of HSCs is the result of autocrine and paracrine feedback loops [14, 36] as well as discrete changes in cell behaviour which are characterised as follows:

1. **Proliferation:** Early expression of PDGF receptors [43] during activation allows the cells to respond to the potent mitogen PDGF [44]. Other mitogens have been identified to play a potential role in fibrogenesis, for example: VEGF, EGF and TGFα.

2. **Chemotaxis:** Migration by HSCs to the site of injury is dictated by cytokine chemoattraction [45], particularly PDGF [46], MCP-1 [47] and CXCR3 [48].

3. **Fibrogenesis:** Activation of rat HSCs in culture has shown to increase matrix production, particularly collagen type I [32, 49]. This is mainly driven by autocrine and paracrine sources of TGFβ.

4. **Contractility:** The contractility of HSCs plays an important role in portal resistance during fibrosis due to their location in the scar regions causing a reduction in blood flow in the sinusoids.

5. **Matrix Degradation:** The course of fibrosis is dictated by the delicate balance in matrix production and degradation. HSCs have been shown to be principle sources of both matrix–metalloproteinases (MMPs) [36] as well as the tissue inhibitors of metalloproteinases (TIMPs) [50].

6. **Retinoid loss:** Activation of HSCs is associated with the loss of the retinoid stored in the perinuclear space. Recent research has demonstrated that upregulation of adipose differentiation-related protein (ADRP) by retinol and palmitate is directly associated with the down regulation of fibrogenic genes in hepatic myofibroblasts [51] suggesting that ADRP expression correlates with the state of HSC activation and potentially represents a new therapeutic target in hepatic fibrosis.

Taken together, these changes in HSC behaviour result in the increased deposition of ECM disrupting normal tissue architecture causing liver failure.

1.2.4.2 Portal Myofibroblasts

Studies by Ramadori's group were the first to show morphologically and functionally distinct populations of fibroblasts within the liver [52, 53] confirming theories that other cell types contribute to ECM production during fibrosis. These cell populations were investigated further by Cassiman *et al* [54] by means of immunohistochemistry to try and identify precursor populations of (myo)fibroblast-like cells in fibrotic liver. They showed that in rat and human cirrhotic livers three different populations of myofibroblast-like cells existed, these were:

(i) Activated hepatic stellate cells (myofibroblasts)

(ii) Interface myofibroblasts

(iii) Peribiliary myofibroblasts

All cells expressed varying levels of αSMA, but were distinguished by their differential expression of other cellular markers such as desmin, GFAP and synaptophysin. These data agreed with previous studies by Tang *et al* [55] which showed that bile duct ligation in rats resulted in the proliferation of portal fibroblasts, identified by expression of αSMA and lack of desmin, that were associated with the scar deposited.

More recently the portal myofibroblast response has been investigated using two animal models of self limited and persistent cholestatic liver injury: arterial liver ischemia and bile duct ligation [56]. Surprisingly, immunohistochemistry revealed an increase in desmin expression suggesting that a proportion of HSCs were beginning to activate during the early stages of liver injury in both animal models. However as fibrosis progressed in both models, the predominant cell type identified was the portal myofibroblast, with few hepatic myofibroblasts observed. It has been postulated that the hepatic myofibroblasts are essential for matrix remodelling and fibrosis regression.

Portal myofibroblasts can be identified by their expression of elastin and αSMA and lack of desmin [57]. In culture their activation was dependent upon two factors, matrix stiffness and TGFβ expression. When placed on a soft support matrix the cells remained quiescent however when this was changed to a stiff support matrix the cells subsequently activated [57]. This data fit with previous

research which has shown that during cholestasis the proliferating biliary epithelial cells release vast amounts of TGFβ2 [58] which stimulates the activation and proliferation of portal myofibroblasts to release TGFβ thus self perpetuating growth [23].

1.2.4.3 Bone Marrow Derived Myofibroblasts

Recent studies by Forbes *et al* [59] proposed that circulating cells may also play an essential role in fibrogenesis. When staining tissue biopsies from male transplant recipients who received donor female livers, they noted that a significant proportion of myofibroblasts in fibrotic areas were positive for the Y chromosome indicating these cells were of bone marrow (BM) origin.

The contribution of the BM to the population of hepatic myofibroblasts was further investigated by Russo *et al* [60]. To do this, they depleted the BM from female mice and replaced it with BM from male mice. Following liver injury, the number of BM derived HSCs and myofibroblasts was markedly increased suggesting that these cells are actively recruited. Furthermore, during liver recovery, the number of BM-derived stellate cells fell noticeably signifying an intra-hepatic source of renewal.

However the contribution of the bone marrow derived myofibroblasts in liver injury is still subject to debate. Bile duct ligation in mice transplanted bone marrow from collagen alpha1(I)-GFP+ reporter mice found that the bone marrow cells detected in the liver did not express αSMA and thus could not be defined as a myofibroblast [61]. The group propose that these cells represent a unique population of fibrocytes which are recruited to the liver following injury however their role in the fibrogenic process is unknown.

1.2.4.4 Biliary Epithelial Cells

Studies of fibrogenesis in other organs, for example the kidney, has shown convincing evidence that the predominant source of fibroblasts are from the epithelia themselves, by undergoing a process called epithelial to mesenchymal transition (EMT) [62, 63] which could be detected by staining with anti-S100A4 antibody (fibroblast specific protein 1), an early marker of the EMT process [64, 65].

The presence of this marker has also been confirmed in diseased liver sections in small duct cells and ductular proliferation [66, 67] and is typically associated with expression of epithelial cell markers, e.g. cytokeratin 19, down regulation of E-cadherin and the nuclear localisation of the downstream TGFβ signalling molecules smad 2 and 3 [26, 67]. In vitro studies have found that the differentiation of biliary epithelial cells is enabled by the treatment of cells with TGFβ and regulated by expression of S100A4 [26]. Furthermore, EMT could be induced in 3D biliary structures in culture through chemokine mediated T cell infiltration, with close proximity observed between infiltrating TGFβ presenting T cells and the expression of mesenchymal markers by the cholangiocytes.

1.2.5 The Inflammatory Response

Hepatic fibrosis caused by persistent infection with hepatitis B and C viruses is characterised by large quantities of inflammatory cell infiltrate. The liver's response to injury can be split into 3 distinct phases, initially inflammatory cells are recruited to the site to try and neutralise the damaging agents and remove necrotic material. This is closely followed by the activation of HSCs into hepatic myofibroblasts which secrete vast amounts of ECM to encapsulate the injury and provide a matrix for hepatocyte regeneration. Finally, if the inflammatory stimulus is removed, the matrix is remodelled and hepatocytes regenerate lost tissue by undergoing proliferation. The complex interactions between the immune mediated response and the resident liver cells are known to play an essential role in determining the outcome of liver injury, whether it leads to fibrosis or regression. For example, animals lacking macrophages or the T/B cell response have been shown to have reduced fibrotic responses [68].

The understanding of HSC biology has led to suggestions that HSCs play an essential role in the recruitment and modulation of the inflammatory response. HSC activation, by hepatocyte necrosis or apoptosis for example, stimulates the secretion of a vast array of chemoattractants and chemokines such as platelet activating factor [69] and MCP-1 [70]. A selection of these chemokines, along with those produced by hepatocytes, biliary epithelial cells and the sinusoidal endothelial cells themselves are presented on the surface of the sinusoidal cells to aid in the recruitment of leukocytes [68]. The chemokine gradient is also responsible for increasing the affinity of the adhesion molecules on the surface of

the sinusoidal endothelium for their target thus favouring the recruitment and infiltration of the inflammatory cells [71].

Following infiltration of the inflammatory cells into the tissue, HSCs have been shown to be important in the presentation of antigen to the lymphocytes allowing them to directly modulate lymphocyte behaviour [72, 73]. Interestingly, recent research has demonstrated that immune cells are also capable of modulating HSC behaviour. Ingestion of disease associated lymphocytes leads to HSC activation [74] representing a novel pathway of fibrogenesis. Some confusion surrounds the function of NK cells during fibrosis with one research group showing that the NK cells perpetuate liver inflammation through TRAIL-mediated hepatocyte apoptosis during HBV infection [75]. However, two other research groups have demonstrated that NK cells had an anti fibrotic response through TRAIL-mediated apoptosis of hepatic myofibroblasts [76, 77].

Positioning of lymphocytes within the liver tissue is an issue which has only been recently investigated. Four weeks of CCl_4 induced liver injury was associated with the infiltration of NK and CD8 T cells and to a lesser extent CD4 T cells [78]. Confocal microscopy revealed that the positioning of lymphocytes was in close proximity to hepatic myofibroblasts in the periportal area and fibrotic scar suggesting a direct interaction between the two cells types [78]. *In vitro* studies of hepatic myofibroblasts, freshly isolated from diseased and normal liver tissue revealed that both cell populations were capable of producing chemotactic factors provoking strong and rapid lymphocyte chemotaxis that could be enhanced following proinflammatory cytokine stimulation [79]. Migration was regulated by both chemokine dependent and independent mechanisms, particularly through HSC expression of ICAM-1 and VCAM-1 and secretion of VEGF, HGF and IL-6.

Kupffer cells, which patrol the liver sinusoids and phagocytose foreign particles, respond to liver injury by the secretion of proinflammatory cytokines which promotes the expression of molecules involved in leukocyte adhesion. Their position in the sinusoids also aids in leukocyte trapping, forcing the cells to interact with the adhesion molecules expressed on the surface of the sinusoidal epithelium. Elegant experiments by Duffield *et al* [5] have indicated that there are two functionally distinct populations of macrophages which have opposing roles in liver injury and repair. The group demonstrated that during injury, macrophages are important in promoting myofibroblast proliferation thus

depletion during this time ameliorates fibrosis. However during fibrosis resolution, the predominant population of macrophages favour myofibroblast apoptosis with depletion resulting in the prevention of matrix degradation.

1.3 Carbon tetrachloride induced liver fibrosis

Animal models of disease are necessary for the advanced understanding of human disease. Currently, there are several well established animal models to study liver fibrosis, the most common of which is iterative toxic damage (e.g. CCl_4 intoxication) [80]. CCl_4 is a hepatotoxin which elicits hepatocyte necrosis and steatosis of the liver and is used to study the effects of acute and chronic liver injury in animals [81].

CCl_4 is administered twice weekly, at a dose of 0.5-2ml/kg, by intraperitoneal injection since subcutaneous injection did not affect serum enzymes markers used to measure hepatotoxicity [82]. CCl_4 is predominately metabolised by cytochrome P450 (CYP) 2E1, which is expressed by hepatocytes in the centrilobular region [83], since CYP2E1 knockout mice are resistant to CCl_4 induced injury [84]. Although CCl_4 is dispersed throughout the whole body following injection, toxic effects are observed in the liver since metabolism is required for the production of the damaging agents [85]. Metabolism begins with the release of the trichloromethyl free radical CCl_3* through reductive cleavage of a carbon-chloride bond [85]. Whilst this free radical is in itself reactive, it can also react with oxygen to form the more reactive trichloromethylperoxyl (CCl_3O_2*) which is more likely to extract hydrogen from polyunsaturated fatty acids initiating lipid peroxidation [85] resulting in cell membrane damage. Resulting liver damage is caused by the free radicals produced by CCl_4 metabolism, which are summarised in figure 1-4.

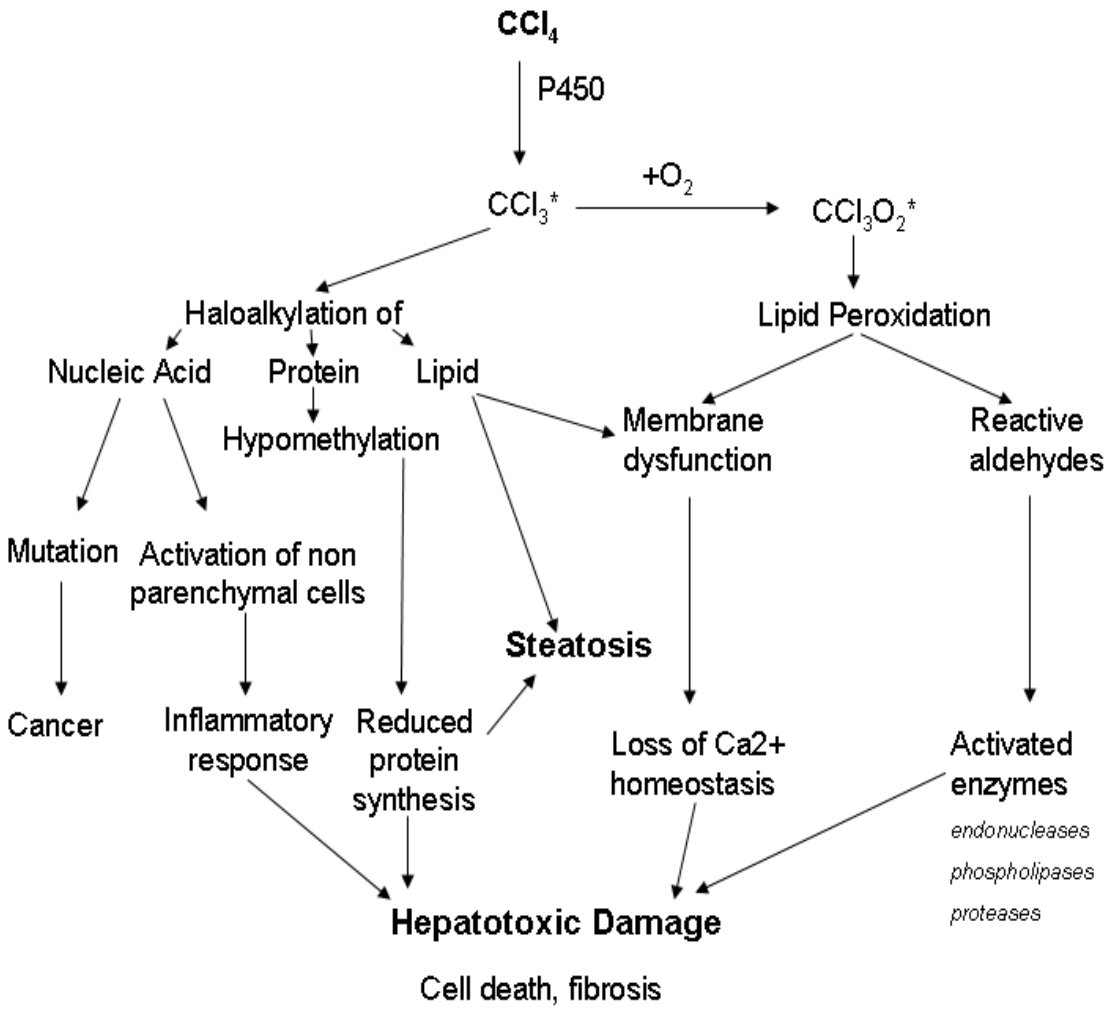

Figure 1-4 Mechanism of CCl_4 induced liver injury. Adapted from [85]. CCl_4 is metabolised by P450, expressed by hepatocytes in centrilobular regions of the liver, generating the free radical CCl_3*. CCl_3* can covalently bind nucleic acids, protein or lipids causing numerous downstream effects, one of which is the activation of non parenchymal cells e.g. kupffer cells of myofibroblasts that stimulates the release inflammatory cytokines and an inflammatory response. If oxygen is present, the highly reactive free radical CCl_3O_2* is produced which removes H^+ from unsaturated fatty acids resulting in membrane dysfunction and the production of reactive aldehydes which inhibit enzymes, damage DNA and block lipoprotein secretion. They also stimulate the activation of enzymes that lead to hepatocyte cell death. Together, all processes result in hepatotoxic damage, fibrosis and ultimately cirrhosis if the injurious stimulus is not removed.

CCl_3* exerts it effects through covalently reacting with biological substances, e.g. nucleic acids, protein and lipids, and altering their activity. For example CCl_4 metabolism is associated with a reduction in protein synthesis due to hypomethylation of ribosomal RNA [86] and steatosis due to the inhibition and/or blockage of lipoprotein secretion from hepatocytes into the circulation [87] possibly due to functional impairment of the Golgi apparatus [88].

Lipid peroxidation, initiated by CCl_3O_2*, results in the release of carbonyl compounds, termed reactive aldehydes, that cause toxic damage to cells through

enzyme inhibition, DNA damage [89] and the blockade of lipoprotein secretion [85]. Furthermore, cellular membranes are disrupted due to extraction of H^+ by the free radicals. When coupled with the loss of calcium homeostasis, due to CCl_4 mediated inhibition of calcium pumps [90], the surge in intracellular calcium concentrations activates catabolic enzymes and destroys cytoskeletal structures resulting in cell death via necrosis [85].

1.4 Resolution of Fibrosis

To date, the majority of anti-fibrotic therapies available for patients deal with the aetiological agent itself rather than the disease mechanism. For some types of liver injury, for example the removal of excess copper or iron in the genetic conditions Wilson's disease and haemachromatosis, or the abstinence from alcohol, this approach is highly effective. For other conditions, the drugs currently available may prevent or slow the progression of fibrosis, for example immunosuppressive drugs are commonly used to treat autoimmune hepatitis. However, for diseases where the underlying cause is not known, it is important that other therapeutic targets are identified which do not necessarily cure fibrosis completely but prevent the progression to cirrhosis and ultimately liver failure. Currently, the only effective method for liver fibrosis is transplantation yet the majority of patients with liver failure will die whilst waiting for a transplant due to the shortage of donors available. The continued understanding of the fibrogenic mechanisms has led to speculation that fibrosis is reversible [36, 91] and the development of drugs which target the fibrogenic mediators. Whilst no drugs have yet been deemed suitable for human use, it has been agreed that the ideal drug should be easy to administer, with few adverse side effects, high liver specificity and promote the resorption of the interstitial ECM generated by the hepatic myofibroblasts.

Several current targeted therapies have been against the signalling pathway for the profibrogenic cytokine TGFβ through use of soluble TGFβ type II receptor [92], neutralising antibodies or molecules which interfere with the downstream signalling pathway e.g. Smads [93]. Whilst this provides a novel therapeutic target, TGFβ is a complex cytokine involved in many biological process thus inhibition may result in uncontrolled inflammation, prevent epithelial differentiation and apoptosis [93]. Other targets include TIMP-1 and the integrin α5β6 expressed by cholangiocytes which tethers latent TGFβ1 [93-95].

1.4.1 Targeting Myofibroblasts

In vitro studies have been essential in determining the role of hepatic myofibroblasts in the initiation, progression and termination of liver injury.

Saile *et al* [96] isolated HSCs from rats to examine mechanisms for terminating uncontrolled proliferation. They noted that culture on plastic resulted in the activation of some HSCs into hepatic myofibroblasts but more importantly activation resulted in the increased expression of CD95 and CD95L allowing the cells to undergo spontaneous cell death which could be blocked by incubation with CD95 blocking antibodies. Studies using an immortalised hepatic myofibroblast cell line, LX-2, have shown that progressive cellular activation was also associated with an increase in TRAIL receptor expression, particularly TRAIL-R2/DR5 which was unique to hepatic myofibroblasts, increasing susceptibility to TRAIL-mediated apoptosis and representing a potential target in the regulation of HSC activation [97].

More importantly, however, *in vitro* studies have revealed that cytokines present in the cell microenvironment may influence the outcome of liver injury. Spontaneous apoptosis of rat hepatic myofibroblast in culture could be prevented through addition of TGFβ, and to a lesser effect TNFα, to the culture medium and was associated with down regulation of CD95L [98]. Furthermore, the anti-apoptotic effect of these cytokines was associated with inhibition of proliferation characterised by G_1 cell cycle arrest [98]. Conversely, the presence of IFNγ in the microenvironment could stimulate apoptosis of hepatic myofibroblasts [99] suggesting that *in vivo* the lifespan of these cells and thus the course of fibrosis was directly related to cytokine signalling.

In vivo translation work by Iredale *et al* [100] investigated the cellular mechanisms during the spontaneous resolution of CCl_4 induced liver fibrosis in rats. Rats were subjected to twice weekly injections of CCl_4 for a period of four weeks, following this they were sacrificed at four different time points after receiving the final dose. Immunohistochemical staining of liver sections from all four time points showed a 12 fold reduction in αSMA positive cells in sections from the 28 day time point. In conjunction with this, dual immunostaining found that TUNEL positive nuclei were within αSMA positive cells suggesting that the hepatic myofibroblasts were undergoing apoptosis. Similarly, a 5 fold decrease in

hepatic myofibroblasts (as determined by αSMA staining) was associated with the progressive resolution of biliary fibrosis following bile duct ligation and subsequent bilio-jejunal anastomosis after 21 days [101]. Both studies support the concept that apoptosis of hepatic myofibroblasts regulates fibrosis resolution.

Proof of concept studies by Wright *et al* [102] showed that the addition of gliotoxin, a fungal toxin, to rat and human hepatic myofibroblasts (characterised by the expression of αSMA) resulted in the cells undergoing apoptosis. Furthermore, administration of gliotoxin to rats with CCl_4 induced fibrosis, resulted in a 57% reduction of hepatic myofibroblasts in a recovery model. Gliotoxin is thought to work by inhibiting the degradation of NF-κB super-repressor IκBα [103, 104], however it has also been suggested that it can work via a mitochondrial dependent pathway through interactions with the adenine nucleotide transporter (ANT) [105].

Oakley *et al* [106] set about to prove that NF-κB signal transduction was the major pathway involved in hepatic myofibroblast activation. They found that rats, which were administered sulfasalazine following CCl_4 induced liver damage, had a reduced fibrosis pathology score as well as a significant dose dependent reduction in the number of hepatic myofibroblasts.

Whilst administration of gliotoxin significantly reduced the number of hepatic myofibroblasts in a recovery model of CCl_4 induced liver fibrosis, its use as an anti fibrotic therapy is somewhat limited. Systemic administration of gliotoxin is known to be associated with immunosuppressive effects through induction of immune cell apoptosis [107, 108] as well as inducing non specific apoptosis of liver cells, e.g. kupffer cells, which are necessary for promoting liver regeneration [109]. To overcome this problem for a range of therapeutics, a vast amount of research is now focused on targeting therapeutics to hepatic myofibroblasts. In 1999, Beljaar *et al* [110] identified that the expression of the mannose-6-phosphate/insulin-like growth factor II (M6P/IGF-II) receptor increased on hepatic myofibroblasts during liver fibrosis [111] and developed a modified version of human serum albumin (HSA) with M6P to specifically target these cells. M6P-HSA was conjugated to gliotoxin via an ester backbone to ensure efficient release following receptor mediated endocytosis and lysosomal degradation [112]. Gliotoxin-M6P-HSA administration at 6 days following bile duct ligation resulted in a significant decrease in the number of αSMA positive cells, similar to

gliotoxin treatment, however gliotoxin-M6P-HSA did not significantly affect other liver cell populations demonstrating that cell specific targeting of gliotoxin is a viable therapeutic option [112].

To overcome the limitations associated with the development of new anti fibrotic therapies a number of drug companies are trying to find novel applications for drugs currently in clinical practice; this is termed drug repositioning [93, 113]. At present, there are a few drugs in clinical use which may possibly be used as an anti-fibrotic therapeutic [114]. Relaxin, a hormone normally associated with pregnancy, has been shown to be able to reduce the deposition of interstitial collagen by hepatic myofibroblasts both *in vitro* and *in vivo* in a rat model of liver fibrosis [115]. The expression levels of peroxisome proliferator-activated receptor γ (PPARγ) have been shown to correlate with HSC activation with agonists reducing proliferation, collagen I gene expression and chemotaxis [116]. More importantly, these agonists are already in clinical use for the treatment of type 2 diabetes and have shown great promise in the clinical trials treatment of NAFLD [117-119].

1.4.2 Synaptophysin & C1-3

Synaptophysin, initially identified in 1985, is a transmembrane glycoprotein found on small electron-translucent (SET) vesicles [120] and is associated with neurotransmitter release and control of exocytosis [121]. Previous research has shown that this was only expressed on neural and neuroendocrine cell types [122], with the exception of rabbit thrombocytes [123]. However a series of immunohistochemical staining experiments carried out by Cassiman *et al* [124] demonstrated that synaptophysin was also a novel marker of quiescent and activated hepatic stellate cells.

This unique marker was exploited by Elrick *et al* [125] in the generation of a monoclonal single chain antibody fragment which was specific for hepatic myofibroblasts. The group identified two peptide regions on the exoplasmic side of the synaptophysin protein (see Figure 1-5) and once synthesised, they could be used to isolate a phage antibody with specificity for either sequence. The result was a single chain antibody fragment with specificity to peptide 2 and was termed C1-3. A sequence of elegant studies to demonstrate functionality proved that the recombinant antibody was capable of binding to human hepatic

myofibroblasts in culture and upon the addition of peptide 2 to the culture, binding with C1-3 was competitively reduced in a dose dependent manner.

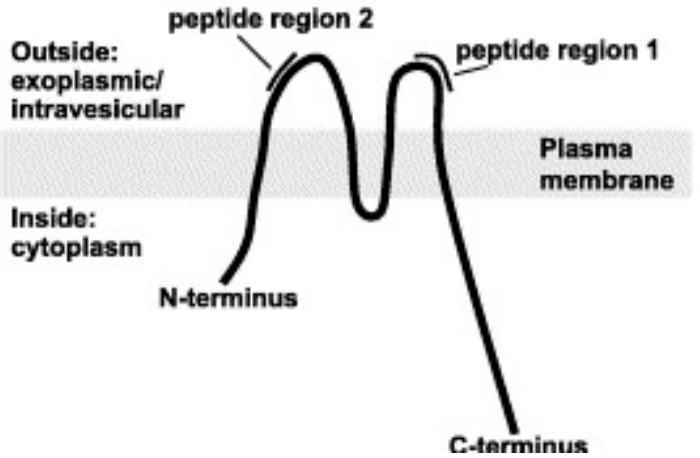

Figure 1-5: taken from [125]. A diagram of the synaptophysin protein in hepatic myofibroblast membrane. The transmembrane spanning glycoprotein has two extracellular domains. On these domains, two peptide sequences were identified and termed peptide 1 and 2. C1-3 binds to the peptide 2 region of synaptophysin with peptide 1 sequence being used as a negative control in ELISA.

Analysis of the liver tissue containing C1-3-FITC found that the antibody specifically labelled hepatic myofibroblasts with no co-localisation with kupffer cells observed. To target the apoptotic effects of gliotoxin the Wright group conjugated the fungal metabolite gliotoxin to C1-3. When injected into fibrotic mice, 60% of the hepatic myofibroblasts underwent apoptosis and fibrosis severity was significantly reduced in a sustained injury model [126].

1.5 Liver Regeneration

The ability of the liver to regenerate was recognised as far back as the ancient Greeks in the myth of Prometheus, who having stolen the secret of fire from the Gods of Olympus was condemned to having a portion of his liver eaten by an eagle. Overnight the liver regenerated providing Prometheus with eternal torture and the eagle with an eternal supply of food [127].

Today, liver regeneration is investigated using a slightly modified method of the two thirds partial hepatectomy (PHx) model first proposed by Higgins and Anderson in 1931 [128]. This is a useful model as the tissue is removed ‘cleanly’ due to the multi-lobular structure of the liver allowing the remaining tissue to regenerate by processes mediating only to the liver tissue itself and not an

inflammatory response which may result from tissue necrosis. The process itself is relatively straight forward and can be accurately monitored.

Liver regeneration is a complex process with many genes involved, the majority of which has been discovered using various knockout strains of mice. Unlike other organs, liver regeneration does not rely upon stem cells to restore tissue mass, instead the mature cells of the liver parenchyma are stimulated to enter the cell cycle and undergo DNA replication [129]. Work to date has shown that this is a highly synchronised event starting with the replication of the hepatocytes followed by biliary cells, kupffer and stellate cells and finally the sinusoidal epithelial cells [127].

The initial stimulus required to initiate the regenerative process is still debated. A recent paper by Tumanov *et al* [130] reported the importance of the adaptive immune system in liver regeneration. They demonstrated that mice deficient in T cells showed reduced capacity for liver regeneration, furthermore mice specifically deficient in T cell lymphotoxin had a decreased ability to initiate DNA synthesis following PHx and had increased liver injury.

Following initiation, liver regeneration can be divided into three main stages: priming, proliferation and termination. Each is a carefully controlled event regulated by many cytokine, growth factor and metabolic pathways. Figure 1-6 summarises the main pathways controlling liver regeneration.

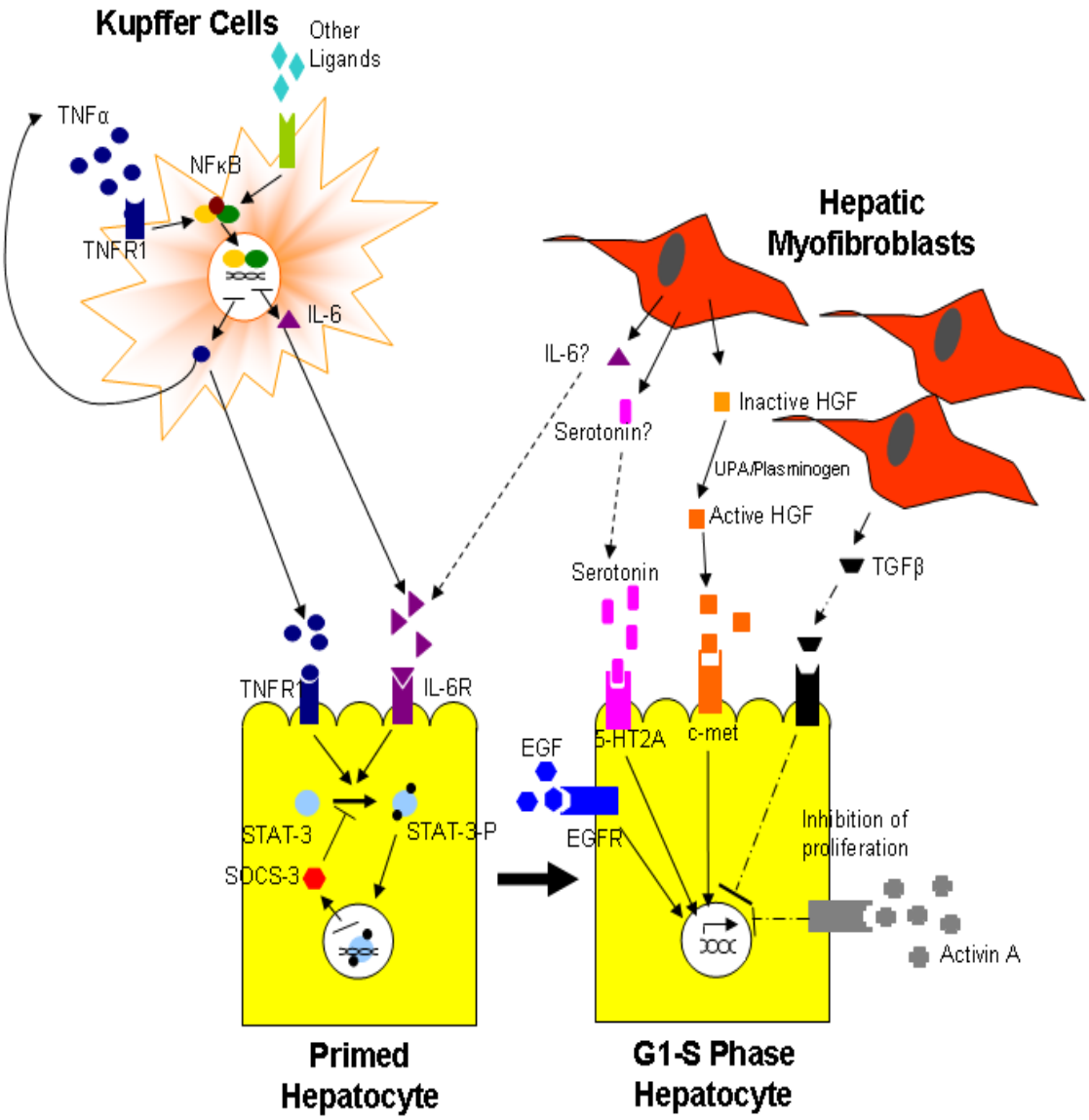

Figure 1-6 Pathways contributing to liver regeneration. Adapted from [129, 131]. After partial hepatectomy kupffer cells and hepatic myofibroblasts are activated by soluble factors such as lipopolysaccharide (LPS), lymphotoxin and vascular endothelial growth factor. TNFα binds to its receptor TNFR1 on kupffer cells leading to the activation of NFκB and the production of IL-6 and more TNFα. TNFα and IL-6 bind to their receptors on hepatocytes and stimulate the activation of STAT-3 by phosphorylation allowing it to translocate to the nucleus to transcribe a number of important genes, one of which is SOCS-3. SOCS-3 is an inhibitor of cytokine signalling through prevention of STAT-3 phosphorylation. Once primed, the hepatocytes are responsive to growth factors which promote their entry into the cell cycle. Proliferation can be inhibited by TGFβ and Activin A.

1.5.1 Priming Phase

Priming of liver regeneration begins in the first few hours following surgery and is thought to be mainly mediated by cytokine pathways. Research using neutralising antibodies and knockout strains of mice has implicated two main cytokines involved in this process, tumour necrosis factor alpha (TNFα) and interleukin 6

(IL-6) [132-136]. The network is initiated through the binding of TNF to its receptor, TNFR1, on non parenchymal cells (NPCs) in the liver (e.g. Kupffer cells) which leads to the activation of the NFκB pathway and the production of IL-6 [129]. IL-6 subsequently binds to its receptor, IL-6R, on hepatocytes stimulating the phosphorylation of the STAT-3 transcription factor allowing it to translocate to the nucleus and transcribe a number of important genes [129]. STAT-3 also leads to the transcription of the gene suppressor of cytokine signalling-3 (SOCS-3), a suppressor of cytokine signalling responsible for the inhibition of STAT-3 phosphorylation to prevent ongoing IL-6 signalling [137].

The role of IL-6 is complex. Whilst it is widely accepted that the production of IL-6 by kupffer cells and hepatic myofibroblasts [131, 138] is a critical event in the priming phase of liver regeneration, the consequences resulting from lack of IL-6 are somewhat debated. Initial work by Cressman *et al* [132] reported that partial hepatectomy in IL-6 knockout mice resulted in severe liver necrosis and mortality. However, in those that survived, hepatocyte replication was severely impaired resulting in delayed regeneration in comparison to wild type mice by up to 5 days. When this was repeated by Sakamoto *et al* [139] they found that IL-6 knockout mice had a reduction in proliferating hepatocytes at 24hrs, determined by BrDU labelling, in comparison to controls however a higher percentage of BrDU positive hepatocytes were observed at 36, 48 and 60hrs following PHx in IL-6 knockout mice. More importantly this study resulted in less mortality with no liver necrosis or differences in liver injury test between the treatment groups.

Work by Wuestefeld *et al* [140] attempted to clarify the role of IL-6 and its family members in liver regeneration using conditional glycoprotein 130 (gp130) knockout mice. Gp130 is a transmembrane protein forming one subunit of the type 1 receptor used in signal transduction by all IL-6 family members. Since gp130 knockout mice die in uteri or shortly after birth due to myocardial hypoplasia and haematopoiesis disorders [141], knockout mice were generated using the Cre/LoxP system. To do this gp130 loxP mice were crossed with *Mx-Cre* mice resulting in approximately 50% of the gp130 litter receiving the *Mx-Cre* transgene. Cre recombinase, under the control of Mx promoter (Mx gene mediates resistance against influenza), was induced through injection of agents (e.g. polyinosinic-polycytidylic acid (pIpC)) that stimulate IFNα expression which in turn activate the promoter [142]. Ten days after gp130 depletion mice were

subjected to two thirds PHx and liver regeneration monitored. Mice lacking an inducible cre recombinase enzyme were used as controls. The group found that mice lacking gp130 had no STAT-3 DNA binding suggesting that activation was cytokine mediated. Furthermore, gene array analysis revealed basal and inducible expression levels of TNFRI and II were significantly reduced in the knockout mice suggesting that these receptors are under IL-6 control. Although DNA proliferation was markedly decreased in conditional gp130 knockout mice, gene array analysis demonstrated that IL-6 had no significant influence on cell cycle progression genes, thus liver regeneration was only delayed not inhibited by gp130 depletion.

Whilst the conflicting data in the literature may reflect a lack of standardisation of experimental conditions in animal studies, a general consensus is that the liver has compensatory mechanisms available to overcome the loss of TNF and IL-6 to allow regeneration to occur.

There is also conflicting evidence surrounding the role of serotonin during the initiation of liver regeneration. Serotonin is both a neurotransmitter and a hormone [143] and is primarily found in the gastrointestinal tract, platelets and central nervous system.

Lesurtel *et al* [144] subjected mice with reduced platelets (due to thrombocytopenia) or inhibited platelet activity (via administration of clopidogrel) to PHx. They found that both defects resulted in decreased liver regeneration with normal proliferation levels restored in the thrombocytopenic mice by the administration of a serotonin agonist. Additionally mice lacking tryptophan-hydroxylase 1 (TPH1), an enzyme essential for the synthesis of peripheral serotonin, had a significant reduction in cellular proliferation following PHx which could be restored following injection of a serotonin precursor 5-HTP to reload their platelets. The authors proposed that the data provide evidence for the role of platelet derived serotonin in the initiation of liver regeneration. Papadimas *et al* [145] exerted a blockade on the serotonin receptor 2 through intraperitoneal injection of ketanserin at different doses and different time points. The group found that ketanserin only arrested liver regeneration when given at 16hr post PHx suggesting that serotonin was only essential close to the G1/S phase transition point and not involved in the initiation of liver regeneration.

Serotonin receptors have recently been identified on hepatic myofibroblasts with expression being induced upon activation [146]. Furthermore, hepatic myofibroblasts were shown to have a functional serotonin transporter as well as participate in active serotonin uptake and release [146]. The data suggest that hepatic myofibroblasts express key regulatory components of the serotonin system which may influence liver regeneration.

1.5.2 Proliferative Phase

The priming phase of liver regeneration corresponds with the passage of hepatocytes from their quiescent G0 state into the cell cycle G1 state. Without the priming phase the liver would be unable to respond to the growth factors thus inhibiting regeneration [147]. The literature to date implicates hepatocyte growth factor (HGF) and the ligands of the epidermal growth factor receptor (EGFR) as the main regulators of cellular proliferation following PHx. The ligands which bind EGFR are as follows: EGF, TGFα, heparin-binding EGF-like growth factor (HB-EGF), amphiregulin, cripto, epiregulin and betacellulin [129, 148].

Hepatocyte Growth Factor

HGF, also known as scatter factor, is synthesised mainly by non parenchymal cells of the liver, e.g. hepatic myofibroblast [131, 138], and is secreted as an inactive single chain polypeptide which is activated through cleavage by either urokinase plasminogen activator (uPa) or HGF activator (HGFa) [149-151]. Studies using knockout mice have demonstrated that HGF and its receptor, c-met, are essential for normal embryo development [152, 153] since mice lacking either gene have a much smaller liver characterised by extensive loss of parenchymal cells resulting in death in uteri.

Following PHx, work by Lindroos *et al* [154] demonstrated an increase in serum levels of active HGF as early as one hour post hepatectomy. Further work by Schuppan *et al* [155] revealed that HGF was capable of binding to matrix proteins, in particularly collagens I, III, V, VI suggesting that the initial source of HGF post hepatectomy may be due to release from the matrix due to remodelling. Approximately three hours following PHx, synthesis of HGF begins by the non parenchymal cells of the liver, particularly the hepatic myofibroblast,

and proceeds for up to 24hrs following surgery [149, 156] allowing for efficient DNA replication.

Further investigation of the HGF signalling pathway was done using a conditional c-met knockout mouse where the c-met gene is flanked by LoxP sites and can be removed upon induction of Cre recombinase. Huh *et al* [157] reported that loss of c-met did not appear to affect the hepatocytes under normal physiological conditions, however massive mortality resulted after PHx with the regenerating livers displaying vast areas of necrosis. Borowiak *et al* [158] also used the Cre/LoxP with a slightly modified protocol to that described by [157].The group monitored the expression of the cyclins by Western blot analysis to investigate hepatocyte proliferation and found that cyclin expression was significantly lower in c-met mutated mice suggesting that c-met signalling is necessary for cell cycle entry after PHx. The group also demonstrated persistently high levels of HGF and IL-6 in the serum of the mutant mice for many days following PHx indicating that the liver was trying to compensate for the lack of c-met signalling.

The difference in animal protocols makes it difficult to interpret the results obtained through the Cre/LoxP removal of the c-met gene. In an attempt to overcome this, a group developed a method to silence either HGF or its receptor, c-met, through RNA interference [159]. siRNA/PEI complexes were injected into rats 24hrs prior to and at the time of PHx and the amount of suppression calculated using RT-PCR. C-met suppression resulted in the inhibition of hepatocyte proliferation for up to 24hrs following surgery in comparison to 90% proliferation observed in controls. This implies that c-met signalling is crucial in the initiation of hepatocyte proliferation and that the liver cannot compensate for its loss. The loss of the silencing plasmid after 24hrs correlates with the near normal levels of cellular proliferation in the mice.

Epidermal Growth Factor

Due to the multiple binding ligands for the EGFR, the associated signalling pathway is more complex than that of HGF. Work by Jones Jr. [160] found that removal of the salivary gland of rats prior to one third and two thirds PHx resulted in severe impairment of DNA replication in animals subjected to the two thirds PHx only. Even at 12 days post surgery the percentage liver weight remained at 55% suggesting that the release of EGF from the salivary gland post

hepatectomy was essential for liver regeneration to begin. Normal levels of DNA synthesis could be achieved by a single dose of EGF into salivectomized rats prior to PHx surgery.

Further work by Berasain *et al* [161] focused on the EGFR ligand amphiregulin and examined its gene expression in healthy and cirrhotic human and rat liver. RT-PCR revealed that amphiregulin mRNA was undetectable in healthy human livers and in rat/mouse livers prior to PHx. However following injury to the liver, either by cirrhosis or PHx, gene transcription of amphiregulin mRNA significantly increased. Amphiregulin knockout mice had severe reduction in cellular proliferation indicating that signalling is necessary in the early stages of liver regeneration and cannot be substituted by other EGFR ligands.

In an attempt to investigate the EGFR signalling pathway itself instead of just the ligands, Paranjpe *et al* [162] designed two EGFR specific short hairpin silencing RNAs to inhibit EGFR expression in the rat liver. Suppression of the EGFR resulted in a significant decrease in cellular proliferation at 24hrs following PHx, as measured by mitotic indices and BrDU incorporation. However liver regeneration, as determined by liver weight, was seemingly unaffected with H&E stains revealing that sh-EGFR treated animals compensated for reduced proliferation through hepatocyte hypertrophy.

Whilst siRNA silencing of genes has provided a useful insight into EGFR signalling and clearly results in suppression of both mRNA and protein levels of EGFR, it is important to interpret these results carefully. Firstly results may be cell specific as transfection efficiency depends upon cell type, with hepatocytes taking up the majority of the plasmid whilst endothelial cells are scarcely affected. Additionally, EGFR is also present in its phosphorylated form in the resting liver meaning that at the time of PHx EGFR signalling can occur.

1.5.3 Termination

Following PHx the liver grows back to its precise mass and does not exceed it with molecules such as TGFβ (produced by hepatic myofibroblasts [163]), IL-1β [164] and Activin A [165, 166] implicated in controlling the process although their exact mechanisms still remain elusive.

The importance of TGFβ was realised when addition of this molecule to hepatocytes *in vitro* resulted in the inhibition of cellular proliferation [167, 168]. This work was taken one step further in 1988 when a group isolated hepatocytes from normal resting liver and compared the mRNA levels of TGFβ from these cells to those isolated from rat livers under various stages of liver regeneration following PHx [169]. The data showed that there was a significant increase in TGFβ mRNA in cells isolated from the regenerating liver which peaked after the majority of hepatocyte proliferation had taken place. However TGFβ over expression in hepatocytes of transgenic mice led to high serum levels of TGFβ1 causing multiple tissue lesions and glomerulonephritis but did not appear to affect liver regeneration [170].

In an attempt to understand the precise mechanistic actions of TGFβ, Oe *et al* [171] selectively deleted the TGFβ type 2 receptor (tgfbr2) in hepatocytes by crossing floxed *tgfbr2* mice with transgenic mice expressing Cre under the control of the albumin promoter. The group found that DNA synthesis peaked much earlier in the knockout mice in comparison to the controls and this was associated with an accelerated entry in the S phase of the cell cycle, as demonstrated by the early upregulation of cyclins D1 and E. However proliferation in the knockout mice halted when the correct liver mass had been reached suggesting that complete TGFβ signalling was not required for termination of liver regeneration. The authors propose that TGFβ is required to limit proliferation of hepatocytes by inhibiting the cells passing from G1 to S phase in the cell cycle. This agrees with previous work published by Russell *et al* [172] which found that intravenous administration of porcine TGFβ1 during PHx and at specified time points following surgery had reduced hepatocyte proliferation in a dose dependent manor however restoration of liver mass occurred as normal.

Work using the knockout mice did reveal an upregulation in Activin A, a dimeric protein thought to be an autocrine growth inhibitor of hepatocytes, suggesting that the liver was trying to compensate for the loss of TGFβ. When the group administered follistatin, a glycoprotein known to bind and inhibit Activin signalling thus promoting continued liver regeneration [165, 166], to the *tgfbr2* knockout mice they found a significant increase in cellular proliferation, as measured by BrDU incorporation, compared to their controls. Interestingly, the increase in

proliferation was not associated with an increase in liver weight in the knockout mice treated with the follistatin. Nevertheless, the experiments suggest that Activin A rather than TGFβ signalling is more important in the termination of liver regeneration.

There is now growing evidence to suggest that termination of liver regeneration is controlled by the remodelling of the ECM. Many *in vitro* studies have demonstrated that the hepatocyte phenotype can be maintained for longer when cultured on a matrix similar to that present in the liver [173-176]. Groups that have investigated the changes in key ECM components following PHx found that between 3-7 days following surgery the decrease in cellular proliferation is associated with an increase in collagen synthesis [177, 178]. Unexpectedly, the study revealed a peak in TIMP-1 at the start of DNA synthesis [177]. This result can be explained by data published by Mohammed *et al* [179] who found that loss of TIMP-1 function in knockout mice resulted in accelerated hepatocyte cell cycle progression as demonstrated by the early expression of cyclin D1 and PCNA. Furthermore, this was associated with an increase in HGF/c-Met signalling suggesting that TIMP-1 is a novel regulator of cell cycle progression through its interactions with the HGF signalling pathway.

The ECM not only provides a scaffold for cellular growth and proliferation. It is also a rich source of signalling for the cells it surrounds mediated via integrins [180]. Recent work investigating the role of integrin signalling revealed that elimination of this signalling pathway by hepatocyte targeted genetic ablation of integrin linked kinase resulted in mice born with livers twice the size of wild type controls and are characterised by increased proliferation of hepatocytes and biliary cells, disorderly hepatic plates and increased deposition of ECM [181]. When subjected to PHx they exhibit a 58% increase in liver mass compared to pre hepatectomy weight [182] suggesting a defect in the mechanism associated with the termination of liver regeneration. This defect was associated with an increase in HGF/c-Met, β-catenin and Hippo kinase signalling pathways.

Whilst the literature alludes to possible mechanisms responsible for the termination of liver regeneration it is difficult to pinpoint an exact answer as there seems to be great redundancy within the pathways.

1.5.4 Model Limitations

The two thirds PHx model adapted from the original 1931 model proposed by Higgins and Anderson [128] is useful in understanding the mechanisms involved in the regenerative process. Although the model has discovered many therapeutic targets which may enhance regeneration, the model does not include outside factors which may influence the regenerative process in the clinical human disease setting. For example the innate immune response or removal of necrotic material [180]. Whilst some may argue that the addition of these factors may complicate matters even further, it is important to provide a realistic environment in order to discover if any therapeutic targets discovered are actually of clinical use.

1.6 Evaluation of Liver Fibrosis

The understanding of the complex mechanisms which initiate and perpetuate liver fibrosis has led to the development of many potential therapeutic agents which specifically target and interfere with the process of fibrosis. The majority of these studies have been tested in animals but in order to test the efficacy in humans, new diagnostic tests are required to evaluate the severity of fibrosis throughout an organ.

Currently the gold standard for the diagnosis of liver disease is histochemical analysis of a needle biopsy. Complications, such as prolonged hospital admission and mortality, are linked to the invasive procedure for 1:1000 to 1:10,000 [183, 184] of patients and is the main reason why this technique is avoided where possible.

Biopsies are typically stained with haematoxylin and eosin (although other stains may be used if required) and graded and staged by a pathologist. Ishtak *et al* [185] used tissue from chronic hepatitis patients to define it as the following:

“Grading may be used to describe the intensity of necroinflammatory activity in chronic hepatitis. Staging, on the other hand, is a measure of fibrosis and architectural alteration, i.e. structural progression of the disease; these features are currently believed to be the consequence of the necroinflammatory process.”

Typically, numerical scores are given to both the staging and grading, in conjunction with written recordings, providing a semi-quantitative assessment of the histological features observed in the tissue. Various scoring systems have been developed for assessing liver tissue, these are METAVIR [186], Scheur [187] and Ishak [188]. However, the biopsy only represents 1/50,000 of the total liver mass [183] and is therefore associated with substantial sampling error, especially in patients with diffuse parenchymal liver disease [189].

Analysis of 124 patients with chronic HCV by Regev *et al* [189] found that in 33.1% of patients a difference of at least one stage was observed between biopsies taken from the left and right lobe of the liver. More importantly in 14.5% of the cohort the pathologists diagnosed stage 3 disease in one biopsy and cirrhosis in the other showing that sampling error may mean that the severity of the disease is under-diagnosed. However, the costs associated with multiple biopsies as well as the increased risks favour the use of other non invasive diagnostic tests.

Currently, serum biochemistry is used to measure the extent of liver damage. These are classified as:

(i) **Hepatocellular leakage enzymes**: Following injury or alteration in membrane permeability to the hepatocyte, enzymes ‘leak out’ into the peripheral blood where they can be measured [190]. The two most commonly measured are alanine aminotransferase (ALT) and aspartate aminotransferase (AST).

(ii) **Cholestatic-induction parameters**: Alkaline phosphatase (ALP) and gamma-glutamyltransferase (γGT) are enzymes of hepatobiliary origin and are induced during cholestasis due to impaired bile flow [190]. Total serum bilirubin also increases during cholestasis due to regurgitation of conjugated bilirubin into the blood [190] or failure to excrete due to obstruction in the liver.

(iii) **Liver function parameters**: Hepatobiliary function is evaluated by measuring markers such as albumin, which may suggest a decrease of liver synthetic capacity [190].

These markers are useful tools in assessing the extent and severity of liver damage, however serum markers are unable to distinguish between the early stages of fibrosis [191] thus many research groups are proposing other novel fibrosis markers. Afdal and Nunes (2004) [183] define the features of an ideal liver fibrosis marker as follows:

(i) Liver specific

(ii) Levels not influenced by alterations in liver, renal or reticuloendothelial functions

(iii) Can measure the stage of fibrosis and the activity associated with matrix deposition and removal

(iv) Easy to perform.

To date many alternative markers of fibrosis have been suggested and typically include enzymes involved in matrix synthesis and degradation [192, 193], extracellular matrix glycoproteins and glycosaminoglycans [193, 194], products of collagen synthesis and degradation. These biomarkers can be subdivided into two categories, those which are pathophysiologically derived from ECM turnover and/or from components produced by the fibrogenic cells themselves (Class 1 biomarkers) or markers which have been statistically proven to indirectly reflect fibrosis (Class 2 biomarkers) [195]. Biomarker combinations currently proposed are summarised in table 1-1.

Index	Parameters	Theory	Advantage	Disadvantage	Reference
Indirect Serum Markers					
AST/ALT ratio	ALT & AST serum enzyme concentration	Enzymes released following hepatocellular injury.	Ratio increases with fibrosis severity.	Confounded by alcohol. Not capable of clearly distinguishing between stages of fibrosis.	[190, 196-199]
AST/platelet ratio (APRI or Wai-index)	AST Platelet count	AST released following hepatocellular injury. Worsening fibrosis associated with increase in platelet sequestration to the spleen.	Differentiate between patients with and without significant fibrosis.	Cannot different between fibrosis stages.	[200, 201]

Index	Parameters	Theory	Advantage	Disadvantage	Reference
Fibrotest/ Fibrosure	α2-globulin γ-globulin α2-macroglobulin Apolipoprotein A1 γGT Billirubin Age Gender	Combines 6 indirect markers of fibrosis with patient age & gender in an algorithm to generate a score which correlates with fibrosis.	Can distinguish between mild, intermediate & significant fibrosis.	Not reliable for HCV patients unless chronic disease.	[202, 203]
ActiTest	As above (Fibrotest) but includes ALT	Reflects fibrosis and necro-inflammatory activity.	Improves diagnosis of the later stages of fibrosis associated with inflammation & necrosis.	Only validated in HCV patients.	[204, 205]
Forns Index	Age Platelet Count Cholesterol γGT	Define thresholds for individuals with low or high probability of significant fibrosis.	Predicts no to low levels of fibrosis.	Cannot detect severe fibrosis Influenced by medications. Staging can be affected by platelet variations. Only validated in HCV patients.	[206]
FibroIndex	AST γGT Platelet Count	Change in FibroIndex correlates with variation in fibrosis stage.	Still being validated.		[207]
FIB-4	Platelet Count AST ALT Age	Similar to fibrotest.	Good at predicting advanced fibrosis. Similar accuracy to Fibrotest.	Only validated in HCV patients with advanced disease.	[208, 209]
Hepascore	Age Gender Bilirubin γGT Hyaluronan α2-macroglobulin	As fibrosis progresses α2-macroglobulin, hyaluronan and bilirubin levels increase.	Hyaluronan improves distinction between significant & advanced fibrosis & cirrhosis.	Cannot distinguish between the early stages of fibrosis.	[191, 210]

Index	Parameters	Theory	Advantage	Disadvantage	Reference
PGAA-Index	Prothrombin time γGT α2-macroglobulin Apolipoprotein A1	As fibrosis progresses α2-macroglobulin levels increase and apolipoprotein A1 levels decrease.	Useful for detecting liver damage in alcoholics.	Can only detect cirrhosis.	[211]
Direct Serum Markers					
Enhanced Liver Fibrosis (ELF) Test	Hyaluronic Acid Type III procollagen N terminal Pro-peptide (PIIINP) TIMP-1	Direct serum markers which reflect ECM turnover.	Validated in alcoholic liver disease, NAFLD & HCV patients. Good at predicting clinical outcome of chronic liver disease.	Sensitivity only allows distinction between no and significant fibrosis.	[212, 213]
ECM related enzymes	e.g. Lysyloxidase Monoamine-oxidase Collagen peptidase	Levels of enzymes reflective of ECM turnover.	Levels of collagen peptidase increase with increasing fibrosis.	Levels do not reliably reflect matrix synthesis.	[183, 214]
Collagen Fragments	e.g. Type I procollagen & PIIINP	Serum mRNA and protein levels measured, reflective of collagen deposition.	Increasing PIIINP correlates with amino-transferase levels and degree of fibrosis.	Limited clinical applicability in liver disease. Not suitable for chronic HCV patients .	[183, 197, 215, 216]
MMPs & TIMPs	e.g. MMP2 TIMP1	Levels of enzymes that regulate ECM accumulation & breakdown.	TIMP1 correlates with cirrhosis in explant tissue. MMP1 correlates with liver inflammation.	Limited clinical value when used in isolation.	[183, 217]
MFAP-4	microfibril-associated protein 4 (MFAP-4)	Ubiquitous protein involved in ECM turnover.	Serum levels increase with progressive fibrosis.	Only validated in HCV patients.	[218]
Hyaluronan	Hyaluronan	GAG secreted by hepatic myofibroblasts.	Levels correlate with inflammation and fibrosis.	Only validated in HCV patients.	[189,192]

Index	Parameters	Theory	Advantage	Disadvantage	Reference
Cytokines	e.g. TGF β CTGF	Cytokines mediate fibrosis.	TGFβ levels correlate with fibrosis severity in HCV patients.	No correlation with amino-transferases Only validated in HCV patients.	[183, 197, 219]
Glycoprotein	e.g. Laminin YKL-40	Laminin synthesised by HSC YKL-40 novel glycoprotein associated with fibrosis.	Laminin more effective than PIINP YKL-40 expressed in fibrotic areas, more accurate than hyaluronan.	Only validated in HCV and alcoholic liver disease patients.	[197, 220]

Table 1-1 Summary of biomarker combinations used in the diagnosis and monitoring of liver fibrosis.

The class 1 biomarkers measure components directly related to fibrosis, however extreme caution is required when interpreting the results to ensure that the patient has no further underlying chronic fibrogenic diseases which may interfere with the test result since no marker is liver specific. Furthermore, the lack of assay standardisation, variations in patient populations, variation of marker being dependent upon the aetiology of liver disease [183] and high costs associated with the tests has prevented many of the biomarkers from being used in clinical situations. Of those which have reached clinical importance, hyaluronan has proved to be the most sensitive and specific [195]. Activation of quiescent HSC to hepatic myofibroblasts in culture is associated with an increase in hyaluronan [221]. This correlates with increasing hyaluronan levels in patients with hepatitis C induced liver fibrosis [194, 222] due to dysfunction of the sinusoidal epithelial cells resulting in reduced clearance from the blood.

Class 2 biomarkers are typically used in multi-parameter combinations, which are selected by statistical models and mathematical algorithms, to aid in the detection and staging of fibrosis [195]. Although they typically measure factors indirectly related to fibrosis, these biomarkers satisfy the majority of diagnostic criteria and are being increasingly used in clinical practice. Of all the different indices listed above, the fibrotest and actitest hold the most promise and are commercially distributed by Biopredictive (Paris, France) and LabCorp (Burlington, USA). Furthermore, following an independent review, they have been recently approved by the French Health Authorities for first line assessment of fibrosis in HCV patients [223, 224].

However, further research is required to generate a fibrosis marker which meets all the criteria of an ideal marker (specified above) since the majority of biochemical and haematological tests, serum markers of connective tissue and the scoring systems described above fail to quantify the extent of fibrosis in approximately 50% of people [225]. Thus various imaging techniques have been proposed, described in table 1-2, which aim to overcome these problems.

Technique	Comments	Advantage	Disadvantage	Reference
Diffusion mediated MRI	Measures the apparent diffusion coefficient (ADC) of water, a parameter that is dependent on the tissue structure.	Fibrotic tissue has distorted architecture due to the deposition of extra ECM components. Thus a cirrhotic liver will have a lower ADC value.	Only validated in chronic HCV patients. Difficult to distinguish early stages of fibrosis.	[226]
Ultrasonography	Use Duplex Doppler ultrasonography to estimate the maximum velocity of blood in the hepatic artery and PV. This value is expressed as an A/P ratio.	The A/P ratio is significantly higher in patients with liver cirrhosis compared to controls.	Only diagnose late stages of fibrosis.	[227]
Transient Elastography	Termed 'Fibroscan'. Combination of ultrasound (5MHz) and low frequency (50Hz) elastic waves, propagation velocity directly related to elasticity.	Liver stiffness directly reflects fibrosis. Reproducible Accurate at predicting significant fibrosis and cirrhosis.	Cannot discriminate between intermediary fibrosis stages. False positive results in acute hepatitis & extrahepatic cholestasis. Unsuitable for obese patients or those with ascites.	[224, 228-230]
Acoustic radiation force impulse imaging (ARFI)	Mechanical excitation of tissue using short duration acoustic waves (~262μs) to generate shear wave propagation and tissue displacement. Quantify shear wave velocity	Reproducible Already in clinical use for other diseases. Accurate at predicting severe fibrosis and cirrhosis. Not influenced by steatosis.	Narrow range of results produced thus difficult to define fibrosis stage. Only preliminary results are currently available. Not tested on patients with ascites.	[224, 231-233]

Table 1-2: Imaging techniques proposed to replace liver biopsy

All the imaging techniques exploit the changes in liver architecture and provide a safe, non invasive and reproducible test for liver fibrosis. However, a major

limitation of these techniques is the failure to accurately distinguish between normal tissue and the early stages of fibrosis [197]. This is crucial in the early diagnosis of liver fibrosis for the implementation of therapeutic strategies as well as accurately monitoring disease progression. Whilst the Fibroscan holds the most promise the technique itself is also subject to some limitations. Its ability to distinguish between the early and intermediary stages is somewhat debated [197, 232], furthermore it is associated with false positive results in patients with acute hepatitis, cholestasis and congestive heart failure, is unsuitable for patients who are obese or suffer from ascites and has mainly been validated in HCV patients.

To date, no serum marker or imaging technique proposed can accurately distinguish between the stages of fibrosis meaning that the liver biopsy remains the gold standard. These diagnostic techniques will be essential upon the implementation of anti fibrotic therapies to monitor alterations in the course of disease and the effectiveness of the therapeutic itself. In order to solve this problem, new imaging techniques or serum markers need to be developed or analysis of liver fibrosis needs to be diagnosed by a combination of different methods [234, 235]. For example the fibroscan is currently being used in conjunction with fibrotest [236], to maximise testing potential and improve the accuracy of fibrosis staging [183, 197]. Furthermore, the majority of tests proposed in tables 1-1 and 1-2 have only been validated in HCV patients thus further evaluations are required before they can be used as standardised screening tools.

1.7 Specific Aims and Objectives

For many years research has demonstrated that the hepatic myofibroblast has been responsible for the initiation and perpetuation of liver fibrosis [14, 101, 237]. Furthermore, proof of concept studies have shown that the apoptosis of these cells, by drugs such as gliotoxin and sulfasalazine results in the resolution of fibrosis and partial return of normal tissue architecture.

However, there is emerging evidence that myofibroblasts may also play a significant role in angiogenesis and ECM remodelling during the resolution of fibrosis [237]. Thus, in order to design drugs capable of targeting the cells involved in fibrosis, it is essential to define the role of the myofibroblasts during liver fibrosis and resolution. More importantly, in order to evaluate the

effectiveness of the new therapeutics it is crucial that a safe, reproducible, accurate and non invasive diagnostic test is available.

This project will utilise the C1-3 antibody to investigate the following:

- Determine whether a quantifiable image of fibrosis can be obtained by using imaging agents conjugated to C1-3
- Investigate the effect of myofibroblast depletion during sustained liver injury
- Investigate the effect of myofibroblast depletion during liver regeneration following two thirds partial hepatectomy.

Chapter 2. Materials and Methods

2.1 Materials

All chemicals were purchased from Sigma-Aldrich (Dorset, UK) unless specified otherwise.

2.2 C1-3 Production

All bacterial culture was performed using aseptic technique with care taken to prevent contamination.

2.2.1 Bacterial Culture & Protein Expression for C1-3

Escherichia coli XL-1 blue cells (Stratagene, Amsterdam, Holland) transfected with the PIMS147 C1-3 [125] plasmid were cultured in baffled flasks containing 50ml sterilised Luria-Bertanni medium (10g/L Bacto-tryptone, 5g/L Bacto-yeast extract and 10g/L Sodium chloride, pH 7.0). Routinely glucose (1%) and antibiotics (Ampicillin 50µg/ml and Tetracycline 15µg/ml, Sigma) were added to ensure selection for transformed cells containing the plasmid.

After overnight incubation at 37ºc, 250rpm in a shaking incubator, one percent of the primary culture was added to 1litre of sterilised TB medium (24g/l Bacto-yeast extract, 12g/l tryptone, 0.5% glycerol) containing phosphate salts (0.17M potassium phosphate monobasic, 0.72M potassium phosphate dibasic), 1% glucose and the antibiotics specified above. The culture was grown for a further 8 hours at 37ºc, 250rpm. Following this the cells were pelleted by centrifugation at 2800*g* for 15 minutes, re-suspended in 1 litre of fresh supplemented TB medium and cultured overnight at 25ºc.

The following morning, the cells were pelleted by centrifugation as described previously, and resuspended in 1 litre of fresh TB medium containing phosphate salts, 1% glucose and ampicillin only. After one hour of culture at 25ºc, the cells were induced to produce the C1-3 antibody by the addition of 500µl of 0.5M IPTG (final concentration 0.5mM). The culture was left for a further 4 hours before being harvested by centrifugation at 6350*g* for 20 minutes.

The pellets were resuspended in 100ml of osmotic shock solution (200mM Tris-Hcl, 20% sucrose, 1mM EDTA pH7.5) with the addition of 50mg of lysozyme to

enzymatically and chemically lyse the cell walls of the bacteria. All solutions had to be ice-cold and the procedure carried out on ice to ensure efficient lysis. After 15 minutes incubation, 100ml of 5mM magnesium sulphate was added and the solution left for a further 15 minutes.

The cells were pelleted by centrifugation at 6350*g* for 30 minutes at 4ºc. The osmotic shock solution containing the recombinant antibody was sterile filtered through 0.45µm filters.

2.3 Protein Isolation

2.3.1 Preparation of Column

The C1-3 was purified via the hexahistidine C-terminal tag tail using Ni^{2+} charged IMAC (immobilised metal ion affinity chromatography) fast flow sepharose resin (Amersham Biosciences). IMAC exploits the interaction between chelated transition metal ions and side chains of certain amino acids on proteins, e.g. histidine.

Briefly, 2ml of nickel sepharose was removed from the stock solution and sedimented by centrifugation at 500*g* for 5 minutes. The ethanol was removed and sepharose resuspended in 5ml of distilled water. The centrifugation step was repeated and supernatant discarded. Finally, 5ml of binding buffer was added (10mM imidazole) and centrifugation repeated. The pellet was resuspended in 5ml fresh binding buffer and was ready for purification.

2.3.2 Protein Purification

The prepared nickel sepharose (described above) was added to the osmotic shock solution and incubated overnight at 4ºc with gentle agitation. The following morning, the osmotic shock solution was allowed to pass through a disposable econo-pac chromatography column (Biorad, Hertfordshire, UK) twice, followed by a final wash of 5ml binding buffer to remove non-specifically bound proteins. This wash was saved for future analysis. The protein was eluted with 10x 1ml volumes of 400mM imidazole and dialysed in 10l PBS overnight to remove the presence of imidazole by diffusion.

2.4 Protein Quantification

2.4.1 ELISA

Enzyme linked immunosorbant assay (ELISA) is a sensitive immunoassay relying on the specific binding of a protein to an antibody or antigen. Two different varieties of ELISA have been used: a binding ELISA to determine ability of an antibody to bind to antigen, and secondly a capture ELISA to calculate antibody concentration.

2.4.2 Peptide1/ 2-BSA conjugation

Initially, conjugation of peptide 1 and 2 (peptide 1, ATDPENIIKEMPMC; peptide 2, YPFRLHQVYFDAPSC) to BSA was carried out. Briefly 40mg of BSA (10mg/ml) was reacted with 1ml 24mM m-maleimido benzoyl-N-hydroxysuccinimide ester (MBS) dissolved in dimethylformamide (DMF). After 30 minutes of reacting, unreacted compounds were removed by PD-10 filtration. Following this, peptide 1 or 2 was dissolved in DMF and 10µmoles added to every 100-200nmoles of the BSA-MBS conjugate and left incubating at 4ºc overnight. Unreacted compounds were removed by PD-10 filtration.

2.4.3 Binding Elisa

Flat bottomed 96-well Immulon-4 microtitre plates (Dynex, Sussex UK) were coated with 2µg (100µl/well) of BSA, BSA-peptide1 or BSA-peptide2 and incubated for 2 hours at room temperature. All steps were carried out on a rocker at 300rpm to ensure components evenly mixed. In between each incubation step, the plate was washed at least three times with PBS+0.05% (v/v) Tween (PBS-T). Non specific binding was blocked by incubating wells with 2% milk protein (w/v) in PBS at 4ºc overnight.

Following washing, the C1-3 and human IgG samples were added to the plate. All samples were serially diluted, briefly 200µl was added to the first well, 100µl of which was subsequently removed and mixed with 100µl PBS and so on. The plate was incubated for one hour, washed and the secondary antibody added, goat anti human C kappa light chain-HRP (Sigma-1/1000 dilution). The antibody was diluted in 2% (w/v) Marvel/PBS. After one hour incubation, the well contents

were removed and washed five times with PBS-T. Bound antibody was detected using TMB tablets as described in 2.4.6.

2.4.4 Capture ELISA

Flat bottomed 96-well Immulon-4 microtitre plates were coated with 0.53µg/well of goat anti human Cκ Light Chain (bound and free, Sigma) for 2hours at room temperature. In between steps, the plate was washed with PBS-T as described previously. Non-specific binding was blocked by incubating wells overnight at 4ºc with 200µl/well of 2% w/v BSA in PBS.

The following day C1-3 protein was diluted 1/10 and then serially diluted across the plate. IgG was prepared at a concentration of 1250ng/ml and serially diluted across the plate, finishing at a concentration of 0.610ng/ml. After 90 minutes incubation at room temperature, the plate was washed and secondary antibody added, HRP-conjugated goat anti human Cκ Light Chain (1/1000 dilution). Finally the plate was washed 5 times with PBS-T and ready for detection of bound antibody (2.4.6).

2.4.5 Synaptophysin binding ELISA

To determine if synaptophysin is a serum marker of fibrosis, serum samples from 4/8/12wk CCl_4 and olive oil control mice were diluted 1/10 in coating buffer (0.1M sodium carbonate, 0.1M sodium bicarbonate pH9.6) and serially diluted across the flat bottomed 96-well Immulon-4 microtitre plates. Plates were incubated for 2 hours at room temperature. Plates were washed twice with PBS-T and blocked overnight with 5% w/v marvel/milk solution in PBS. After five washes with PBS-T, the plate was incubated with C1-3 (2µg/ml) or rabbit anti albumin (MP Biomedicals, USA (1.25µg/ml)) in 5% w/v marvel/milk solution in PBS for 1 hour at room temperature. The plates were washed 5 times with PBS-T and incubated with the appropriate secondary antibody, goat anti human Cκ light chain-HRP (1:1000) or goat anti rabbit-HRP (1:3000) in 2% w/v marvel/milk in PBS for a further 1 hour at room temperature. Finally the plate was washed five times with PBS-T and ready for detection (2.4.6).

2.4.6 Detection of bound antibody

Bound antibody was detected by incubation with 3,3',5,5'-Tetramethylbenzidine dihydrochloride monohydrate (TMB) tablets (Sigma). 1mg of TMB was dissolved in 10ml of 0.05M phosphate-citrate buffer pH5 with the addition of 2µl of 30% hydrogen peroxide. After 10 minutes, the reaction was stopped by the addition of 50µl 2M H_2SO_4, turning the reaction product from blue to yellow. This colour was then analysed using a spectrophotometer at 450nm.

2.5 Conjugation of C1-3 to other compounds

2.5.1 Removal of Endotoxin

Before conjugation could take place it was necessary to remove endotoxin from the C1-3 preparation using Q maxi H columns (Fisher Scientific, Loughborough, UK). Briefly, the columns were washed sequentially with 17ml of sterile water, 17ml 0.5M sodium hydroxide, 3x17ml sterile water and 2x17ml PBS pH 7.4 by loading each solution into the device followed by centrifugation at 2000g for 5 minutes.

The antibody was loaded onto the column and centrifuged as above for ten minutes. The flow through, containing the antibody, was sterile filtered through a 0.45µm filter and stored for downstream applications.

2.5.2 Conjugation to Alexa Fluorophore 594

Conjugation of C1-3 and CSBD9 (control scAb) [126, 238] to alexa fluorophore 594 was carried out using a kit from Molecular Probes (A-10239, Invitrogen, Paisley, UK). Absorption and emission of this fluorophore peak at approximately 590nm and 617nm, respectively.

Briefly, 50µl of 1M sodium bicarbonate buffer, pH8, was added to 0.5ml of the C1-3 antibody (2mg/ml) to increase the pH. This mixture was added to one vial of fluorophore and incubated on a magnetic stirrer for 2 hours. Following this, unconjugated fluorophore was removed via gel filtration through sepharose. To determine if conjugation was successful the samples were run on an SDS-PAGE gel.

2.5.3 Conjugation to FITC

Fluorescein isothiocyanate (FITC) powder, purchased from Thermo Scientific (Loughborough, UK), was prepared at a concentration of 10mg/ml in DMF. The reaction, which involved the isothiocyanate groups reacting with the free amine groups on C1-3, must be performed in an amine free buffer and is most effective at pH 8-9. Thus, PD-10 columns (GE Healthcare, Buckinghamshire, UK) were equilibrated with 50mM borate buffer pH 8.5 and used for buffer exchange by adding 2.5ml of C1-3 in PBS to the column and centrifuging at 1000g for 2 minutes. A 20 fold molar excess of FITC was added to the C1-3, in the conjugation buffer, and incubated at room temperature for 1 hour with occasional mixing. Unconjugated fluorophore was removed via PD-10 (GE Healthcare) columns equilibrated with PBS and centrifuged as before.

2.5.4 Conjugation to Gliotoxin

The conjugation process is based on [239] and outlined in Figure 2-1. All products used for the reaction were free from endotoxin.

750nmole of endotoxin free C1-3 was reacted with 22µmole of S-acetyl thioglycolic acid N-hydroxysuccinimide (SATA) and 1mM EDTA for 1 hour. Unreacted SATA was removed by PD-10 gel filtration. Following this, reactive sulphydral groups in the C1-3-SATA were exposed (deblocked) by incubation with 460µmole hydroxylamine for 1 hour.

12µmoles of gliotoxin, prepared as a 2mg/ml stock in DMSO, was activated through available hydroxyl groups by reaction with 60µmole of N-p-maleimidophenyl isocyanate (PMPI, ratio of 1:5).

After one hour of reacting, 12µmole of gliotoxin-PMPI was added to 600nmole of C1-3-SATA-deblocked and incubated for a further 2 hours. Unreacted compounds were removed by PD-10 gel filtration.

The C1-3-gliotoxin was aliquoted and stored at -20ºc.

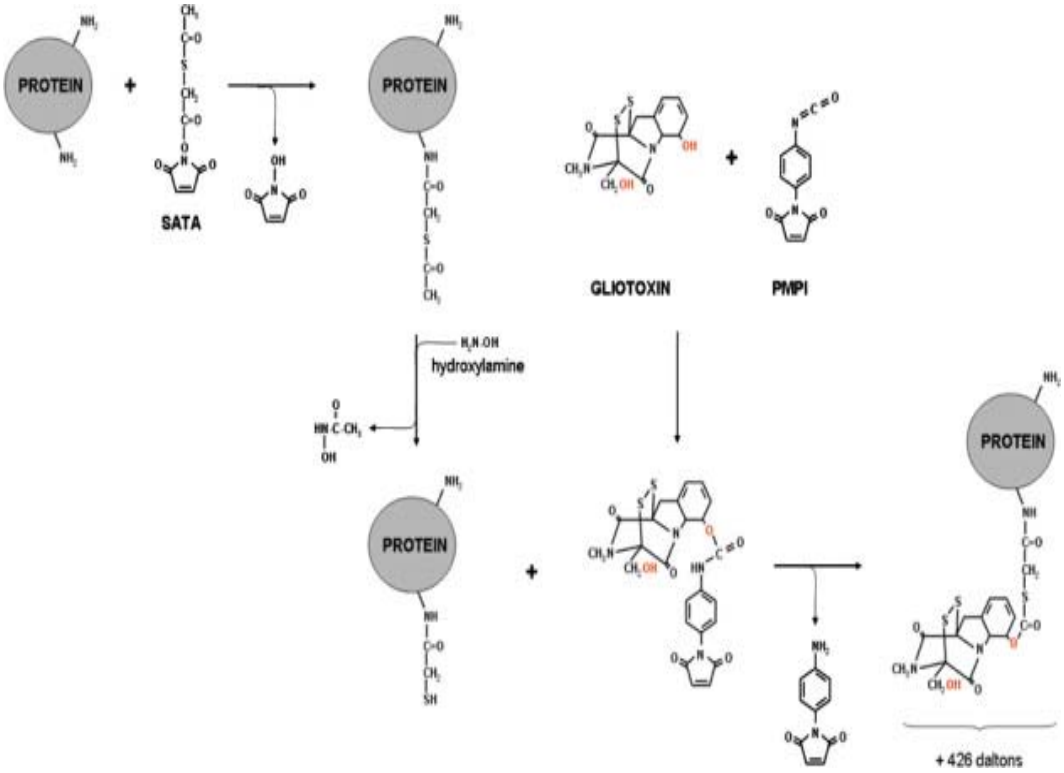

Figure 2-1. Taken from [126] a schematic diagram illustrating the reactions involved in conjugating C1-3 to gliotoxin. Primary amine groups on C1-3 were thiolated by the addition of SATA. After a 1 hour incubation, excess SATA was removed by PD-10 filtration. C1-3-SATA conjugates were de-blocked in the presence of hydroxylamine for 1 hour. Whilst incubating, gliotoxin was conjugated by reaction with PMPI for 1hr. Once complete, gliotoxin-PMPI was reacted with the deblocked C1-3-SATA for a further 3 hours with excess compounds removed via PD-10 filtration.

2.6 Protein Isolation and Analysis

2.6.1 Preparation of whole cell extracts

Medium was aspirated from the well and cells washed twice with 1xPBS. After washing, cells were scraped directly into either 100µl of reducing loading buffer (62.5mM Tris Buffer pH 6.8, 10% v/v glycerol, 2% w/v SDS, 100mM DL-Dithiothreitol (DTT) and 0.02% w/v bromophenol blue) or 500µl of 1xPBS (per well of a 24 well plate). The PBS/cell suspension was transferred to a sterile eppendorf and centrifuged at 3000g for 15 minutes. The supernatant was then carefully removed and the cell pellet resuspended in a known volume of 20mM Tris pH 7.4. 5µl of the sample was removed and used for the determination of protein concentration via the Lowry method (2.6.4). Samples were frozen and stored short term at -20°C or long term at -80°C.

2.6.2 Preparation of whole tissue samples

Tissue samples were removed from mice and snap frozen in liquid nitrogen. Samples were weighed and homogenised in 20% w/v TKMS buffer (50mM Tris, 25mM potassium chloride, 5mM magnesium chloride and 250mM sucrose pH7.4). 5µl of the sample was removed and used for the determination of protein concentration via a Lowry assay (2.6.4). Samples were frozen and stored short term at -20°C or long term at -80°C.

2.6.3 Preparation of bacterial lysates and scAb samples

Osmotic shock solution for SDS-PAGE analysis was filtered through a 0.2µm filter to remove contaminating bacterial DNA. Samples were diluted 1:5 with reducing loading buffer.

Unless specified otherwise, scAb samples for SDS-PAGE analysis were diluted 1:1 with reducing loading buffer. Samples were frozen and stored short term at -20°Cor long term at -80°C.

2.6.4 Lowry Assay

Protein concentration was determined by using a modified version of the Lowry assay described in 1951 [240]. It relies on the principle that under alkaline conditions copper complexes with protein and upon the addition and binding of Folin-phenol reagent, the complex is reduced and a blue colouration formed.

Buffer ABC was prepared immediately prior to use and was composed of Lowry A (2% w/v Na_2CO_3 /4% w/v NaOH), B (2% w/v sodium tartrate) and C (1% w/v copper sulphate) mixed at a ratio of 100:1:1 (v:v:v).

Bovine serum albumin (BSA) standards were prepared ranging from 0-20µg/µl from a 20mg/ml (20µg/µl) stock of BSA diluted in dH_2O. 5µl of each standard or sample was aliquoted into an eppendorf, diluted with 50µl of dH_2O and 1ml buffer ABC and left for 10 minutes at room temperature before the addition of 100µl of Folins reagent (Fluca, Switzerland, diluted 1:1 with dH_2O). Samples were incubated for a further 30 minutes at room temperature to allow colour development. Samples were then transferred into plastic cuvettes and absorbance at 750nm was determined spectro-photometrically. A calibration curve was plotted using the absorbence of standards. The equation of the line

was used to calculate the protein concentration of the unknown samples by measuring their absorbance and rearranging the equation of the straight line in terms of x. (y = mx + c where y represents the absorbance, m represents the gradient of the line and c represents intercept with the axis).

2.6.5 SDS-PAGE

The use of sodium-dodecyl sulphate polyacrylamide gel electrophoresis (SDS-PAGE) to analyse proteins is based on the original method of Laemmli in 1970 [241]. When using an electrical current to drive macro-molecules through a fixed pore size gel, three factors influence the rate of movement – size, charge and degree of folding. SDS is an anionic detergent that denatures proteins by binding to the polypeptide backbone. When used in conjunction with reducing agents such as DTT, it converts highly folded heterogeneously charged proteins to linear structures with negative charge that varies per unit length. Thus the proteins will now migrate through the gel, from negative to positive, according to size. Proteins are run alongside a marker of known molecular weight (Invitrogen) in order to allow an estimation of the molecular weight of a certain band.

A separating gel (375mM Tris buffer pH8.8, 0.1% w/v SDS, 0.05% w/v ammonium persulphate (APS) and 0.05% v/v TEMED) containing either 7.5, 9 or 12% acrylamide was cast between two plates set 1mm apart. The gel was covered with a thin layer of isopropanol to ensure a level interface. Once polymerisation had occurred, the isopropanol was removed and the gel washed with water. A 4% stacking gel (4% w/v acrylamide in 125mM Tris buffer pH 6.8, 0.1% w/v SDS, 0.05% APS and 0.1% TEMED) was carefully poured on top and wells created using combs.

The protein samples were heated to 90°C for approximately 5 minutes to ensure that all structure was removed and 10µl of sample (concentration dependent upon protein of interest, typically 10-20µg) loaded per well. The gels were placed in the tank with electrophoresis running buffer ((ERB) 20mM Tris, 160mM glycine and 0.08% w/v SDS, pH 8.3) and were run at 100V initially, ensuring that the protein formed a linear band at the interface. Following this the voltage was increased to 150V and left until the dye had reached the bottom of the gel.

Once the dye front had reached the end of the separating gel, the gels were removed and either stained (2.6.6) or total protein was electro-transferred onto nitrocellulose membrane for immunodetection of specific proteins (2.6.7).

2.6.6 Gel staining

Gels were removed from the electrophoresis equipment and washed briefly in water. Following washing, the gel was stained with coomassie blue (0.5% w/v coomassie blue in 25% v/v isopropanol / 10% v/v acetic acid) for 1 hour and destained for a further 4-24 hours depending upon the number of washes. Destaining solution consists of 10% acetic acid and 10% methanol in deionised water. Coomassie blue weakly binds to histidine and arginine as well as aromatic amino acids via weak Van der Waals forces (physisorption).

2.6.7 Western Blotting

Following separation of the proteins according to size, it was necessary to transfer them onto a nitrocellulose membrane (Amersham) for analysis by Western blotting. The membrane was placed on top of the resolved gel and sandwiched between filter paper and scotchbrite pads in a cassette, all of which had been pre-soaked in transfer buffer for 5 minutes. This was then submerged in transfer buffer (0.025M Tris, 0.19M Glycine, 20% v/v methanol pH 8.3) and subjected to 100V for one hour.

Once transferred, non specific binding sites were blocked by incubation with 3% marvel (w/v) dissolved in TBS (20mM Tris, 200mM sodium chloride pH7.4)+ 0.05% tween 20 (v/v) for one hour at room temperature. The membranes were subsequently washed with TBS-T and incubated with the primary antibody, diluted in 0.3% marvel in TBS-T, for 1 hour at room temperature. The bound antibody was detected using species specific IgG secondary antibodies directly conjugated to HRP (Horse-radish peroxidase). This enzyme catalyses the oxidation of luminol, present in the ECL reagents (Amersham), resulting in the production of light which is detectable on hyperfilm (Amersham). Antibody dilutions in table 2-1.

Antibody	Dilution
Goat anti Human Cκ Light Chain-HRP (Sigma)	1:1000
Rabbit anti gliotoxin	1:3000
Goat anti Rabbit-HRP (Dako)	1:3000
Mouse anti actin (Millipore)	1:3000
Goat anti Mouse-HRP (Dako)	1:3000
Rabbit anti Synaptophysin (Chemicon)	1:1000
Mouse anti Synaptophysin (Dako)	1:1000

Table 2-1 Dilutions of primary and secondary antibodies used for Western blotting

2.7 Cell Culture

2.7.1 Isolation of Mouse Hepatic Myofibroblasts

3-4 C57Bl6 mice were schedule 1 killed and the whole liver removed. Liver tissue was mashed through a sterile tea strainer with the addition of 140mg pronase (Roche, Hertfordshire, UK) and 2mg DNAse in 40ml of Hanks balanced salt solution (HBSS) [0.14M NaCl, 5.4mM KCl. 0.34mM $Na_2HPO_4.7H_20$, 0.44mM KH_2PO_4, 5.6mM D-glucose and 15.7mM $NaHCO_3$, pH7.4] containing 6mM sterile Hepes, 1mM $CaCl_2$ and 0.035% (w/v) $NaHCO_3$. A further 10ml of HBSS+ supplemented with 25mg collagenase B (Roche) was added to the liver pureé and left at 37°Cto digest for 30 minutes. The cell suspension was filtered through sterile 125µm nylon mesh and centrifuged at 1100*g* for 7 minutes. Pellets were resuspended in 40ml fresh HBSS+ supplemented with 30mg pronase (Roche) and 2mg DNAse and incubated for a further 30 minutes at 37°C. The cell suspension was centrifuged as previously described and resuspended in 60ml HBSS+ and 13ml optiprep. This mixture was equally divided between two 50ml falcon tubes, carefully overlayed with a further 1ml HBSS+ per tube and subjected to density gradient centrifugation at 1400*g* for 20 minutes. The HSC rich upper phase was carefully removed and mixed with at least 1:2 HBSS+ and centrifuged for 7 minutes at 1100*g*. Pellets were resuspended in culture medium (Dulbecco's modification of Eagle's medium (DMEM) supplemented with 16% foetal calf serum (FCS) and 80U/ml penicillin/streptomycin) and seeded into 6 well plates.

2.7.2 Isolation of Human Hepatic Myofibroblasts

Explant liver tissue, obtained with full ethical consent from patients undergoing partial hepatectomy (Freeman Hospital, Newcastle, UK), was perfused using a

continuous flow pump system through manual insertion of perfusion tubing into available vessels at the cut surface with calcium free HBSS containing 6mM Hepes and 0.035% (w/v) $NaHCO_3$ to clear blood from the tissue. The tissue was then perfused with HBSS+ supplemented with 30mg collagenase B (Roche) and 235mg Pronase until the tissue was pliable to touch. The tissue was then dispersed in 100ml HBSS+ containing 35mg pronase (Roche) and 2mg DNAse, filtered through sterile 125µm nylon mesh and centrifuged at 1100*g* for 7 minutes. Pellets were resuspended in fresh HBSS+ containing 1mg DNAse and re-pelleted as previously described and repeated a further two times. After the three washes, the pellets were resuspended in 60ml HBSS+, 1mg DNAse and 13ml optiprep, carefully overlayed with a further 1ml of HBSS+ and subjected to density gradient centrifugation at 1400*g* for 20 minutes. The HSC rich upper phase was carefully removed and mixed with at least 1:2 HBSS+ and centrifuged for 7 minutes at 1100*g*. Pellets were resuspended in culture medium (DMEM supplemented with 16% foetal calf serum (FCS) and 80U/ml penicillin/streptomycin) and seeded into 6 well plates

2.7.3 Maintenance of Cells

Cos 7 cells were routinely maintained at 37°C in a humidified atmosphere of 95% air and 5% CO_2 in 75cm^2 plastic culture vessels. Cells were cultured in DMEM containing 1g/l of glucose supplemented with 10% (v/v) FCS, 80U/ml penicillin and 80U/ml streptomycin. Human and mouse hepatic myofibroblasts were cultured in DMEM containing 4.5g/l of glucose supplemented with 16% (v/v) FCS, 80U/ml penicillin and 80U/ml streptomycin. Culture medium was changed every 2-3 days.

2.7.4 Passage of Cells

All cells were anchorage dependent and grown as a monolayer until 80-100% confluence and then passaged. Medium was aspirated from the cells and washed once in 1xPBS (4mls per 75cm^2 flask) to remove any remaining medium. Cells were detached by incubation with 1xTrypsin-EDTA diluted in 1xPBS for Cos 7 cells or 5xTrypsin-EDTA for hepatic myofibroblasts (4ml per 75cm^2 flask) in the conditions described in 2.7.3 for 10 minutes. Gentle tapping of the culture vessel encouraged detachment of cells. Following detachment, 4ml of fresh media was added to the trypsin to inhibit its activity and the suspension transferred to a 50ml

falcon tube for centrifugation at 1000g for 3 minutes. The supernatant was discarded and the pellet resuspended in appropriate fresh culture medium. Cells were then seeded accordingly for cell maintenance or experimental protocol as detailed throughout.

2.7.5 Cell Storage

Cell stocks for all cell lines were routinely frozen down and stored in liquid nitrogen for long-term storage. Cells were detached and pelleted as previously described in 2.7.4 and resuspended in 90% FCS + 10% DMSO, typically 2ml per pellet harvested from a confluent 75cm^2 flask. The suspension was aliquoted into sterile cryovials (1ml per cyrovial) and placed in an isopropanol filled cooling aid (Mr Frosty™, Nalgene) and left in the -80°C freezer overnight. Cells were cooled at a rate of approximately 1°C per hour and then transferred to liquid nitrogen for long-term storage.

2.7.6 Revival of cells stocks

Cells were removed from liquid nitrogen and rapidly thawed at 37°C, transferred to a 50ml falcon tube and re-suspended in 10ml of fresh warmed medium. The cell suspension was then centrifuged for 4 minutes at 500g and the supernatant was discarded. The pelleted cells were then resuspended in 10ml of fresh medium, added to a 25cm^2 flask and allowed to attach overnight. Once confluence was reached cells were subcultured as previously described and transferred to a 75cm^2 flask.

2.7.7 Assessment of cell viability and number

Cell viability was determined using trypan blue exclusion. Freshly isolated cells were resuspended in 10ml fresh medium, a 100µl aliquot of this was added to 200µl fresh medium and 100µl 0.4% trypan blue solution (Gibco). 10µl of the cell suspension was added to an Improved Neubauer Haemocytometer and viable and non-viable cells counted. Viable cells have an intact membrane and are able to exclude the dye whereas non-viable cells take up the dye and are blue. Total cell number and the number of non-viable cells in a known volume of cell suspension were calculated and used to determine the percentage viability of the freshly isolated cells along with the total cell number.

2.7.8 C1-3 uptake

The ability of C1-3 to bind to its target receptor synaptophysin was assessed by the incubation of the antibody with mouse hepatic myofibroblasts. Cells were detached as described in 2.7.4 and total cell number determined as described above. Cells were resuspended to a density of $1.33*10^5$/ml and seeded in a fresh well (1.5ml/well of a 6 well plate). Cells were incubated overnight under standard conditions (37°Cin a humidified atmosphere of 95% air and 5% CO_2.) The following day the medium was aspirated and cells washed in 1xPBS. A specified concentration of C1-3 antibody was added to the total medium required for all wells and once mixed the medium was distributed evenly between the wells. Once incubation was complete, the medium was removed and cells gently washed in 1xPBS. Cells were directly harvested into 100µl/well reducing loading buffer ready for Western blot analysis.

2.7.9 In vitro assessment of gliotoxin activity

Mouse hepatic myofibroblasts, between passages 1-4, were seeded into 24 well plates at a density of $0.5x10^5$ per well and left for 24 hours to adhere and proliferate. Following this, C1-3 (4.5µg/ml), C1-3-GT (4.5µg/ml), free gliotoxin in DMSO (1.5µM) and DMSO were added to the cells in 300µl serum-free media and treated for 24 hours. Adherent cells, as a measure of cell viability, were counted from 5 random fields of view before the addition of treatment and subsequently at 1, 2, 4, 6 and 24 hours. Cell viability is expressed as a percentage of remaining adherent cells relative to time zero. All experiments performed in triplicate.

2.7.10 Cell transfection

Cells were transfected essentially as detailed in the manufacturer's protocol and cultured under standard conditions (37°C in a humidified atmosphere of 95% air and 5% CO_2).

Briefly, cos-7 cells were resuspended at a density of $1.5*10^5$/ml and seeded in 6 well plates (1.5ml/well of a 6 well plate). Cells were left for 24 hours to adhere to culture plate before transfection. Genejuice transfection reagent (Merck, Nottingham, UK) was added to 100µl of serum free media in a sterile eppendorf at a ratio of 3µl Genejuice to 1µg plasmid DNA and incubated at room

temperature for 5 minutes. Plasmid DNA was added to the mixture and left to incubate for a further 15 minutes at room temperature. The entire volume of transfection medium was added drop wise to the cells in 1.5ml of complete medium and gently rocked to ensure even distribution.

2.7.11 Assessment of transfection efficiency

To assess transfection efficiency, cells were transfected as outlined in 2.7.9 with different concentrations of the eGFP (pEGF-N1, Stratagene) reporter construct for 24 hours. The number of positive cells were counted and expressed as a percentage of the total number of cells per field of view.

2.8 Plasmid DNA constructs

2.8.1 Synaptophysin constructs

Mouse and human synaptophysin plasmids were purchased from Invitrogen (Paisley, UK). The sequences were transferred from the ORF prokaryote vector to the pTREX-DEST30 vector (Invitrogen) via site specific recombination mediated by LR Clonase II enzyme (Invitrogen) as outlined in the manufacturer's protocol. Briefly, 150ng of the entry clone (3µl) and destination vector (1µl) were incubated with 4µl TE buffer (10mM Tris, 1mM EDTA, pH 8 with HCl) and 2µl LR Clonase II for 1 hour at 25°C. The reaction was terminated by the addition of 40µg of proteinase K and incubating the samples at 37°C for 10 minutes. Successful recombination was confirmed via PCR using synaptophysin US and DS 2,3 and 4 primers detailed in table 2-5.

2.8.2 TOPO Cloning of Blunt-End PCR Products

To confirm PCR results, PCR products were routinely cloned into the PCR®-Blunt TOPO® vector (Invitrogen) according to the manufacturer's instructions. In brief, 25ng (1µl) of PCR®-Blunt was added to 100ng (5µl) of blunt PCR product, 1µl 10x ligation buffer (60mM Tris-HCl pH 75, 60mM $MgCl_2$, 50mM NaCl, 1mg/ml BSA, 70mM β-mercaptoethanol, 1mM ATP, 20mM dithiothreitol and 10mM spermidine), 2µl sterile H_2O and 1µl (4 Units) of T4 DNA ligase. For control reactions, the PCR product was replaced with 5µl sterile water. All reactions were incubated at 16°C for 1 hour. 2µl of the ligation reaction was transformed into TOP10 competent cells, as detailed in 2.8.3, and selected for kanamycin

resistance (50µg/ml). Plasmids were isolated by miniprep (2.8.5) and subjected to EcoRI restriction digest (2µl plasmid DNA, 1µl BSA 1mg/ml, 2µl buffer H, 4µl sterile H_2O and 1µl (12 Units) EcoRI) for 1 hour at 37°C to confirm PCR product insertion. To analyse, samples were mixed with loading dye and run on an agarose gel (2.12.7).

2.8.3 Competent cell transformation

Constructs were routinely propagated in TOP10 *E.coli* cells (Invitrogen) for synaptophysin plasmids or XL-1 blue *E.coli* cells (Stratagene) for PIMS147 C1-3 plasmid according to the manufacturer's protocol. Briefly, 50-100ng of plasmid DNA was added to 50µl of competent cells and incubated on ice for 30 minutes, causing the DNA to condense on the surface of the bacteria. The solution was then heat shocked at 42°C for 45 seconds and 250µl of sterile LB media added. The *E. coli* were incubated for 1 hour at 37°C (250rpm) to recover followed by plating out. 50-200µl of the bacterial suspension was spread onto the surface of 100mm petri dishes filled with solidified LB-agar with antibiotics (Synaptophysin: 100µg/ml ampicillin C1-3: 50µg/ml ampicillin and 15µg/ml tetracycline) to select for cells which had successfully been transformed.

The dishes were given 10 minutes to absorb the liquid and then incubated upside down at 37°C overnight (16 hours). Dishes were inspected for growth the following morning and well defined individual colonies were selected and used to inoculate 5ml of LB medium containing the appropriate antibiotic overnight at 37°C. Following overnight incubation the culture was either used for miniprep or used to inoculate LB for a large scale expression and maxi prepped as described in 2.8.5 and 2.8.6.

2.8.4 Storage of plasmid stocks

Glycerol stocks were prepared for plasmid DNA constructs by adding 500µl of the overnight culture to 500µl of sterile LB containing 30% glycerol. This was then immediately stored at -80°C.

When required, this stock was then used to produce more plasmid DNA by streaking out a small amount onto an agar plate with the appropriate antibiotic and grown overnight at 37°C. A single colony was then picked and used to inoculate liquid cultures, typically 1 colony was added to 5ml LB supplemented

with the appropriate antibiotic and incubated at 37°C overnight and then used for miniprep. Alternatively, the 5ml overnight culture was used to inoculate LB for a large scale expression with plasmid DNA being purified by maxiprep.

2.8.5 Miniprep of plasmid DNA

The purification process is based upon an alkaline lysis procedure followed by salt and pH dependent binding of plasmid DNA to the anion-exchange resin. The miniprep kit, provided by Qiagen (Southampton, UK), is designed for the purification of a maximum of 20µg plasmid DNA from 1-5ml of overnight culture. Briefly, bacteria from 1ml of the overnight culture were pelleted by centrifugation at 3000g for fifteen minutes at 4°C and the supernatant discarded. The bacterial cell pellet was then re-suspended in 250µl of buffer P1 (containing RNase), 250µl of buffer P2 (alkaline salt buffer containing SDS) was added and mixed by gentle inversion until the solution became clear and viscous. 350µl of buffer N3 was added to neutralise the solution and cause contaminating genomic DNA and membrane to precipitate. The precipitate was pelleted by further centrifugation at 10000g for 10 minutes and the supernatant applied to a Qiaprep spin column and centrifuged at 10000g for 1 minute. The flow through was discarded and the column was washed in 500µl of buffer PB and centrifuged for another minute. Any remaining contaminants were removed by a final wash step with 750µl of buffer PE and centrifugation at 10000g for 1 minute. Any flow through was discarded and the Qiaspin columns centrifuged for a further minute to ensure all residue was removed. The Qiaspin column was transferred to a sterile RNase-free eppendorf and 50µl of sterile H_2O was applied to the column and incubated for 1 minute before being centrifuged for 1 minute at 10000g to elute the DNA.

2.8.6 Maxiprep of plasmid DNA

Maxiprep kits, provided by Qiagen, are designed for the purification of plasmid DNA, maximum of 100µg, from 100-500ml overnight culture of transformed *E.coli* cells. In brief, 100ml of bacteria from an overnight culture were pelleted by centrifugation at 6000g for 15 minutes at 4°C. The supernatant was discarded and the pellet re-suspend in 10ml of Buffer P1 (containing RNase), 10ml of buffer P2 (alkaline salt buffer containing SDS) was then added and mixed by inversion. The mix was incubated at room temperature for 5 minutes and then 10ml of chilled buffer P3 was added, mixed immediately and incubated on ice for 20

minutes whilst contaminating genomic DNA and membranes precipitated. The precipitate was pelleted by centrifugation at 20000g for 30 minutes at 4°C and the supernatant applied to an Qiagen maxi column equilibrated with 10ml buffer QBT. Any contaminating RNA, proteins and low molecular weight impurities were removed by a medium salt wash, i.e. two 30ml washes with buffer QC, and any flow through discarded. DNA was removed from the column under high salt conditions by the addition of 15ml of buffer QF (containing isopropanol) to the column and flow through collected. DNA was then precipitated out of the solution by adding 10ml of 100% sterile isopropanol and pelleted by centrifugation at 15000g for 30 minutes at 4°C and the supernatant discarded. 5ml of 70% EtOH was added to the pellet to remove precipitated salt and centrifuged for a further 10 minutes at 15000g. The supernatant was removed and the pellet allowed to air dry. Upon drying the DNA pellet was resuspended in sterile ddH_2O and quantified using a spectrophotometer (2.8.7).

2.8.7 DNA quantification

The concentration of the DNA isolated was determined using UV spectrophotometry at 260nm. The DNA was diluted 1:100 with sterile water and added to a cuvette. The absorbance at 260nm was used to determine the concentration on the basis that an absorbance of 1.0 corresponds to 50µg/ml double stranded DNA.

The purity of the DNA was determined by measuring the absorbance values at 260nm and 280nm, DNA maximally absorbs at 260nm whereas protein absorbs at 280nm. These values are typically expressed as a ratio, with a pure DNA sample having a ratio value of 1.8 or greater.

2.9 Animal Work

2.9.1 Mice

C57Bl6 mice were purchased from Charles River and housed in the Comparative Biology Centre at Newcastle University. Mice were housed in an air conditioned environment at 20°C± 3^{o}C and a humidity of 50 ± 10% with a 12 hour light/dark cycle. Animals were cared for as per Home Office regulations.

Corticotrophin releasing hormone (Crh) transgenic mice were purchased from Jackson laboratories, St Louis and housed in the Comparative Biology Centre at Newcastle University. The rat Crh gene was expressed under the control of the metallothionine promoter in transgenic mice resulting in a mouse model of chronic pituitary activation. Mice developed symptoms characteristic of Cushing's syndrome with excess fat accumulation, muscle atrophy, thinning of the skin and alopecia.

2.9.2 Carbon tetrachloride-induced liver injury

To cause centrilobular damage which typically represents liver disease in humans the chemical CCl_4 was used. CCl_4 was diluted 1:1 with olive oil and given twice a week via intraperitoneal injection at a dose of 1ml/kg of body weight. This was carried out for up to a maximum of 12 weeks.

2.9.3 Partial Hepatectomy

This technique was based upon the two thirds PHx methods first proposed by Higgins and Anderson in 1931 [128].

Mice were anesthetized with a mixture of isoflurane/oxygen, and right medial, left medial, and left lateral lobes were excised and weighed after separate ligations resulting in removal of ~70% of the hepatic mass. At each time point, livers were harvested, weighed, and processed for subsequent analysis. Preoperative and regenerated liver weight was expressed as liver-to-body-weight ratio and used to calculate the relative growth of residual liver lobes. All surgical work was performed by Dr Fiona Oakley (Newcastle University).

2.9.4 Monitoring cellular proliferation

Bromodeoxyuridine (BrDU), an analogue of thymidine, is incorporated into the DNA of replicating cells and is a useful monitor of cellular proliferation. BrDU, prepared at 20mg/ml in an isotonic buffer (typically PBS), was administered via i.p. injection to mice (200mg/kg) 4 hours prior to sacrifice.

2.9.5 Serum enzyme assay

Serum samples were collected by tail bleeding and terminal bleed after autopsy. Blood was allowed to clot and then centrifuged at 10000g for 10 minutes, the

serum was collected and analysed by the Clinical Biochemistry Department at the Royal Victoria Infirmary, Newcastle.

2.10 Imaging

2.10.1 OPT Imaging

Optical projection tomography (OPT) allows the three dimensional imaging of fixed biological specimens typically over 1cm across. It has been generated to fill the gap between confocal microscopy and MRI imaging and is typically used to visualise gene expression patterns in human embryos.

2.10.2 Sample Preparation

One lobe from the liver was perfused with HBSS+ and stored in 10% formalin. The formalin fixed liver samples were embedded in 1% low melting point agarose and left to set overnight. The agarose plug was then dehydrated in increasing concentrations of methanol (10%, 25%, 50%, 75%, 90%, 100%), followed by four final washes with 100% methanol to ensure all water had been removed. The samples were finally cleared in three 1 hour washes of BABB (1:2 v/v Benzyl Alcohol:Benzyl Benzoate) followed by 1 final overnight incubation in BABB.

2.10.3 Sample Scanning

The first sample to be scanned was removed from BABB solution and blotted dry. The bottom of the agarose plug was attached to a small metal stub and placed onto the microscope. The samples were suspended in BABB whilst scanning to reduce light scattering and reduces heterogeneities of refractive index throughout the specimen.

Each sample was rotated 1º and subjected to excitation at wavelengths of 488nm and 543nm. All data were written to a CD and manipulated post scanning to create a 3D image. Figure 2-2 illustrates how OPT works.

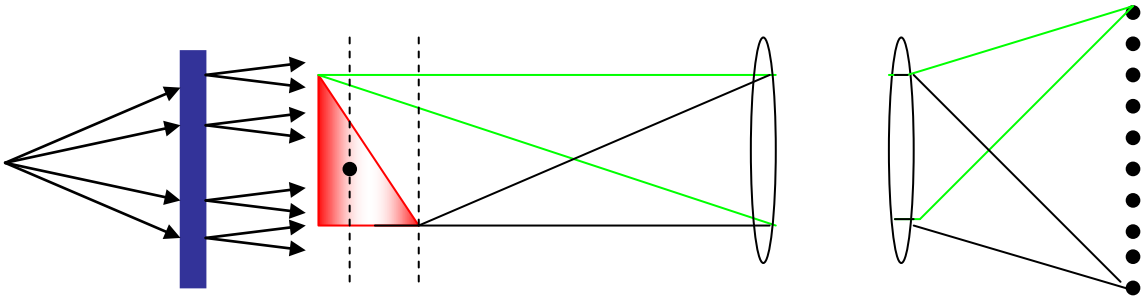

Figure 2-2: Overview of OPT. Light passes through the diffuser (blue) converting it into an even illumination and then through the specimen. The light is focused by the optics onto a CCD imaging chip (row of black dots). The intensity of the light at each position is recorded on the CCD chip which then approximates a projection through the focused part of the specimen.

2.10.4 IVIS Imaging

In vivo imaging system (IVIS) allows the non-invasive visualisation of fluorophores and luminescence present in the body of a rodent. All procedures adhered to the strict guidelines detailed by the Home Office. Animals were anaesthetised with isoflurane/oxygen mix and their stomach, abdomen and lower body regions shaved to prevent the fur blocking the visualisation of the fluorescence. Anaesthesia was maintained during the imaging procedure with up to 5 animals being imaged at any one time.

Typically, a background picture was taken with an automatic, 1 second and 10 second exposure time before any antibody was injected. Once this had been completed animals were either injected intraperitoneally or intraveneously with the C1-3-AF antibody with a specified dose of 8mg/kg and imaged immediately (*i.p.* injection only), 10 minutes, 20 minutes, 30 minutes, 45 minutes, 1 hour and 2 hours following injection at the exposures stated previously. Once imaging studies were complete, all animals were sacrificed and their organs excised and imaged as previously described.

2.11 Immunohistochemistry and Immunocytochemistry

2.11.1 Immunohistochemistry

All tissues were fixed in 10% formalin diluted in 1 x PBS for a minimum of twenty fours hours before processing. Once processed (sequentially through increasing concentrations of ethanol), tissue was mounted in paraffin and 4µm sections were cut and mounted onto super frost plus slides. Sections were de-waxed in xylene for 10 minutes and then re-hydrated through 5 minute incubations in 100%

ethanol followed by 90% ethanol. Tissue sections were then incubated with 0.45% H_2O_2 in methanol for 10 minutes at room temperature to quench endogenous peroxide activity and washed for 5 minutes in 1 x PBS. Antigen retrieval was carried out using either 0.01M citrate buffer (see section 2.11.2) or 10µg/ml proteinase K digestion (see section 2.11.3). Non-specific binding of antibodies was prevented by incubating tissue sections in 20% (v/v) FCS in 1 x PBS for 20 minutes prior to incubation with primary antibody diluted in 0.05% FCS in PBS (for dilutions see table 2-2) for 1 hour at room temperature or at 4°C overnight. Sections were then washed three times for 5 minutes in 1 x PBS and incubated with the appropriate HRP conjugated secondary antibody diluted in 0.05% (v/v) FCS in 1 x PBS (see table 2.11.1) for 1 hour at room temperature followed by three 5 minute washes in 1 x PBS. HRP activity was visualised using diaminobenzidine (DAB) chromogen (Dako) to develop colour essentially as outlined in the manufacturer's instructions. DAB was applied to the slide and incubated for 5 minutes, or as optimised for individual antibodies. In all cases control sections were stained without primary antibody incubation for each individual antibody used. After incubation with DAB slides were washed briefly in water and then counterstained for 30 seconds in haematoxylin and washed in acidified water for 10 seconds. Finally, the slides were sequentially dehydrated through 50%, 75%, 95%, 2x100% ethanol and finally into xylene before mounting in Depex.

2.11.2 Citrate buffer pressure cooker antigen retrieval

Slides were added to 0.01M citrate buffer vigorously boiling in a pressure cooker. When full pressure had been reached, the slides were timed for 1 minute before removing from the heat and rapidly cooled whilst the pressure was released. Slides were washed twice in 1xPBS before continuing with the staining protocol.

2.11.3 Proteinase K antigen retrieval

Tissue sections were digested in 10µg/ml proteinase K diluted in 1 x PBS for 25 minutes at 37°C. Slides were rinsed in 1 x PBS before commencing with immunostaining protocol.

2.11.4 Vector Laboratories ABC method

To increase staining sensitivity, an ABC kit produced by vector laboratories (Peterborough, UK) was used. The kit relies on the high binding affinity that avidin has for biotin, in addition to its four binding sites for biotin. These properties allow macromolecular (avidin:biotin complexes (ABC)) complexes to be formed between avidin and the biotinylated secondary antibody thus amplifying the bound antibody.

Before the ABC complex can be applied, endogenous avidin/biotin activity in the liver tissue was blocked using the avidin/biotin blocking kit (Vector Labs). Briefly, slides were incubated with reagent A for 15 minutes, washed twice in 1 x PBS, and incubated with reagent B for a further 15 minutes. Slides were rinsed with 1 x PBS before continuing the staining protocol. This step was typically carried out prior to the FCS block.

After primary antibody incubation, slides were washed and incubated with a biotinylated secondary antibody, see table 2-2 for dilutions, for 1 hour at room temperature. After two washes in PBS, slides were incubated with RTU Vectastain Elite ABC peroxidase reagent for 30 minutes at room temperature followed by three washes in 1xPBS. HRP activity was visualised, counterstained and mounted as described in 2.11.1.

2.11.5 Picro-sirius red staining

Picro-sirius red stain specifically binds to collagens [242, 243] thus can be used to monitor collagen deposition during fibrosis. Slides were dewaxed and rehydrated, as detailed in 2.11.1, and placed in the picro-sirius red stain (0.036mM in saturated picric acid) for 2 hours at room temperature. Excess stain was removed by 2 washes in acidified H_20 (0.5% v/v acetic acid in deionised H_20), then slides were dehydrated in 2 changes of 100% ethanol, cleared in xylene before mounting in Depex.

Antigen	Dilution	Antigen Retrieval	Comments and Source RT=incubate at room temperature O/N= Overnight incubation
α SMA-FITC	1:1000 IHC 1:200 ICC	Citrate Buffer	Mouse monoclonal (Sigma) directly conjugated to FITC. RT
Synaptophysin	1:5000 IHC	Citrate Buffer	Rabbit polyclonal from Abcam. O/N
BrDU	1:10 IHC	Citrate Buffer	Mouse monoclonal from BD Biosciences, no FCS block required O/N
NIMP	1:200 IHC	Proteinase K	Rat polyclonal from AbD Serotec (Kidlington, UK) Requires ABC staining O/N
C1-3-AF	60µg/ml ICC	N/A	Native staining only RT
IL-6	1:50 IHC	Citrate Buffer	Rabbit polyclonal from Santa Cruz (USA) O/N
Rabbit anti FITC HRP	1:200 IHC	N/A	Rabbit polyclonal from Dako RT
Rabbit Anti Rat IgG Biotinylated	1:200 IHC	N/A	AbD Serotec RT
Goat anti Mouse HRP	1:300 IHC	N/A	Goat polyclonal from Dako RT
Goat anti Rabbit HRP	1:300 IHC	N/A	Goat polyclonal from Dako RT

Table 2-2 Antibody dilutions for IHC and ICC

2.11.6 Immunocytochemistry

For hepatic myofibroblast staining only, cells were seeded on to 22mm^2 square coverslips that had been sterilised with 70% ethanol prior to placement in one well of a 6 well plate.

Plates were removed from incubator, medium aspirated, washed in 1 x PBS and 60µg/ml C1-3-AF added in Hepes/HBSS solution. Cells were left for 2 hours at 37°C/5% CO_2. Following incubation the antibody was removed and cells were washed twice in 1 x PBS. 2ml of fixative (2% v/v formaldehyde/ 0.2% v/v glutaraldehyde in 1 x PBS pH 7.4) was added to each well and cells were incubated for 15 minutes at room temperature. Fixative was removed and cells were washed twice for 5 minutes in 1 x PBS. For myofibroblast staining, non-specific protein binding was blocked by incubation with 2ml 20% (v/v) FCS in 1 x PBS per well for 20 minutes at room temperature whilst being gently rocked. The

blocking solution was then discarded and αSMA-FITC added at the required dilution (as detailed in table 2-2) in 0.05% (v/v) FCS in 1 x PBS. Cells were incubated in αSMA-FITC for 1 hour at room temperature with gentle agitation. Primary antibody was then removed and cells were washed two times for 5 minutes in 1 x PBS. Cell nuclei were stained with 6µg/ml 4',6-diamidino-2-phenylindole (DAPI, a fluorescent stain which strongly binds DNA) in deionised H_2O (2ml per well) and either visualised immediately using confocal microscopy (transfected cells) or mounted on super frost plus slides (myofibroblasts) in vectashield (Vector Labs) anti fade.

2.12 Isolation and Quantification of RNA

2.12.1 Trizol RNA purification

Medium was removed and cells were washed twice in sterile 1 X PBS. For a 6 well plate 1ml of Trizol was added to each well and placed on rotating plate at high speed for 5 minutes to disrupt cells. Trizol was then removed and put into an RNase/DNase free eppendorf. For whole tissue samples, a small portion of the tissue was placed into a RNase/DNase free eppendorf and was homogenised in 1ml of Trizol.

RNA was extracted from sample by the addition of 200µl of chloroform to the Trizol solution and mixed well using a vortex. Samples were centrifuged for 15 minutes at 10000g at 4°C. The upper aqueous layer was removed and placed into a fresh eppendorf, 500µl of cold isopropanol was added and incubated on ice for 10 minutes. Samples were then centrifuged at 10000g for 15 minutes at 4°C. The supernatant was discarded, the pellet dislodged and washed in 70% ethanol before centrifugation at 10000g for 15 minutes at 4°C. The supernatant was discarded and the pellet was allowed dry in air before being re-suspended in sterile pharmacy grade H_2O. RNA was aliqouted and stored at –80°C with freeze thaw being avoided as much as feasibily possible.

2.12.2 Determining RNA integrity and concentration

RNA was quantified at 260nm, and purity determined by the ratio of absorbance at 260nm and 280nm readings. RNA was diluted in 200µl of sterile H_2O and transferred into a quartz cuvette, the absorbance was scanned between 260 and 280nm versus 200µl of H_2O to correct for background. RNA concentration was

then calculated based on 1 x 260nm being equivalent to 25µg RNA/ml. RNA integrity was routinely checked on an agarose gel containing ethidium bromide and viewed under UV light; two distinct bands were visualised, 28S and 18S respectively. Assessment of RNA purity was made by determining the 260/280 ratio which should be 2.0 for pure RNA. Ratios lower than 2.0 may indicate protein or DNA contamination.

2.12.3 DNase treatment of RNA (Promega)

RNA was DNase treated to remove any genomic DNA contamination. RNA was diluted in 50µl of sterile H_2O; 0.1 Volume of RQ1 10x DNase I Reaction Buffer and 0.1 Volume DNase I and was then added to the sample (e.g. If resuspended in 50µl H_2O then add 5µl DNase I Buffer and 5µL (5 Units) DNase I). The sample was mixed gently and incubated at 37°C for 30 minutes, the reaction was stopped by adding 0.1 volume of RQ1 DNase stop solution (5µl). The sample was mixed and then incubated at 65°C for 10 minutes to terminate reaction.

2.12.4 1st strand cDNA synthesis

Moloney murine leukaemia virus (MMLV) reverse transcriptase RNase H minus point mutant is an RNA dependent DNA polymerase used for the synthesis of cDNA. The point -H mutant lacks RNase H activity allowing optimal conditions for the generation of full length cDNA from long RNA templates. MMLV (-H); is thermostable, reducing any problems associated with secondary structure and gives higher yields of cDNA than MMLV. RNA was diluted to a starting concentration of 200ng/µl.

First strand cDNA was produced by adding 400ng RNA (typically 2 µl) to 2 µl water and 1µl of oligo dT (stock concentration of 50 µg/ml). The reaction was heated to 85ºc for 3 minutes to remove secondary RNA structure, followed by rapid cooling on ice and 15 µl of megamix added to each tube (table 2-3).

	µl/tube
5x MMLV buffer (Promega) 250mM Tris-HCl (pH 8.3 at 25°C), 375mM KCl, 15mM $MgCl_2$, 50mM DTT	4
Pharmacy Grade Water	7.5
10mM dNTPs	2
MMLV Reverse Transcriptase RNase H minus (Promega)	1 (50 Units)

Table 2-3 Components of mastermix required for 1st cDNA synthesis

The reaction was incubated for a further 1 hour at 42ºC. Typically 2-5µl of cDNA was used directly for PCR, or frozen and stored at -20°Cfor later use.

2.12.5 PCR

PCR is a very important tool in molecular biology and is used to amplify specific DNA sequences. Phusion high fidelity DNA polymerase uses a novel pyrococcus like enzyme with a processivity-enhancing domain catalysing the polymerisation of nucleotides into duplex DNA in the 5' → 3' direction in the presence of magnesium and has proof reading capability 3' → 5' which permits the removal of base misinsertions resulting in the products generated having fewer errors. 2µl of the first strand cDNA was added to 18µl of megamix containing the following components (Table 2-4):

	µl/tube
5 x Phusion HF Buffer (New England Biolabs)	4
10mM dNTPs	0.4
0.5µM upstream primer stock	2
0.5µM downstream primer stock	2
Pharmacy grade water	9.4
Phusion high fidelity DNA polymerase	0.2 (0.4 Units)

Table 2-4 Mastermix components required for PCR.

The reaction (illustrated in Figure 2-3) was initially heated to 98ºC for 30 seconds, followed by 35 cycles of 98ºC for 10 seconds, annealing temperature for 30 seconds and 72ºC for 30 seconds. After the 35 cycles there was a final elongation step for 10 minutes at 72ºC. The annealing temperature varied according to the primer being used, but was typically 3ºC higher than the lowest primer melting point.

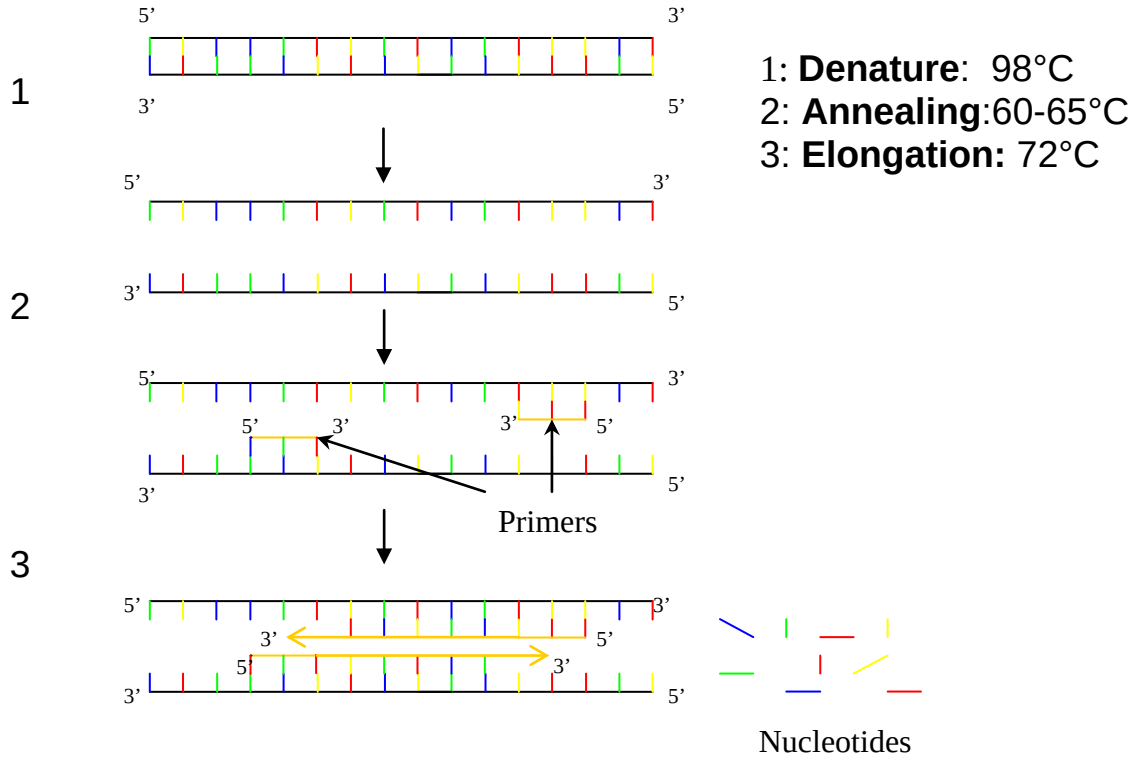

Figure 2-3: Schematic diagram of PCR reaction. The cDNA is initially denatured at 98°Cfor 30 seconds followed by 35 cycles of denature (10 seconds), annealing (30 seconds) and elongation (30 seconds). To complete the reaction, a final elongation step is carried out at 72°Cfor 10 minutes.

The PCR program was optimised for each individual set of primers as detailed in table 2-5.

Primer Name	Sequence	Melting Point	Annealing temperature
Synaptophysin upstream 1	ATGGACGTGGTGAATCAGCTGGT	67.20 ºC	
Synaptophysin downstream 2	GCCCCCATGGAGTAGAGGAA	59.97 ºC	62.9ºC
Synaptophysin downstream 3	CATCTGATTGGAGAAGGAGGTGGG	60.40 ºC	63.4ºC
Synaptophysin downstream 4	GGGTGCATCAAAGTACACTTGG	60.69 ºC	63.6ºC
GAPDH upstream	TGACATCAAGAAGGTGGTGAAG	42.1ºC	
GAPDH downstream 2	TCTTACTCCTTGGAGGCCATGT	44.9ºc	42ºc

Table 2-5 DNA oligonucleotide sequences used in PCR.

2.12.6 Primer Design

Primer pairs were routinely designed to amplify specific DNA sequences of interest. DNA sequences were acquired from the NCBI database (www.ncbi.nlm.nih.gov). BLAST was then used to check the specificity of chosen primer sequences and also to assess the possibility of dimerisation. The following guidelines were generally followed: primers should contain 40-60% G and C and have a length of approx 18-30 bases, the G and C content of each primer should be similar in order to keep the Tm values within the same region and primers pairs were not complementary to one another to avoid the formation of primer dimmers. Tm = 2°C x (A + T) + 4°C x (G + C).

2.12.7 Agarose gel electrophoresis

This technique allows the separation of DNA fragments according to size. Agarose, a polysaccharide extracted from seaweed, is dissolved in a heated buffer which upon cooling forms a solid matrix. If a current is applied using a conducting buffer, DNA loaded onto the gel will migrate according to size and degree of folding. Due to the negative charge of the sugar-phosphate backbone of nucleic acids they migrate towards the positive electrode. The migration process is monitored by using ethidium bromide.

Agarose powder was dissolved in 1x TAE buffer by boiling the solution until all traces of powder were gone. 50x TAE stock consisted of 242g Tris base, 57.1ml acetic acid, 100ml 0.5M EDTA, and water to 1 litre. The percentage of agarose gel used was dependent upon the size of the nucleic fragment that was to be analysed. High percentage gels are used for small fragments and low percentage for large fragments. Ethidium bromide was added to the gel solution to intercalate into the DNA backbone and fluoresce, meaning that the bands can be visualized when viewed under UV light. Once the solution had cooled slightly, it was poured into a casting stand and allowed to set for thirty minutes. The set gel was transferred to an electrophoresis tank and submerged in 1x TAE buffer. 10µl of a 100bp DNA ladder (Promega) was loaded to allow size approximation of DNA bands. 10µl of DNA was added to 2µl of 6x loading dye (Promega) and added to the wells.

The gel was run at 80V for approximately 45 minutes and visualized using a Fluorchem (Alpha Innotech) gel doc system.

2.12.8 Real-time PCR using TaqMan

All cDNA samples were diluted to 10ng/µl, 5µl (50ng) of which was added to each well in a 96 well plate (Applied Biosystems, Warrington, UK) with samples run in duplicate. 8µl of TaqMan mastermix (Applied Biosystems: 6.5µl 2x TaqMan universal mastermix, 0.65µl 20x primer/probe and 0.85µl pharmacy grade sterile water) to each well, with control wells containing mastermix only. All TaqMan primers used are detailed in table 2-6.

Gene Name	Applied Biosystems Assay ID Number	Gene Group
18S	HS99999901_s1	Eukaryotic 18S rRNA
α smooth muscle actin	Mm01546133_m1	Cytoskeletal protein
Synaptophysin	Mm00436850_m1	Membrane traffic regulatory protein
Collagen 1a1	Mm00801666_g1	Extracellular matrix structural protein
Interleukin 6	Mm00446190_m1	Cytokine
Interleukin 1β	Mm00434228_m1	Cytokine
Epidermal growth factor	Mm00438696_m1	Growth factor
Hepatocyte growth factor	Mm01135185_m1	Growth factor
Tumour necrosis factor α	Mm00443258_m1	Cytokine

Transforming growth factor β	Mm03024053_m1	Cytokine
Cyclin D1	Mm00432359_m1	Kinase modulator
Cyclin E1	Mm01266311_m1	Kinase modulator
Cyclin-dependent kinase 2	Mm00443947_m1	Protein kinase
Tissue inhibitor of metalloproteinases 1	Mm00441818_m1	Protease inhibitor

Table 2-6 Summary of TaqMan primers

All primers used for TaqMan were conjugated to the fluorescent dye FAM and analysed using FAM detector settings on an Applied Biosystems 7500 PCR machine. The programme used was as follows:

1. 50°Cfor 2 minutes
2. 95°C for 10 minutes
3. 40 cycles of 95°C for 15 seconds and 60°C for 1 minute

To calculate C_T values, threshold limits were manually adjusted to represent the exponential phase of amplification. Relative quantitation of gene expression relative to an endogenous control 18S, were calculated using the comparative C_T method as described in the Applied Biosystems RT-PCR guide and as validated in [244]. Briefly, the mean and standard deviation (SD) of the C_T values were calculated for each target gene and 18S. The ΔC_T was calculated by subtracting the 18S C_T from the target gene C_T. The SD for the ΔC_T was calculated as follows: $SD= (SD_1^2 + SD_2^2)^{1/2}$ where $SD_{1/2}$ are the SD of 18S and the target gene. The $\Delta\Delta C_T$ was calculated by subtracting the average ΔC_T of the designated control (i.e. olive oil/ sham mice) from the ΔC_T of the remaining values. Fold change, relative to the designated control was calculated using the following equation: fold change = $2^{-\Delta\Delta CT}$ with SD range calculated by SD plus = $(2^{-\Delta\Delta CT-SD})$ – Fold change and SD minus = Fold change - $(2^{-\Delta\Delta CT+SD})$.

2.13 Statistical Analysis

Data between treatment groups were tested for statistical significance using the Student's two tailed *t* Test. Data were considered significant when $p<0.05$ unless otherwise stated. Sample power calculations based on a previous model of myofibroblast depletion [126] suggest that animal group sizes of 6 are sufficient to obtain statistical significance.

Chapter 3. Production of a recombinant single chain antibody fragment, C1-3, and analysis of the expression of its antigen synaptophysin

3.1 Introduction

Single chain antibody fragments (scAbs) are fusion proteins of the variable region of the heavy (V_H) and light (V_L) immunoglobulin chain and are connected by a short linker peptide. They are typically produced by phage display, where an antigen of interest is immobilised on the surface of a well and a phage antibody specific for that sequence remains bound whilst the rest are washed away. Bound antibodies are eluted and are further enriched and purified by numerous rounds of panning [125]. The sequence of the desired phage-antibody can be sub cloned into an expression vector and expressed in bacterial cells, allowing for unlimited production.

C1-3, a scAb with a human constant kappa domain, was generated by the Wright lab in 2005 and shown to specifically target and bind hepatic myofibroblasts *in vitro* [125] via the synaptophysin protein. Furthermore, the group demonstrated that conjugation of the scAb to the toxin tributyl-tin was able to induce apoptosis of cultured hepatic myofibroblasts.

Synaptophysin is a 38kDa transmembrane glycoprotein found on neural and neuroendocrine cells and is associated with neurotransmitter release and control of exocytosis [120]. Cassiman *et al* [124] established that synaptophysin was a unique marker in the liver, with the protein expressed on the surface of quiescent hepatic stellate cells and hepatic myofibroblasts.

The use of scAbs as imaging agents and for delivering therapeutics is continually increasing as their small size allows rapid distribution and excretion throughout the body. In liver disease, research to date has established that the hepatic myofibroblast is the key cell involved in liver fibrosis, with its survival determining fibrosis progression or resolution. The generation of a scAb which specifically targets this cell has the potential to revolutionise the diagnosis and treatment of liver fibrosis, however in order to investigate this large quantities of the scAb need to be produced and the interactions with its receptor analysed.

3.2 Results

3.2.1 C1-3 Production

C1-3 production was induced by the addition of Isopropyl-β-D-thiogalactosidase (IPTG) to proliferating XL-1 blue cells containing the PIMS147 expression vector, as described in the methods chapter. IPTG cannot be metabolised by *E.coli* cells thus the concentration remains constant allowing for maximal production of the scAb. To isolate the scAb, the bacterial cells were lysed via enzymatic and chemical means allowing final purification via the hexahistidine tag by immobilised metal ion chelate affinity chromatography (IMAC).

Non-specifically bound proteins were removed from the column with a 10mM imidazole wash, a compound able to displace the bond between proteins and nickel sepharose. A higher concentration of imidazole was used to elute the C1-3 from the column, with excess imidazole removed by overnight dialysis in PBS. Samples from the osmotic shock solution before and after incubation with the nickel sepharose were routinely run on an SDS-PAGE gel alongside the binding buffer wash and eluted C1-3. Figure 3-1 is an example of a typical SDS page gel, the arrow shows a decrease in the C1-3 in the osmotic shock solution following incubation with the nickel sepharose indicating that all C1-3 was bound to the sepharose in the column. The majority of the bands present in the osmotic shock solution are reduced following incubation with the nickel sepharose. This suggests that these proteins are binding in a non specific manner to the nickel sepharose as they are removed in the binding buffer wash. Furthermore, the binding buffer wash shows that little C1-3 was removed from the column during this stage and was eluted with the higher concentration of imidazole. This can be more clearly seen using Western blot analysis with the antibody Goat anti human Cκ light chain (Sigma) which specifically binds to the C1-3 scAb. Both the western blot and the SDS-PAGE gel reveal two distinct bands which are smaller than the expected weight for the C1-3 and are likely degradation products of the C1-3 protein.

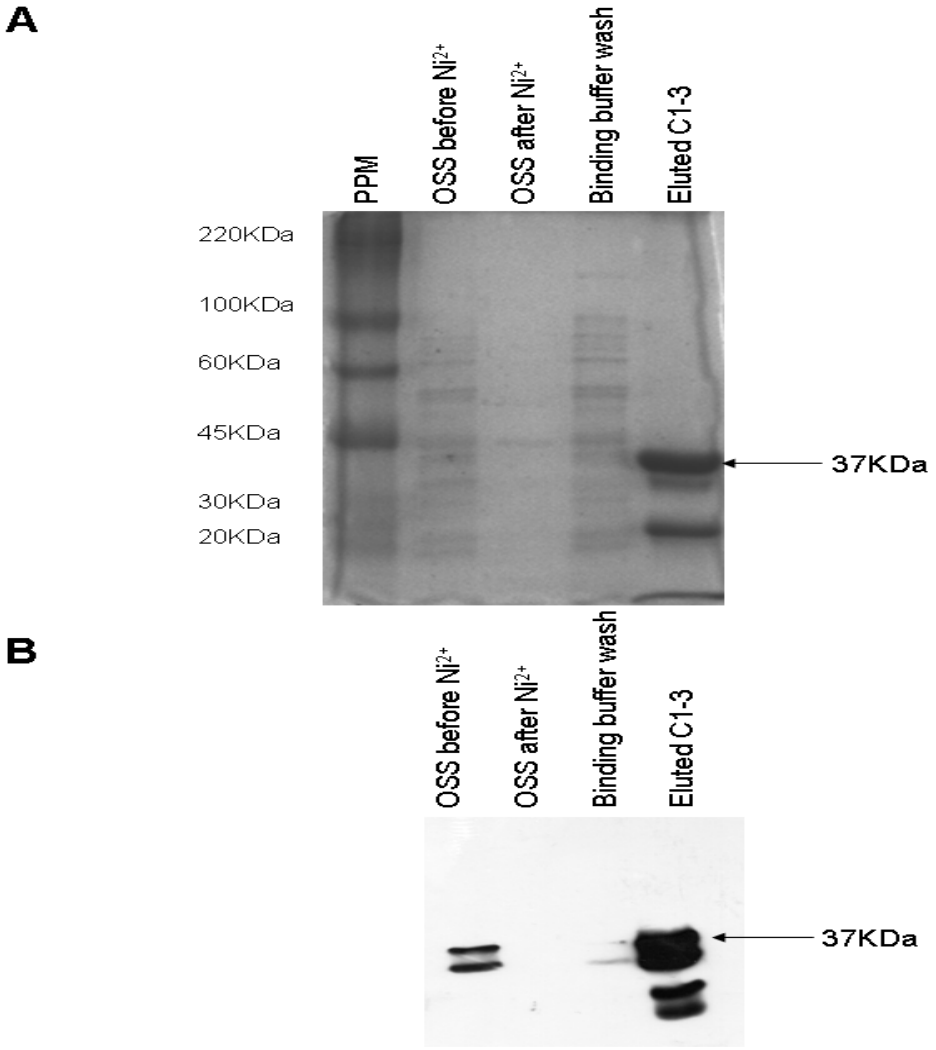

Figure 3-1 SDS-PAGE and WB analysis of osmotic shock solution and eluted C1-3. A: Osmotic shocked solution (OSS) before and after incubation with nickel sepharose, as well as binding buffer wash and eluted C1-3 were diluted 1:5 in reducing loading buffer and denatured at 90°Cfor 5mins. 10µl of each sample was loaded onto a 9% SDS-PAGE gel and separated according to size. To visualise proteins, gels were stained for 1hr with coomassie blue, destined by numerous washes with 10% v/v methanol and acetic acid in deionised H_2O. B: Following electrophoresis proteins were transferred to nitrocellulose membrane, blocked with 3% milk marvel solution and probed with goat anti human Cκ light chain antibody. Results are typical of 5 different C1-3 preparations.

To be able to use the scAb in downstream applications it was important to confirm that it was capable of binding to its target antigen, peptide 2. To do this a binding ELISA was conducted using peptide 1, as a negative control, alongside peptide 2.

Figure 3-2 shows that C1-3 was able to bind to its receptor peptide 2 with little binding to peptide 1.

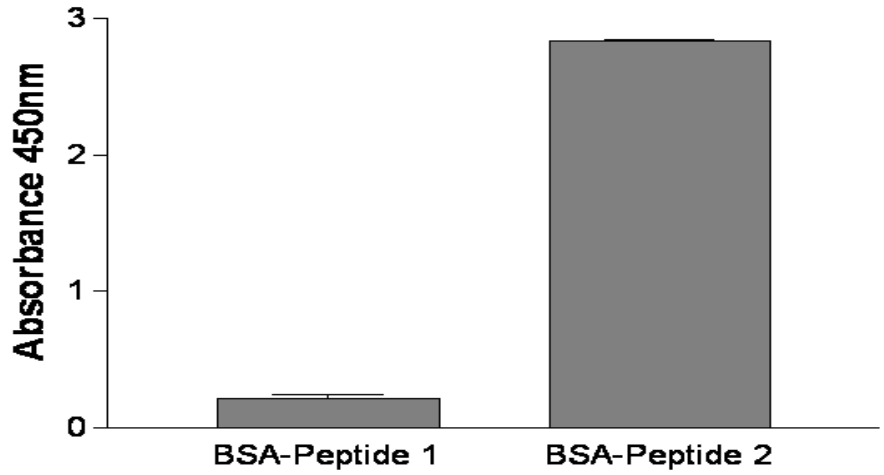

Figure 3-2 Peptide 1 and 2 binding ELISA for C1-3. 96 well plates were coated with BSA-conjugated peptide 1 or peptide 2. ScAb samples of unknown concentrations were initially diluted 1:10 with PBS then serially diluted across the plate. Bound antibody was detected using a secondary HRP conjugated goat-anti human Cκ light chain antibody and quantified by measuring a colorimetric reaction by the addition of TMB and the absorbance at 450nm noted. All experiments were performed in triplicate and the absorbance at dilution 5 (1/160) plotted. Data presented are the mean and SD of three well replicates and are representative of 5 separate C1-3 preparations.

To determine the concentration of the C1-3 antibody, two methods were used. The simplest was running diluted C1-3 on an SDS page gel alongside known concentrations of BSA protein standards however this is subject to user error in the estimation of band size. Figure 3-3 is an example of a typical SDS page gel, it shows that the C1-3 protein sample is of a similar concentration to BSA standard 0.5μg/μl, thus when the 1:1 dilution of C1-3 to loading buffer is taken into consideration this gives the C1-3 a concentration of 1μg/μl.

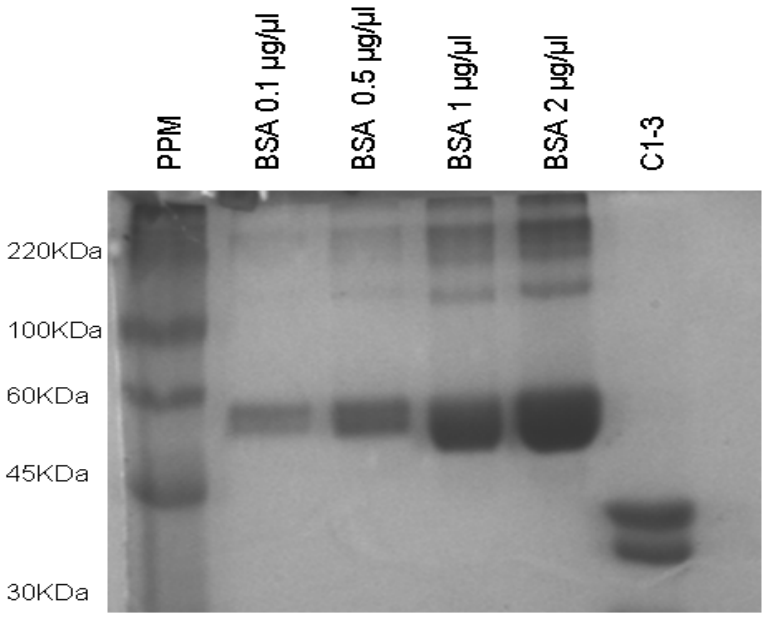

Figure 3-3 SDS-PAGE analysis of C1-3 vs. BSA standards. 20mg/ml BSA was diluted to the following concentrations in reducing loading buffer: 0.01µg/µl, 0.5µg/µl, 1µg/µl and 2µg/µl. C1-3 was diluted 1:1 in reducing loading buffer. All samples were denatured at 90°Cfor 5 minutes prior to loading of 10µl onto a 9% SDS-PAGE gel. To visualise proteins, gels were stained for 1hr with coomassie blue, destined by numerous washes with 10% v/v methanol and acetic acid in deionised H_2O. Data are representative of 5 different C1-3 preparations.

A more accurate method of quantification could be achieved by performing a capture ELISA (Figure 3-4). C1-3, of an unknown concentration, was initially diluted 1/10 and then serially diluted across a plate alongside known concentrations of human IgG. C1-3 concentration was determined from the linear portion of the curve and corrected for dilution factor and for the presence of an extra human kappa light chain domain on the human IgG antibody. The corrected concentration of C1-3 is shown in table 3-1. However this method also has the potential for error as multiple dilutions of C1-3 may have similar absorbency values in the liner portion of the IgG concentration curve leading to different C1-3 concentrations. Ideally both SDS-PAGE and ELISA methods should be used to ensure accurate quantification.

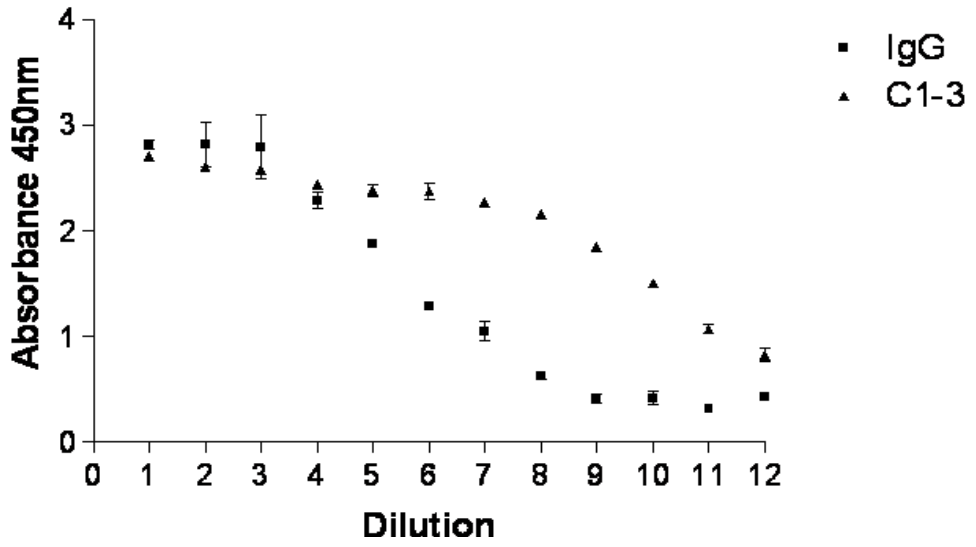

Figure 3-4 Quantification of C1-3 using a capture ELISA. 96 well plates were coated with goat anti human Cκ light chain antibody and blocked with 2% milk marvel solution. C1-3, of an unknown concentration, was initially diluted 1:10 then serially diluted across the plate. IgG with an initial concentration of 1.25mg/ml was serially diluted as previously described. Bound antibody was detected by using a secondary HRP conjugated goat-anti human Cκ light chain antibody and quantified by measuring a colorimetric reaction by the addition of TMB and the absorbance at 450nm noted. All experiments were performed in triplicate and the data plotted are the mean and SD for each dilution. Data are representative of 5 different C1-3 preparations.

Sample	Concentration Determined by Capture ELISA	Corrected for Sample Dilution	Adjusted for IgG
C1-3	19.53ng/ml	0.4mg/ml	0.8mg/ml

Table 3-1 Adjusted concentration of C1-3. C1-3 concentration was determined from the linear portion of the curve and corrected for dilution factor and for the presence of an extra human kappa light chain domain on the human IgG antibody. For example dilution 11 of C1-3 is equal to dilution 7 of IgG with a concentration of 19.53ng/ml. To correct for dilution this number is multiplied by 2^{11} and finally by 10 to account for initial 1:10 dilution. Finally the value is adjusted for the presence of 2 human Cκ light binding domains by multiplying by 2.

3.2.2 Synaptophysin

To investigate whether the synaptophysin protein was expressed by both human and mouse hepatic myofibroblasts, primers were designed to 4 conserved regions of the synaptophysin mRNA sequence forming 1 upstream and 3 downstream primers (Figure 3-5).

```
5' ATGGACGTGGTGAATCAGCTGGT 3' US
   CCAAGTGTACTTTGATGCACCC     DS4
   CTTCCTCTACTCCATGGGGGC      DS2
   CCCACCTCCTTCTCCAATCAGATG   DS3
```

Figure 3-5 Conserved regions in rat/human/mouse synaptophysin sequence. Rat, human and mouse cDNA sequences were aligned and conserved regions identified. US primer contains ATG start codon and the three further sequences identified were reverse complemented for use as downstream primers. DS4 is part of the peptide 2 cDNA sequence and DS3 amplifies the whole transcribed cDNA sequence.

PCR confirmed partial 5' synaptophysin gene expression in myofibroblast samples since the full length of the gene could not be amplified. Full length synaptophysin mRNA was only present in samples from mouse brain and a human neural cell line, SY5Y, which were being used as positive controls since both are known to express the synaptophysin protein [245] (Figure 3-6).

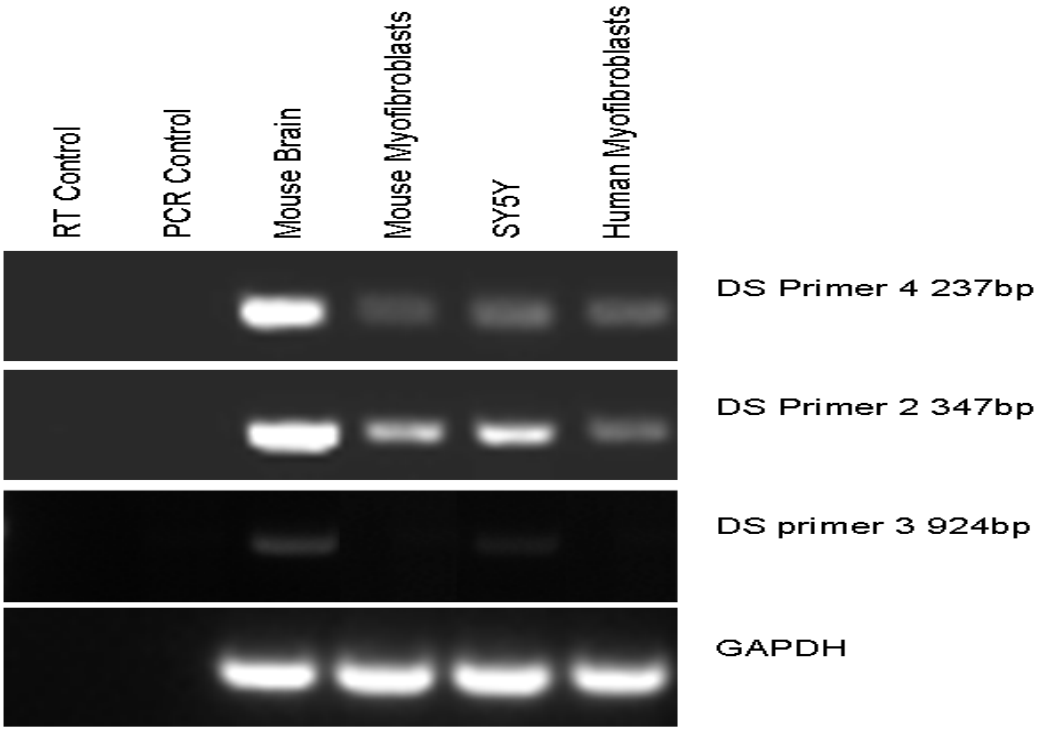

Figure 3-6 Synaptophysin expression in neural and hepatic myofibroblast samples. RNA was isolated from brain, SY5Y cells and hepatic myofibroblast cells using Trizol, quantified and reverse transcribed using oligo dT. 40ng were added to PCR mastermix containing 0.5μM required primers. Samples separated according to size on an agarose gel containing ethidium bromide to allow visualisation of the PCR products. GAPDH is a housekeeping gene and is used to confirm cDNA integrity. Data are representative of 3 technical replicates and of 5 different cell protein samples.

To ensure that the bands amplified were in fact synaptophysin, the PCR products were cloned into the Zero Blunt TOPO vector (Invitrogen) and sent away for sequencing. Table 3-2 shows the results obtained.

	Synaptophysin mRNA Expression		
	SYN1US – SYN4 DS 237bp	SYN1US – SYN2 DS 347bp	SYN1US – SYN3 DS 924bp
Mouse Brain	N/D	100% alignment with synaptophysin sequence	N/D
Mouse Hepatic Myofibroblasts	100% alignment with synaptophysin sequence	96% alignment with synaptophysin sequence	N/D
Human SY5Y	99% alignment with synaptophysin sequence	100% alignment with synaptophysin sequence	99% alignment with synaptophysin sequence
Human Hepatic Myofibroblasts	100% alignment with synaptophysin sequence	100% alignment with synaptophysin sequence	N/D

Table 3-2 Synaptophysin sequencing results. Blunt end PCR products were cloned into Zero Blunt TOPO vector (Invitrogen) as detailed in 2.8.2. Results were inputted into a BLAST search to determine alignment with synaptophysin sequence. N/D= not detected. Data are representative of 3 sequencing attempts.

The table shows that the approximately 1/3 of the synaptophysin sequence could be cloned for mouse brain, human SY5Y and human hepatic myofibroblast samples with only 96% sequence alignment achieved with mouse hepatic myofibroblast samples. This difference could reflect a genuine difference in the synaptophysin sequence or a mutation introduced by the high fidelity DNA polymerase. However, since the full sequence for synaptophysin could not be cloned from either hepatic myofibroblast samples it is unknown whether genuine differences occur. The full synaptophysin sequence could only be cloned from the human SY5Y sample.

Matching protein samples were used to confirm protein expression by Western blot analysis (Figure 3-7).

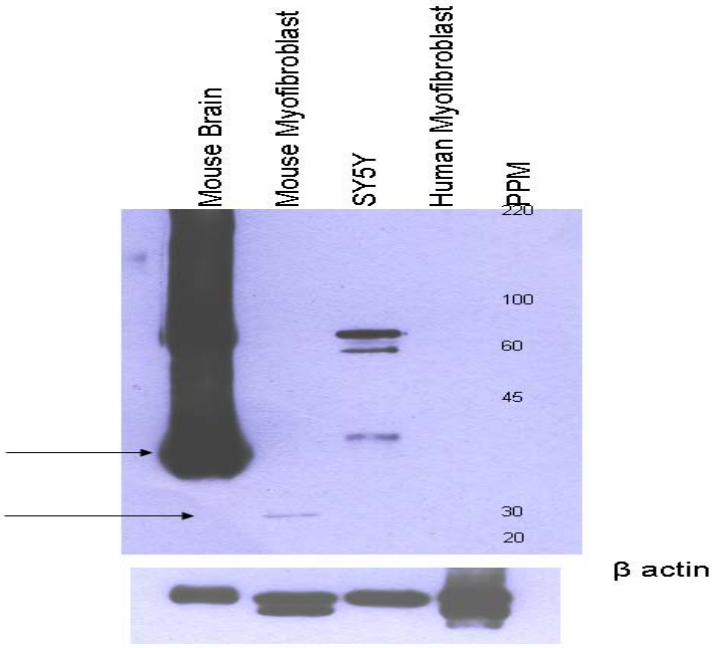

Figure 3-7 Western blot analysis of synaptophysin expression. Protein concentration from whole cell lysates was determined by Lowry analysis and samples diluted to 1.5µg/µl in reducing loading buffer. Samples were denatured by heating to 90°Cfor 5 minutes with 10µl loaded onto a 9% SDS-PAGE gel and separated according to size alongside a prestained protein marker (PPM). Proteins were transferred to nitrocellulose membrane, blocked with 3% milk marvel solution and probed with rabbit anti synaptophysin or mouse anti βactin primary antibodies. βactin is an internal housekeeping gene and serves as a loading control for Western blots. Data are representative of 3 technical repeats and are typical of 5 different cell protein samples.

No synaptophysin protein could be detected in the human hepatic myofibroblast sample and only a slight band at approximately 30KDa was present in the mouse hepatic myofibroblast sample using commercially available antibodies which bind to the C terminal region of the protein. Furthermore, the bands present in mouse brain and human SY5Y samples appear to be different sizes suggesting that synaptophysin may be modified post translation, e.g. glycosylation. The smaller band in the mouse hepatic myofibroblast sample would indicate that the synaptophysin protein has been decreased in size, possibly the result of a splice variant.

To confirm that C1-3 was capable of binding to its target cell *in vitro*, it was conjugated to alexa fluorophore 594 and incubated with hepatic myofibroblasts isolated from healthy mouse and human livers. To confirm myofibroblast phenotype, cells were dual labelled with C1-3-AF in combination with αSMA (figures 3-8 and 3-9).

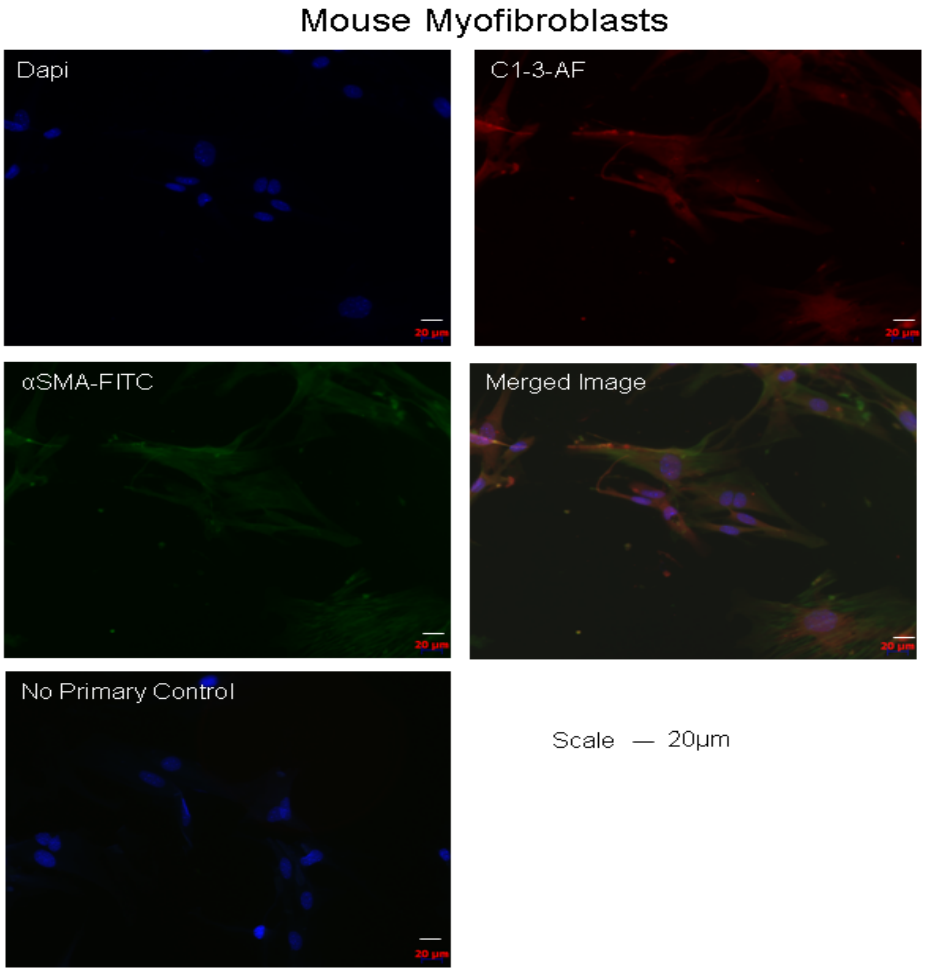

Figure 3-8 Mouse hepatic myofibroblasts incubated with C1-3-AF594 and αSMA Cells were isolated from C75Bl6 murine livers and cultured on tissue culture plastic causing cellular activation into a hepatic myofibroblast phenotype. Myofibroblasts were used for ICC staining between passages 1-4. Briefly, 22mmx22mm coverslips were sterilised with 70% ethanol and placed into a well of a 6 well plate. Cell numbers were determined using a haemocytometer and an equal number of cells seeded per well. Once confluency was reached, cells were incubated with 60µg/ml C1-3-AF for 2hrs in HEPES/HBSS for 2hrs at 37°C. Following this cells were fixed with 2% formaldehyde/0.2% glutaraldehyde in PBS and permeabilised with ice cold methanol. Cells were co-stained with aSMA-FITC. Finally, cell nuclei were stained with DAPI, mounted on slides and visualised using a Zeiss fluorescent microscope. Images taken at x200 magnification. Images are representative of staining from 3 different cell preparations.

Figures 3-8 and 3-9 show representative images of the dual ICC staining and demonstrates co-localisation of the C1-3-AF with hepatic myofibroblasts expressing αSMA.

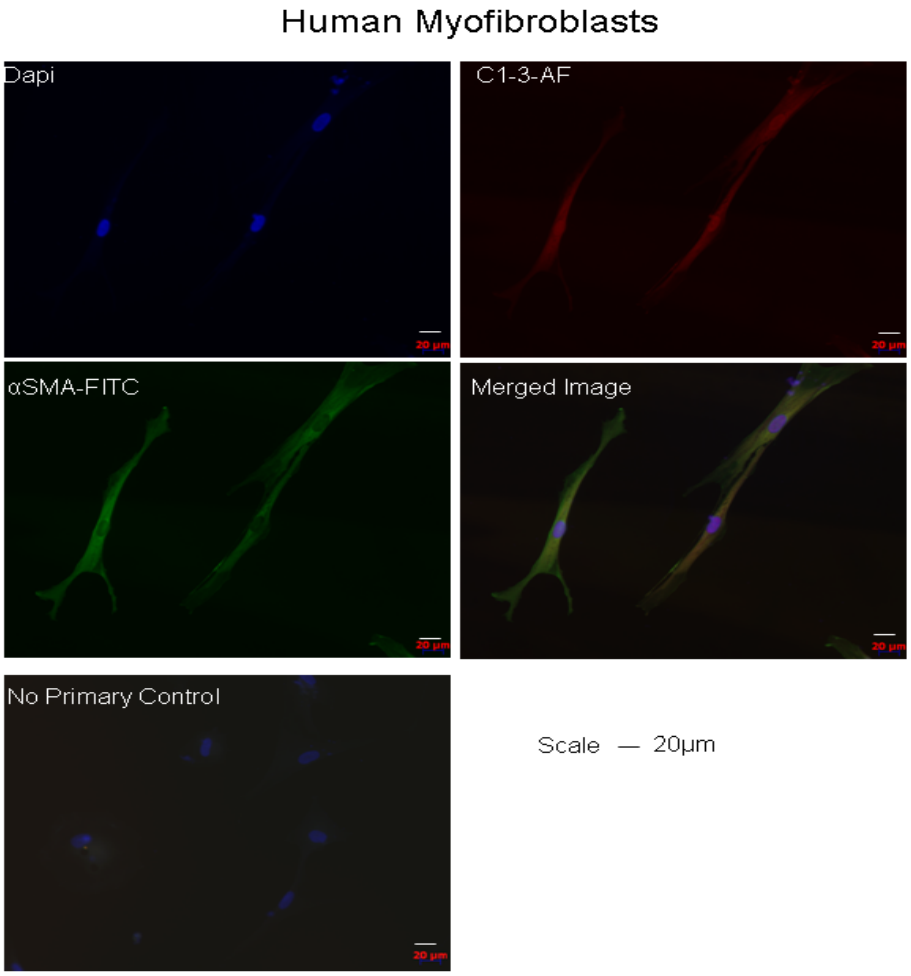

Figure 3-9 Human hepatic myofibroblasts incubated with C1-3-AF594 and αSMA Cells were isolated from human explant livers and cultured on tissue culture plastic causing cellular activation into a hepatic myofibroblast phenotype. Myofibroblasts were used for ICC staining between passages 1-4. Briefly, 22mmx22mm coverslips were sterilised with 70% ethanol and placed into a well of a 6 well plate. Cell numbers were determined using a haemocytometer and an equal number of cells seeded per well. Once confluency was reached, cells were incubated with 60µg/ml C1-3-AF for 2hrs in HEPES/HBSS for 2hrs at 37°C. Following this cells were fixed with 2% formaldehyde/0.2% glutaraldehyde in PBS and permeabilised with ice cold methanol. Cells were co-stained with aSMA-FITC. Finally, cell nuclei were stained with DAPI, mounted on slides and visualised using a Zeiss fluorescent microscope. Images taken at x200 magnification. Images are representative of 2 different cell preparations.

Whilst the images in figures 3-8 and 3-9 illustrate C1-3 binding to hepatic myofibroblasts, it does not confirm that the scAb is specifically binding to synaptophysin. To demonstrate this, cos-7 cells were transfected with plasmid DNA containing mouse and human synaptophysin expression sequences. To determine optimal transfection conditions, cos-7 cells were initially transfected with 2 concentrations of the pEgfp-N1 reporter construct (Figure 3-10A) and the number of green cells counted to determine transfection efficiency (Figure 3-10B). The data showed that 2µg of pEgfp-N1 plasmid DNA provided the highest transfection efficiency and this was confirmed with the mouse and human synaptophysin plasmid DNA (Figure 3-10C). The Western blot probed with a

commercial synaptophysin primary antibody revealed multiple bands at the predicted protein size suggesting that synaptophysin may be modified post translation, e.g. glycosylation.

Following transfection, the binding of C1-3-AF to synaptophysin was investigated. Since previous studies have shown that C1-3 staining works best under native conditions, i.e. no fixation, cells were incubated with either C1-3-AF or a commercially available synaptophysin antibody (chemicon, CCN) conjugated to alexa fluorophore AF594 under both native and fixed conditions. Representative images are shown in figure 3-11.

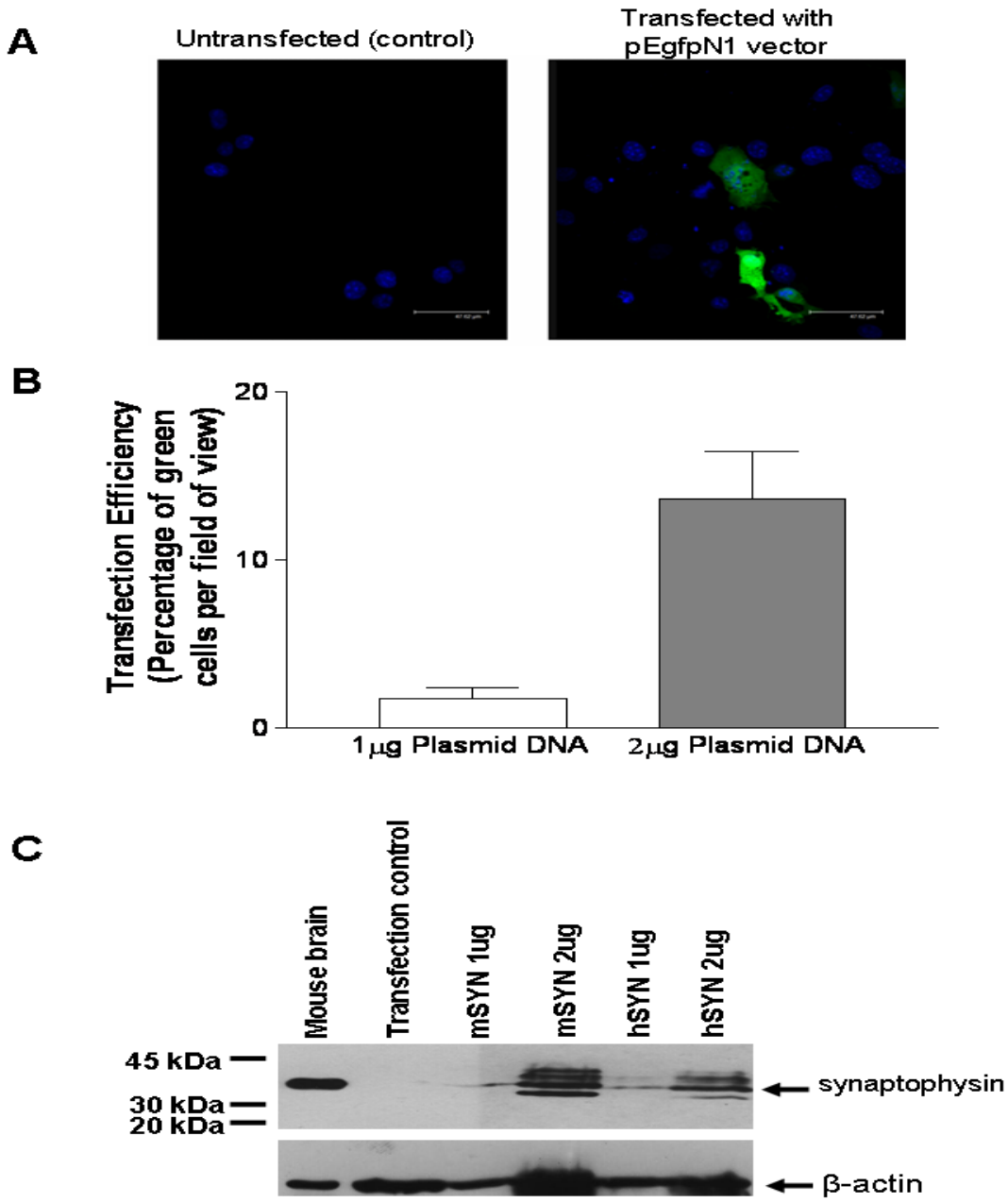

Figure 3-10 Transfection of cos-7 cells with eGFP and synaptophysin. A: Cos-7 cells were equally seeded into 6 well plates and transfected with two different concentrations of pEgfp-N1 plasmid DNA vector. Images are representative of fixed untransfected cells and cells transfected with 2μg of mouse synaptophysin (mSYN) and human synaptophysin (hSYN). Cell nuclei stained with DAPI. Pictures taken at x60 magnification, Scale bar=47.62μm. B: For quantification, the number of eGFP positive cells were counted in 5 random fields of view at x400 magnification and expressed as a percentage of the total cell number per field of view. C: Untransfected and transfected cells were harvested into 100μl of reducing loading buffer, 10μl of which was loaded onto a 9% SDS-PAGE gel. Separated proteins were transferred onto a nitrocellulose membrane, blocked with 3% milk marvel solution and probed with Chemicon rabbit anti synaptophysin primary antibody. Data are representative of 3 individual experimental repeats.

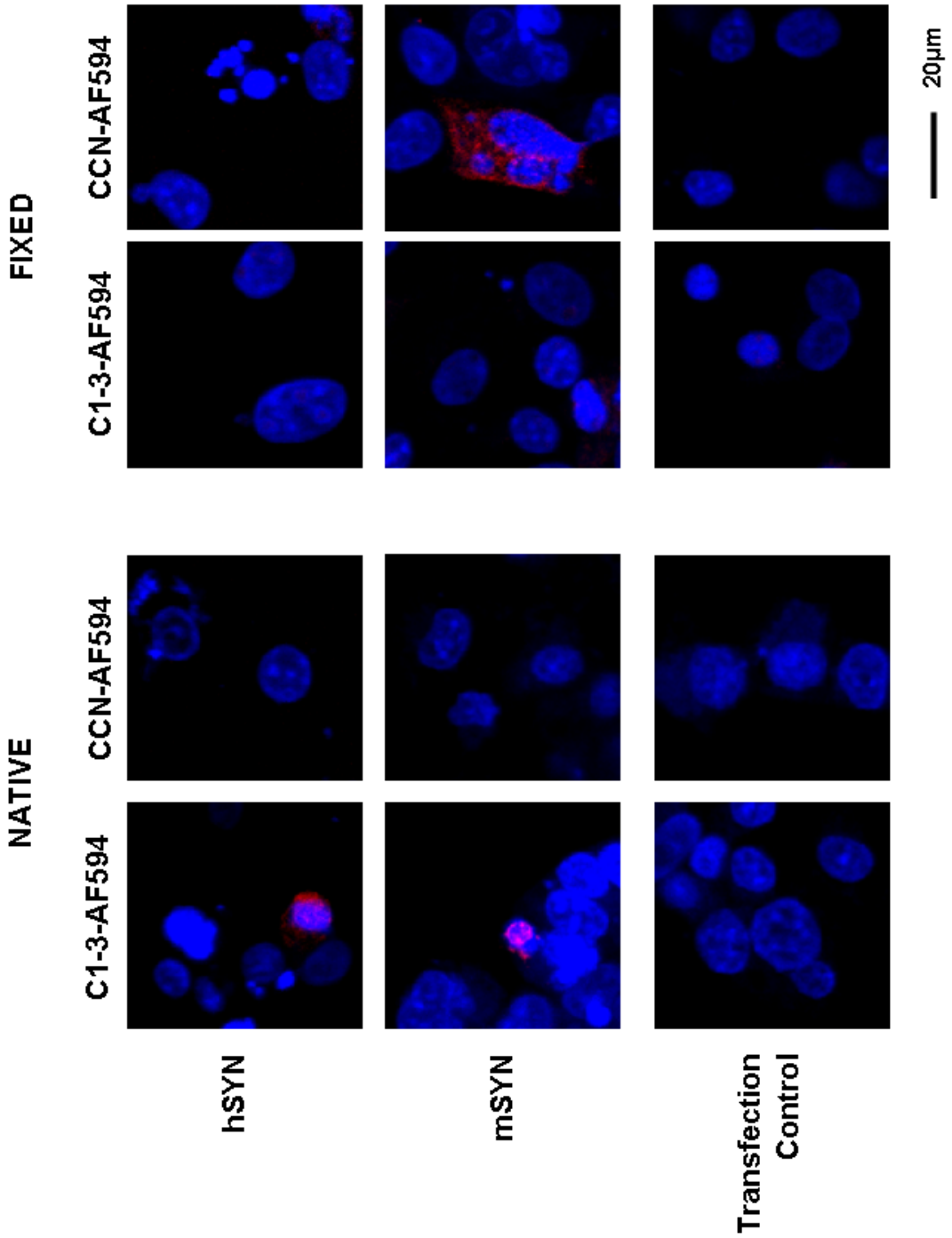

Figure 3-11 C1-3-AF and CCN-AF staining of transfected cos-7 cells under native and fixed conditions. Cos-7 cells were equally seeded into 6 well plates and transfected with 2µg of human and mouse synaptophysin plasmids for 24hrs at 37°C, 5% CO2. Following this cells were incubated with C1-3-AF or CCN-AF in HEPES/HBSS for 2hrs under native conditions before or after fixation. Cell nuclei were stained with DAPI and pictures taken at x60 magnification. Transfection control represents untransfected cells incubated with specified antibodies. Data are representative images of staining observed and are typical of 3 individual experimental repeats. Scale bar=20µm.

The data in figure 3-10 show that C1-3-AF can bind to synaptophysin transfected cells under native conditions only whereas the chemicon synaptophysin antibody (CCN-AF) can only bind after cell fixation and permeabilisation. This is due to the location of the antigen to which the antibody binds, for example peptide 2 is

expressed on the cell surface thus C1-3-AF can bind under native conditions whereas CCN-AF binds to the C terminal region of the synaptophysin protein thus can only bind after permeabilisation. To verify that C1-3-AF is specifically targeting and binding synaptophysin positive cells, peptide 2 could be added to the culture medium as a competitor for the C1-3 binding site and has previously been shown to reduce C1-3 staining in a dose dependent manner [125].

The granular appearance of the C1-3-AF staining under native conditions suggests that the scAb is being actively taken up into the hepatic myofibroblast cell. To determine if this was the case, mouse hepatic myofibroblasts were incubated with increasing concentrations of C1-3 for 3 different time periods. After extensive washing, cells were harvested into reducing loading buffer and analysed by Western blot. Figure 3-12 shows that there is an increasing uptake of C1-3 by the cells with increasing C1-3 concentration. C1-3 incubation for 2hrs compared to 1hr resulted in increased uptake suggesting this was due to active uptake by receptor mediated endocytosis rather than non specific mechanisms. After overnight incubation, C1-3 concentration on the Western blot appears to be lower when directly compared to the 2hr incubation time point suggesting that C1-3 is being broken down by the cells.

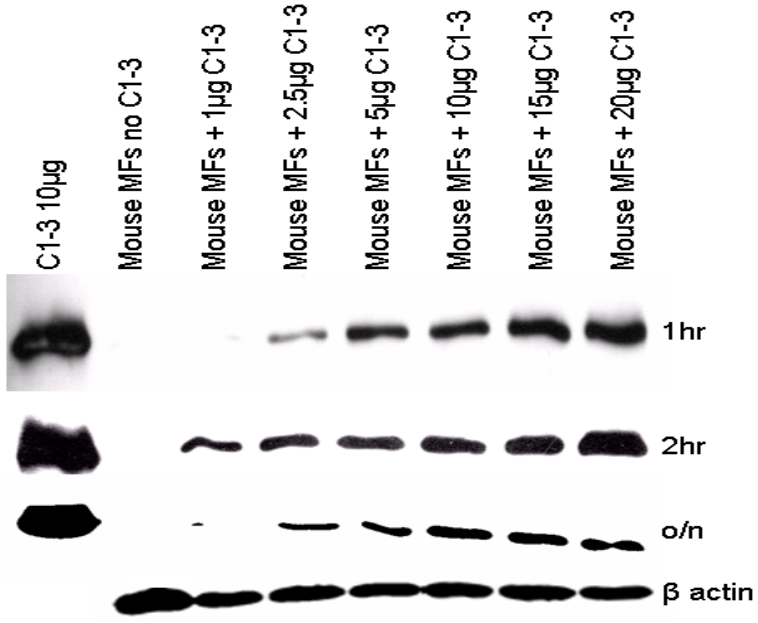

Figure 3-12 C1-3 uptake by mouse hepatic myofibroblasts. Equal number of mouse hepatic myofibroblasts were seeded into 6 well plates and allowed to adhere to the plastic. Specified amounts of C1-3 were added to the cells in HEPES/HBSS and allowed to incubate for the required time. Following this, cells were thoroughly washed in PBS and directly harvested into 100µl reducing loading buffer. 10µl of each sample was loaded onto a 9% SDS-PAGE gel and separated proteins transferred onto nitrocellulose membrane. Membranes were blocked and probed with Goat anti human Cκ light chain. Data are representative of 3 experimental repeats.

The problems associated with the current diagnostic protocols for liver disease have led to a surge in publications proposing novel serum markers which exploit the changes in matrix deposition however to date non are liver specific. Little information is known about synaptophysin expression and function on quiescent HSCs and hepatic myofibroblasts thus a binding ELISA was used to detect the presence of synaptophysin in serum isolated from fibrotic and non fibrotic mice. Figure 3-13 represents the absorbance mean and SD obtained at a serum dilution of 1/160. The data show low absorbance readings for wells probed with C1-3 to detect synaptophysin, with no differences observed between the treatment groups. If synaptophysin was a serum marker of fibrosis, absorbance levels would be expected to significantly increase in comparison to the olive oil controls. Albumin detection in all treatment groups confirmed that the assay was working efficiently.

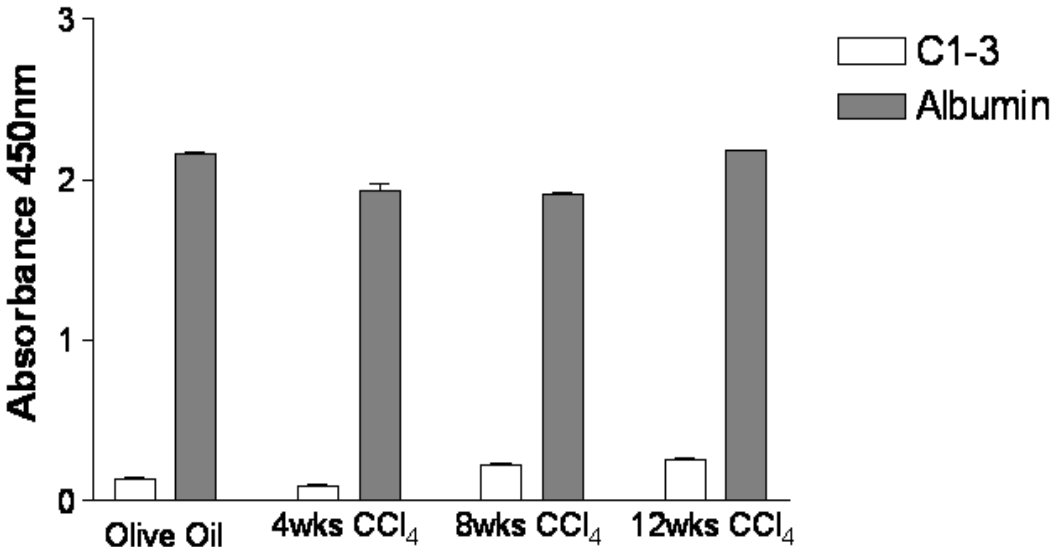

Figure 3-13 C1-3 ELISA to detect synaptophysin in the serum of fibrotic and non fibrotic mice. Whole blood was extracted following schedule 1 termination from olive oil control mice and mice treated for 4, 8 and 12wks with CCl4. Isolated serum was initially diluted 1/10 then serially diluted across a 96well plate. Serum was incubated with either C1-3, to detect synaptophysin, or rat anti albumin, as a positive control since it is the most abundant plasma protein in the blood. All experiments performed in triplicate. Data are the mean and SD of absorbance values obtained at a serum dilution of 1/160 of triplicate samples and are representative of 3 experimental repeats.

3.3 Discussion

Hepatic myofibroblasts have been identified as the pivotal cell type involved in liver fibrogenesis, dictating disease progression or regression. A vast amount of research has been dedicated to investigating the mechanistic actions of hepatic myofibroblasts in an effort to develop targeted therapeutics which act as a 'magic bullet' to slow liver fibrosis progression or even stimulate liver regeneration following chronic injury. Targeted therapeutics have many advantages over untargeted ones, such as reduced chance of adverse side effects and lower levels of therapeutic dose required. However it is essential that the target antigen is tissue/cell specific since presence of the antigen outside of the disease site could have unprecedented consequences.

Single chain recombinant antibodies are currently used in clinical practice to image tumours [246], target drugs [247] and neutralise cytokines in diseases associated with cytokine dysregulation [248]. Advances in recombinant DNA technology have allowed the production of recombinant antibodies where the target antigen can be designed to user specification allowing unlimited potential as clinical therapeutics.

In 2005, Elrick, Leel *et al* published a novel method for targeting hepatic myofibroblasts using a recombinant scAb developed by the group and was termed C1-3. *In vitro* studies showed that C1-3-FITC was capable of specifically binding hepatic myofibroblasts, even when co cultured with other cell types e.g. hepatocytes. Furthermore binding of C1-3-FITC to hepatic myofibroblasts was blocked upon the addition of extracellular synaptophysin to the cell culture medium. The group also demonstrated that C1-3 could be successfully conjugated to apoptosis inducing agents, such as tributyl tin isothiocyanate and gliotoxin, to successfully deplete hepatic myofibroblasts *in vitro* and in *in vivo* models of liver fibrosis [125, 126, 249].

C1-3 specifically binds a region of the synaptophysin protein expressed on the surface of hepatic myofibroblasts, termed peptide 2. Synaptophysin was identified as a novel marker of human and rat hepatic myofibroblasts in 1999 [124], and whilst its function on neural cells involves neurotransmitter exocytosis, its function for quiescent HSCs and hepatic myofibroblasts is unknown. In order to utilise this scAb in further studies, large quantities of the antibody need to be

produced for further conjugation reactions. Typically, 1 litre of bacterial culture yielded 5-8mg of C1-3 and over 150mg was produced over two years. This chapter investigated the production of C1-3 and the binding to its antigen, synaptophysin.

The data in this chapter show that C1-3 could be produced in large quantities with further analysis confirming antigen binding ability and purity. Once produced, its binding to synaptophysin was further investigated.

Primers designed to four conserved regions of the mouse/rat/human synaptophysin cDNA sequences were used to confirm synaptophysin expression in both mouse and human hepatic myofibroblast samples, with neural samples from mouse brain and the human cell line SY5Y being used as positive controls. PCR products were subcloned into a commercial sequencing vector to ensure that the correct product had been amplified. The sequencing results verified synaptophysin mRNA expression in all hepatic myofibroblast and neural samples however the full sequence could only be successfully cloned from the human neural cell line SY5Y. Two thirds of the sequence, which incorporates the peptide 2 binding site, was successfully amplified from all samples using downstream primer 2 (as detailed in table 2-5). To determine if a splice variant of synaptophysin is expressed by hepatic myofibroblasts, a poly T primer could be used in conjunction with the upstream synaptophysin primer. This would amplify the whole synaptophysin sequence and allow for further sequencing analysis.

Matching protein samples were analysed for synaptophysin protein expression by Western blotting. Bands of slightly different sizes were observed in human and mouse neural samples, with the differences possibly reflecting post translational modifications. However a much smaller band was observed in mouse hepatic myofibroblast samples suggesting a splice variant of the synaptophysin sequence exists that may possibly create a functionally distinct protein. Interestingly, no protein expression was detected in human hepatic myofibroblast samples. This result was obtained for two commercially available anti synaptophysin antibodies which bind to the C terminal region of the protein. Future work would involve the optimisation of C1-3 antibody for use in Western blotting as it has been previously shown to detect the peptide 2 synaptophysin sequence [125].

Immunocytochemistry (ICC) confirmed that C1-3 was capable of binding to both mouse and human hepatic myofibroblasts *in vitro* as previously described [125, 249], with hepatic myofibroblast phenotype verified by αSMA staining. Similarly, ICC of synaptophysin transfected cells has shown for the first time that C1-3 actually binds the synaptophysin protein and is internalised, possibly by receptor mediated endocytosis, as demonstrated by the granular staining pattern and Western blotting, However further work is required to elucidate the precise mechanisms involved in C1-3 uptake.

Currently, there are no published scientific studies which have investigated synaptophysin function on quiescent HSCs and hepatic myofibroblasts. With a growing interest in serum markers for diagnosing liver fibrosis, serum samples from fibrotic and non fibrotic mice were analysed by binding ELISA for synaptophysin presence. The studies revealed that synaptophysin could not be detected in serum, confirming that synaptophysin could not be used as a serum marker of liver fibrosis.

Whilst the data in this chapter confirm that C1-3 binds to synaptophysin and that mRNA expression can be detected by PCR, further work needs to be carried out to determine if splice variants of synaptophysin are expressed by hepatic myofibroblasts.

Chapter 4. The use of C1-3 as an imaging agent

4.1 Introduction

Liver disease is a leading cause of morbidity and mortality in the Western world and, with an ever increasing incidence, is placing a huge burden on the health system. Liver fibrosis is the result of the body's wound healing response to injury which can be triggered by numerous aetiologies. It is a carefully balanced 'see-saw', for example if the insult is removed the balance tips in favour of regeneration however if it persists the body tries to encapsulate the injury and the deposition of ECM results in the disruption of normal tissue architecture resulting in organ functional impairment [15].

Due to the huge compensatory ability of the liver, liver disease is typically not detected until the end stages however it can be detected at earlier stages using routine blood tests which detect serum concentrations of amino transferases such as ALT and AST [190]. It is crucial to be able to accurately quantify and stage fibrosis in order to monitor disease progression and the effects of any treatment, especially for viral hepatitis that require constant monitoring to check treatment regimes [250]. Currently, the gold standard for disease staging is using a liver biopsy, however many clinicians avoid this technique due to the small sample size of tissue in comparison to the liver making the result prone to error as well as a risk of bleeding and in rare cases results in death [183, 184, 189]. This problem has led to a surge in publications proposing novel serum markers and new imaging techniques [197], however the majority of serum markers are not organ specific and whilst the imaging techniques hold more promise, a lack of standardisation and normal results have prevented them being more widely used.

This chapter investigates using C1-3 as an imaging agent to quantify and stage liver fibrosis. It is widely accepted that the hepatic myofibroblast is the key cell type involved in liver fibrosis [36] and are characteristically associated with the 'scar-regions' of the liver tissue [251]. Our lab hypothesize that the number of hepatic myofibroblasts present is indicative of the stage of fibrosis, with more hepatic myofibroblasts being present in chronic liver disease.

4.2 Results

C1-3 and CSDB9 (a control scAb which binds to microcystin, was kindly provided by Angela Douglass, Aberdeen University) were conjugated to alexa fluorophore 594 (AF594). Conjugation was confirmed by SDS-PAGE analysis with a distinct increase in molecular weight observed in the C1-3-AF and CSBD9-AF lanes (Figure 4-1).

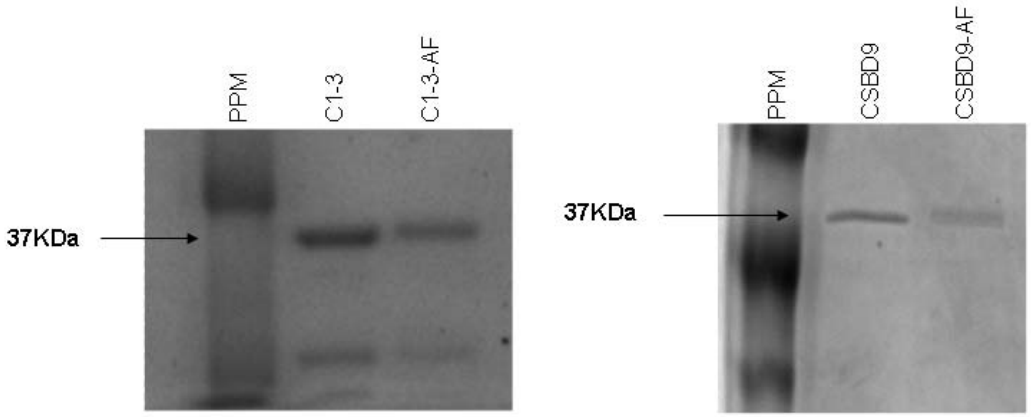

Figure 4-1 SDS-PAGE analysis of C1-3 and CSBD9 before and after conjugation to AF594. Samples of unconjugated and conjugated antibody were diluted 1:1 with reducing loading buffer. Following denaturation, 10µl of each sample was loaded into a well of a 7.5% SDS-PAGE gel alongside a prestained protein marker (PPM) and separated according to size. To visualise the proteins, each gel was stained for 1hr with coomassie blue, destained for 24hr to remove excess stain. Results for C1-3-AF conjugation are typical of 5 separate conjugation reactions. SDS-PAGE analysis is typical of 3 technical and repeats.

Prior to its use *in vivo*, C1-3-AF was checked to ensure it was capable of binding to its antigen using a binding ELISA and incubating it with mouse hepatic myofibroblasts. For the binding ELISA, C1-3 and C1-3-AF were initially diluted 1/10 then serially diluted across a 96 well plate coated with antigens peptide 1 and 2. Figure 4-2A is a typical representation of the data obtained and shows that both C1-3 and C1-3-AF bind to their antigen peptide 2 but not peptide 1.

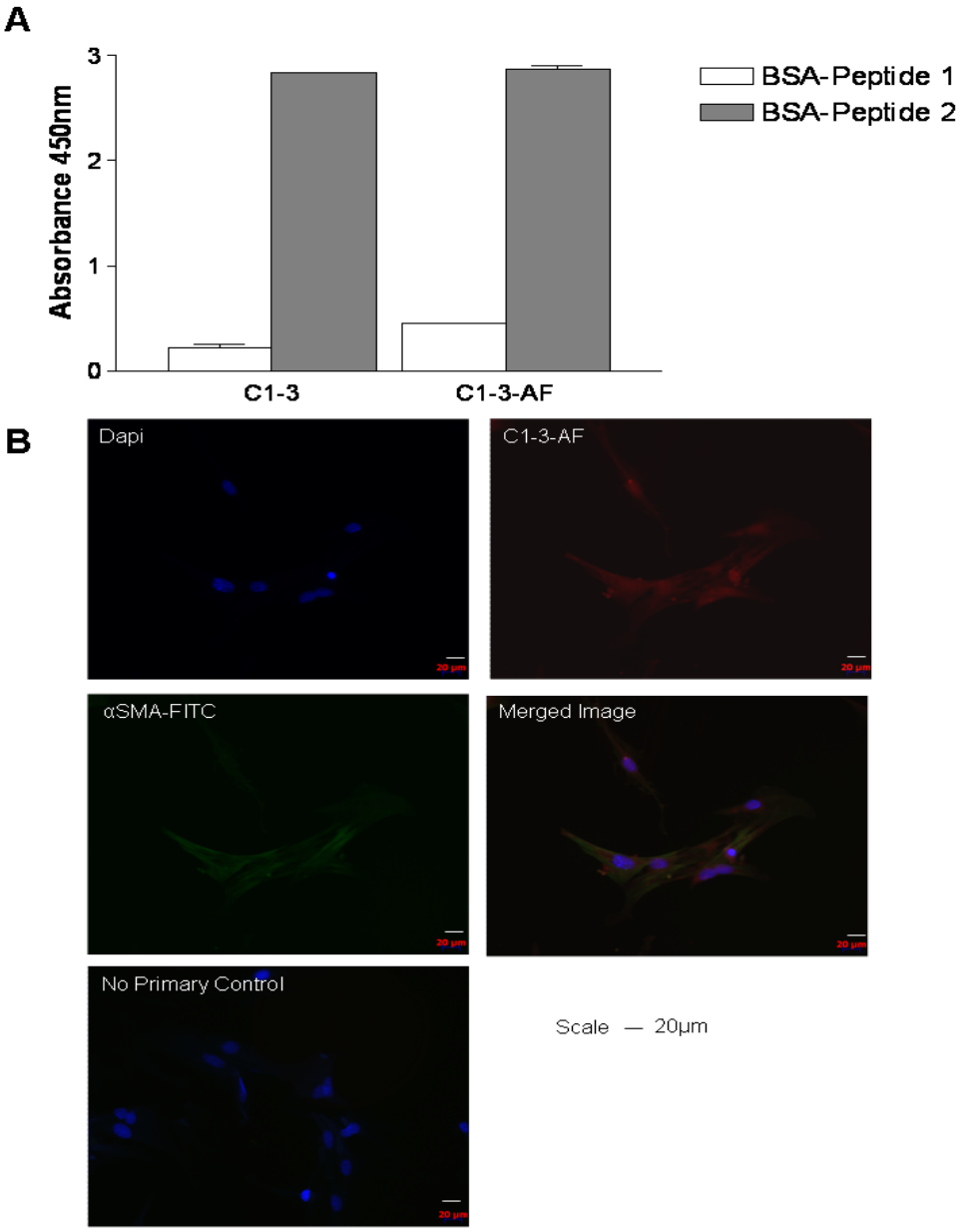

Figure 4-2 Peptide 1 and 2 binding ELISA and ICC of mouse hepatic myofibroblasts to check binding ability of C1-3-AF. A: 96 well plates were coated with BSA-conjugated peptide 1 or peptide 2. Antibody samples of unknown concentrations were initially diluted 1:10 with PBS then serially diluted across the plate. Bound antibody was detected using a secondary HRP conjugated goat-anti human Cκ light chain antibody and quantified by measuring a colorimetric reaction by the addition of TMB and the absorbance at 450nm noted. All experiments were performed in triplicate and the mean and SD of the absorbance at dilution 5 (1/160) plotted. Data are representative of 3 experimental repeats using different preparations of C1-3 and C1-3-AF. B: Following isolation from C75Bl6 mouse livers and subsequent activation on tissue culture plastic, mouse myofibroblasts were used for ICC staining between passages 1-4. Cells were incubated with 60µg/ml C1-3-AF for 2hrs in HEPES/HBSS for 2hrs at 37°C. Following this cells were fixed with 2% formaldehyde/0.2% glutaraldehyde in PBS and permeabilised with ice cold methanol. Cells were co-stained with aSMA-FITC. Finally, cell nuclei were stained with DAPI, mounted on slides and visualised using a Zeiss fluorescent microscope. Images taken at x200 magnification Results are typical of 3 individual experimental repeats.

Previous research by the Wright group has shown that synaptophysin expression increases following activation of a quiescent HSC to a myofibroblast phenotype (unpublished observations). Thus following isolation of mouse hepatic myofibroblasts, cells were cells were dual labelled with C1-3-AF and aSMA-FITC. Figure 4-2B shows that C1-3-AF colocalises with aSMA-FITC where as no staining was observed in the no antibody controls.

To test C1-3-AF as an imaging agent *in vivo,* a CCl_4 model of chronic liver injury was set up dosing C57Bl6 mice twice weekly for seven weeks. 24hr after the final dose on the eighth week, control and CCl_4 mice were either injected with C1-3-AF, CSBD9-AF (scab control) or PBS (vehicle control) and sacrificed 3hrs later (see Figure 4-3).

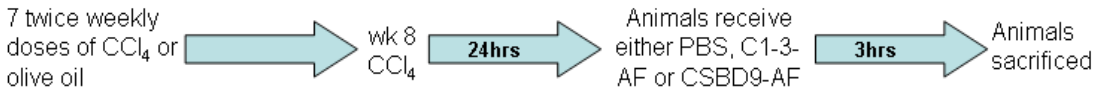

Figure 4-3 Overview of OPT imaging study. Animals received twice weekly injections of CCl_4 or olive oil for 8 weeks. 24hrs after the final dose the CCl_4 and olive oil mice were further subdivided into 3 groups to receive either PBS, C1-3-AF or CSBD9-AF via i.p. injection. 3hrs after dosing all animals were schedule 1 killed and the livers removed along with a blood sample for serum analysis. Each liver was split into 3 samples and either perfused for OPT analysis, fixed in formalin or snap frozen in liquid nitrogen. Each treatment group is representative of 3 animals.

To ensure that CCl_4 treatment had resulted in liver damage, whole blood was removed following schedule 1 termination and serum sent for ALP and ALT analysis. ALT, an enzyme associated with hepatocytes, is released into the circulation following hepatocyte cell death. ALP is an enzyme of hepatobiliary origin and is induced during cholestasis due to impaired bile flow.

Figure 4-4 shows the mean and SD for ALT serum concentrations for each treatment group. Since CCl_4 treatment does not tend to cause cholestasis [81], ALP levels were below the threshold limit which could be accurately detected. ALT levels were significantly higher in CCl_4 treated mice than the control treatment group.

A small portion of each liver (typically $1cm^3$) was perfused with an isotonic buffer and prepared for OPT analysis. OPT is typically used for investigating gene expression in embryos however it is able to show antibody distribution within a tissue. Each piece of liver tissue was subjected to both 488nm and 543nm wavelengths whilst being slowly rotated and images captured. Exposure to 488nm was essential to determine tissue morphology as the liver is very autofluorescent in this spectrum

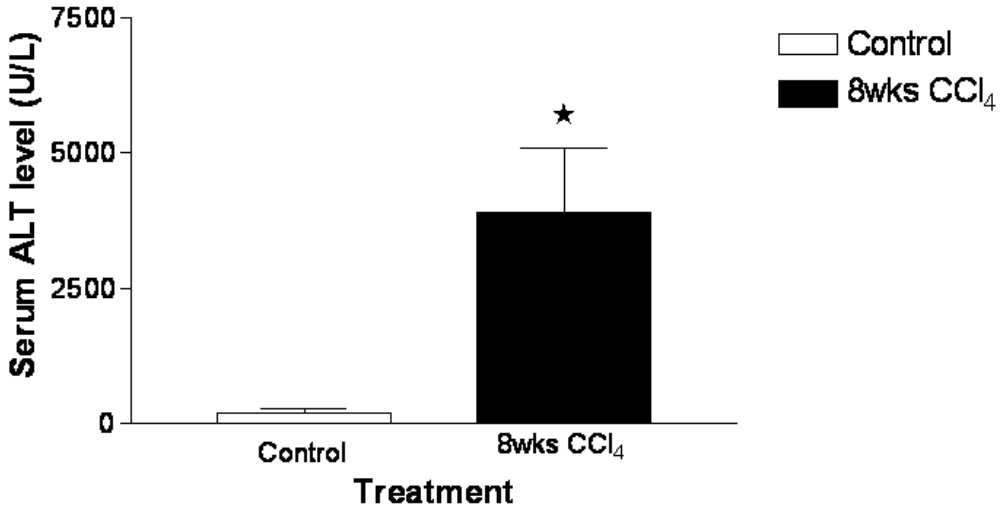

Figure 4-4 Serum concentration of ALT in control and CCl_4 treated mice. Mice were schedule 1 killed and whole blood was removed and allowed to clot at room temperature for 1hr. Serum was removed following centrifugation and diluted in 0.9% (w/v) sodium chloride. All serum samples were analysed by Newcastle Clinical Biochemistry Department. Data are the mean and SD for each treatment group (n=9) and were tested for statistical significance using the Student's two tailed t test. Serum ALT levels in 8wk CCl4 animals were significantly higher than the control treatment group ($p<0.05$).

.

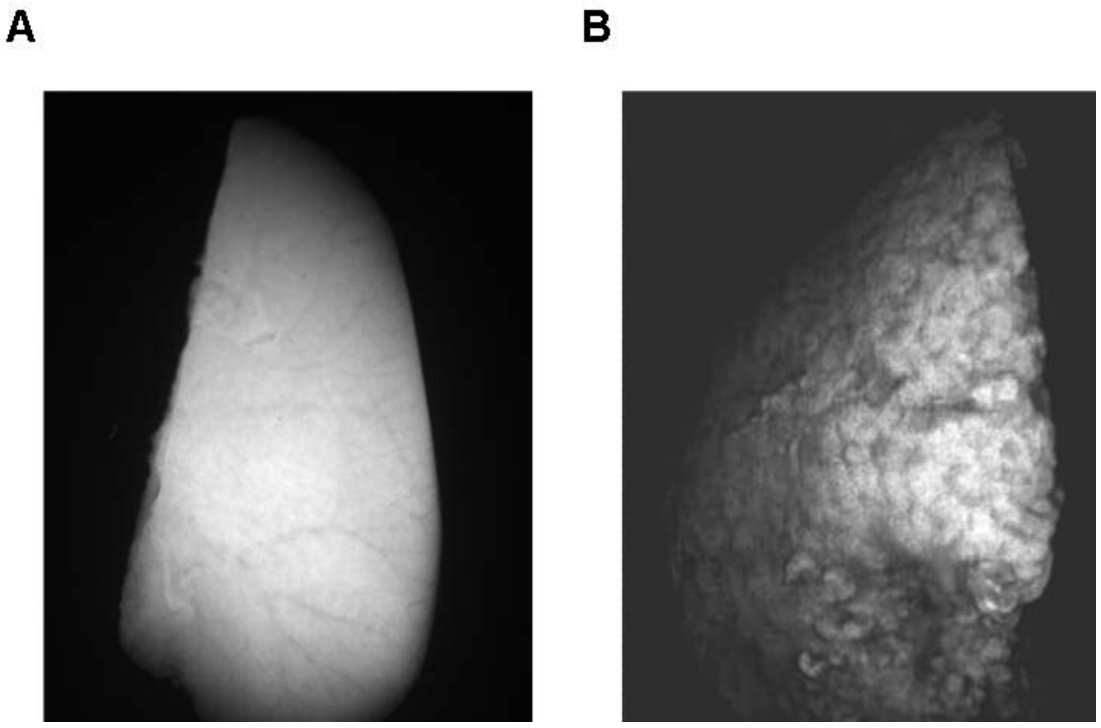

Figure 4-5 Images of control and CCl_4 liver scanned with 488nm wavelength using OPT setup. Perfused liver samples were fixed in formalin for 48hrs and embedded in low melting point agarose. The agarose plug was dehydrated in increasing concentrations of methanol and cleared in BABB (1:2 v/v Benzyl Alcohol:Benzyl Benzoate). For OPT analysis, each agarose plug was glued to a metal holder and placed onto the microscope. The sample was suspended in BABB and an image captured at every 1° rotation using the specified 488nm wavelength. A: Image from a control liver from a PBS injected animal B: Images from a fibrotic liver from a PBS injected animal.

Figure 4-5 is a snapshot of the liver tissue scanned from a PBS olive oil control mouse and a CCl_4 treated mouse. The differences in tissue architecture are quite dramatic, blood vessels which can be clearly seen in the olive oil controls (Figure 4-5A) are lost in the CCl_4 treated mice (Figure 4-5B) due to the deposition of extracellular matrix.

To visualise distribution of the labelled antibodies, the tissue was also subjected to a wavelength scan at 543nm. Figure 4-6 shows representative images from XYZ planes of olive oil control injected with C1-3-AF and CCl_4 animals injected with PBS, C1-3-AF and CSBD9-AF.

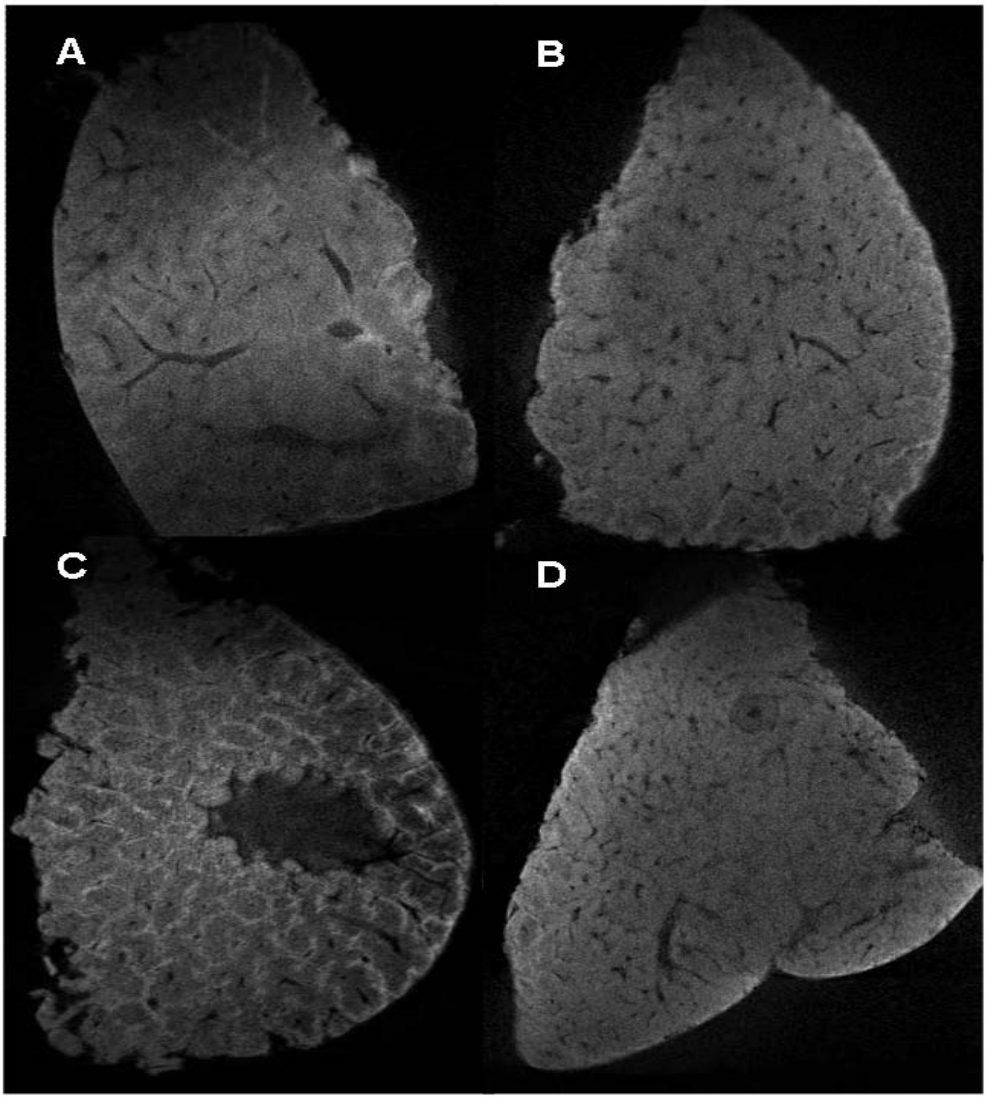

Figure 4-6 OPT images from XYZ planes of olive oil control injected with C1-3-AF and CCl_4 animals injected with PBS, C1-3-AF and CSBD9-AF (A-D respectively). Samples were scanned, as previously described, using both 488nm and 543nm wavelengths to visualise tissue structure and bound antibody. Images from each 1° rotation were manipulated post scanning to generate a 3D model of the tissue sample allowing images to be taken throughout the XYZ planes. All images are grey scales with bound antibody represented by the lighter pixels. Images are representative of data obtained per treatment group (n=3).

All images are grey scale with lighter pixels representing bound antibody, however it is important to note that the technique results in 'noise' around the edge of the tissue and should not be mistaken for bound antibody. Figure 4-6A and C show bound antibody in non fibrotic and fibrotic tissue respectively. Whilst a small amount of bound C1-3-AF can be visualised in the non fibrotic tissue, there is a large increase in pixel intensity in the fibrotic tissue which seems to be in the 'scar-associated' regions. There are no lighter pixels in the scar regions in the liver samples from CCl_4 mice injected with PBS or CSBD9-AF (Figure 4-6 B&D) confirming that there is no bound antibody

To emphasize bound C1-3-AF antibody, images could be manipulated post scanning to colour pixels above a certain threshold (Figure 4-7) allowing the distribution of hepatic myofibroblasts to be easily visualised within the tissue.

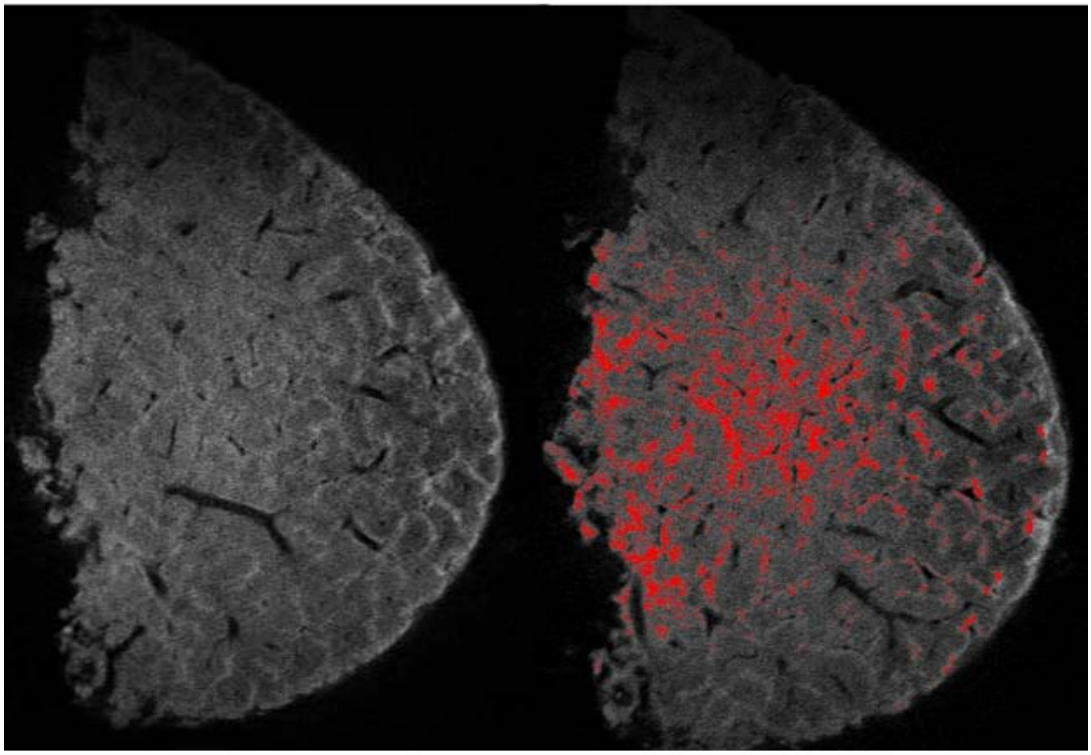

Figure 4-7 OPT images manipulated to emphasise positive staining. All images generated by the OPT software are grey scale with bound antibody represented by lighter pixels. The OPT software designed by Edinburgh University allows the user to measure individual pixel intensity and set a threshold level meaning anything above that intensity represents bound antibody and is coloured red. Following analysis the images could be edited to remove 'noise' generated by light scattering around the edge of the tissue so it was not mistaken as bound antibody. The data shown are typical before and after images following pixel manipulation.

Whilst the data provide proof of concept that a recombinant antibody can be used to visualise fibrosis, a major limitation with OPT is sample size. Specimens over $1cm^3$ in size have poor resolution therefore this technique could not be used for whole liver samples. Furthermore, due to the 'noise' the amount of bound antibody cannot be accurately quantified thus the technique cannot be used to stage and grade fibrosis.

Recent advances in scientific equipment have led to the development of an in vivo imaging system (IVIS) capable of live animal imaging. To ensure that C1-3-AF was suitable for this system a mouse and its organs were scanned at all pre-set wavelengths to look at tissue autofluorescence (figure 4-8).

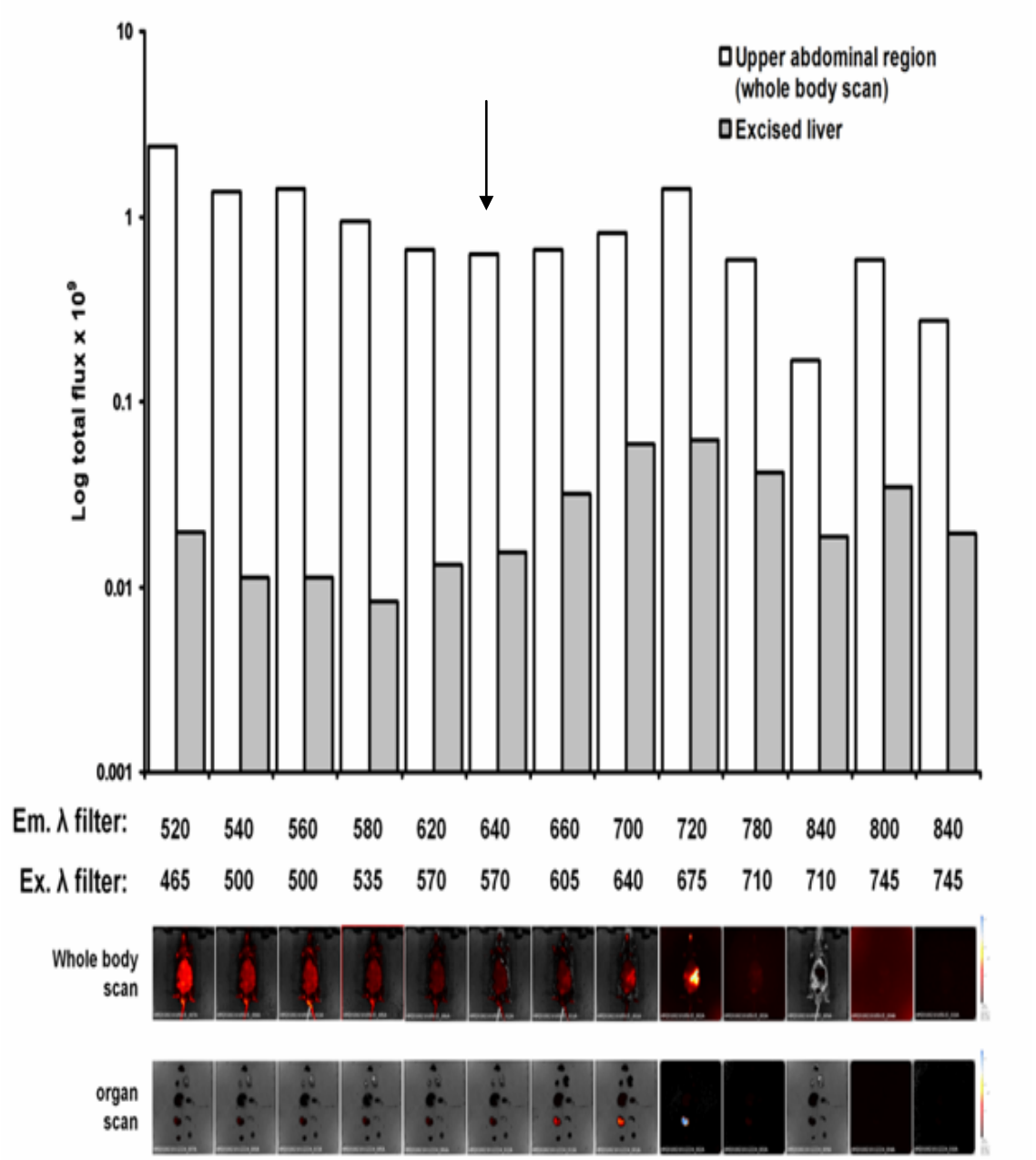

Figure 4-8 Autofluorescence scan of whole body and organs. A C57Bl6 mouse was anaesthetised and scanned at all pre-set wavelengths available on the IVIS/Living Image system. Following this the mouse was schedule 1 killed and its organs (brain, heart, lung, liver, kidney, spleen, stomach & pancreas) removed and imaged as before. All data generated using set exposure time of 1 second. Regions of interest were drawn around the upper abdominal area and excised liver and the total flux measured. The arrow on the bar chart represents the total flux for AF594 excitation/emission filter wavelengths.

The arrow on the bar chart illustrates the autofluorescence of the whole body and liver tissue expected for AF594 in comparison to all other wavelengths pre-set on the machine. Whilst the longer wavelengths have reduced autofluorescence in the whole body scans there is an increase in the autofluorescence of the excised liver tissue. Thus the chosen fluorophore, AF594, should be suitable for animal imaging.

An animal study was set up to determine if IVIS, in combination with C1-3-AF, could be utilised to quantify different stages of fibrosis of the whole liver tissue. C57Bl6 mice were dosed for either 4, 8 or 12 weeks with CCl_4 to induce different grades of liver injury whilst controls received olive oil (Figure 4-9).

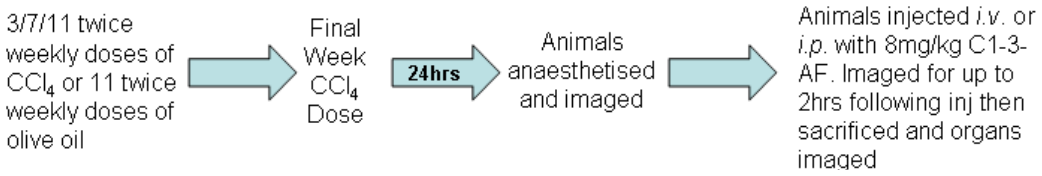

Figure 4-9 Overview of imaging animal study. Animals were subjected to twice weekly doses of CCl_4 to induce centrilobular liver fibrosis for either three, seven or eleven weeks. Dosing was staggered so that all mice received their final dose of CCl_4 during the same week. 24hrs following the final dose animals were anaesthetised and a background fluorescence scan taken at the appropriate wavelength. Mice were injected via i.v. or i.p. injection and imaged immediately after (i.p. only), 10min, 20min, 30min, 45min, 60min and 120min (i.p. only) following injection. After the final image, mice were schedule 1 killed and organs (brain, heart, lung, liver, kidney, spleen, stomach & pancreas) removed and imaged as before. Auto, 1 second and 10 second exposure setting were used at each time point.

Figure 4-10 to 4-13 are the images for each of the treatment groups over the 1hr time course and were generated using a manually set 10 second exposure time. Both whole body scans and organ scan were deemed necessary to determine if the total flux value *in vivo* was representative of organ flux since tissues have different absorption properties and autofluorescence.

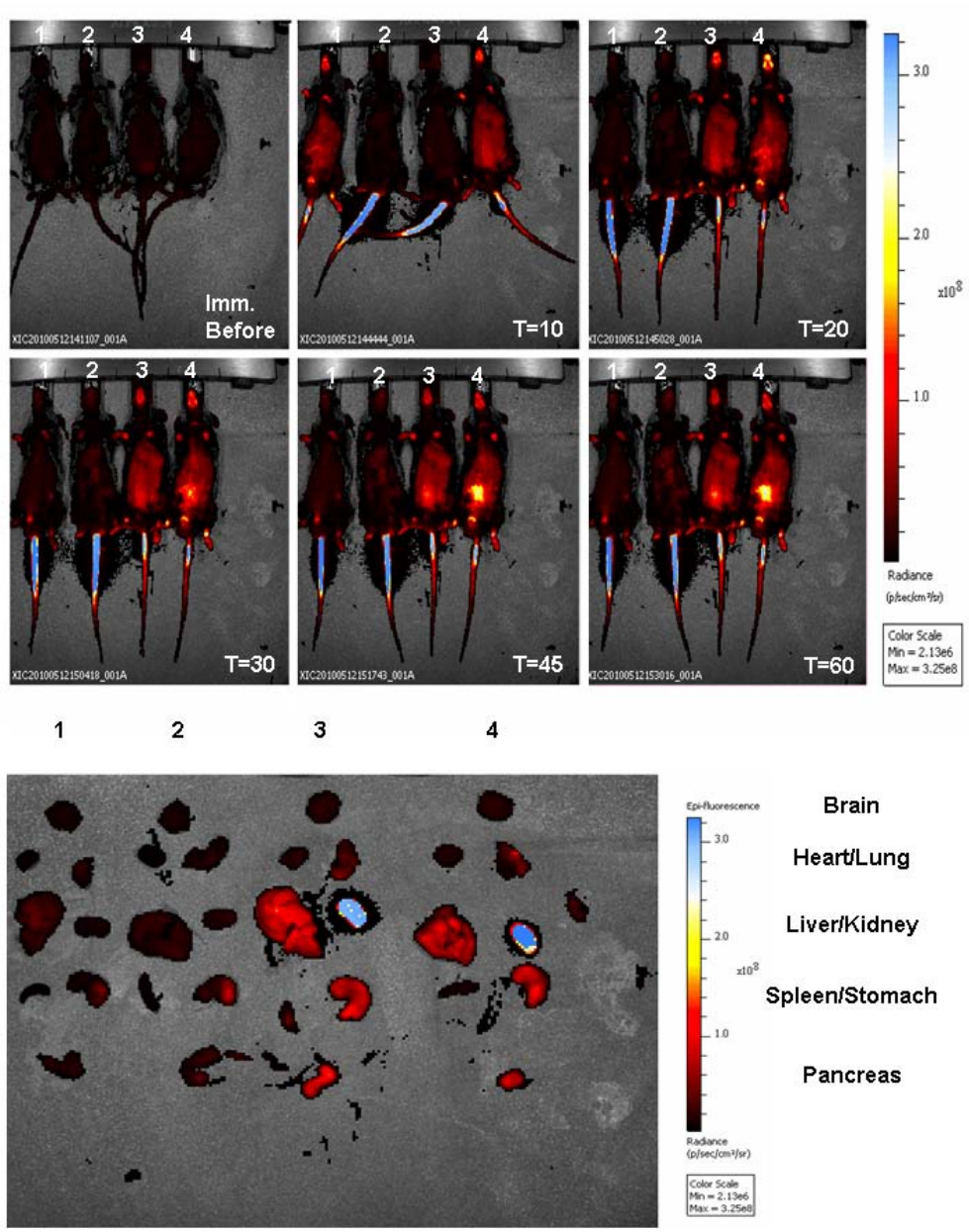

Figure 4-10 Whole body and organ scan from control mice which have received C1-3-AF via *i.v.* injection. Images generated with a 10 second exposure since both auto and 1 second setting revealed little fluorescence. All images (both body and organ scan) were manipulated post scanning to be on the same radiance scale so data can be directly compared. All 4 mice (labelled 1-4 in the live scans and with respective organs) were injected with 8mg/kg or C1-3-AF and the antibody distribution monitored over time.

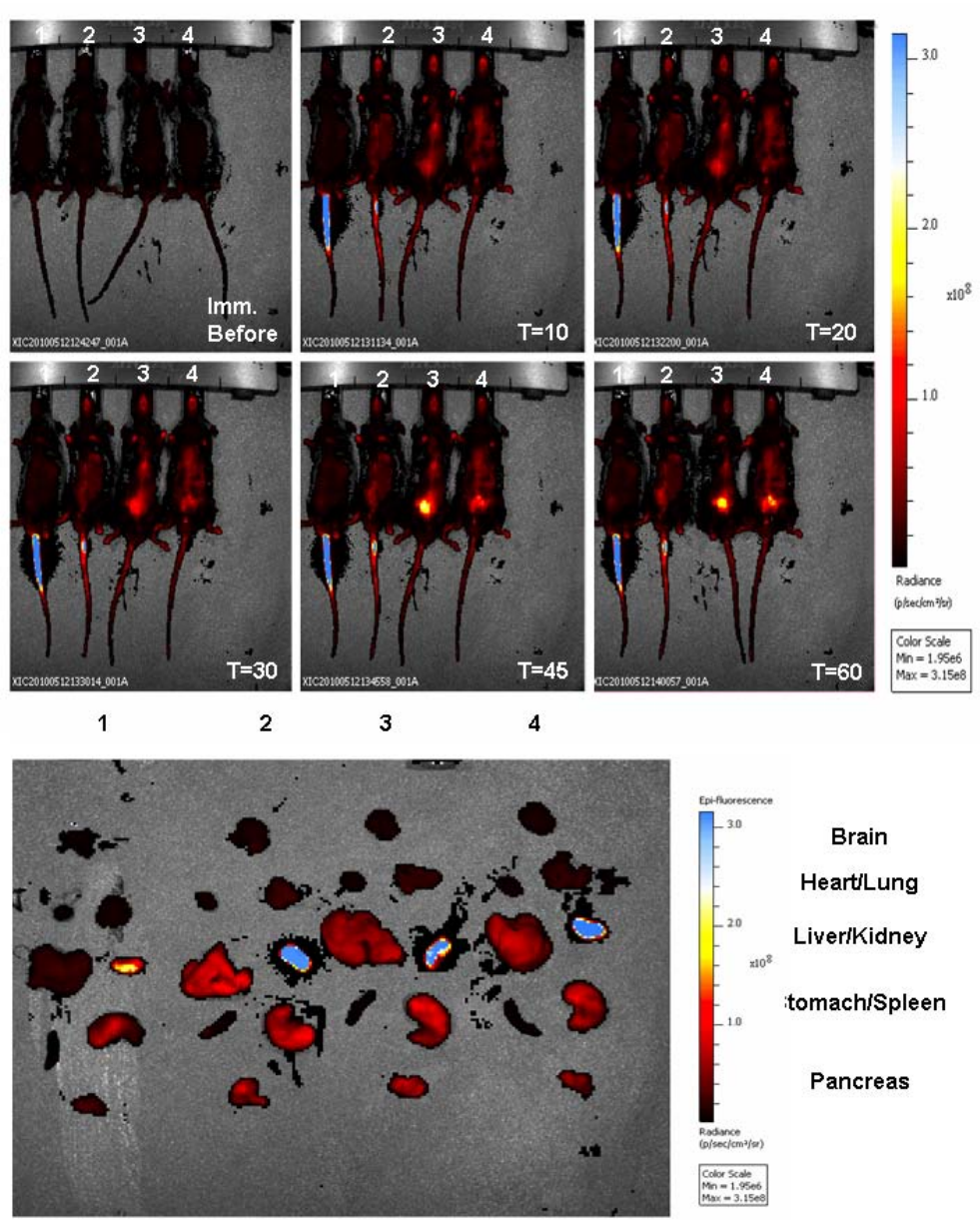

Figure 4-11 Whole body and organ scan from 4wk CCl_4 mice which have received C1-3-AF via *i.v.* injection. Images generated with a 10 second exposure since both auto and 1 second setting revealed little fluorescence. All images (both body and organ scan) were manipulated post scanning to be on the same radiance scale so data can be directly compared. All 4 mice (labelled 1-4 in the live scans and with respective organs) were injected with 8mg/kg or C1-3-AF and the antibody distribution monitored over time.

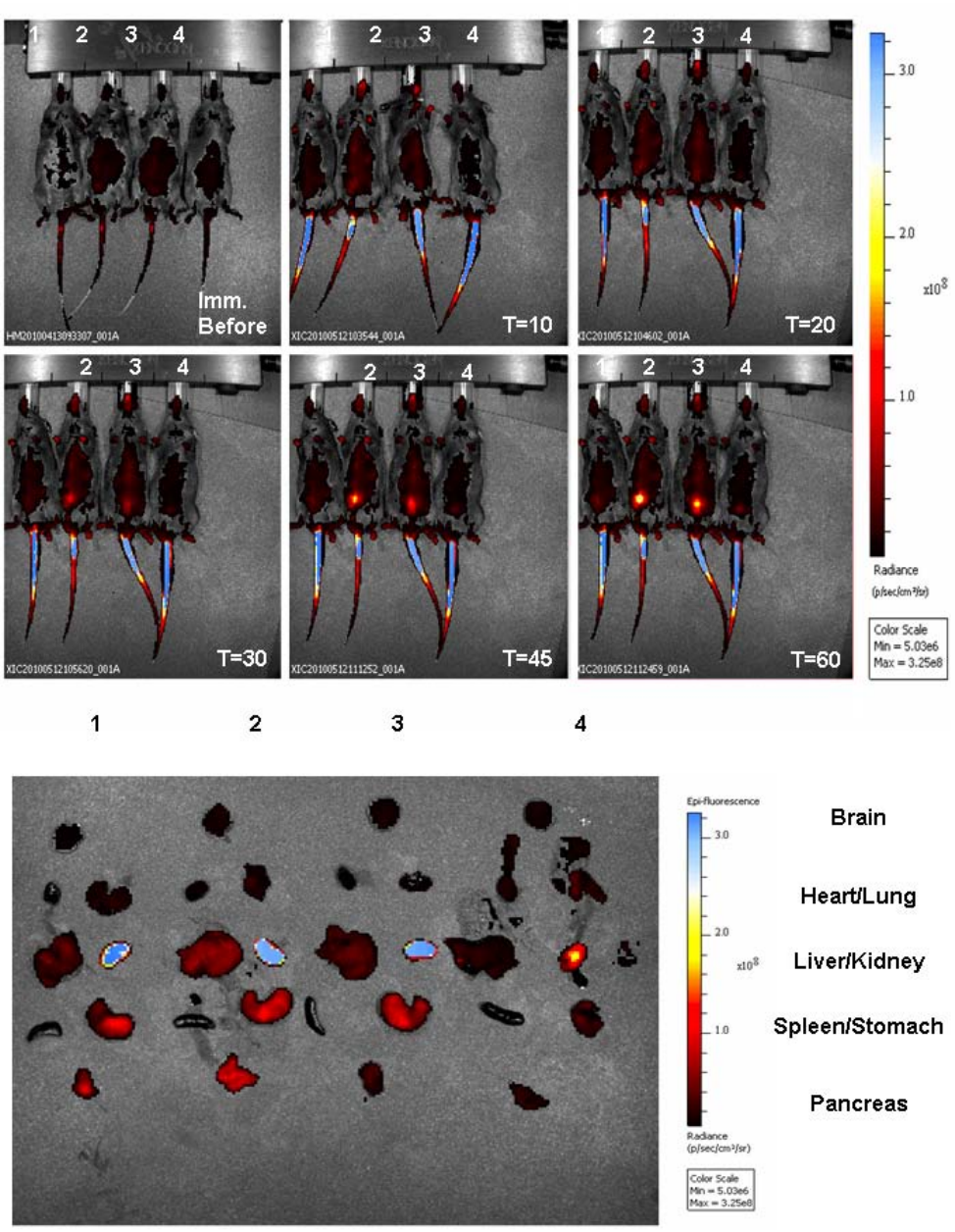

Figure 4-12 Whole body and organ scan from 8wk CCl_4 mice which have received C1-3-AF via *i.v.* injection. Images generated with a 10 second exposure since both auto and 1 second setting revealed little fluorescence. All images (both body and organ scan) were manipulated post scanning to be on the same radiance scale so data can be directly compared. All 4 mice (labelled 1-4 in the live scans and with respective organs) were injected with 8mg/kg or C1-3-AF and the antibody distribution monitored over time.

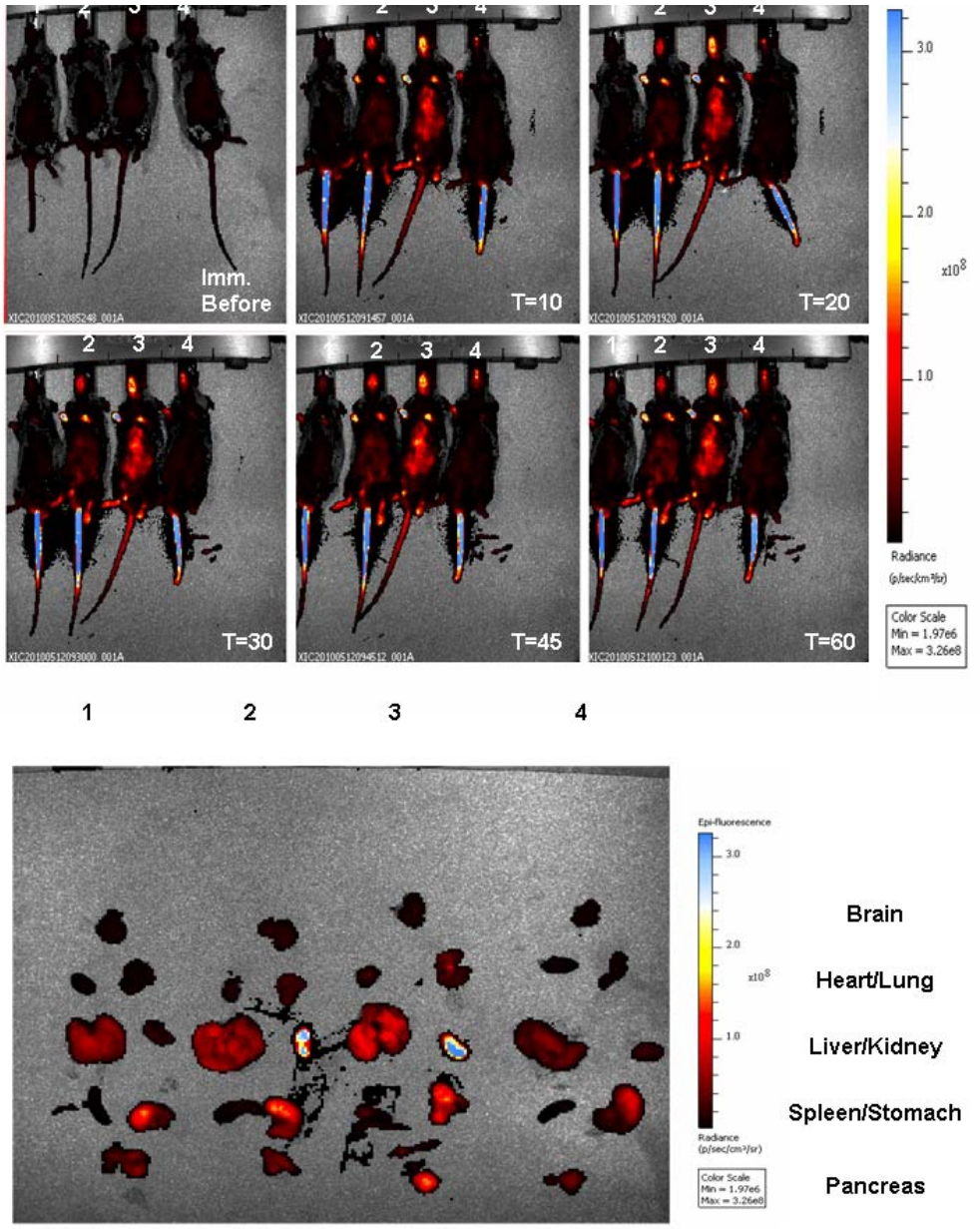

Figure 4-13 Whole body and organ scan from 12wk CCl_4 mice which have received C1-3-AF via *i.v.* injection. Images generated with a 10 second exposure since both auto and 1 second setting revealed little fluorescence. All images (both body and organ scan) were manipulated post scanning to be on the same radiance scale so data can be directly compared. All 4 mice (labelled 1-4 in the live scans and with respective organs) were injected with 8mg/kg or C1-3-AF and the antibody distribution monitored over time.

For analysis, images from each treatment group were set to the same radiance scale so that fluorescence could be visually compared between the images over the study time course. Regions of interest (ROI) were manually drawn around the upper abdominal area, bladder and each individual excised organ to allow for total flux calculation (Figure 4-14).

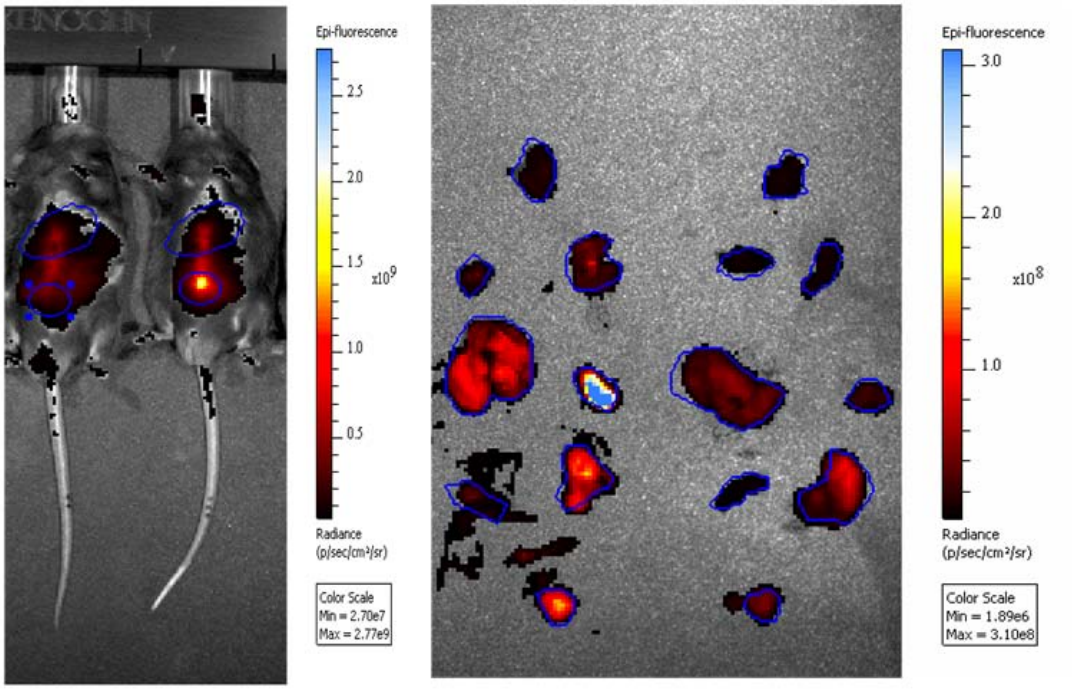

Figure 4-14 Example of the regions of interest used to calculate total flux. Images were manipulated post scanning using Living Image 4.0 software using the analysis tools to draw ROI around the areas where total flux measurements were required. For the whole body scans total flux was measured in the upper abdominal region (for C1-3-AF uptake) and the bladder (for C1-3-AF excretion).

Figure 4-15 shows the average total flux for the upper abdominal and bladder regions for each treatment group over the time course. Interestingly Figure 4-15A shows that there were no significant differences in the upper abdominal total flux readings over the time course however it is difficult to interpret the finding since some *i.v.* injections were unsuccessful and remained within the tail sheath, as represented by the highly fluorescent tails in figures 4-10 to 4-13. Antibody which did enter the circulation was increasingly excreted from the body over the 1hr time course as shown by the increase in bladder total flux (Figure 4-15).

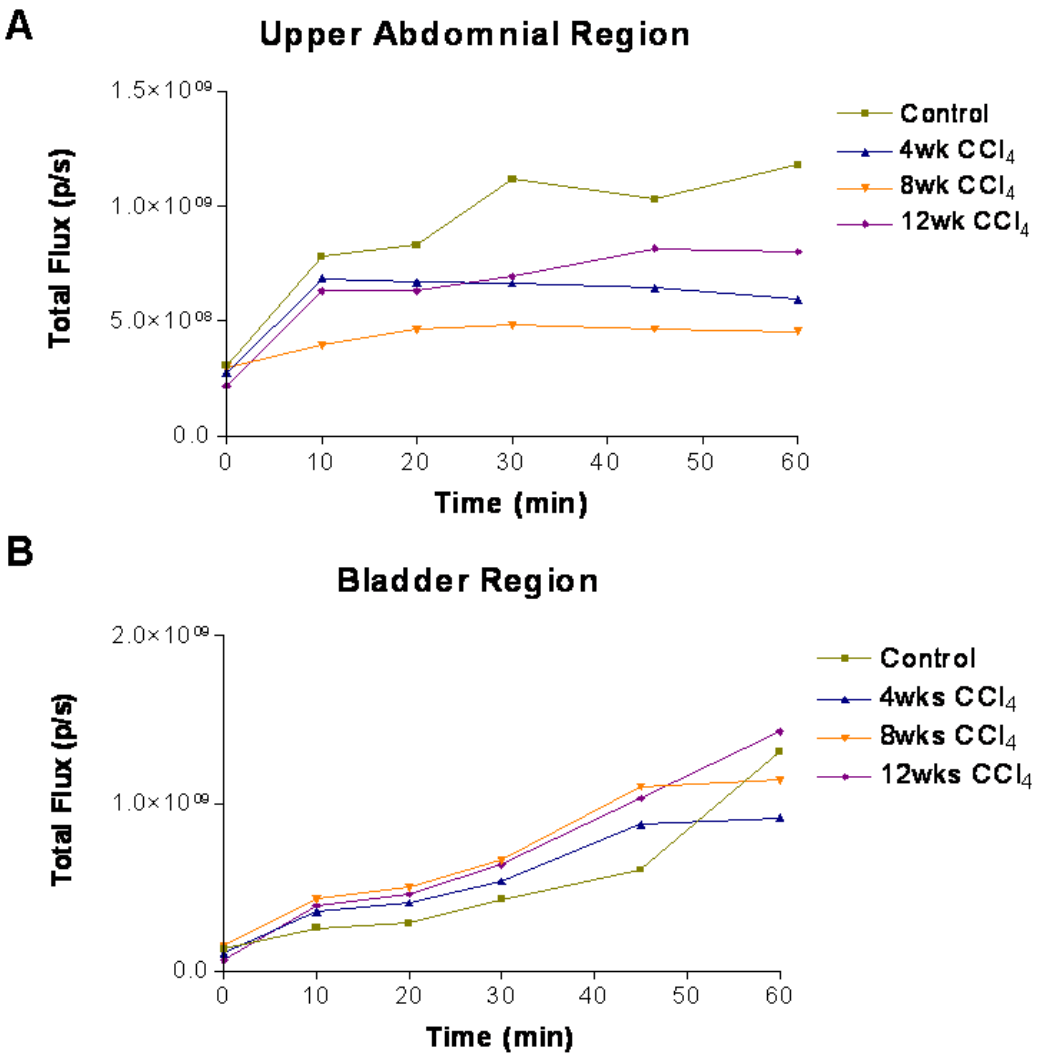

Figure 4-15 Total flux readings for both upper abdominal and bladder region for each treatment group during the 1hr time course. Images were manipulated post scanning using Living Image 4.0 software using the analysis tools to draw ROI around the areas where total flux measurements were required. Data are mean total flux for each treatment group over the time course. SD not plotted for clarity.

The data from figure 4-15 agree with figure 4-16 which show the total flux from the organs excised following imaging. There were no significant differences observed in the total liver flux between the treatment groups. The kidneys also show a high amount of flux which demonstrates that C1-3-AF is being excreted from the body, correlating with the increasing bladder flux in figure 4-15. The stomach has a high flux value which may be explained by the autofluorescence of chlorophyll in the mouse diet.

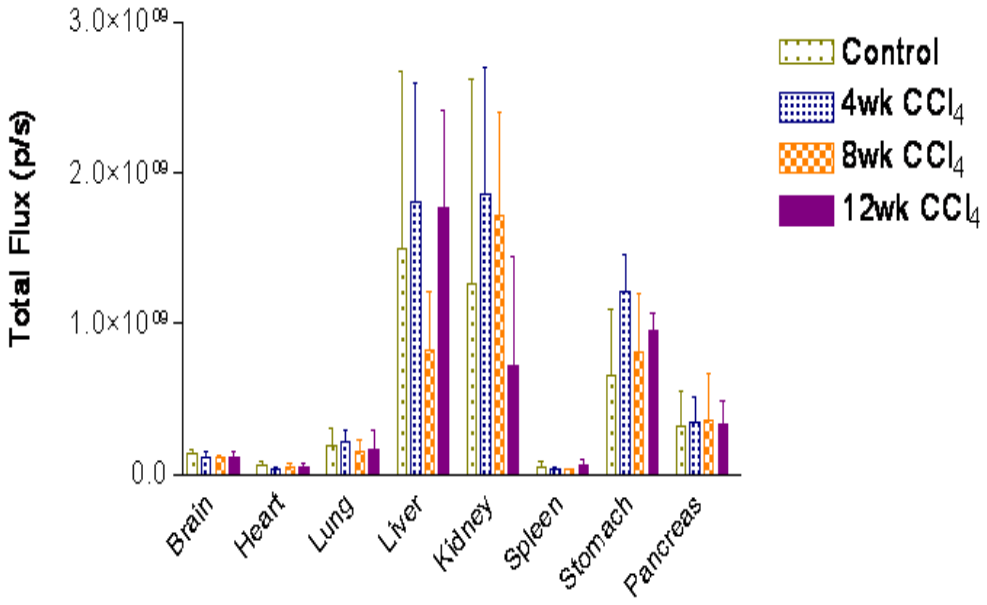

Figure 4-16 Total flux for all treatment group organs excised following imaging. Images were manipulated post scanning using Living Image 4.0 software using the analysis tools to draw ROI around the areas where total flux measurements were required. Data are the mean and SD of the total flux for each treatment group (n=4 per group) over the time course

Whilst *i.v.* injection of C1-3-AF is representative of the current clinical situation, the difficulty of the injection increases the chances of the C1-3-AF antibody missing the mouse tail vein and remaining in the tail sheath. This presents a major problem when trying to investigate whether C1-3-AF can be used as a non invasive *in vivo* measure of liver fibrosis since it cannot be guaranteed that each animal receives the same dose of antibody. Therefore it was deemed necessary to repeat the experiment and inject the C1-3-AF antibody directly into the intraperitoneal cavity.

Figure 4-17 to 4-20 represent images taken at the specified time points for control, 4 wk, 8wk and 12wk CCl_4 mice respectively which received C1-3-AF via intraperitoneal injection. Data presented are from 1 second exposure only, settings auto and 10 second resulted in either too little or a saturated signal. An uninjected control mouse was included for each treatment group to provide a reference point for tissue and organ autofluorescence.

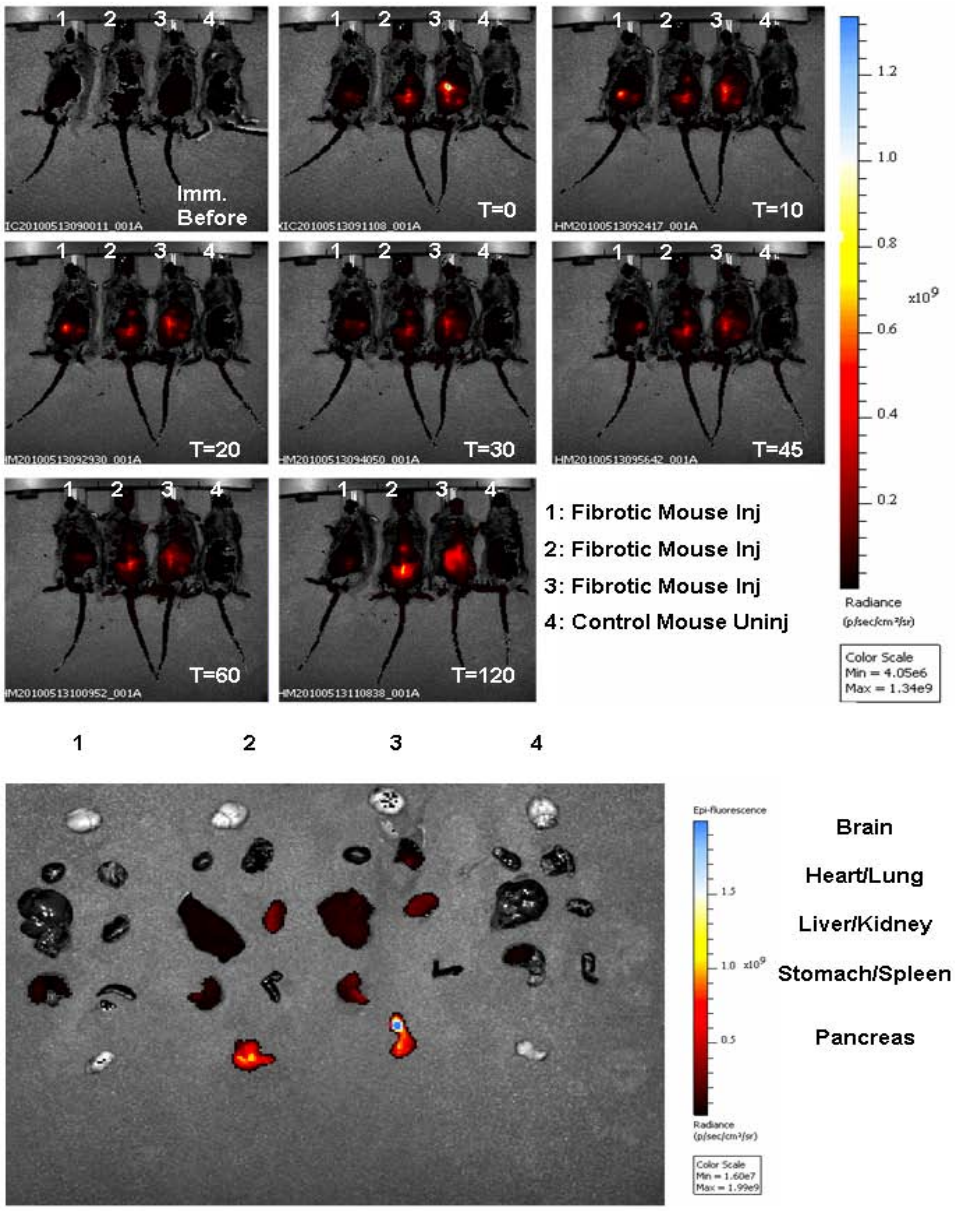

Figure 4-17 Whole body and organ scan from control mice which have received C1-3-AF via *i.p.* injection. Images generated with a 1 second exposure since both auto and 10 second setting revealed too little or too much fluorescence. All images (both body and organ scan) were manipulated post scanning to be on the same radiance scale so data can be directly compared. Mice 1-3 were injected *i.p*. with 8mg/kg C1-3-AF.

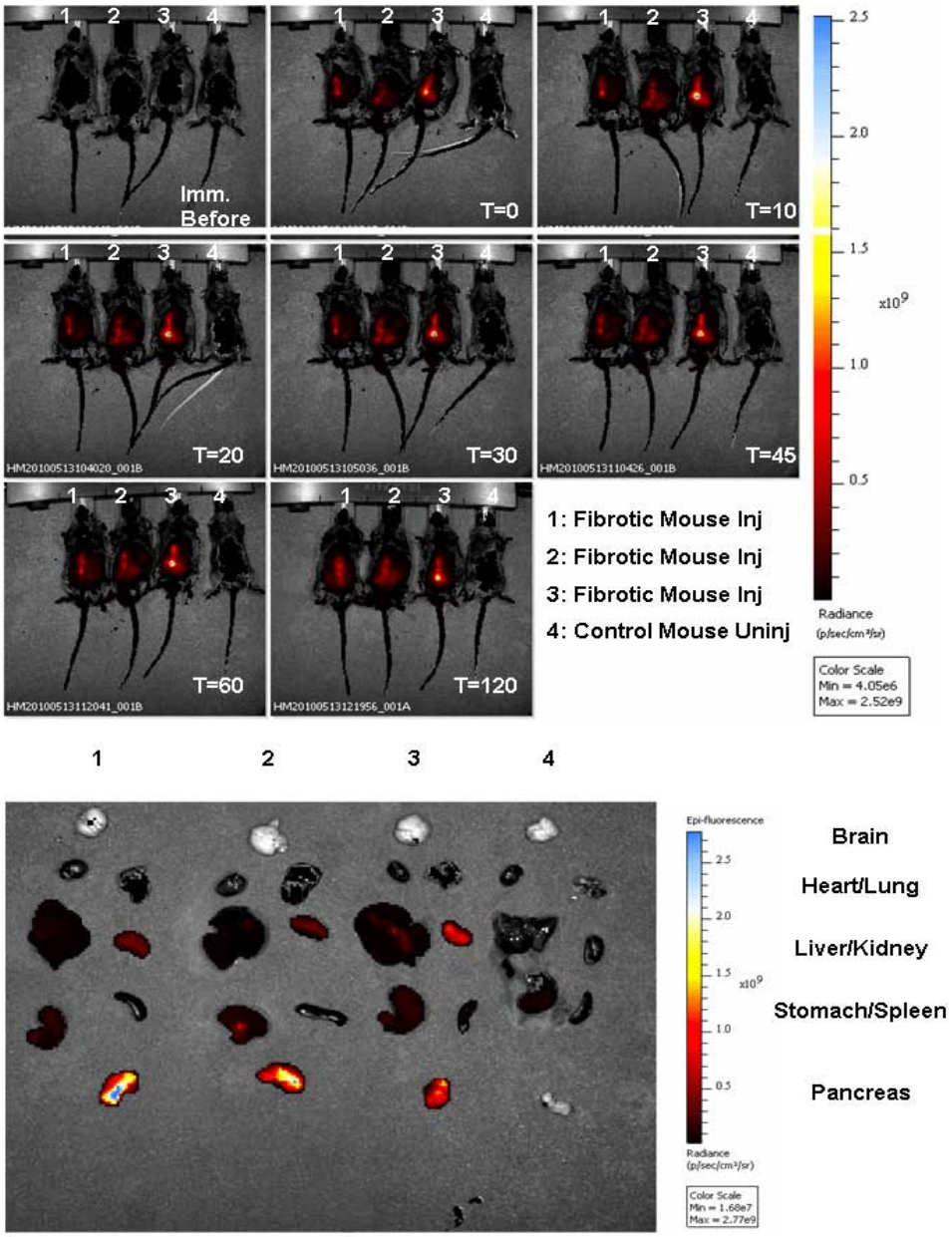

Figure 4-18 Whole body and organ scan from 4wks CCl_4 mice which have received C1-3-AF via *i.p.* injection. Images generated with a 1 second exposure since both auto and 10 second setting revealed too little or too much fluorescence. All images (both body and organ scan) were manipulated post scanning to be on the same radiance scale so data can be directly compared. Mice 1-3 were injected *i.p*. with 8mg/kg C1-3-AF.

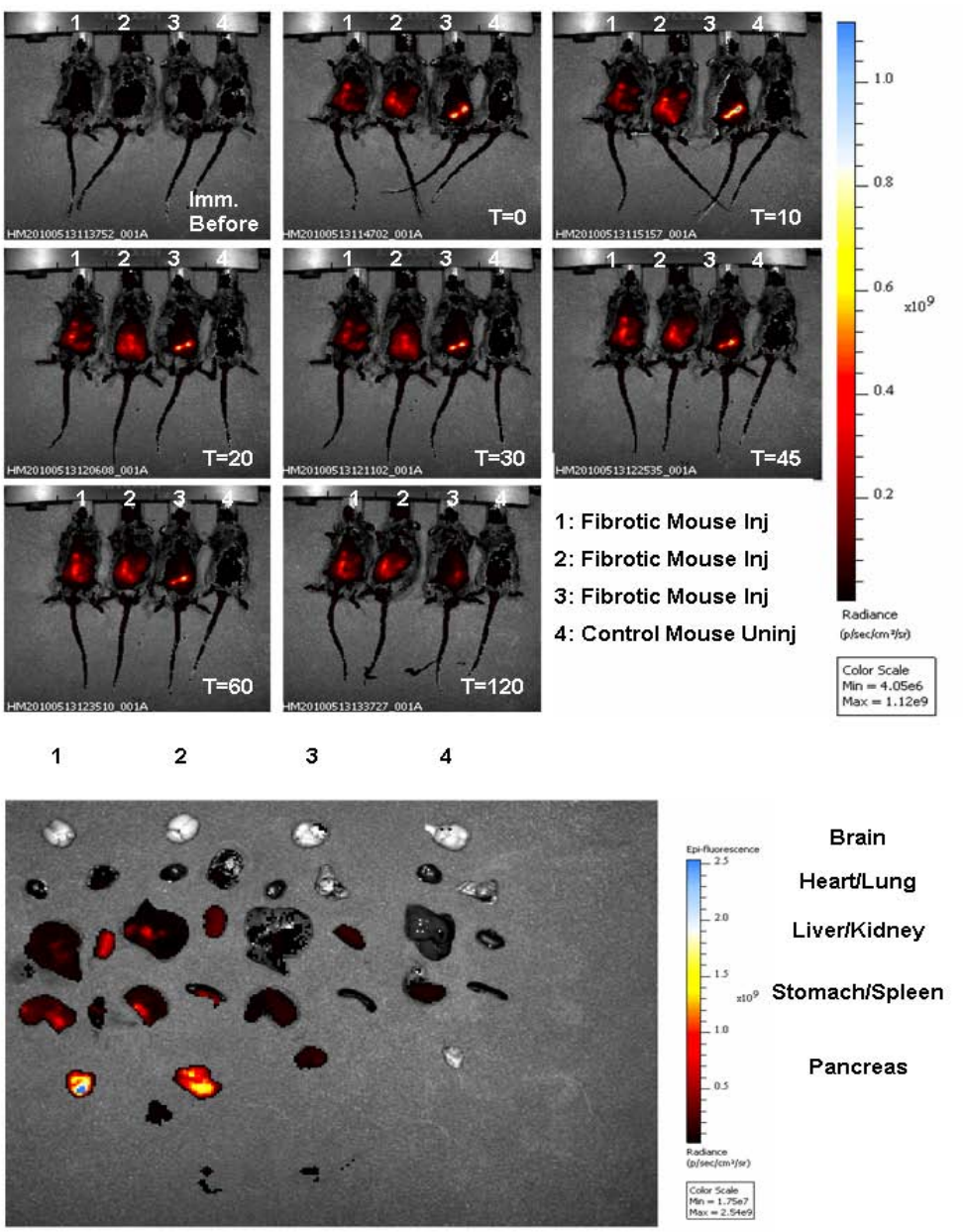

Figure 4-19 Whole body and organ scan from 8wks CCl_4 mice which have received C1-3-AF via *i.p.* injection. Images generated with a 1 second exposure since both auto and 10 second setting revealed too little or too much fluorescence. All images (both body and organ scan) were manipulated post scanning to be on the same radiance scale so data can be directly compared. Mice 1-3 were injected *i.p*. with 8mg/kg C1-3-AF.

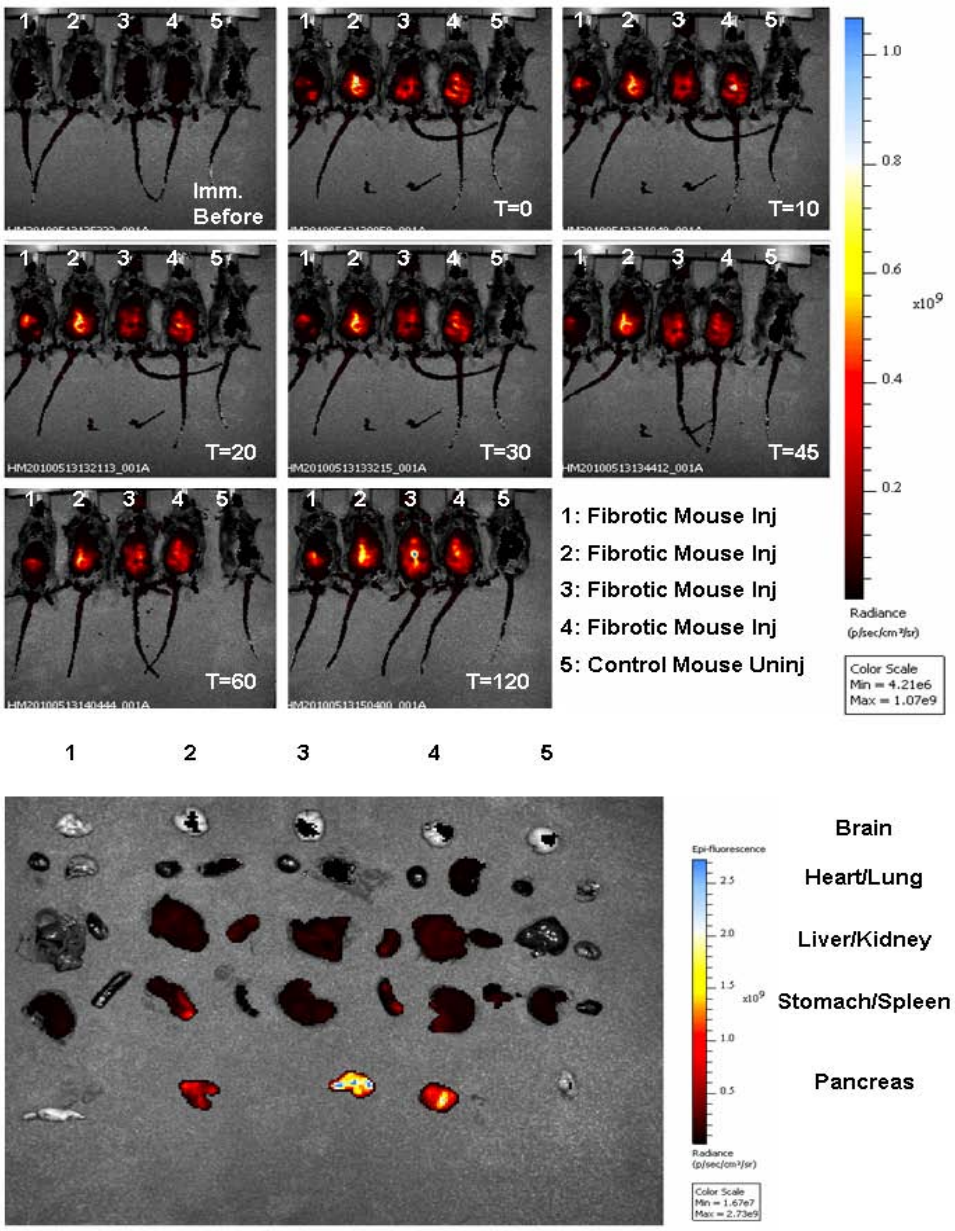

Figure 4-20 Whole body and organ scan from 12wks CCl_4 mice which have received C1-3-AF via *i.p.* injection. Images generated with a 1 second exposure since both auto and 10 second setting revealed too little or too much fluorescence. All images (both body and organ scan) were manipulated post scanning to be on the same radiance scale so data can be directly compared. Mice 1-4 were injected *i.p*. with 8mg/kg C1-3-AF.

As described previously, total flux was measured over the time course by drawing a box around the upper abdominal region to measure liver fluorescence and around the bladder to measure excretion of the fluorophore from the body. The data in figure 4-21 show that there is a significantly higher total flux value in the upper abdominal region of CCl_4 treated mice (at selected time points) in comparison to the control and uninjected mice. Furthermore, this value is higher in the 4wk CCl_4 mice in comparison with the 8wk and 12wk CCl_4 mice.

The total flux in the bladder region follows a different pattern, an initial peak between 0-20 minutes suggests quick excretion of excess fluorophore from the body followed by a gradual increase between 45 minutes to 2 hours where remaining fluorophore is removed.

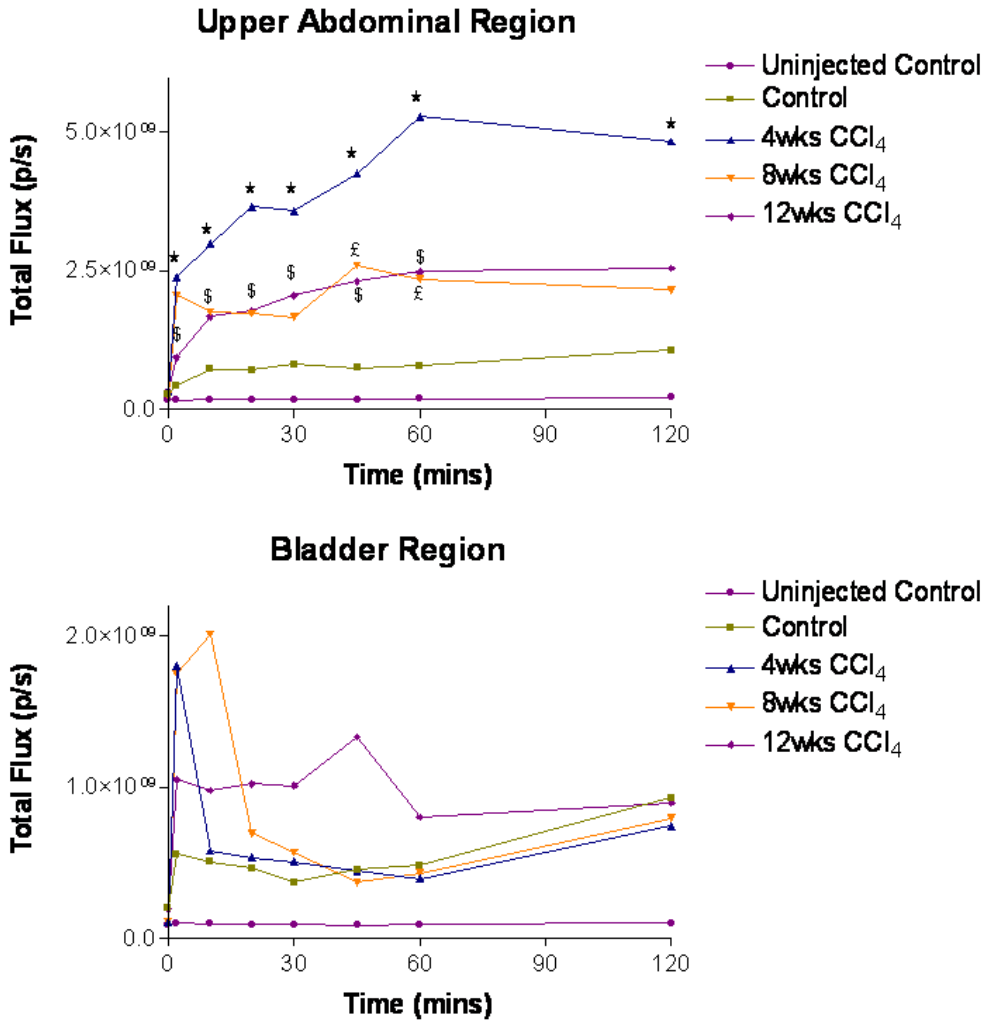

Figure 4-21 Total flux readings for both upper abdominal and bladder region for each treatment group during the 2hr time course. Images were manipulated post scanning using Living Image 4.0 software using the analysis tools to draw ROI around the areas where total flux measurements were required. Data are mean total flux for each treatment group over the time course. SD not plotted for clarity. Data tested for statistical significance using the Student's two tailed T test, * represent significance between 4wk CCl_4 and control £ represent significance between 8wk CCl_4 and control and $ represent significance between 12wk CCl_4 and control ($p<0.05$). Animal group numbers: Uninjected control n=4, Control/4wks CCl_4/8wks CCl_4 n=3; 12wks CCl_4 n=4.

Following time course completion, the major organs were excised from each animal and total flux measured as previously described.

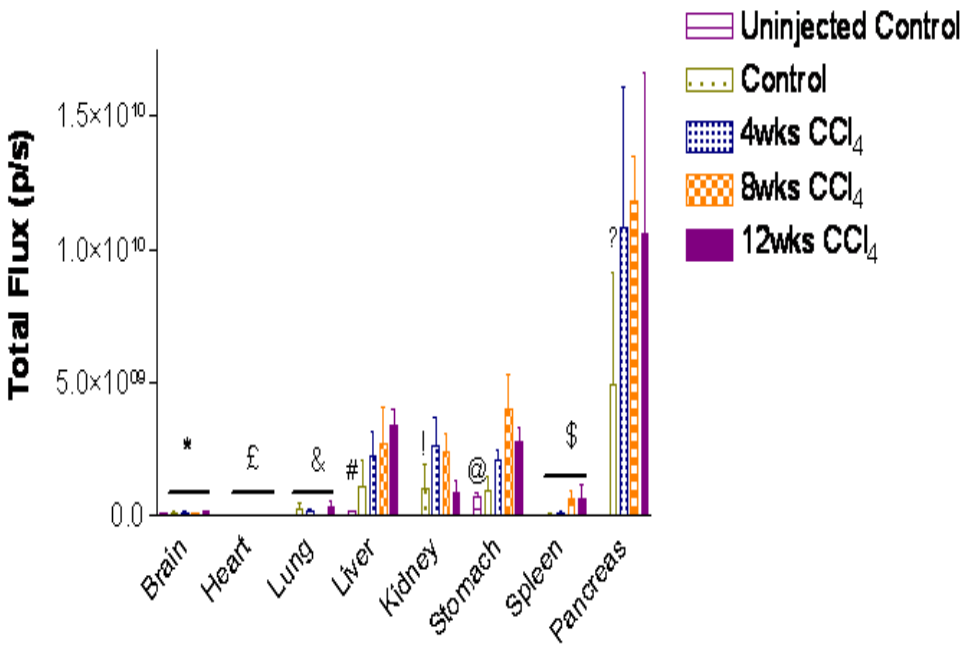

Figure 4-22 Total flux for all *i.p.* injected treatment group organs excised following imaging. Images were manipulated post scanning using Living Image 4.0 software using the analysis tools to draw ROI around the areas where total flux measurements were required. Data are the mean total flux for each treatment group (n=3 per group 4,8 CCl_4 and control injected groups, n=4 12wk CCl_4 and uninjected controls) over the time course. . Data tested for statistical significance using the Student's two tailed T test; * illustrates significantly lower total flux in brain tissue from injected animals in comparison to the liver ($p<0.0001$); kidney ($p<0.0001$); stomach ($p<0.0005$); pancreas ($p<0.0001$) from injected animals. £ illustrates significantly lower total flux in the hearts from injected animals in comparison to the liver ($p<0.00001$); kidney ($p<0.0005$); stomach ($p<0.0005$); pancreas ($p<0.0001$) from injected animals. & illustrates significantly lower total flux in the lungs from injected animals in comparison to the liver ($p<0.0001$); kidney ($p<0.001$); stomach ($p<0.00001$); pancreas ($p<0.00001$) from injected animals. $ illustrates significantly lower total flux in the spleen from injected animals in comparison to the liver ($p<0.0001$); kidney ($p<0.005$); stomach ($p<0.0005$); pancreas ($p<0.0001$) from injected animals. #,!,@ and ? represent significantly lower total flux in the organs from the uninjected animals compared with the injected animals (# p<005; !,@ ? p<0.05).

The bar chart in figure 4-22 shows that total flux are significantly higher in the liver, kidney, stomach and pancreas of injected animals in comparison to the other organs. This shows that the C1-3-AF antibody is binding to synaptophysin positive cells in the liver and pancreas as the total flux in these organs is significantly higher than the uninjected controls. The high total flux in the kidney, combined with the increasing total flux in the bladder regions (figure 4-21) would suggest that the antibody is being actively excreted, since the total flux is significantly higher in the injected animals compared to the uninjected controls. Interestingly, the total stomach flux is higher in the injected animals in comparison to the uninjected controls. Whilst some of this is due to the presence of autofluorescence compounds in the diet, the data would suggest that C1-3-AF

is binding to synaptophysin positive cells in this organ. However, there is no evidence in the literature that synaptophysin is expressed by cells in the stomach.

Figure 4-23 illustrates total liver flux for both *i.v.* and *i.p.* injected animals. Whilst no change in liver flux is seen in the *i.v.* injected animals, probably due to the difficulty of injection, a clear increase can be seen in the liver of the CCl_4 compared to the injected controls. More importantly this increase is significantly higher in mice treated 12 weeks with CCl_4 in comparison to the controls.

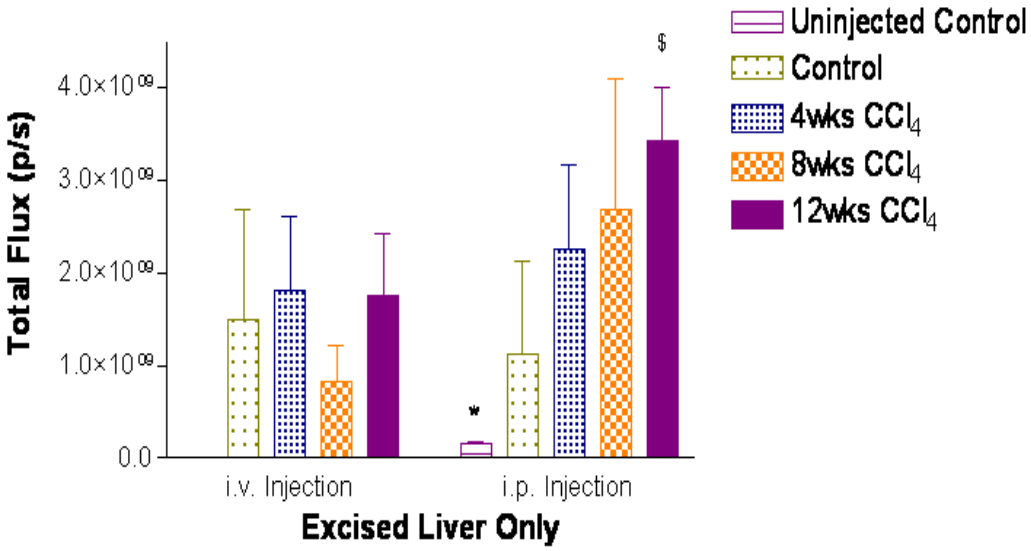

Figure 4-23 Total flux of the excised liver from all treatment groups. Images were manipulated post scanning using Living Image 4.0 software using the analysis tools to draw ROI around the areas where total flux measurements were required. Data are the mean total flux for each treatment group (I.V. n=4 per treatment group, I.P.n=3 per 4,8 CCl_4 and control injected groups, n=4 12wk CCl_4 and uninjected controls) over the time course Data tested for statistical significance using Student's two tailed T test $ represents significance between 12wks CCl_4 and control ($p<0.01$); * represent significantly lower total flux in the uninjected controls in comparison to the injected animals ($p<0.005$).

To confirm that the CCl_4 treatment had resulted in liver damage, whole blood was removed from each animal following schedule 1 termination and serum sent for ALT/ALP analysis. As expected, ALP levels were below the threshold level for accurate quantification since CCl_4 is not known to cause cholestasis. ALT analysis showed a significant increase in serum ALT concentrations in the CCl_4 treated mice in comparison to the controls indicating liver damage had occurred (Figure 4-24).

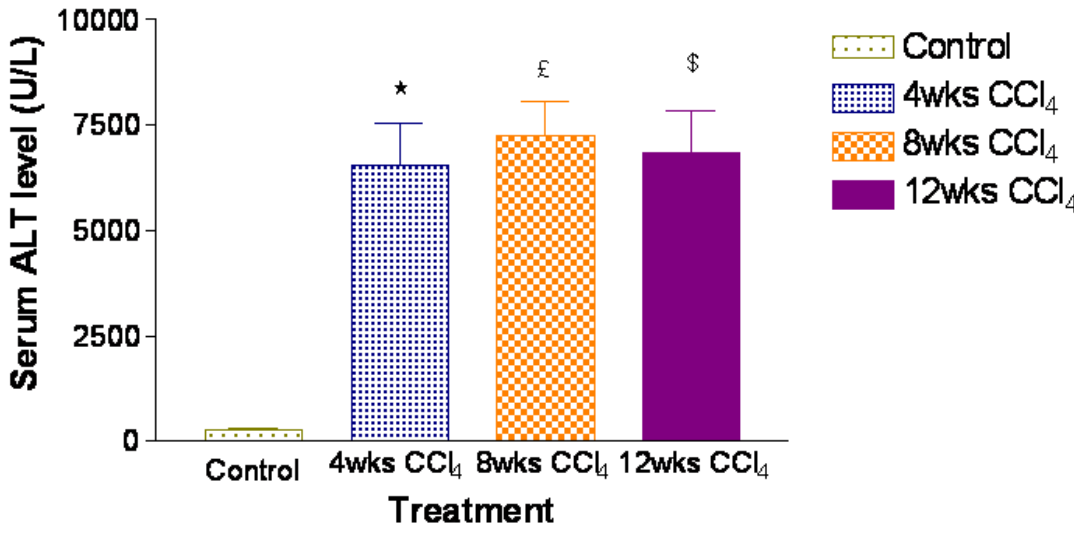

Figure 4-24: Serum ALT concentration for all treatment groups. Mice were schedule 1 killed and whole blood was removed and allowed to clot at room temperature for 1hr. Serum was removed following centrifugation and diluted in 0.9% sodium chloride. All serum samples were analysed by Newcastle Clinical Biochemistry Department. Data are the mean and SD for each treatment group and were tested for statistical significance using the Student's two tailed. * represent significance between 4wk CCl_4 ($p<0.001$) and control £ represent significance between 8wk CCl_4 and control ($p<0.001$) and $ represent significance between 12wk CCl_4 and control ($p<0.001$).

To determine if this result reflected the number of hepatic myofibroblasts present in the liver tissue, formalin fixed liver tissue was stained with α-SMA-antibody. For quantification, slides were examined at x200 magnification and the percentage area of positive staining per field of view was determined using Leica software and is shown in figure 4-25.

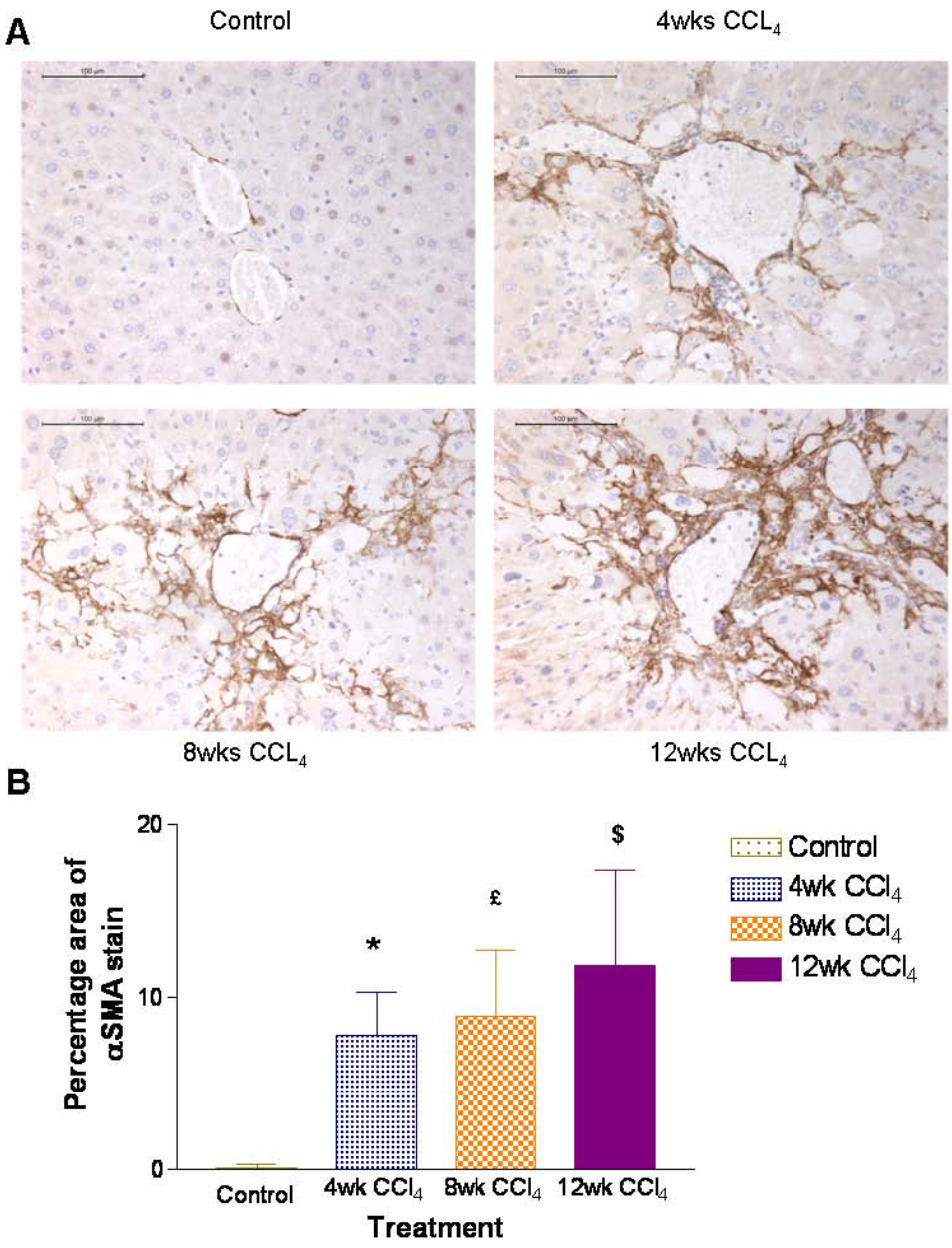

Figure 4-25 α-SMA IHC staining and quantification. A: Formalin fixed paraffin embedded tissue samples from each animal were cut into 4µm sections. Sections were dewaxed, subjected to heat induced antigen retrieval, blocked and incubated for 1hr with Mouse anti αSMA-FITC antibody. After extensive washing, bound antibody was detected with Rabbit anti FITC-HRP secondary antibody and visualised with DAB chromagen. Finally, sections were counterstained with haematoxylin and mounted. All images taken at x200 magnification. B: For quantification, pictures were taken around 10 random CLV at x200 magnification and subjected to analysis using Leica software to determine the percentage area of the αSMA stain. Data are the mean and SD of percentage area of the αSMA stain for each treatment group and were tested for statistical significance using Student's two tailed T test. * represent significance between 4wk CCl_4 ($p<0.001$) and control; £ represent significance between 8wk CCl_4 and 4wk CCl_4 ($p<0.05$); $ represent significance between 12wk CCl_4 and 8wk CCl_4 ($p<0.001$). Scale bar = 100µm.

Quantification of the α-SMA stain in figure 4-25 reveals that there is a significant increase in the percentage area of positive staining in the CCl_4 mice in comparison with the control which significantly increases with treatment time.

Sections of the liver tissue were also stained with picro-sirius red to allow quantification of collagen deposited in response to injury. Upon inspection under the light microscope at x200 magnification, CLV were located and moved to the corner of the field of view so the band of collagen could be quantified by software analysis as previously described.

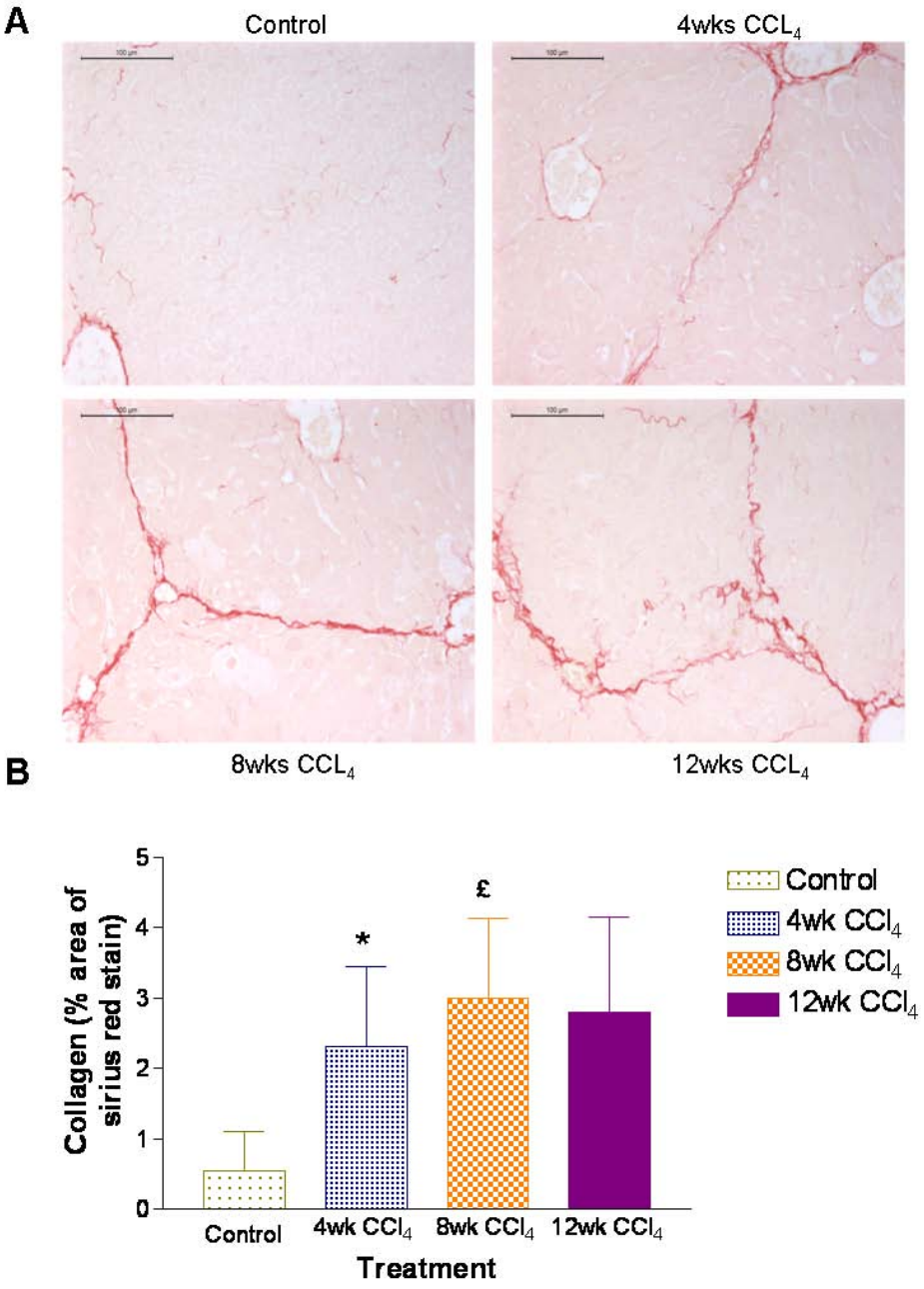

Figure 4-26 Picro-Sirius red staining and quantification. A: Formalin fixed paraffin embedded tissue samples from each animal were cut into 4µm sections. Sections were dewaxed and incubated in picro-sirius red stain for 2hrs at room temperature. Excess stain was removed by 2 washes in acidified H_2O (0.5% acetic acid in deionised water) and sections dehydrated in two changes of 100% ethanol. Sections were mounted and images taken at x200 magnification. B: For quantification 10 random CLV were located and moved to the corner of the field of view to allow quantification of the band of collagen by Leica software analysis. Data are mean and SD of percentage area of picro-sirius red stain and were tested for statistical significance using Student's two tailed T test. * represent significance between 4wk CCl_4 ($p<0.001$) and control; £ represent significance between 8wk CCl_4 and 4wk CCl_4 ($p<0.001$). Scale bar = 100µm.

Images in figure 4-26A are typical representations of picro-sirius staining observed in all treatment groups. Quantification of the collagen staining (figure 4-26B) revealed a significant increase in the percentage of area stained in all CCl_4 treated mice in comparison with the controls. Initially there is a significant increase in positive staining between control-4wks CCl_4 and 4-8wks CCl_4, however no difference is observed between 8 -12wks of CCl_4 treatment.

Whilst the αSMA and picro-sirius red staining show an increase in αSMA staining and collagen deposition with increasing treatment time, the organ flux data revealed a significant increase in the 12wk CCl_4 liver in comparison to the injected controls. However, the upper abdominal flux during the whole body scan is somewhat different, with 4 wk CCl_4 treatment resulting in a higher flux than the two other CCl_4 groups. One possible explanation which may account for this is the liver tissue itself quenching the fluorescence. A simple experiment was setup to test this theory which involved imaging a dose of C1-3-AF fluorophore next to and under an uninjected liver. As anticipated, the placing of the fluorophore tube under the liver resulted in 99% quenching of the fluorophore signal (Figure 4-27) suggesting that the flux values obtained throughout the experiment may not be representative of the true values.

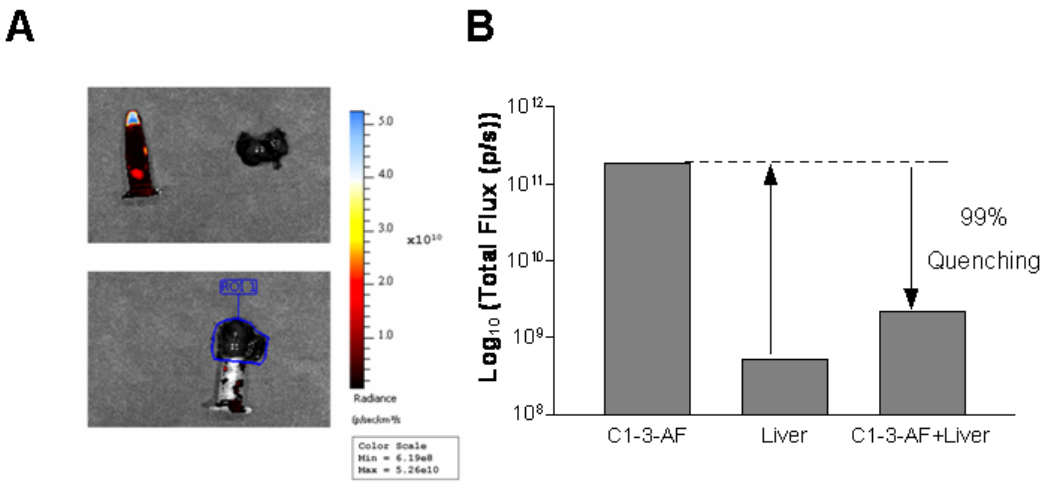

Figure 4-27 Quenching of C1-3-AF fluorescence by the liver. A: A liver from an uninjected C57Bl6 mouse was imaged alongside a 100µl dose of C1-3-AF antibody (0.2mg) using manually set 1 second exposure. The fluorophore tube was placed underneath the excised liver and imaged as before. The total flux for each of the three regions was determined using Living Images 4.0 software. B: The arrows on the bar chart highlight the quenching of the fluorophore signal by the liver.

Since the pilot IVIS data revealed the high binding capacity of C1-3-AF in the pancreas as well as the liver, a second animal study was set up to investigate whether it was able to distinguish pancreatic islet cell mass. Tg (CRH) mice,

which appear cusingoid by 21 weeks of age, are known to have increased β cell mass to compensate for their insulin resistance and are therefore predicted to have a higher pancreatic flux value than C57Bl6 controls [252]. The study was set up as before, with the animals being imaged immediately before injection to measure background fluorescence, then at 1minute, 10 minutes, 20 minutes, 30 minutes, 1hr and 2hrs following *i.p.* injection. An uninjected C57Bl6 mouse was imaged alongside the CRH to provide a background reference point for the whole body and organ scans. It was decided not to inject the antibody intravenously since this had proved difficult in the previous study.

Figure 4-28 and 4-29 are images taken at the specified time points for CRH and control mice respectively. Data presented are from 1 second exposure only since auto and 10 second exposures resulted in too little or too much fluorescence. The images in both figures show an increase in fluorescence in the upper abdominal and bladder regions after C1-3-AF injection. In some mice there appears to be a large amount of fluorescence in the lower abdominal region which may be the result of some antibody accidentally entering the intestines due to a bad injection. Figure 4-29 shows 5 mice being imaged over the experiment time course however it is clearly visible that mice 1 and 2 have received a bad injection with the antibody being injected subcutaneous instead of into the intraperitoneal cavity. As a result of this, it was decided to exclude their organs from the final organ scan since it would be difficult to calculate the exact dosage that these mice received and in turn normalise the data.

Upper abdominal and bladder flux were calculated for the CRH mice and the 3 injected female C57Bl6 controls as previously described. The average total flux for each region and treatment group is illustrated in figure 4-30. A significantly higher flux was observed in the upper abdominal region of the CRH mice in comparison to the controls at 1 and 2hr time points following injection. Interestingly, the total flux in the bladder region was significantly higher in CRH mice in comparison to the C57Bl6 controls suggesting that either the CRH mice excrete the antibody more rapidly than the controls or that the control mice received a lower dose of C1-3-AF due to some antibody going subcutaneous. However, due to the lack of CRH mice available at the time of the study it was not possible to repeat this experiment.

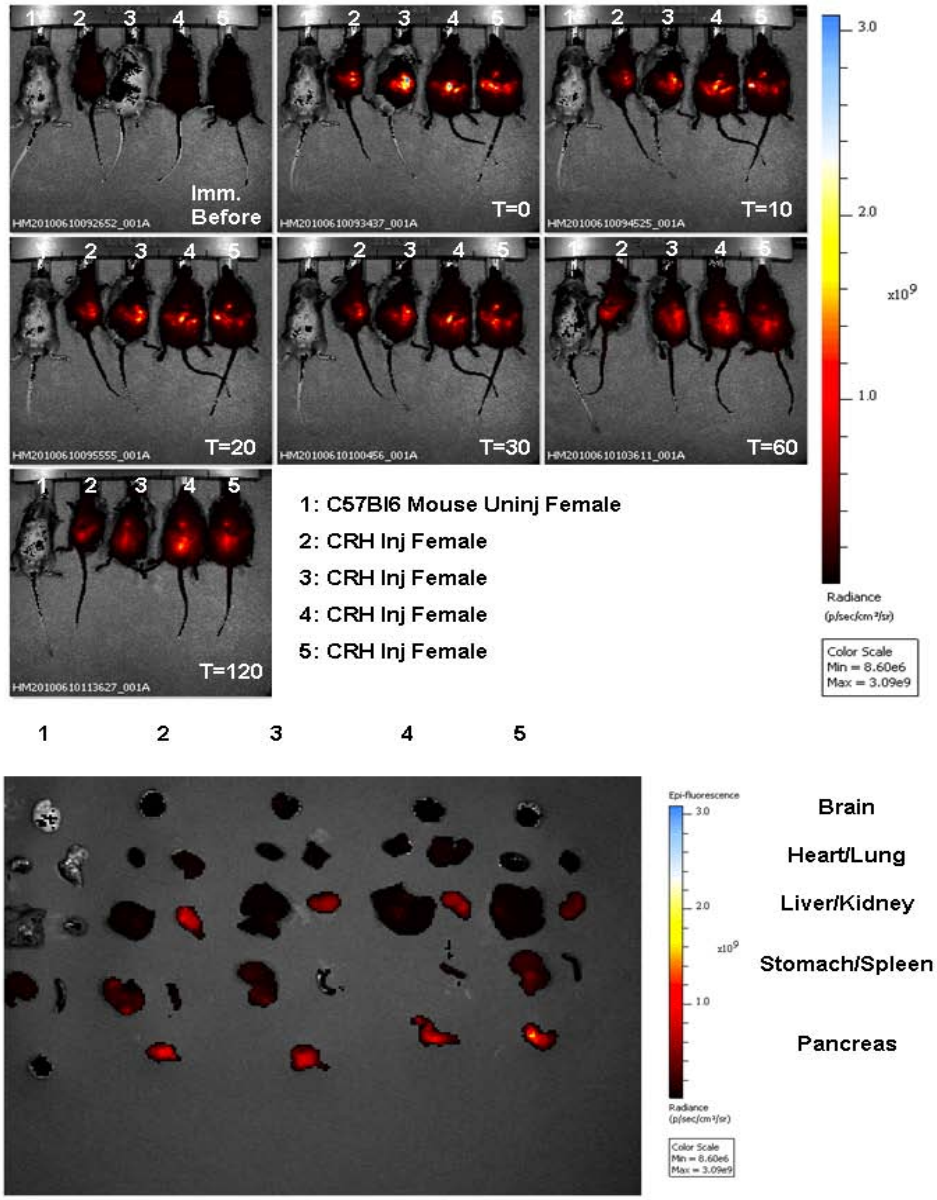

Figure 4-28 Whole body and organ scan from CRH mice which have received C1-3-AF via *i.p.* injection. Images generated with a 1 second exposure since both auto and 10 second setting revealed too little or too much fluorescence. All images (both body and organ scan) were manipulated post scanning to be on the same radiance scale so data can be directly compared.

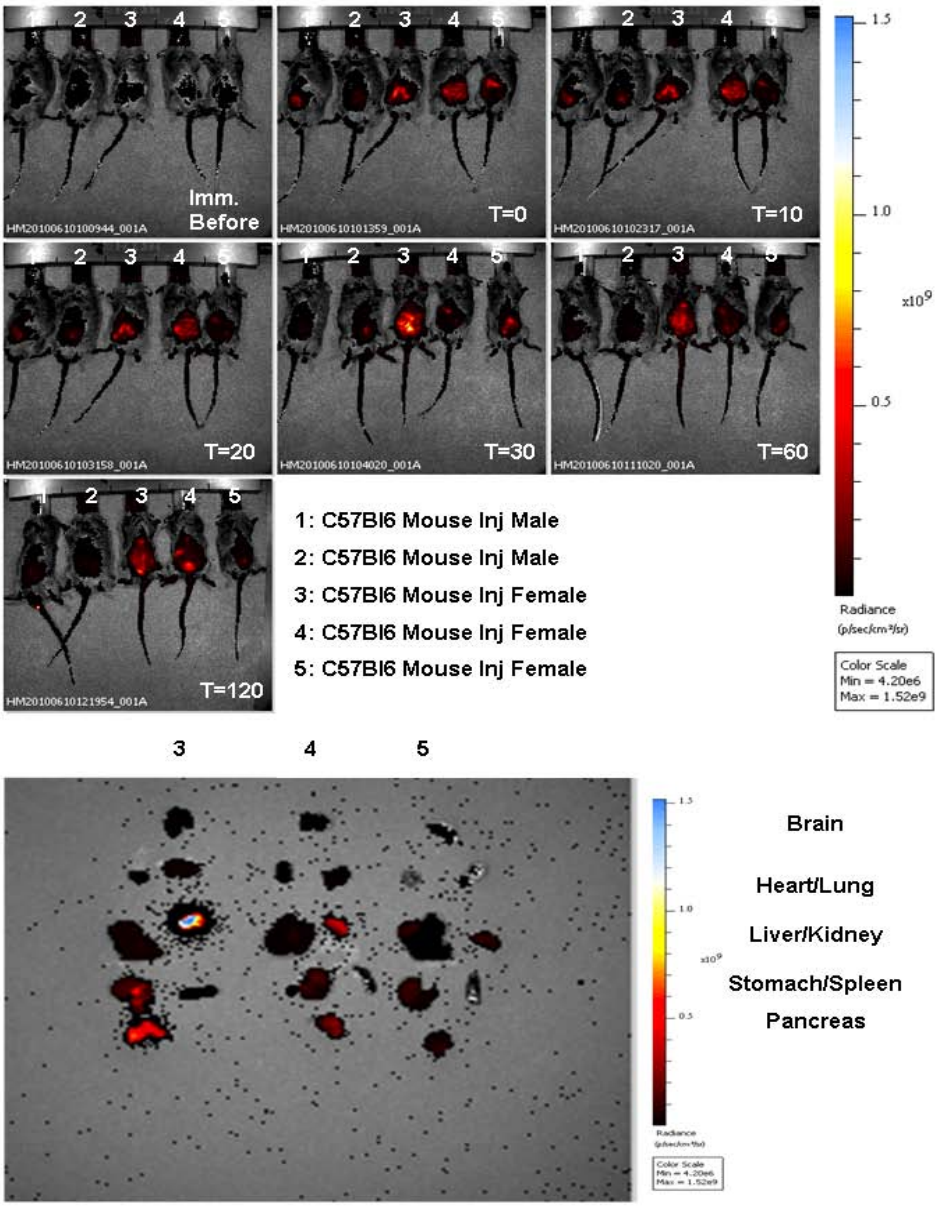

Figure 4-29 Whole body and organ scan from control mice which have received C1-3-AF via *i.p.* injection. Images generated with a 1 second exposure since both auto and 10 second setting revealed too little or too much fluorescence. All images (both body and organ scan) were manipulated post scanning to be on the same radiance scale so data can be directly compared. Both mice 1 & 2 injections went subcutaneous instead of intraperitoneal thus organs have been excluded from the final scan.

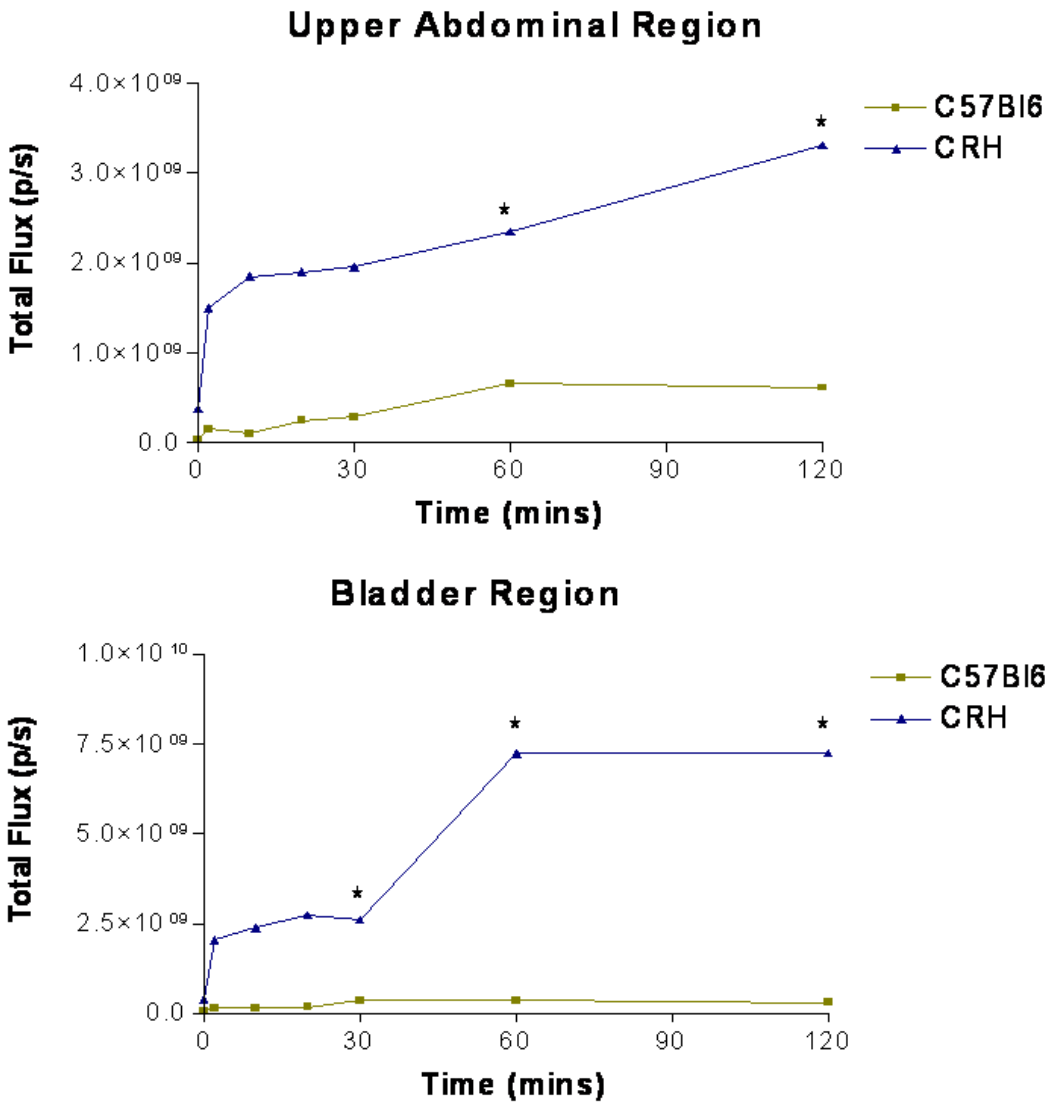

Figure 4-30 Total flux readings for both upper abdominal and bladder region for each treatment group during the 2hr time course. Images were manipulated post scanning using Living Image 4.0 software using the analysis tools to draw ROI around the areas where total flux measurements were required. Data are the mean total flux for each treatment group over the time course (n=3 per treatment group). Data tested for statistical significance using the Student's two tailed T test, * represent significance between C57Bl6 and CRH ($p<0.05$).

Previous work by Wallace *et al* [252] has shown that pancreata in CRH mice are significantly smaller compared to C57Bl6 wild type controls. Thus total flux was expressed per gram of pancreas weight for each group and is illustrated in figure 4-31. The data show that CRH mice had a significantly higher total flux value per gram of pancreatic weight compared to C57Bl6 controls. This correlates with previous data published [252] and shows that an increase in islet cell mass in CRH can be quantified by C1-3-AF imaging.

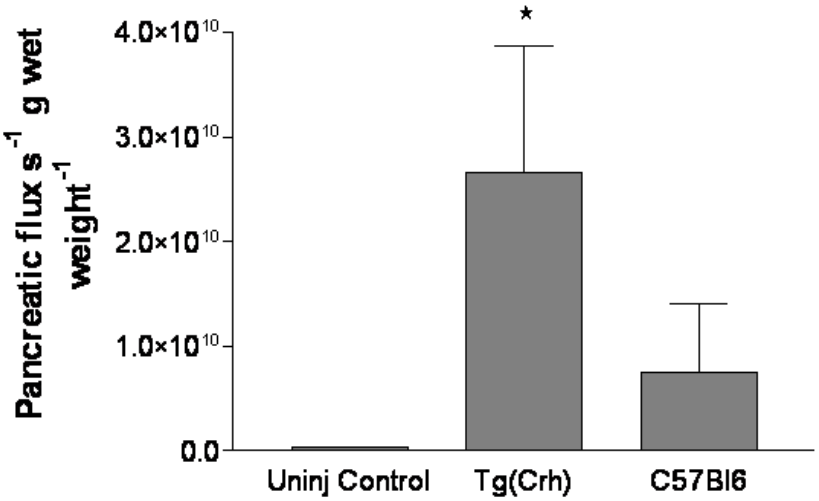

Figure 4-31 Pancreatic flux for each group. Images were manipulated post scanning using Living Image 4.0 software using the analysis tools to draw ROI around the areas where total flux measurements were required. Uninjected control represents female C57Bl6 mouse. Tg(CRH) and C57Bl6 were injected with 8mg/kg C1-3-AF. Data are the mean total flux for the pancreata. Data tested for statistical significance using the Student's two tailed T test, * represent significance between C57Bl6 and CRH ($p<0.05$).

4.3 Discussion

Recent advances in scientific research have led to a greater understanding of the mechanisms involved during fibrosis and the proposal that fibrosis may in fact be reversible [126, 253]. Therefore if diagnosed during the early stages therapeutic strategies could be implemented to halt or even reverse disease progression before end stage liver failure is reached.

C1-3, a single chain antibody fragment, was generated by the Wright group in 2005 and was shown to specifically target synaptophysin positive hepatic myofibroblasts in the liver [125]. Since hepatic myofibroblasts have been shown to be the principal cell type involved in fibrosis progression and matrix deposition [36, 91] it has been postulated that the number of hepatic myofibroblasts present within the tissue may be indicative of the stage of fibrosis.

Single chain antibodies are being increasingly used in clinical practice to target therapies [247] and image tumours [246] due to their specificity, ability to penetrate tissue and fast excretion from the body. Therefore this chapter set out to investigate whether C1-3 would be a suitable imaging agent to successfully distinguish between the stages of fibrosis.

In order to address this question, C1-3 was successfully conjugated to alexa fluorophore 594 and its binding activity tested *in vitro*. *In vivo* function was tested in an animal model of liver fibrosis, where mice had been treated with CCl_4 to induce centrilobular damage due to hepatocyte apoptosis and necrosis. OPT analysis showed clear distribution of C1-3-AF in the fibrotic liver, particularly in scar regions around CLV. As expected, C1-3-AF was also present in the control non fibrotic livers, albeit to a lesser extent. This is because synaptophysin is expressed by both quiescent HSCs and hepatic myofibroblasts thus under normal conditions there are a few quiescent HSCs which reside in the space of Dissé, sensing the microenvironment [124]. Bound antibody could be easily visualised by colouring pixels above a threshold limit, as determined by analysis of control samples. Whilst this highlighted the difference in antibody distribution between the treatment groups, the lack of ability to actually quantify the number of coloured pixels and normalise for ‘noise’ makes it impossible to conclude if any significant differences were observed.

Whilst the data provide proof of concept that single chain antibodies can be used to successfully image liver fibrosis, as with many of the new detections methods recently proposed there are major limitations with regard to OPT technology. OPT has been developed to fill the gap between confocal microscopy and MRI imaging and is typically used to map gene expression pathways in embryos over 1cm across [254]. The technique relies on shadows generated when light is shone at the sample and the intensity at each point recorded. A computer programme translates the data into a 3D image which can be further manipulated with imaging software. The liver samples used for analysis were approximately $1cm^3$ and even at this size there was poor resolution within the centre of the tissue due to insufficient lighting. To compensate for this, threshold values could be altered post-scanning to increase pixel intensity however this tended to increase the noise surrounding the tissue thus a compromise had to be made. More importantly, however, OPT is subject to the same complications and sampling errors as a needle biopsy and whilst it provides a novel method for assessing hepatic myofibroblast numbers it is unlikely that this technique will be used in a clinical setting.

The emergence of a highly sensitive, non invasive imaging system that allows the visualisation and tracking of fluorophores in the body and tissue of live animals led to the novel proposal that C1-3-AF could be used as a non invasive measure of liver fibrosis. To test this theory, three different stages of liver fibrosis were generated in mice by dosing for 4, 8 and 12 weeks with CCl_4 whilst control mice received olive oil. After their final dose of CCl_4 or olive oil, each treatment group was injected with C1-3-AF and its distribution monitored over time using Xenogen's IVIS® 200 series imager. To replicate a clinical setting, C1-3-AF was injected into mice via two routes, either intravenously or in the intraperitoneal cavity. It was predicted that i.v. injection would provide the most useful data since distribution of the antibody to the liver would be much quicker in the circulatory system and would reduce the possibility of non specific background fluorescence. However, injection of the antibody into the tail vein was more difficult than first thought and on many occasions a substantial proportion of the dose remained within the tail sheath thus no difference in upper abdominal and organ flux was observed between the fibrotic stages.

I.P. injection proved much more successful and showed that at specific time points (particularly 45 and 60 minutes after injection) there was a significantly higher upper abdominal total flux in comparison with the injected control animals. Interestingly, the upper abdominal flux was highest in the mice treated for 4 weeks with CCl_4 suggesting that there are a higher number of synaptophysin positive hepatic myofibroblasts involved during the early stages of liver disease. To determine if this is an accurate representation of the number of synaptophysin positive hepatic myofibroblast it would be necessary to quantify cell number by IHC staining and RT-PCR analysis.

To determine if the whole body readings actually reflected the fluorescence of the organ, following completion of the time course the mice were schedule 1 killed and organs removed. In order to fully account for the whole body readings, it was deemed necessary to remove the brain, heart, lungs, kidney, pancreas, spleen and stomach as well as the liver to ensure that C1-3-AF was specifically targeting its antigen. The data revealed an increase in liver total flux with increasing CCl_4 treatment time however this difference was only significant for the 12wk CCl_4 mice in comparison to the olive oil controls. This suggests that there is an increasing number of synaptophysin positive hepatic myofibroblasts throughout disease progression and that this number corresponds to the stage of fibrosis. Immunohistochemical staining revealed a similar trend with collagen deposition significantly increasing during treatment time due to the significant increase in the number of αSMA positive myofibroblasts. This work agrees with a previous study which similarly demonstrated that αSMA could be used a marker to stage fibrosis and to monitor therapeutic treatments since the number of αSMA cells reflected the disease status [251].

Whilst the liver organ flux values provide proof of concept that C1-3-AF can be detect advanced fibrosis, it should be noted that these values were not reflective of the upper abdominal flux values in the whole body scans. The organ scan revealed significantly higher total flux in the liver, kidney, stomach and spleen in comparison to the brain, heart, lungs and spleen of injected animals. A high total flux in the kidney was due to excretion of the excess antibody, as shown by the increase in total flux in the bladder regions during the liver animal imaging. Interestingly, quantification revealed that animals injected C1-3-AF had a significantly higher stomach total flux compared to the uninjected controls. Whilst

the autofluorescence of chlorophyll in the mouse diet contributes to the total value, the data suggest that C1-3-AF is binding to cells within the stomach. As there is no evidence in the literature that the stomach contains synaptophysin positive cells, it would be necessary to carry out synaptophysin IHC on stomach tissue to investigate this further. The high total flux reading for the pancreas can be accounted for by the expression of synaptophysin in the islet cells [255]. It is therefore possible that the slight difference in total flux readings in the whole body scan may be enhanced or accounted for by the fluorescence of the pancreas and the stomach.

A simple experiment, where an uninjected liver was placed over a dose of C1-3-AF, proved that the liver was capable of quenching up to 99% of the fluorescent signal therefore an animal experiment was set up to determine if the total flux readings in the upper abdominal region were dependent upon the expression of synaptophysin in the pancreas. Total flux in the upper abdominal region of CRH mice, known to have increased islet cell mass due to insulin resistance [252], was significantly higher than C57Bl6 wild type controls. Furthermore, they had a significantly higher total flux per gram of pancreas weight than the controls indicating that C1-3-AF was a useful tool in measuring islet cell mass. However, due to the difference in bladder total flux suggesting different dosing of C1-3-AF fluorophore and lack of animals, it would be necessary to repeat this experiment to confirm the result.

This chapter shows that C1-3-AF may be useful in quantifying the number of synaptophysin positive hepatic myofibroblasts in explant liver tissue, with the number of hepatic myofibroblasts increasing with disease progression. However its use as a non invasive marker of liver fibrosis may be limited due to the expression of synaptophysin in the pancreas which in turn affects the total flux measurement of the upper abdominal region as well as the quenching of the fluorescent signal by the liver. One way to overcome this may be to use a fluorophore which emits near the infrared end of the spectrum, since the absorbance spectra of the body fluids and tissues are much lower in the near infrared region [256]. Ideally, 3D scans would be conducted on each individual mouse to map the fluorescence to a particular organ allowing for more accurate flux values to be calculated; however with the technology currently available during this pilot study this was not feasibly possible.

Finally, it is important to note another limitation of C1-3-AF as an imaging agent. Immunohistochemical studies of the fibrogenic response during liver disease caused by different aetiological agents have revealed that there are functionally and morphologically distinct populations of myofibroblasts present during fibrosis [52, 53]. More importantly however, studies have shown that during portal fibrosis, for example, the portal fibroblast is dominant and is closely associated with scar regions [55]. Unfortunately, these cells do not express synaptophysin [124] therefore an animal study of obstructive cholestasis would be necessary to determine the involvement of synaptophysin positive hepatic myofibroblasts during disease progression.

Chapter 5. Use of C1-3-GT to investigate the role of hepatic myofibroblasts in liver regeneration

5.1 Introduction

The liver has a remarkable ability to regenerate following injury or loss of tissue. It is generally mediated by replication of existing hepatocytes although a progenitor cell repopulation can occur if hepatocyte replication is inhibited [129, 257]. The complex pathways governing the initiation and termination of liver regeneration have been under investigation for years yet many areas are still not well understood.

Although the stimulus for the initiation of liver regeneration is unclear, it is widely accepted that hepatic myofibroblasts and macrophages are the main source of IL-6 and TNFα [131-133, 135, 138], the two cytokines responsible for priming hepatocytes to respond to the mitogens HGF and EGF [160, 258]. Once primed, the hepatocytes undergo 2-3 rounds of cell division to restore liver mass after 70% hepatectomy.

Hepatic myofibroblasts are thought to play a key role in liver regeneration, not only providing the key cytokines responsible for priming hepatocytes but are also a source of serotonin [146], a neurotransmitter which is believed to play a pivotal role in regeneration. However, researchers investigating the possible reversal of liver fibrosis have shown that the induced apoptosis of these cells results in degradation of the collagen scar and an improvement in tissue function [100, 102, 249].

C1-3-GT has been shown to target hepatic myofibroblasts *in vivo* and significantly reduce fibrosis severity in a recovery model [126]. Thus, this antibody will therefore be used in a two thirds partial hepatectomy (PHx) model to investigate the role hepatic myofibroblasts in liver regeneration.

5.2 Results

Prior to the investigation, C1-3 was conjugated to gliotoxin as described in the materials and methods sections. Successful conjugation was confirmed by SDS-PAGE (figure 5-1), where a distinct increase in molecular weight could be seen in the C1-3-GT sample in comparison to C1-3. Western blotting using rabbit anti gliotoxin antibody proved that this increase was due to gliotoxin conjugation.

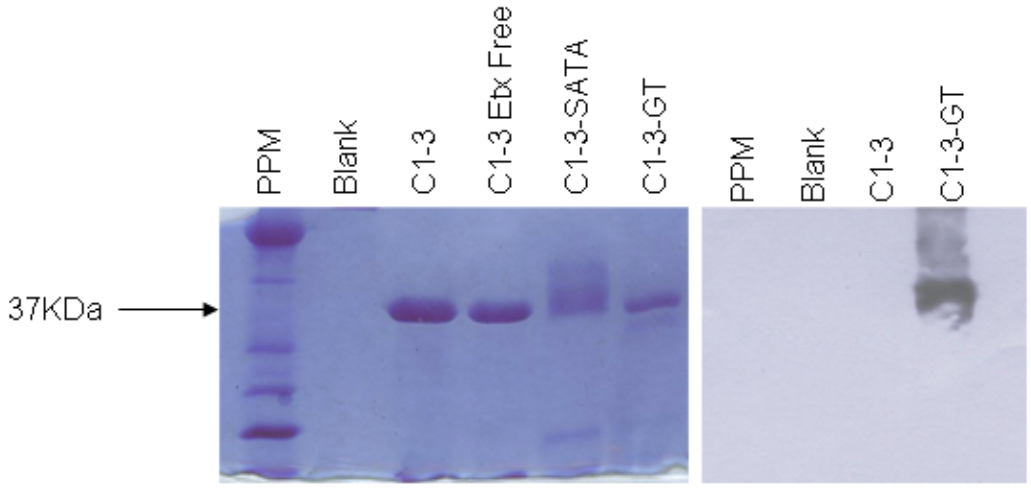

Figure 5-1 SDS-PAGE and Western blot analysis of samples from the C1-3-GT conjugation process. Samples were taken throughout the conjugation process and diluted 1:1 with reducing loading buffer. After denaturation, 10µl of each sample was loaded onto a 9% SDS-PAGE gel alongside a prestained protein marker and separated according to its size. To visualise the proteins, each gel was stained for 1hr with coomassie blue, destained for 24hr to remove excess stain. For Western blot analysis, proteins were transferred to a nitrocellulose membrane, blocked with 3% milk marvel solution, and probed with rabbit anti gliotoxin. Results are typical of 5 individual antibody conjugation reactions.

To ensure that conjugation of gliotoxin had not resulted in functional impairment of the antibody a binding ELISA was used. Figure 5-2 shows that C1-3-GT is able to bind to its antigen peptide 2 with C1-3 being used as a positive control.

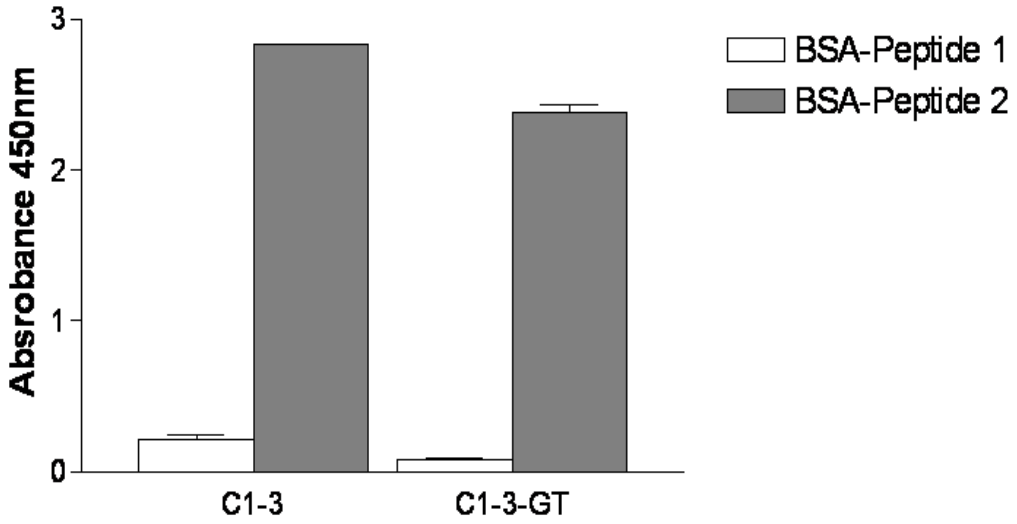

Figure 5-2 Peptide 1 and 2 binding ELISA for C1-3 and C1-3-GT. 96 well plates were coated with BSA-conjugated peptide 1 or peptide 2. Antibody samples of unknown concentrations were initially diluted 1:10 with PBS then serially diluted across the plate. Bound antibody was detected using a secondary HRP conjugated goat-anti human Cκ light chain antibody and quantified by measuring a colorimetric reaction by the addition of TMB and the absorbance at 450nm noted. All experiments were performed in triplicate and the absorbance at dilution 5 (1/160) plotted. Results are typical of 5 separate antibody conjugation reactions.

Following confirmation of binding ability, C1-3-GT was routinely checked by addition to cultures of activated human and mouse hepatic myofibroblasts. Figure 5-3 is an example of the results obtained from *in vitro* cell detachment assays. Adherent cells were counted from 5 random fields of view per treatment group and expressed as a percentage of cells attached using the average cell number from time zero. Both C1-3 and DMSO (vehicle control for free gliotoxin) did not affect cell attachment however the addition of free gliotoxin rapidly induced cell apoptosis and detachment. C1-3-GT caused a much slower detachment of cells, possibly due to the process required for the uptake and processing of the C1-3 antibody itself. Even after 24 hours, approx 35% remained attached in the C1-3-GT treatment group compared to those treated with free GT which may be explained by the heterogeneity of synaptophysin expression on hepatic myofibroblasts. Whilst cell detachment is not a direct measure of apoptosis in itself, it provides a very quick and crude measurement to confirm that the C1-3-GT is working. To confirm apoptosis, it would be necessary to measure caspase 3 activity in the live cell cultures using commercially available kits.

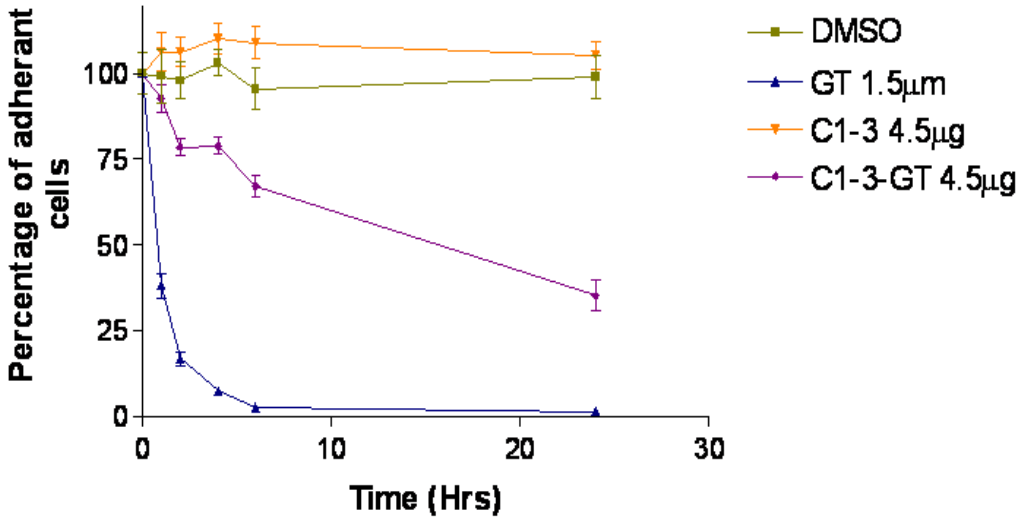

Figure 5-3 *In vitro* assessment of C1-3 & C1-3-GT activity. Hepatic myofibroblasts were isolated from C57Bl6 mouse livers and cultured on plastic for 1-2 weeks until fully activated. Cells were seeded at equal densities into 24 well plates and incubated with either 4.5µg C1-3, 4.5µg C1-3-GT (to give approximately 450 pmol GT/well), DMSO or GT (450pmol GT/well) in serum free medium for up to 24hrs. The number of adherent cells were counted in 5 random fields of view at the specified time points and expressed as a percentage of cells attached. Experiments were performed in triplicate and data at each time point are the mean and SD per treatment group. Data are representative of 2 experimental repeats.

An animal study to investigate the role of hepatic myofibroblasts in liver regeneration was set up using the two thirds PHx model. This is a popular model used to investigate liver regeneration as tissue is easily removed due to the multi lobular structure of the liver thus the regenerative process is not influenced by outside factors e.g. necrosis or inflammation. Mice were dosed with C1-3-GT at critical time points to ensure hepatic myofibroblast depletion before and after surgery whilst control animals received C1-3. Each mouse was weighed before surgery and the amount of liver removed recorded. Sham hepatectomies were performed to ensure that the surgical procedure itself did not have any impact on the regenerative process, where the mice were subjected to the same procedure except that the liver was not removed. This is outlined by the schematic diagram in Figure 5-4.

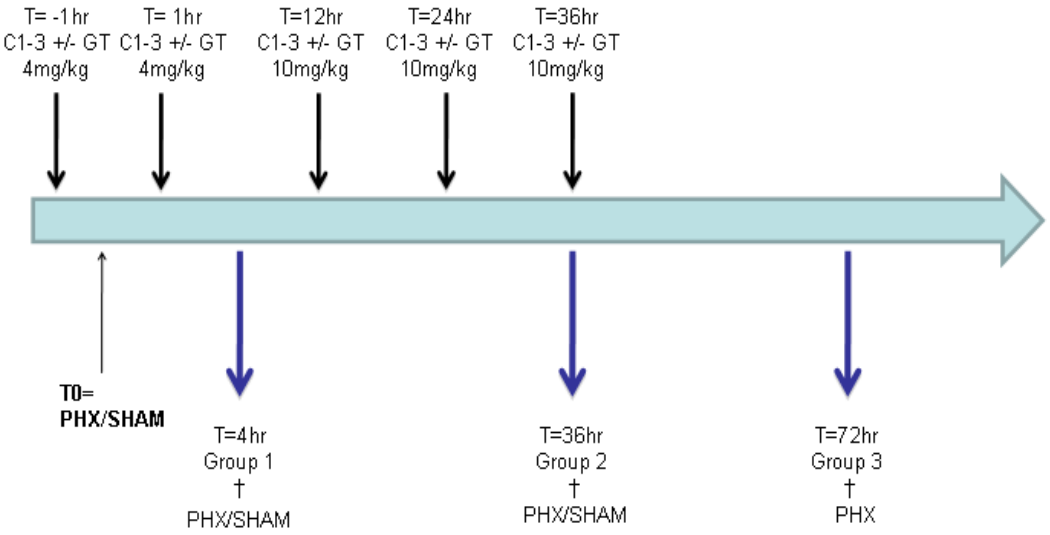

Figure 5-4 Overview of partial hepatectomy animal study. Male C57Bl6 mice were injected with 4mg/kg of C1-3+/-GT 1 hr prior to and at 1, 12, 24 and 36hrs following two thirds PHx surgery. Mice were schedule 1 killed at 4, 36 and 72hrs following surgery which were key time points identified in the liver regeneration process. Sham hepatectomies were performed to ensure the results were not due to the procedure itself and were subjected to the same surgery except no liver tissue was removed. Animals were weighed prior to and after surgery. Liver tissue removed at the time of surgery and following sacrifice was recorded as a measure of liver regeneration. Whole blood samples were taken at the time of sacrifice for serum analysis of liver enzyme markers. Animal group numbers: C1-3 4hr n=5; 36hr n=6; 72hr n=4. C1-3-GT 4hr n=4; 36hr n=3; 72hr n=4. Sham n=3 per treatment group and time point.

At each time point the mice were sacrificed and their livers removed and weighed. To verify that the remaining liver weight could be used as a measure of liver regeneration between the treatment groups, the liver removed during surgery was expressed as a percentage of the total body weight. As shown in figure 5-5A, there is no significant difference in the percentage of liver removed between treatment groups.

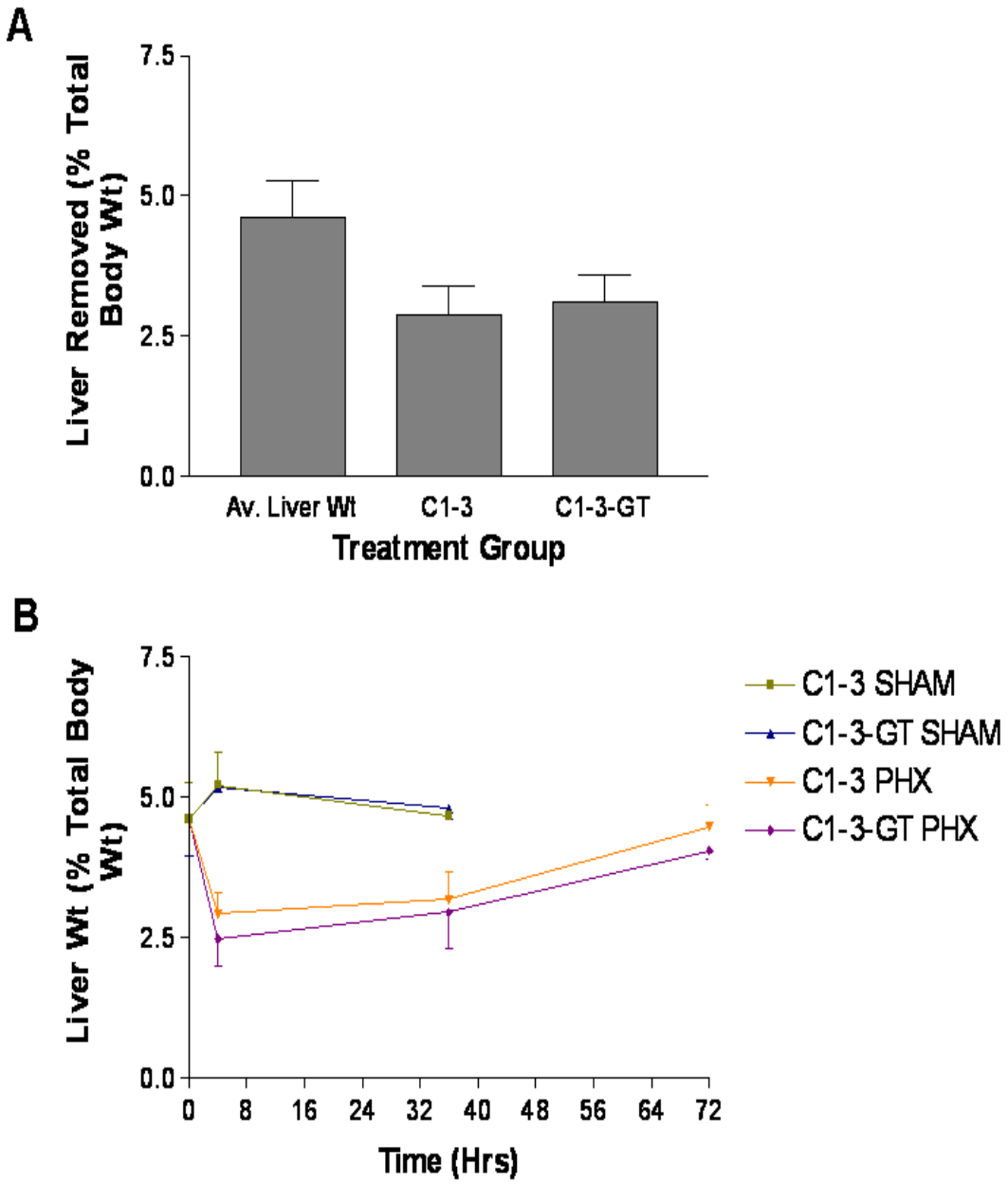

Figure 5-5 Assessment of liver regeneration using liver weight. A: Animals were weighed prior to surgery and the amount of liver removed during surgery recorded. Data are the mean and SD of the percentage of total liver removed with respect to (wrt) body weight for all C1-3 and C1-3-GT treatment groups. Average liver weight is the mean and SD from 5 wild type C57Bl6 mice which were weighed prior to schedule 1 killing and their liver weights noted. B: At each time point, animals were weighed prior to schedule 1 sacrifice and the remaining liver removed and weighed. Data represent the remaining liver weight wrt body weight. Data are the mean and SD for each treatment group at each specified time point. Animal group numbers: C1-3 4hr n=5; 36hr n=6; 72hr n=4. C1-3-GT 4hr n=4; 36hr n=3; 72hr n=4. Sham n=4 per treatment group and time point.

Figure 5-5B displays the remaining liver weight, once the animal has been sacrificed, as a percentage of body weight. The graph shows that whilst the liver of the sham mice remains relatively stable, there is a sharp decrease in liver weight in mice subjected to PHx at 4hr followed by a gradual increase in weight over 36-72hrs. This clearly demonstrates that the livers in these mice are

regenerating however no significant differences were observed between the treatment groups.

Following sacrifice serum was sent for analysis of the liver enzymes ALT and ALP. These enzymes are markers of hepatocyte damage and cholestasis respectively, however since PHx does not incur much damage to the liver or blockage of bile flow it was expected that there should be no difference in these enzymes between the treatment groups. The results are shown in figure 5-6.

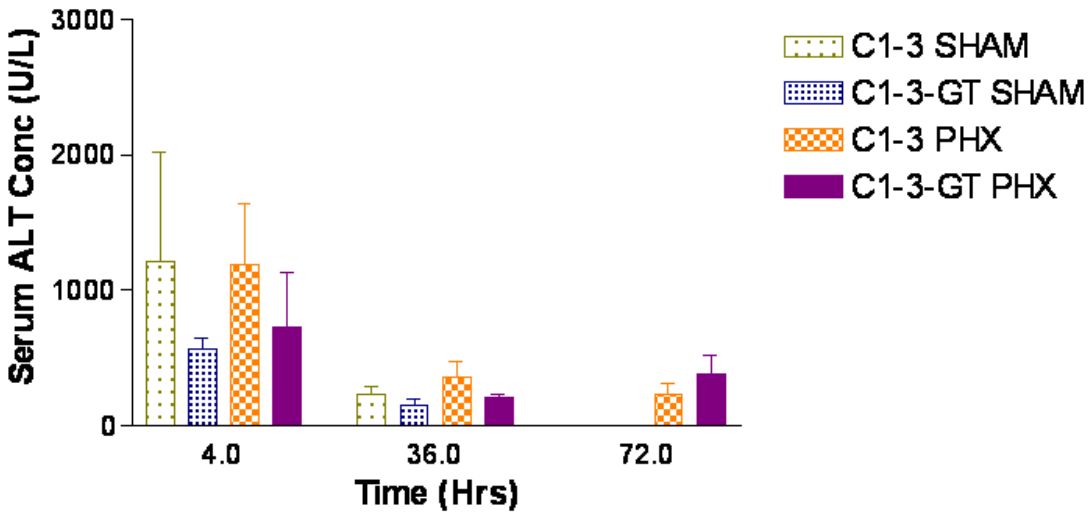

Figure 5-6 ALT serum concentration in partial hepatectomy and sham mice. Mice were schedule 1 killed and whole blood was removed and allowed to clot at room temperature for 1hr. Serum was removed following centrifugation and diluted in 0.9% sodium chloride. All serum samples were analysed by Newcastle Clinical Biochemistry Department. Data are the mean and SD for each treatment group. Animal group numbers: C1-3 4hr n=5; 36hr n=6; 72hr n=4. C1-3-GT 4hr n=4; 36hr n=3; 72hr n=4. Sham n=3 per treatment group and time point.

Interestingly, ALT levels rose in both sham and PHx groups at 4hrs (Figure 5-6), possibly the result of the surgical procedure itself, nevertheless there were no significant differences between groups. As expected, ALP remained below threshold limits thus could not be accurately measured.

To investigate whether the hepatic myofibroblasts had in fact been targeted and depleted by C1-3-GT, portions of the liver from each group were stained for the presence of αSMA positive myofibroblasts. Slides from olive oil control and 4wk CCl_4 mice were included as staining controls since it is widely known that CCl_4 treatment elicits hepatic myofibroblast proliferation, representative images are shown in figure 5-7. Upon inspection of the tissue under the light microscope, it

was discovered that α-SMA positive cells were present in specific regions of the tissue, and more importantly they were surrounding either the centrilobular veins or the portal tracts. Thus, for quantification 10 random PT regions and 10 random CLV regions were photographed at x200 magnification and the number of positive cells counted. An image representing each treatment group and time points are shown in figures 5-8 to 5-9. The images show that 4wk CCl_4 treatment resulted in an increase in the number of αSMA positive hepatic myofibroblasts surrounding the CLV only. However, only a few αSMA positive hepatic myofibroblasts are observed surrounding the PT and CLV in PHx mice suggesting that they are not a major cell involved in the response to PHx unlike CCl_4 treatment. Quantification of αSMA positive cells is shown in figure 5-10.

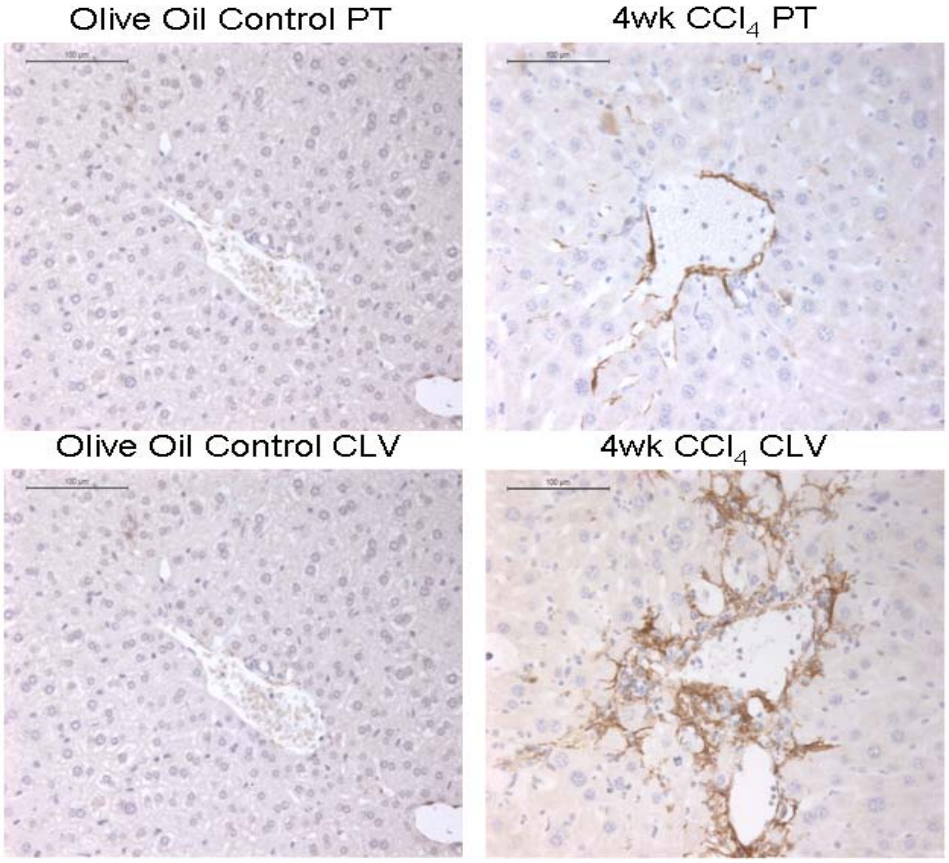

Figure 5-7 Immunohistochemical staining of αSMA cells in olive oil control and 4wk CCl4 liver tissue. Formalin fixed paraffin embedded tissue samples from each animal were cut into 4μm sections. Sections were dewaxed, subjected to heat induced antigen retrieval, blocked and incubated for 1hr with mouse anti αSMA-FITC antibody. After extensive washing, bound antibody was detected with rabbit anti FITC-HRP secondary antibody and visualised with DAB chromagen. Finally, sections were counterstained with haematoxylin and mounted. All images taken at x200 magnification. The images from the olive oil control and 4wk CCl_4 groups are representative of 5 individual animals. Images are representative of the 10 random PT and CLV photographed from each treatment group. Scale bar=100μm.

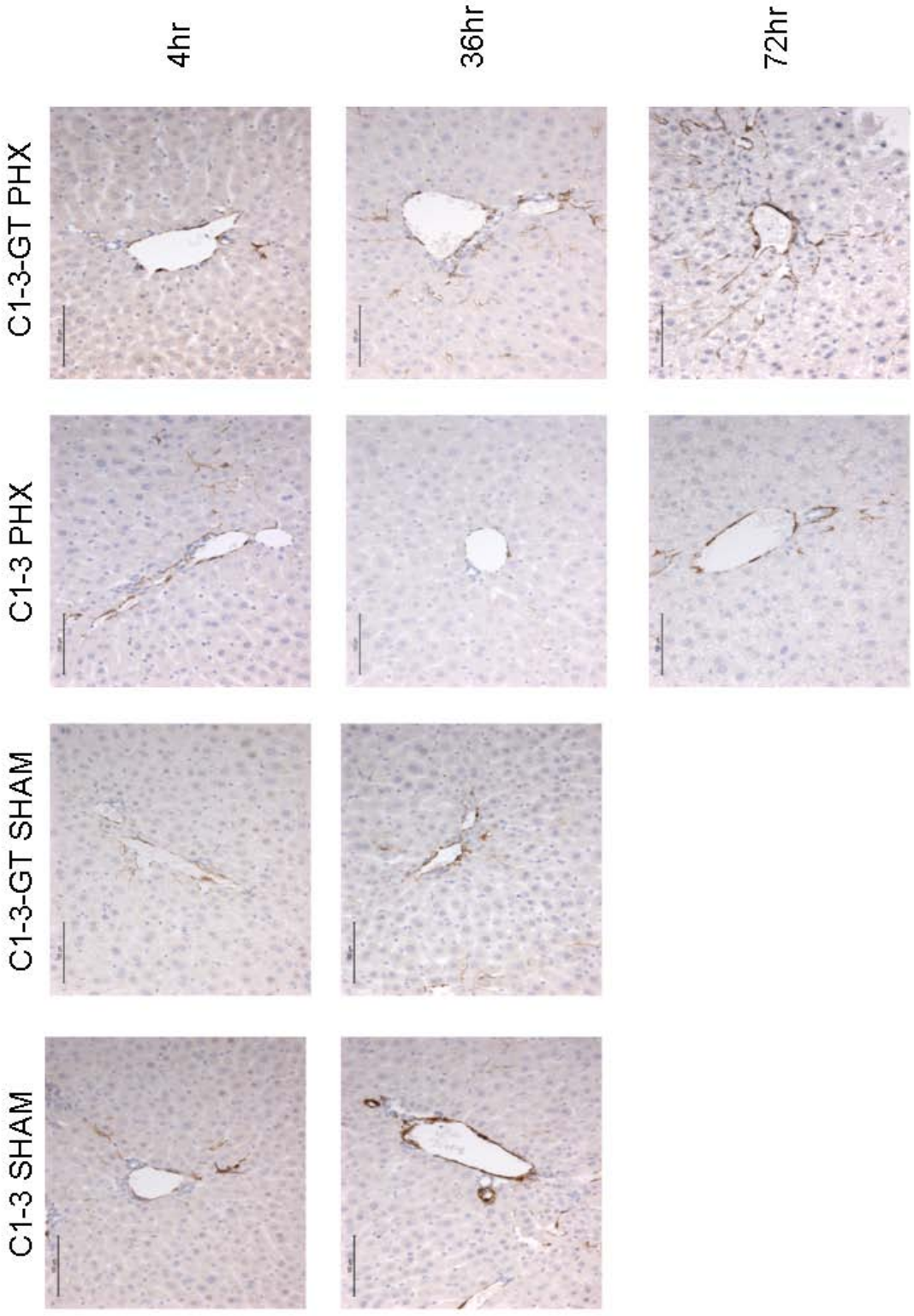

Figure 5-8 Immunohistochemical staining of α-SMA cells surrounding PT. Formalin fixed paraffin embedded tissue samples from each animal were cut into 4µm sections. Sections were dewaxed, subjected to heat induced antigen retrieval, blocked and incubated for 1hr with mouse anti αSMA-FITC antibody. After extensive washing, bound antibody was detected with rabbit anti FITC-HRP secondary antibody and visualised with DAB chromagen. Finally, sections were counterstained with haematoxylin and mounted. All images taken at x200 magnification. Images are representative of the 10 random PT photographed from each treatment group. Scale bar=100µm. Animal group numbers: C1-3 4hr n=5; 36hr n=6; 72hr n=4. C1-3-GT 4hr n=4; 36hr n=3; 72hr n=4. Sham n=3 per treatment group and time point.

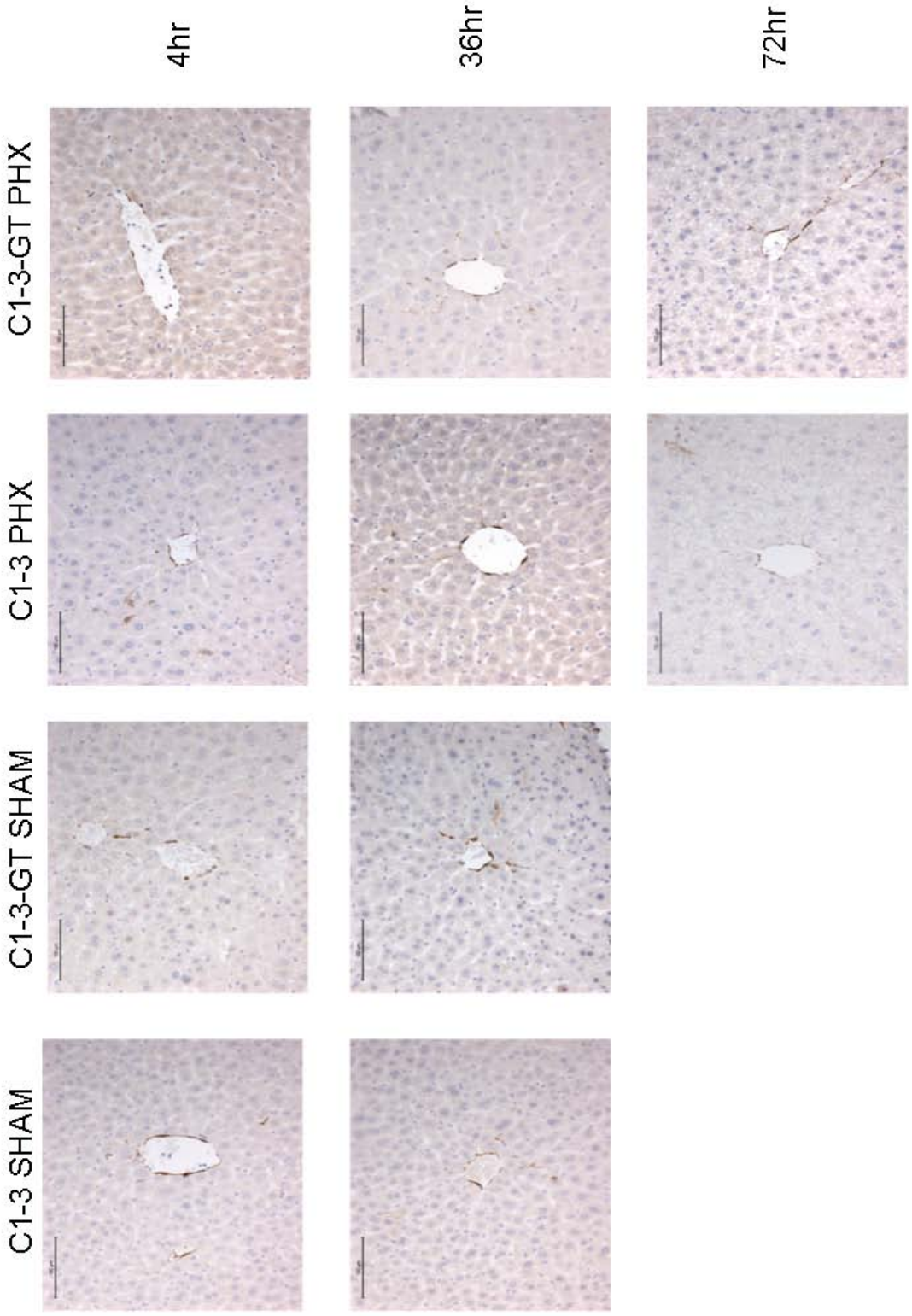

Figure 5-9 Immunohistochemical staining of α-SMA cells surrounding CLV. Formalin fixed paraffin embedded tissue samples from each animal were cut into 4µm sections. Sections were dewaxed, subjected to heat induced antigen retrieval, blocked and incubated for 1hr with mouse anti αSMA-FITC antibody. After extensive washing, bound antibody was detected with rabbit anti FITC-HRP secondary antibody and visualised with DAB chromagen. Finally, sections were counterstained with haematoxylin and mounted. All images taken at x200 magnification. Images are representative of the 10 random CLV photographed from each treatment group. Scale bar=100µm. Animal group numbers: C1-3 4hr n=5; 36hr n=6; 72hr n=4. C1-3-GT 4hr n=4; 36hr n=3; 72hr n=4. Sham n=3 per treatment group and time point.

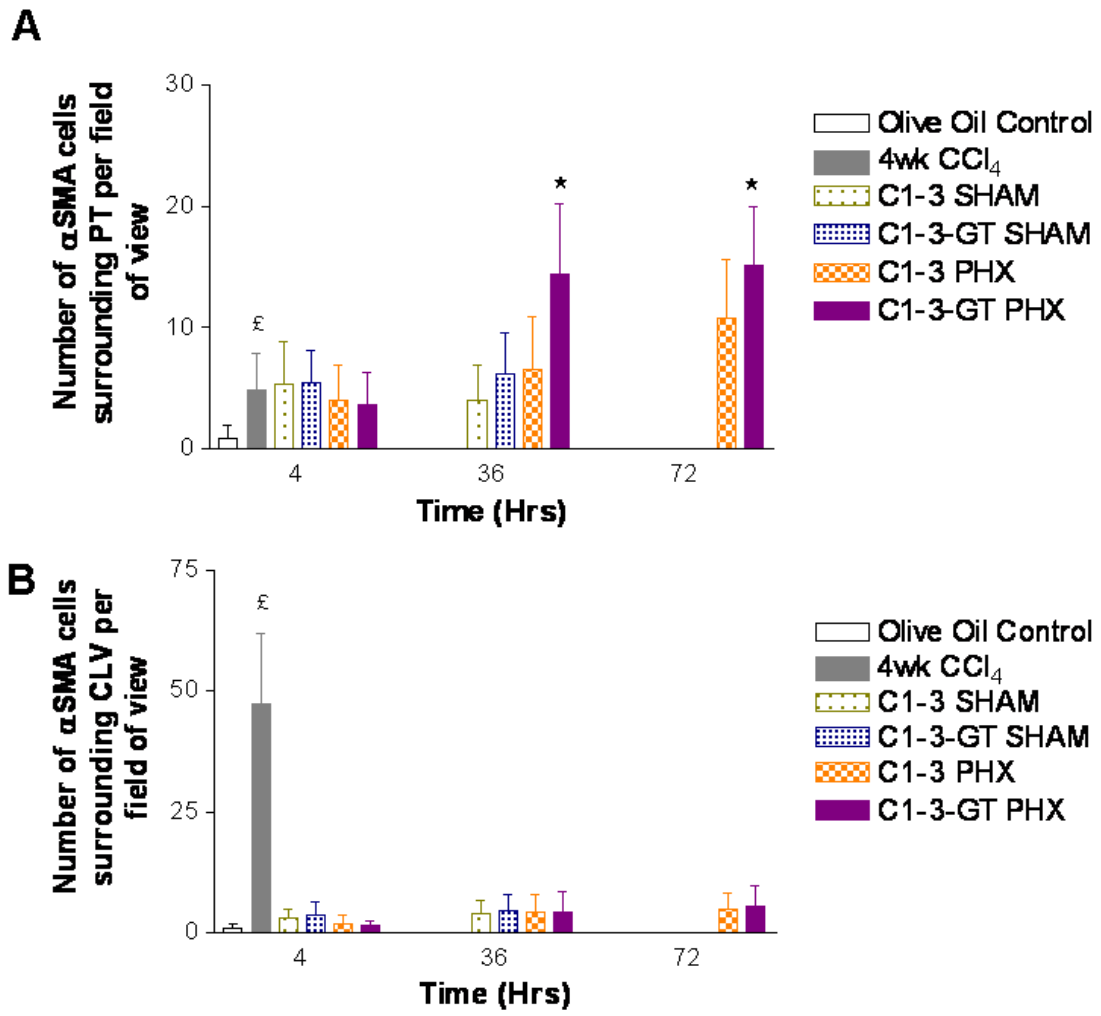

Figure 5-10 Quantification of αSMA cells around PT and CLV. For quantification, pictures were taken around 10 random PT (A) and CLV (B) at x20 magnification and the number of αSMA positive cells with clear nuclear staining counted. Data are the mean and SD of the number of αSMA cells for each treatment group at each time point and were tested for statistical significance using Student's two tailed T test. * represents significance between C1-3-GT PHX in comparison to C1-3 PHX ($p<0.001$); £ represent statistical significance between no treatment and 4wk CCl_4 ($p<0.0001$). The data from the no treatment and 4wk CCl_4 groups are representative of 5 individual animals and 10 random fields of view for both PT and CLV. PHx animal group numbers: C1-3 4hr n=5; 36hr n=6; 72hr n=4. C1-3-GT 4hr n=4; 36hr n=3; 72hr n=4. Sham n=3 per treatment group and time point.

Treatment of mice with C1-3-GT resulted is a significant increase in the number of αSMA positive cells surrounding portal tracts at 36 and 72hrs (Figure 5-10A) whereas no significant difference was observed between the treatment groups of αSMA positive cells around centrilobular veins (Figure 5-10B). The αSMA counts in the 4 wk CCl_4 treated animals show that liver regeneration following PHx invokes the proliferation of hepatic myofibroblasts surrounding PT rather than the CLV.

Next, RT-PCR was used to quantify total gene expression of αSMA in liver samples from each treatment group and normalised to an 18S rRNA standard. The data in figure 5-11 show a significant increase in expression of the αSMA gene 4hrs after surgery in C1-3-GT treated PHx mice in comparison to the C1-3 PHx controls. This increase is mirrored by an increase in the number of αSMA positive cells at 36 and 72hr in C1-3-GT PHx mice (figure 5-10).

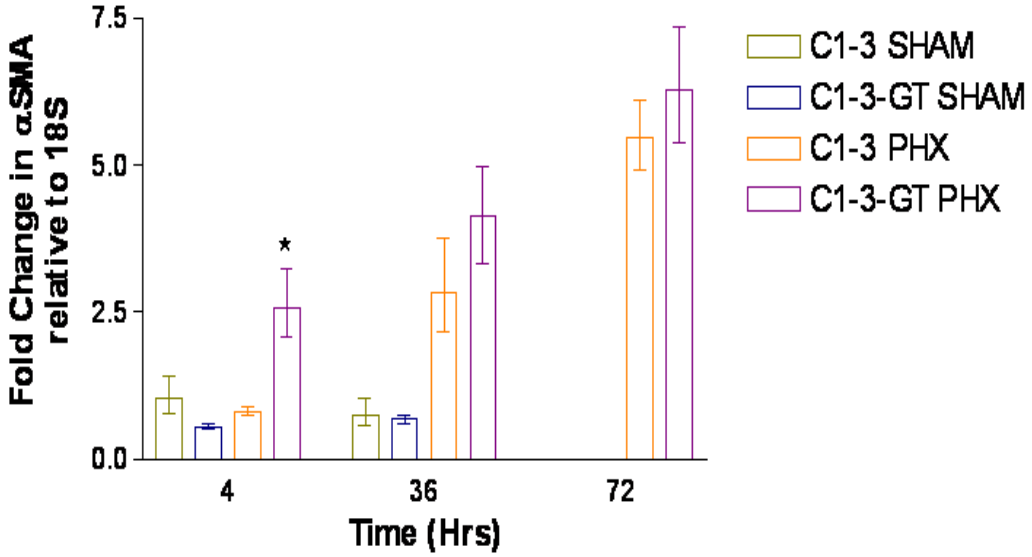

Figure 5-11 Relative gene expression levels of α-SMA sham and PHx mice. RNA was isolated from each mouse liver using Trizol, quantified and reverse transcribed using oligo dT. RT-PCR was carried out for 40 cycles and analysed using Applied Biosystems TaqMan software. Data are the mean and SD of the fold change relative to 18S standard and normalised to αSMA expression in C1-3 SHAM operated mice at 4hrs. Data tested for statistical significance using Student's two tailed T test, * represent significance between C1-3-GT PHX and C1-3 PHX ($p<0.01$). Animal group numbers: C1-3 4hr n=5; 36hr n=6; 72hr n=4. C1-3-GT 4hr n=4; 36hr n=3; 72hr n=4. Sham n=3 per treatment group and time point. All samples performed in duplicate.

To determine if the increase in αSMA gene expression and cell number was reflective of the number of synaptophysin expressing hepatic myofibroblasts, liver tissue from all animals was stained for the presence of synaptophysin and the number of positive cells surrounding PT and CLV counted at x400 magnification. Mouse pancreatic tissue, used as a positive control to ensure the antibody was working correctly, shows staining of synaptophysin positive beta cells in the pancreatic islets (figure 5-12). Liver tissue from olive oil controls and 4wk CCl_4 mice were included as a positive control since previous work by our group has demonstrated successful C1-3-GT mediated hepatic myofibroblast depletion in 8wk CCl_4 mice [126]. Representative images from these two treatment groups are shown in figure 5-13. Representative images from each treatment group and time point are illustrated in figures 5-14 and 5-15, and quantified in figure 5-16.

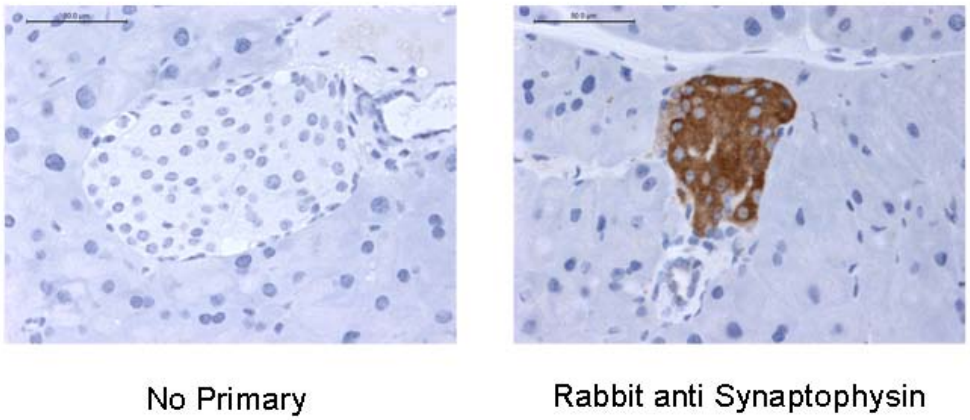

Figure 5-12 Immunohistochemical staining of synaptophysin in mouse pancreatic tissue. Formalin fixed paraffin embedded tissue samples from each animal were cut into 4µm sections. Sections were dewaxed, subjected to heat induced antigen retrieval, blocked and incubated overnight with rabbit anti synaptophysin antibody. After extensive washing, bound antibody was detected with goat anti rabbit HRP secondary antibody and visualised with DAB chromagen. Finally, sections were counterstained with haematoxylin and mounted. All images taken at x 400 magnification and are representative of the staining observed in the pancreatic tissue.

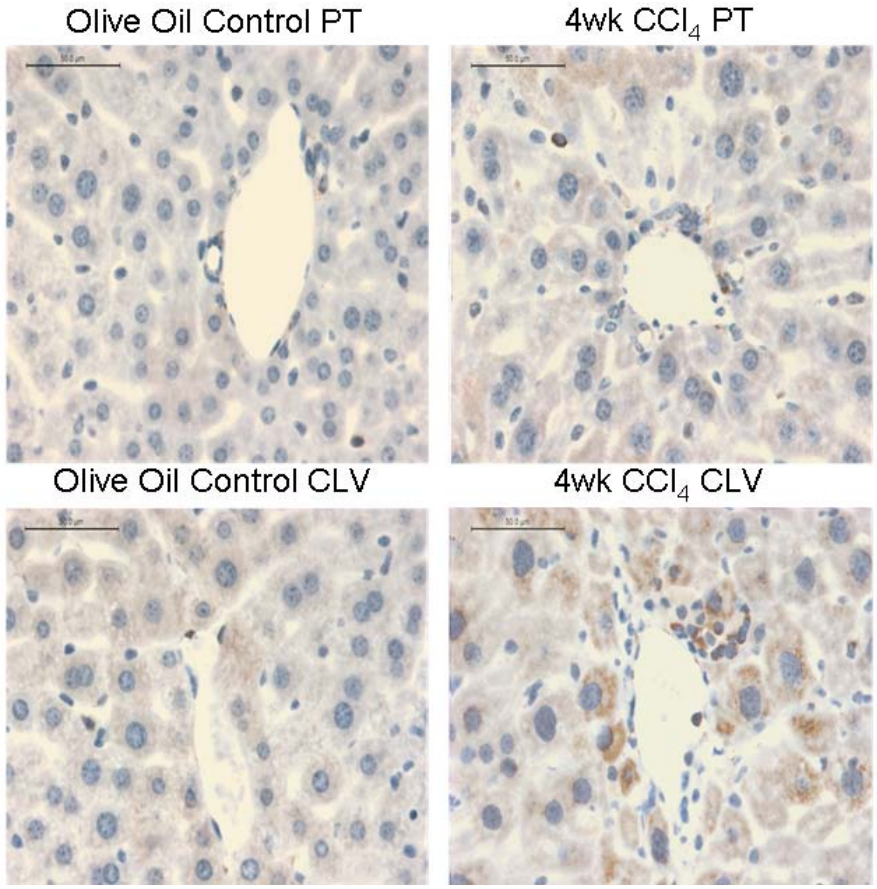

Figure 5-13 Immunohistochemical staining of synaptophysin cells in untreated and 4wk CCl_4 liver tissue. Formalin fixed paraffin embedded tissue samples from each animal were cut into 4µm sections. Sections were dewaxed, subjected to heat induced antigen retrieval, blocked and incubated overnight with Rabbit anti Synaptophysin antibody. After extensive washing, bound antibody was detected with Goat anti Rabbit HRP secondary antibody and visualised with DAB chromagen. Finally, sections were counterstained with haematoxylin and mounted. All images taken at x 400 magnification. The images from the olive oil controls and 4wk CCl_4 groups are representative of 5 individual animals. Images are representative of the 10 random PT and CLV photographed from each treatment group. Scale bar=50µm.

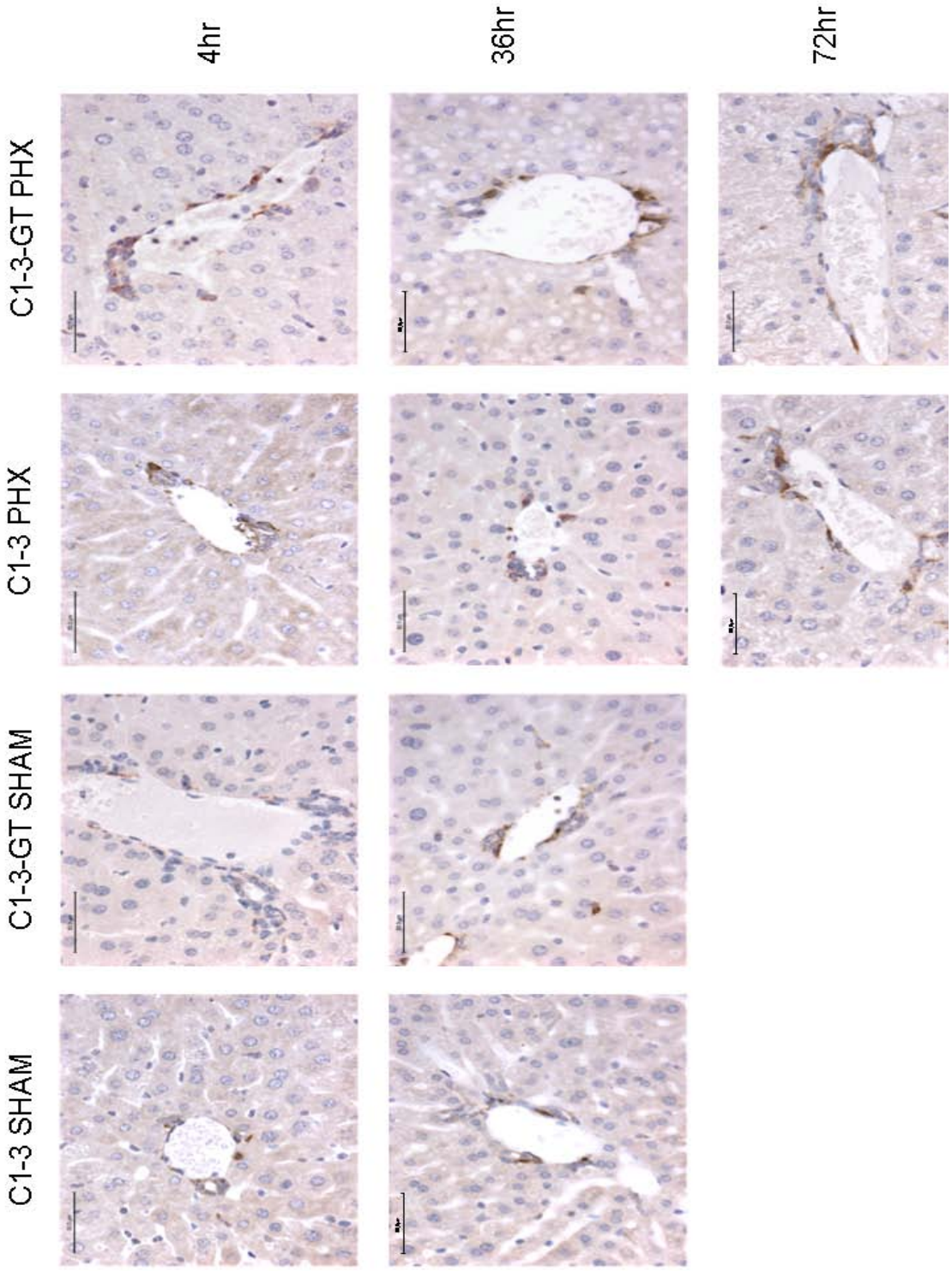

Figure 5-14 Immunohistochemical staining of synaptophysin around PT. Formalin fixed paraffin embedded tissue samples from each animal were cut into 4µm sections. Sections were dewaxed, subjected to heat induced antigen retrieval, blocked and incubated overnight with rabbit anti synaptophysin antibody. After extensive washing, bound antibody was detected with goat anti rabbit HRP secondary antibody and visualised with DAB chromagen. Finally, sections were counterstained with haematoxylin and mounted. All images taken at x 400 magnification. Images are representative of the 10 random PT photographed from each treatment group. Scale bar=50µm.

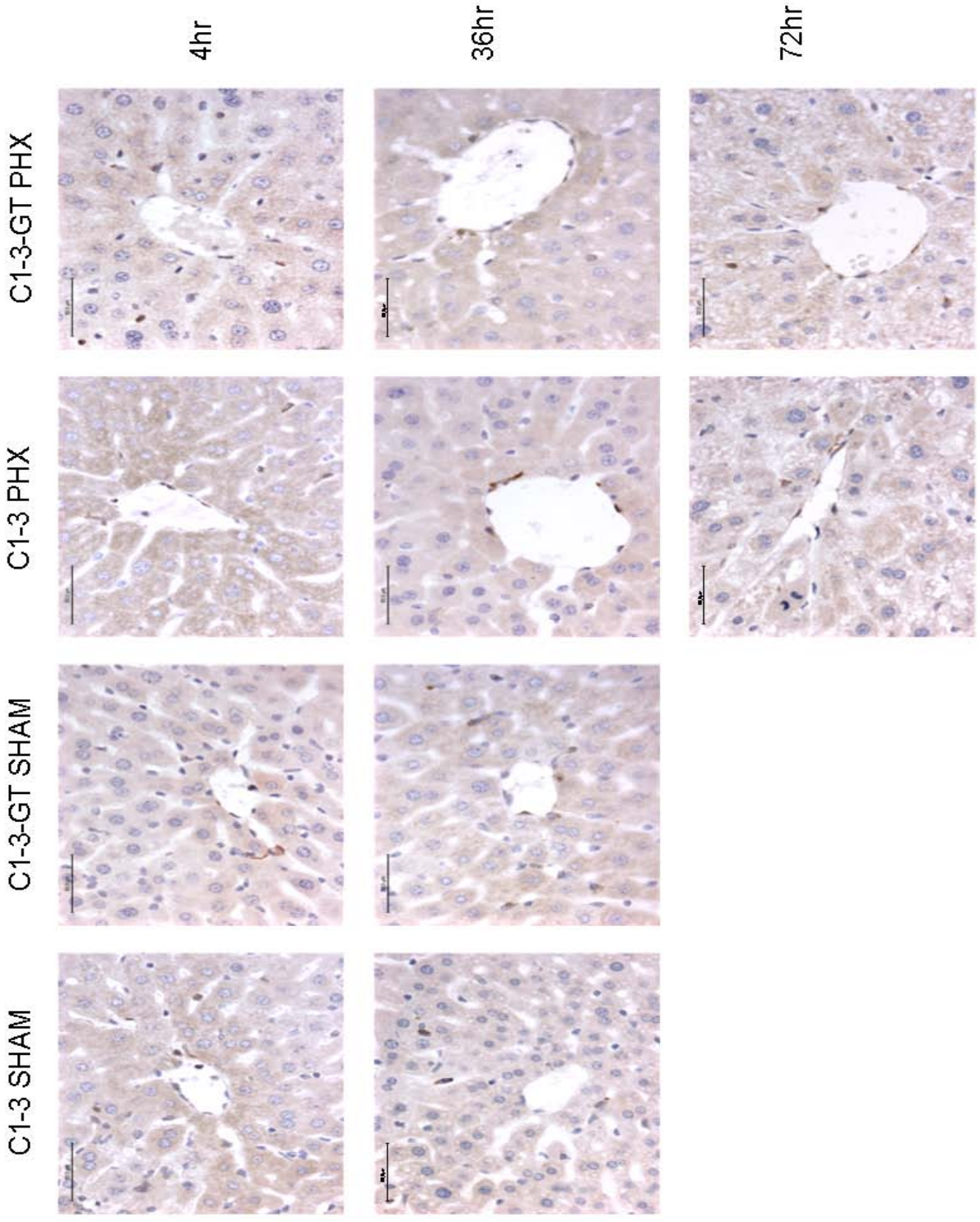

Figure 5-15 Immunohistochemical staining of synaptophysin around CLV. Formalin fixed paraffin embedded tissue samples from each animal were cut into 4µm sections. Sections were dewaxed, subjected to heat induced antigen retrieval, blocked and incubated overnight with rabbit anti synaptophysin antibody. After extensive washing, bound antibody was detected with goat anti rabbit HRP secondary antibody and visualised with DAB chromagen. Finally, sections were counterstained with haematoxylin and mounted. All images taken at x 40 magnification. Images are representative of the 10 random CLV photographed from each treatment group. Scale bar =50µm.

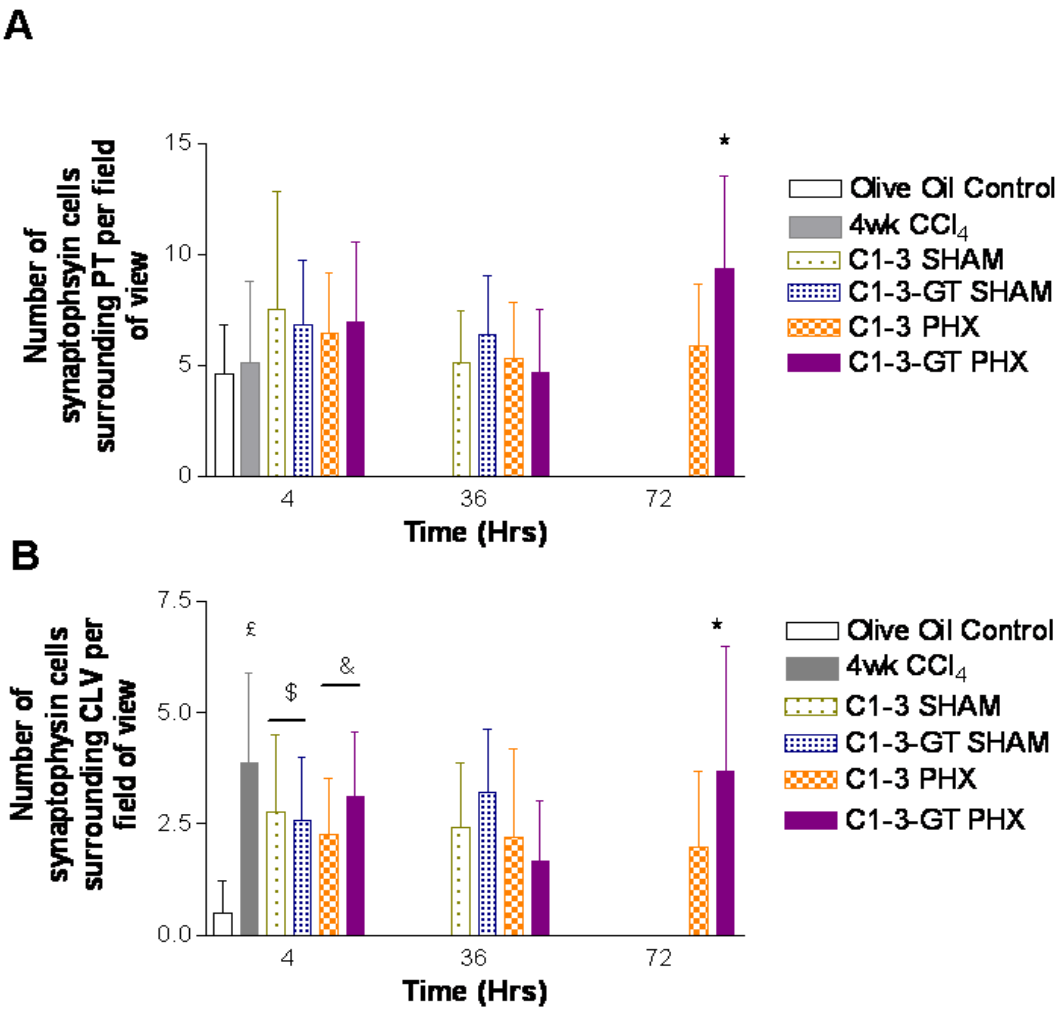

Figure 5-16 Quantification of synaptophysin cells around PT and CLV. For quantification, pictures were taken around 10 random PT (A) and CLV (B) at x400 magnification and the number of synaptophysin positive cells with clear nuclear staining counted. Data are the mean and SD of the number of synaptophysin cells for each treatment group at each time point and were tested for statistical significance using Student's two tailed T test, * represents significance between C1-3-GT PHX in comparison to C1-3 PHX (A: $p<0.005$) (B: $p<0.0005$); £ represents significance between olive oil control and 4wk CCl_4 ($p<0.0001$); $ represents a significant increase in synaptophysin positive cells surrounding CLV in sham mice in comparison to olive oil control ($p<0.0001$); & represents a significant increase in synaptophysin positive cells surrounding CLV in PHx mice in comparison to olive oil control ($p<0.0001$).

Quantification revealed a significant increase in the number of synaptophysin positive cells surrounding both PT and CLV in C1-3-GT PHx mice at 72hrs in comparison to C1-3 controls. No significant differences were observed at other time points (Figure 5-16). Synaptophysin counts from olive oil control and 4wk CCl_4 mice revealed that the number of synaptophysin positive cells surrounding CLV was significantly higher in CCl_4, sham and PHx mice in comparison to the no treatment controls. This suggests that the surgical procedure itself causes the proliferation of a few synaptophysin positive hepatic myofibroblast.

Synaptophysin gene expression was further quantified using RT-PCR and the data (figure 5-17).

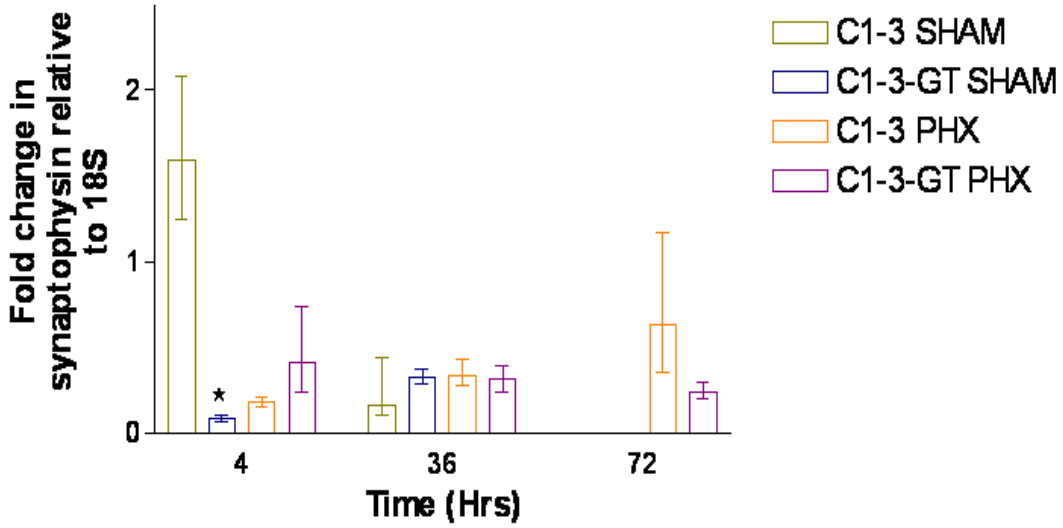

Figure 5-17 Relative gene expression levels of synaptophysin in sham and PHx mice. RNA was isolated from each mouse liver using Trizol, quantified and reverse transcribed using oligo dT. RT-PCR was carried out for 40 cycles and analysed using Applied Biosystems TaqMan software. Data are the mean and SD of the fold change relative to 18S standard and normalised to synaptophysin expression in C1-3 SHAM operated mice at 4hrs. Data tested for statistical significance using Student's two tailed T test, * represents significance between C1-3-GT SHAM and C1-3 SHAM ($p<0.05$). Animal group numbers: C1-3 4hr n=5; 36hr n=6; 72hr n=4. C1-3-GT 4hr n=4; 36hr n=3; 72hr n=4. Sham n=3 per treatment group and time point. All samples performed in duplicate.

Whilst C1-3-GT caused a significant decrease in synaptophysin gene expression in sham mice at 4hrs (Figure 5-17), no significant difference were observed in the PHx groups at any of the time points. Furthermore, at 36hrs there are no significant differences in synaptophysin gene expression between the treatment groups which are reflective of the quantified IHC staining in figure 5-16.

Liver regeneration begins with the priming of hepatocytes to respond to growth factors in order to begin the 2-3 rounds of proliferation required to restore liver mass. The two key cytokines implicated in this process are TNFα and IL-6, which are produced by kupffer cells and hepatic myofibroblasts, were quantified by RT-PCR and are shown in figure 5-18.

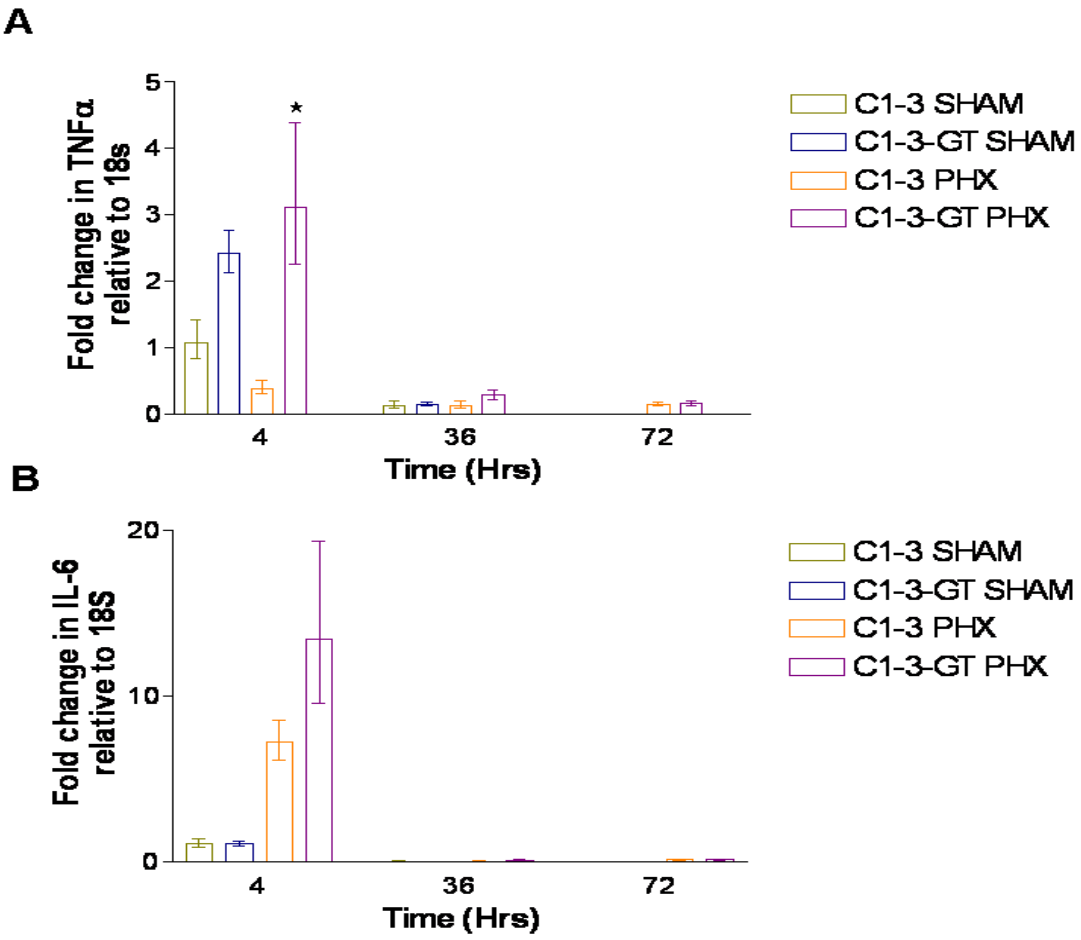

Figure 5-18 Relative gene expression levels of TNFα and IL-6 in sham and PHx mice. RNA was isolated from each mouse liver using Trizol, quantified and reverse transcribed using oligo dT. RT-PCR was carried out for 40 cycles and analysed using Applied Biosystems TaqMan software. Data are the mean and SD of the fold change relative to 18S standard and normalised to TNFα (A) or IL-6 expression (B) in C1-3 SHAM operated mice at 4hrs. Data tested for statistical significance using Student's two tailed T test, * represents significance between C1-3-GT PHX and C1-3 PHX ($p<0.001$). Animal group numbers: C1-3 4hr n=5; 36hr n=6; 72hr n=4. C1-3-GT 4hr n=4; 36hr n=3; 72hr n=4. Sham n=3 per treatment group and time point. All samples performed in duplicate.

As demonstrated in figure 5-18, PHx mice treated with C1-3-GT had a significant increase in TNFα gene expression at 4hr in comparison to mice treated with C1-3. An increase in IL-6 gene was also observed at the same point in the same treatment group however this difference was not significant. TNFα and IL-6 cytokines are only necessary during the initial stages of liver regeneration to prime the hepatocytes to respond to growth factors which may explain why gene expression levels fell dramatically at 36 and 72hrs. IL-6 protein expression was also quantified by immunohistochemistry using an anti-IL6 antibody. Positive cells were counted using the same guidelines set up for the αSMA staining. Figures 5-19 and 5-20 are representative images from each treatment group at each time point.

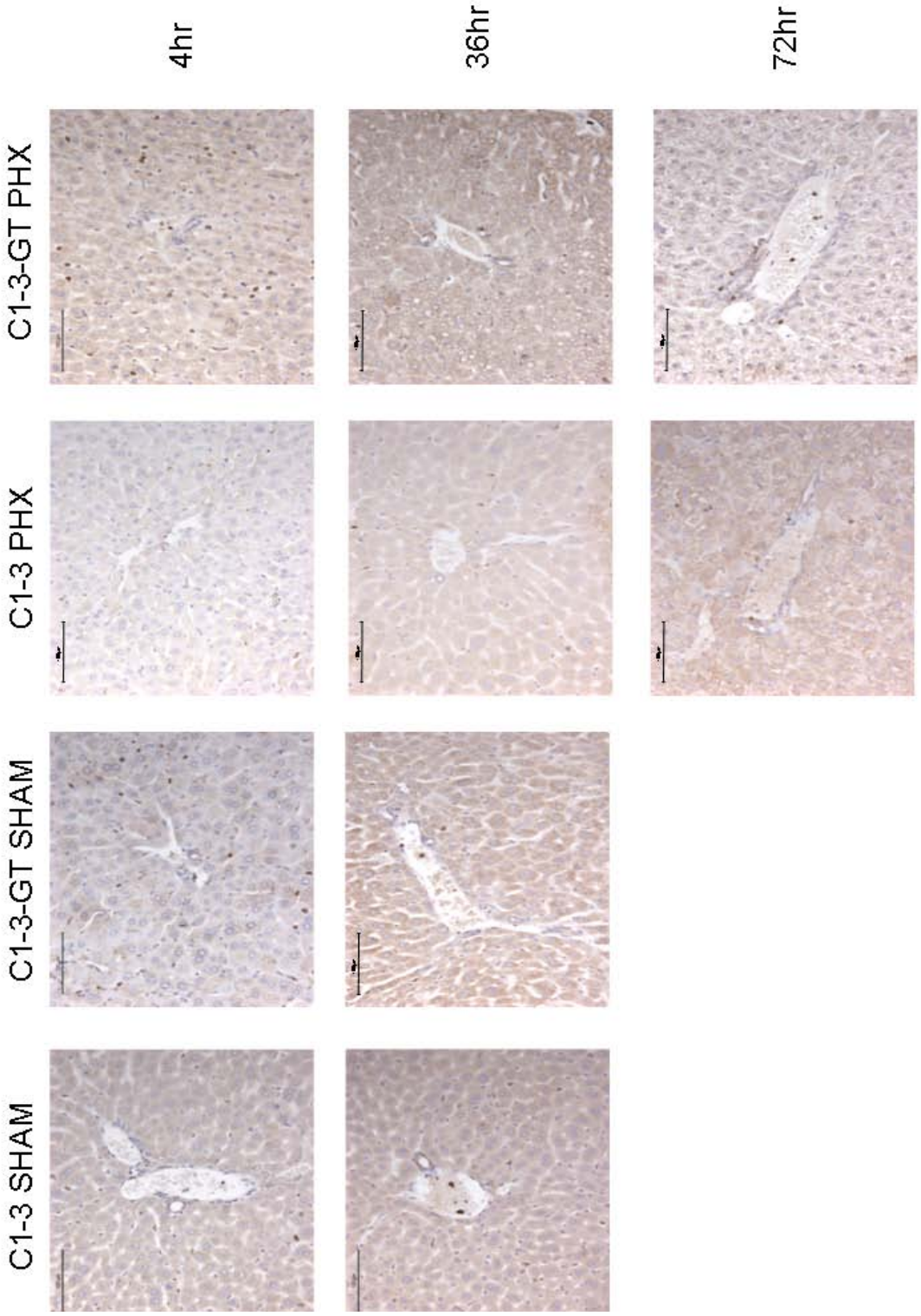

Figure 5-19 Immunohistochemical staining of IL-6 around PT. Formalin fixed paraffin embedded tissue samples from each animal were cut into 4µm sections. Sections were dewaxed, subjected to heat induced antigen retrieval, blocked and incubated overnight with rabbit anti IL-6 antibody. After extensive washing, bound antibody was detected with goat anti rabbit HRP secondary antibody and visualised with DAB chromagen. Finally, sections were counterstained with haematoxylin and mounted. All images taken at x 200 magnification. Images are representative of the 10 random PT photographed from each treatment group. Scale bar=100µm.

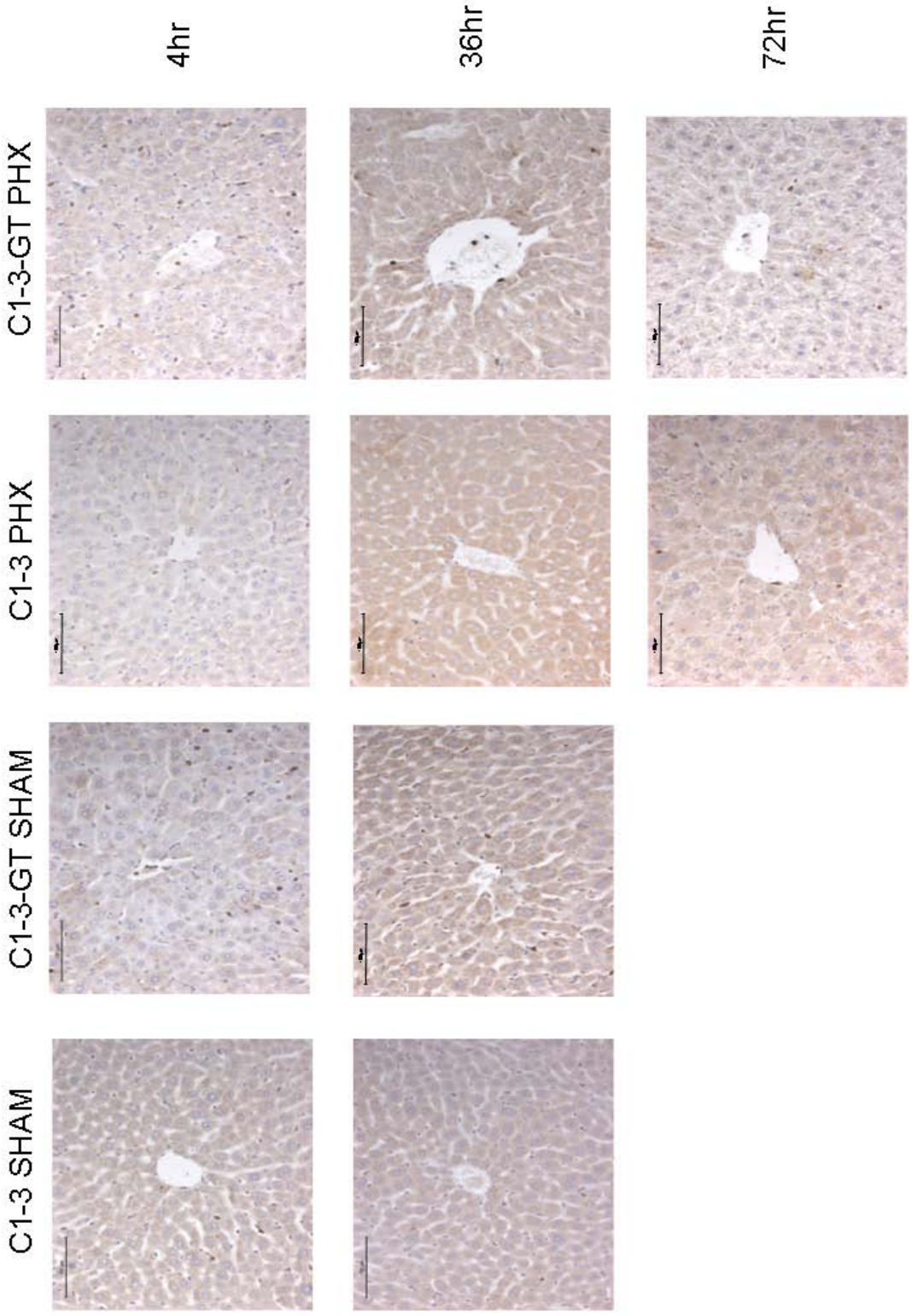

Figure 5-20 Immunohistochemical staining of IL-6 around CLV. Formalin fixed paraffin embedded tissue samples from each animal were cut into 4μm sections. Sections were dewaxed, subjected to heat induced antigen retrieval, blocked and incubated overnight with rabbit anti IL-6 antibody. After extensive washing, bound antibody was detected with goat anti rabbit HRP secondary antibody and visualised with DAB chromagen. Finally, sections were counterstained with haematoxylin and mounted. All images taken at x 200 magnification. Images are representative of the 10 random CLV photographed from each treatment group. Scale bar=100μm.

Both groups treated with C1-3-GT saw a significant increase in the number of IL-6 positive cells surrounding both portal tracts and CLV at 4hr (Figure 5-21). No differences were seen between the groups at any further time points as IL-6 is only required for the priming phase.

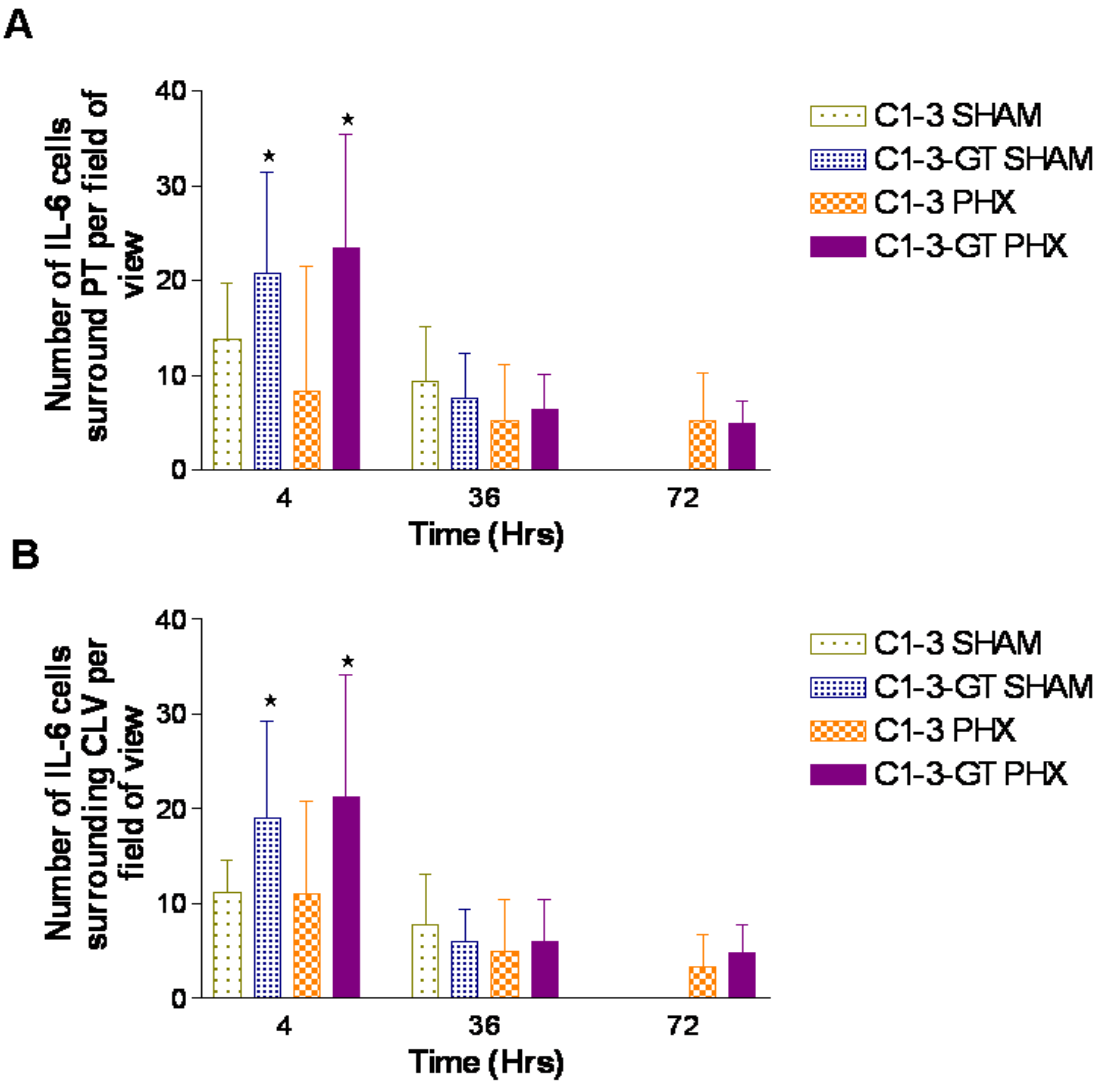

Figure 5-21 Quantification of IL-6 cells around PT and CLV. For quantification, pictures were taken around 10 random PT (A) and CLV (B) at x400 magnification and the number of IL-6 positive cells with clear nuclear staining counted. Data are the mean and SD of the number of IL-6 cells for each treatment group at each time point and were tested for statistical significance using Student's two tailed T test, * represents significance between C1-3-GT in comparison to C1-3 treatment groups (A: $p<0.005$) (B: $p<0.0005$).

Researchers have demonstrated that hepatocyte growth factor, synthesised by non-parenchymal cells particularly the hepatic myofibroblast, and epidermal growth factor, are the two main growth factors involved in stimulating the hepatocytes to proliferate. These growth factors, which are found in the tissue in the first 4hrs following PHx, were quantified using RT-PCR (figure 5-22).

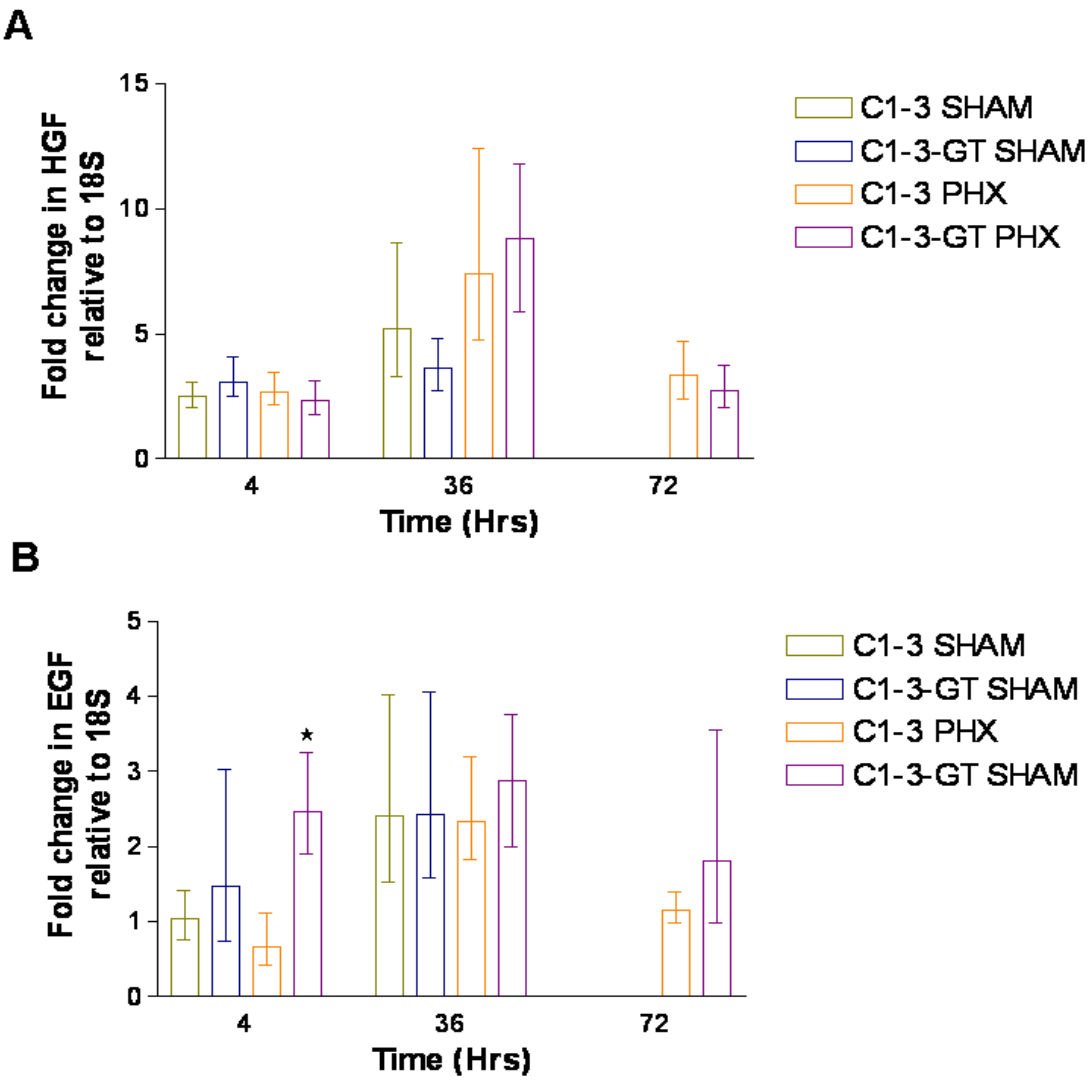

Figure 5-22 Relative gene expression levels of HGF and EGF in sham and PHx mice. RNA was isolated from each mouse liver using Trizol, quantified and reverse transcribed using oligo dT. RT-PCR was carried out for 40 cycles and analysed using Applied Biosystems TaqMan software. Data are the mean and SD of the fold change relative to 18S standard and normalised to HGF (A) or EGF (B) expression in C1-3 SHAM operated mice at 4hrs. Data tested for statistical significance using Student's two tailed T test, B: * represents significance between C1-3-GT PHX and C1-3 PHX ($p<0.05$). Animal group numbers: C1-3 4hr n=5; 36hr n=6; 72hr n=4. C1-3-GT 4hr n=4; 36hr n=3; 72hr n=4. Sham n=3 per treatment group and time point. All samples performed in duplicate.

Figure 5-22A shows that at 4hrs there was no difference in HGF gene expression between treatment groups which suggests that intracellular sources of HGF are being released to stimulate hepatocyte proliferation. At 36 and 72hr HGF gene expression was not significantly different when compared to the sham controls.

EGF gene expression did not vary significantly at 36hr and 72hr post hepatectomy (Figure 5-22B). However, C1-3-GT treatment of PHx mice resulted in a significant increase in EGF gene expression at 4hrs in comparison to the C1-3 PHx group.

To determine if the changes in growth factor and cytokine gene expression between the treatment groups had any significant effect on cellular proliferation, bromodeoxyuridine (BrDU) was injected into each animal 4 hours prior to sacrifice. BrDU is a synthetic nucleotide that is an analogue of thymidine and is incorporated into the newly synthesised DNA of proliferating cells. Images in figure 5-23 and 5-24 are typical representations of BrDU staining around CLV and PT at each time point and are quantified in figure 5-25 and 5-26. Quantification was carried out as previously described however the number of positive parenchymal (e.g. hepatocytes) and non parenchymal (e.g. hepatic myofibroblasts) cells, as distinguished by cell morphology, were counted separately.

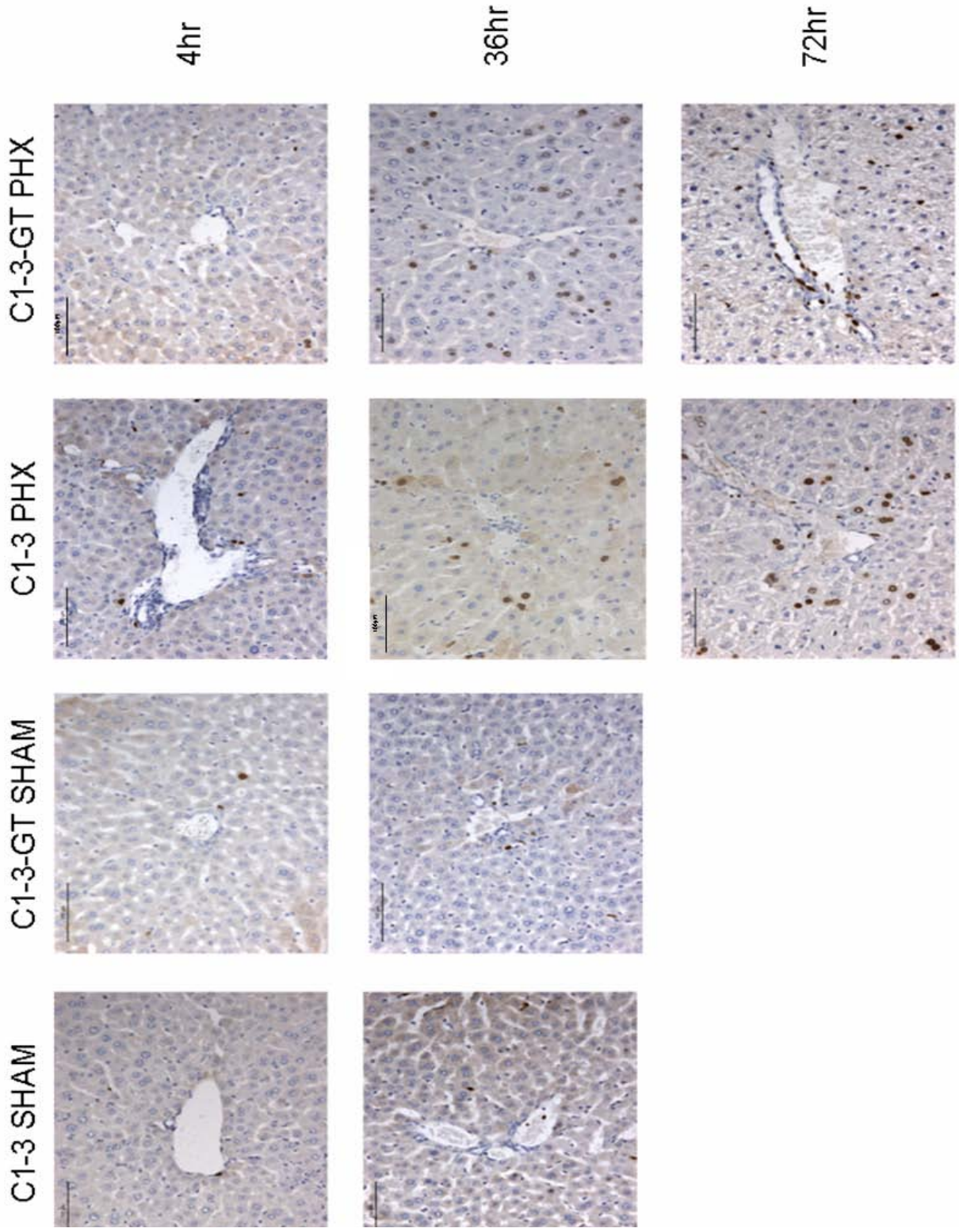

Figure 5-23 Immunohistochemical staining of BrDU around PT. Formalin fixed paraffin embedded liver tissue from each animal were cut into 4µm sections. Slides were dewaxed, subjected to heat induced antigen retrieval and incubated with mouse anti BrDU primary antibody overnight at 4°C. After extensive washing, bound antibody was detected using a goat anti mouse-HRP secondary antibody and visualised with DAB chromagen. Sections were lightly counterstained with haematoxylin and mounted with coverslips. All images taken at x200 magnification and are representative of the 10 random PT photographed from each treatment group.

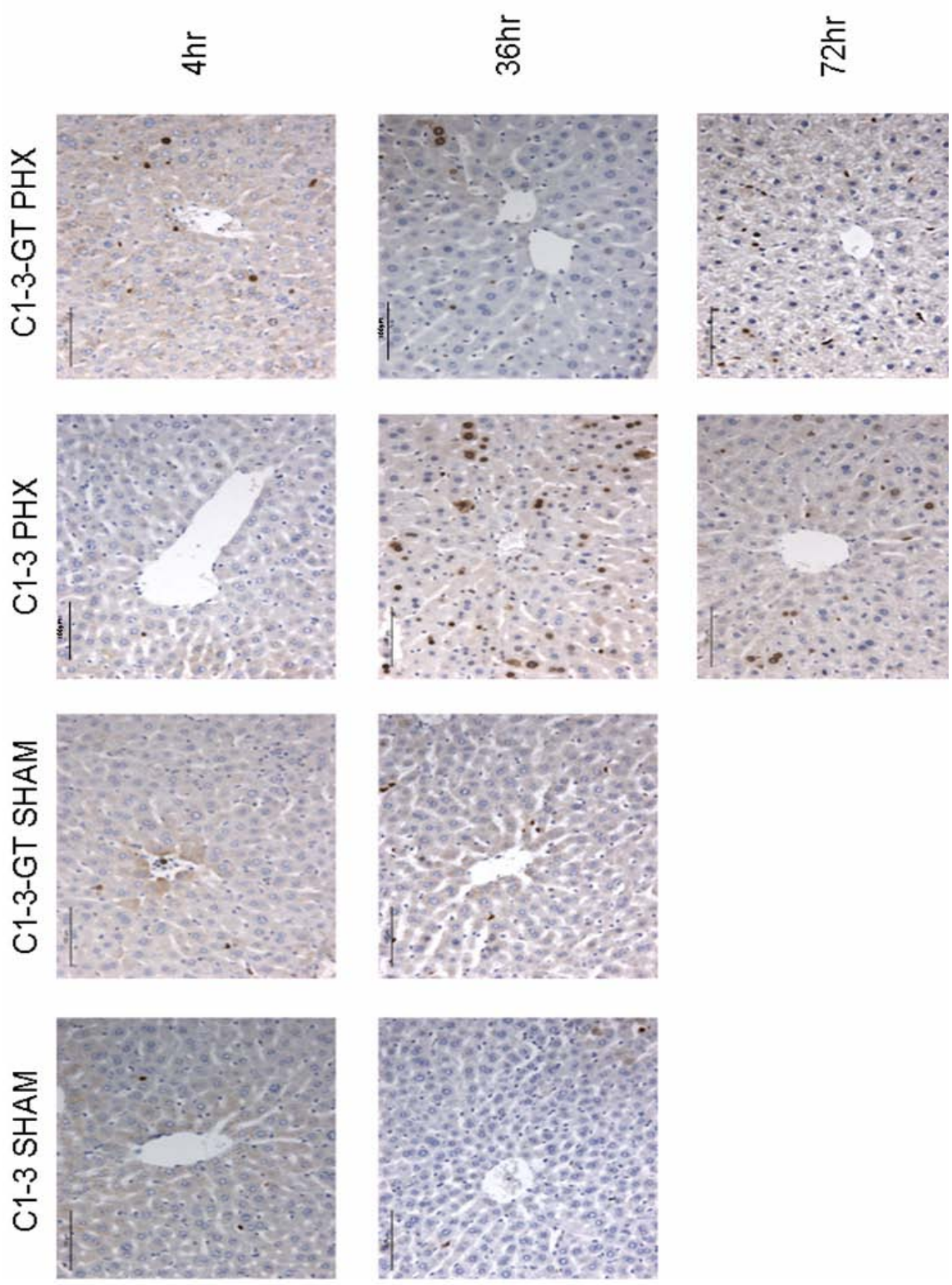

Figure 5-24 Immunohistochemical staining of BrDU around CLV. Formalin fixed paraffin embedded liver tissue from each animal were cut into 4µm sections. Slides were dewaxed, subjected to heat induced antigen retrieval and incubated with mouse anti BrDU primary antibody overnight at 4°C. After extensive washing, bound antibody was detected using a goat anti mouse-HRP secondary antibody and visualised with DAB chromagen. Sections were lightly counterstained with haematoxylin and mounted with coverslips. All images taken at x200 magnification and are representative of the 10 random CLV photographed from each treatment group.

Quantification of these cells shows that at 4hr there is a significant increase in the number of proliferating parenchymal cells surrounding both PT and CLV in PHx mice treated with C1-3-GT compared to the C1-3 PHx control (Figures 5-25A and 5-26A). C1-3-GT treatment of sham operated mice resulted in a significant decrease in the number of proliferating non parenchymal cells surrounding the PT (Figure 5-25B)

At 36hr, there is no difference in the number of BrDU positive parenchymal and non parenchymal cells in the sham groups however treatment of PHx mice with C1-3-GT results in a significant decrease in the number of BrDU positive parenchymal and non parenchymal cells surrounding both PT and CLV in comparison to the C1-3 controls (Figures 5-25 and 5-26). Finally, at 72hr there is only a significant increase in the number of non parenchymal cells surrounding PT in PHx mice treated with C1-3-GT (Figure 5-25B).

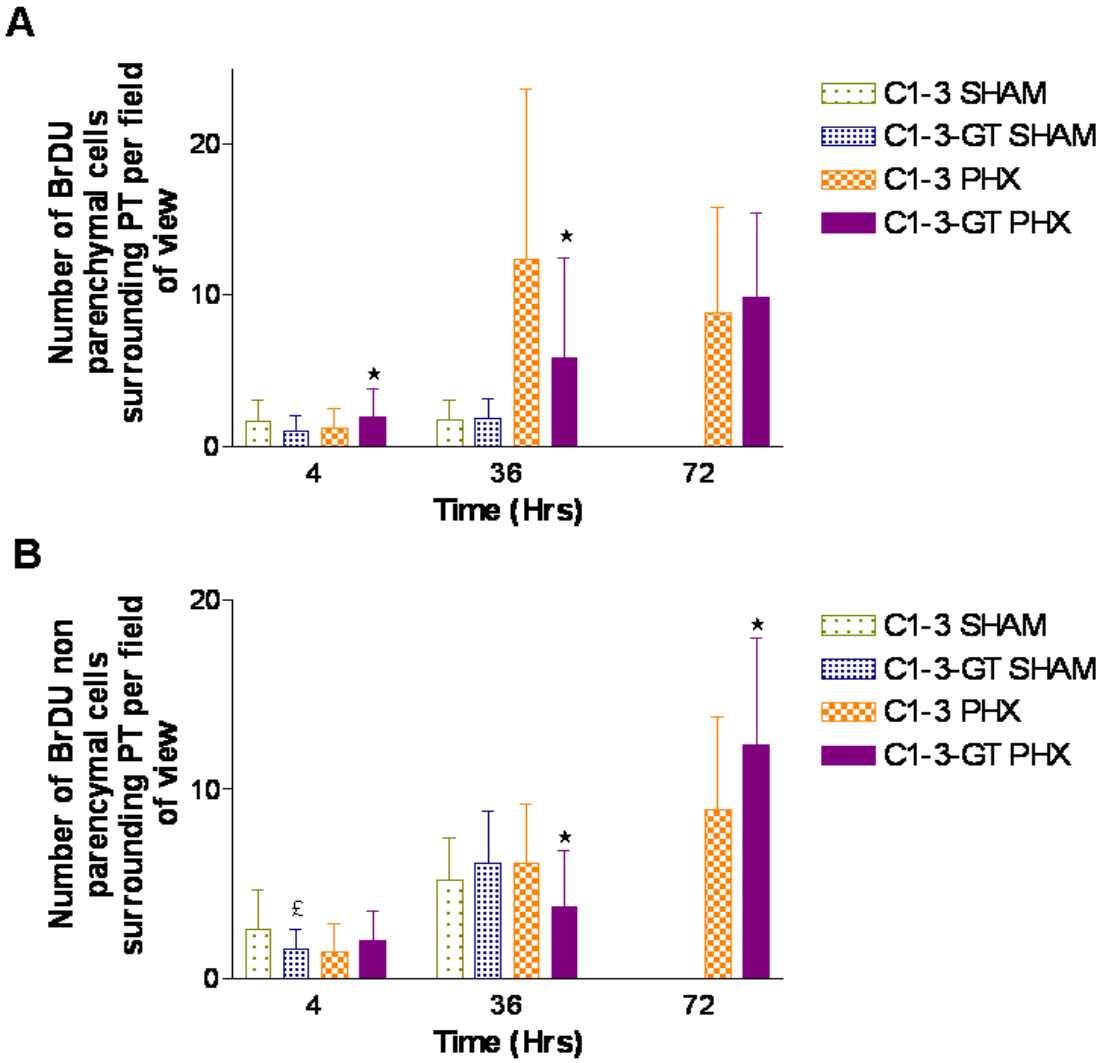

Figure 5-25 BrDU quantification of parenchymal and non parenchymal cells surrounding PT. For quantification, the number of parenchymal (A) and non parenchymal (B) cells with clear BrDU nuclear staining surrounding 10 random PT regions were counted at x200 magnification. Data presented are the mean and SD of the average number of cells for each treatment group at each time point. Statistical significance was tested using Student's two tailed T test * represents significance between C1-3-GT PHX and its respective C1-3 PHx control £ represents significance between C1-3-GT SHAM and C1-3 SHAM control. (A: 4hr $p<0.05$ 36hr $p<0.005$) (B £4hr $p<0.05$ *36hr $p<0.005$ *72hr $p<0.05$).

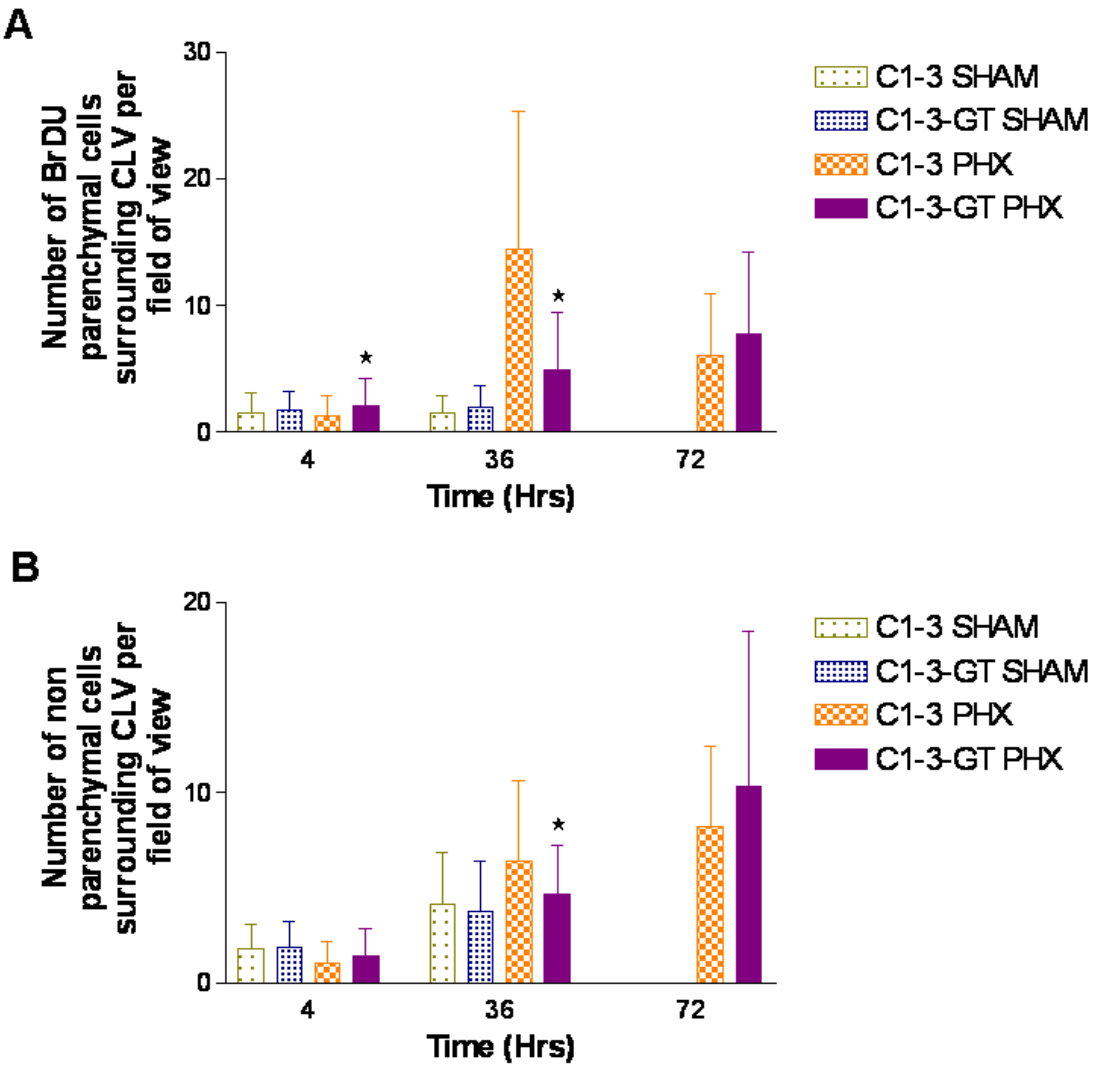

Figure 5-26 BrDU quantification of parenchymal and non parenchymal cells surrounding CLV. For quantification, the number of parenchymal (A) and non parenchymal (B) cells with clear BrDU nuclear staining surrounding 10 random CLV regions were counted at x200 magnification. Data presented are the mean and SD of the average number of cells for each treatment group at each time point. Statistical significance was tested using Student's two tailed T test, * represents significance between C1-3-GT PHX and its respective C1-3 PHX control (A: 4hr $p<0.05$ 36hr $p<0.0001$) (B: 36hr $p<0.05$).

Relative gene expression levels of the cellular markers of proliferation were quantified using TaqMan probes (figure 5-27). Cyclin D1, E1 and cyclin-dependent kinase 2 (CDK2) are essential for the transition of cells from G1 (growth) to S (synthesis) phase of the cell cycle. The data in figure 5-27A and C show that cyclin D1 and CDK2 expression is significantly higher in C1-3-GT PHx mice at 4hrs in comparison to the C1-3 control. Whilst levels of cyclin D1 remain relatively stable at 36 and 72hr in the PHx mice, there is a significant decrease in cyclin D1 expression in the sham operated mice at 36hr that correlates with the reduced number of BrDU positive parenchymal cells in figures 5-25A and 5-26A.

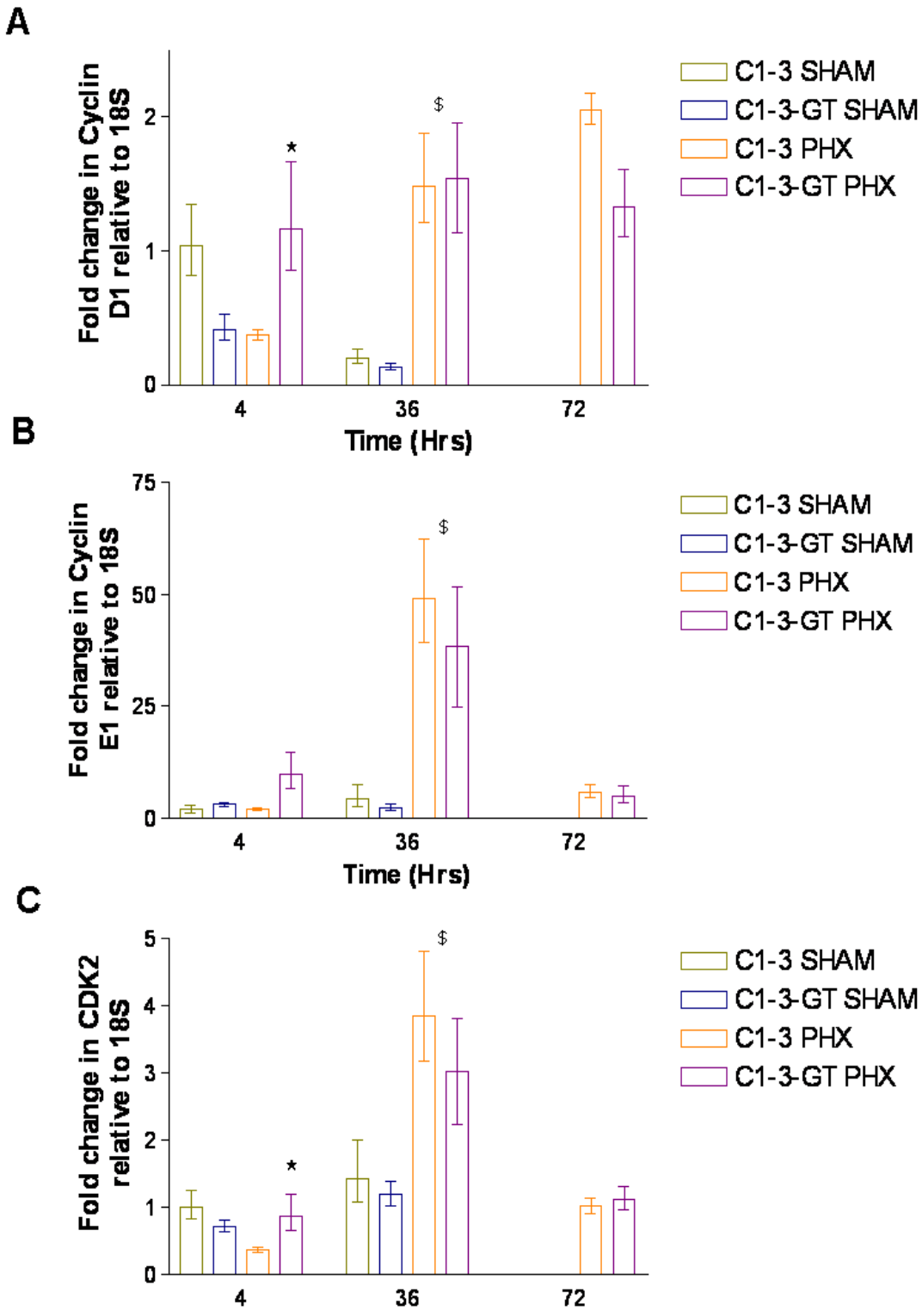

Figure 5-27 Relative gene expression levels of Cyclin D1, E1 and CDK2 in sham and PHx mice. RNA was isolated from each mouse liver using Trizol, quantified and reverse transcribed using oligo dT. RT-PCR was carried out for 40 cycles and analysed using Applied Biosystems TaqMan software. Data are the mean and SD of the fold change of cyclin D1(A), cyclin E1(B) and CDK2 (C) relative to 18S standard and normalised to expression levels in C1-3 SHAM operated mice at 4hrs. Data tested for statistical significance using Student's two tailed T test, A/C: * represents significance between C1-3-GT PHX vs. C1-3 PHX ($p<0.005$); $ represents significance between PHX vs. SHAM mice at 36hrs ($p<0.0005$). Animal group numbers: C1-3 4hr n=5; 36hr n=6; 72hr n=4. C1-3-GT 4hr n=4; 36hr n=3; 72hr n=4. Sham n=3 per treatment group and time point. All samples performed in duplicate.

The data in figure 5-27B and C follow a similar trend, with a significant increase in cyclin E1 and CDK2 gene expression at 36hr in the PHx mice in comparison to the sham operated controls. However, unlike the BrDU data in figures 5-25 and 5-26, there are no significant differences in gene expression levels of the cellular proliferation markers between the C1-3 and C1-3-GT treatment groups.

Collagen type I is a fibrillary collagen and is one of the common components of the interstitial ECM surrounding PT and CLV. Hepatic myofibroblasts are the principal cell type involved in collagen type I production and during centrilobular induced liver fibrosis the deposition of collagen type I disrupts the basement-membrane like matrix resulting in functional impairment and organ failure. Relative expression levels of collagen type I was quantified using RT-PCR (figure 5-28). Collagen 1a1 is the gene which encodes the major component of collagen type I.

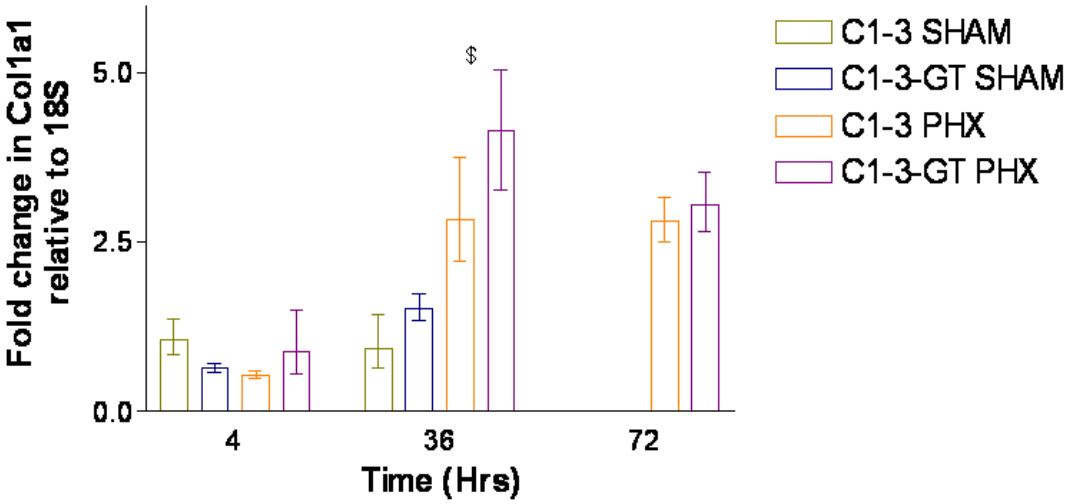

Figure 5-28 Relative gene expression levels of collagen 1a1 in sham and PHx mice. RNA was isolated from each mouse liver using Trizol, quantified and reverse transcribed using oligo dT. RT-PCR was carried out for 40 cycles and analysed using Applied Biosystems TaqMan software. Data are the mean and SD of the fold change relative to 18S standard and normalised to expression levels in C1-3 SHAM operated mice at 4hrs. Data tested for statistical significance using Student's two tailed T test, $ represents significance between PHX vs. SHAM mice at 36hrs ($p<0.001$). Animal group numbers: C1-3 4hr n=5; 36hr n=6; 72hr n=4. C1-3-GT 4hr n=4; 36hr n=3; 72hr n=4. Sham n=3 per treatment group and time point. All samples performed in duplicate.

The data in figure 5-28 show a significant increase in col1a1 expression in PHx mice at 36hr following surgery in comparison to sham controls which would correlate with the deposition of interstitial matrix around new PT and CLV. Although a significant increase in hepatic myofibroblasts around PT was observed in C1-3-GT PHx mice at 36 and 72hrs (figure 5-10), this was not associated with an increase in col1a1 gene expression.

Following PHx the liver grows back to its precise mass and does not exceed it with molecules such as TGFβ, IL-1β and Activin A implicated in controlling the process however their exact mechanisms still remain elusive. Relative expression levels of TGFβ1 and IL-1β were quantified by RT-PCR and are illustrated in figure 5-29.

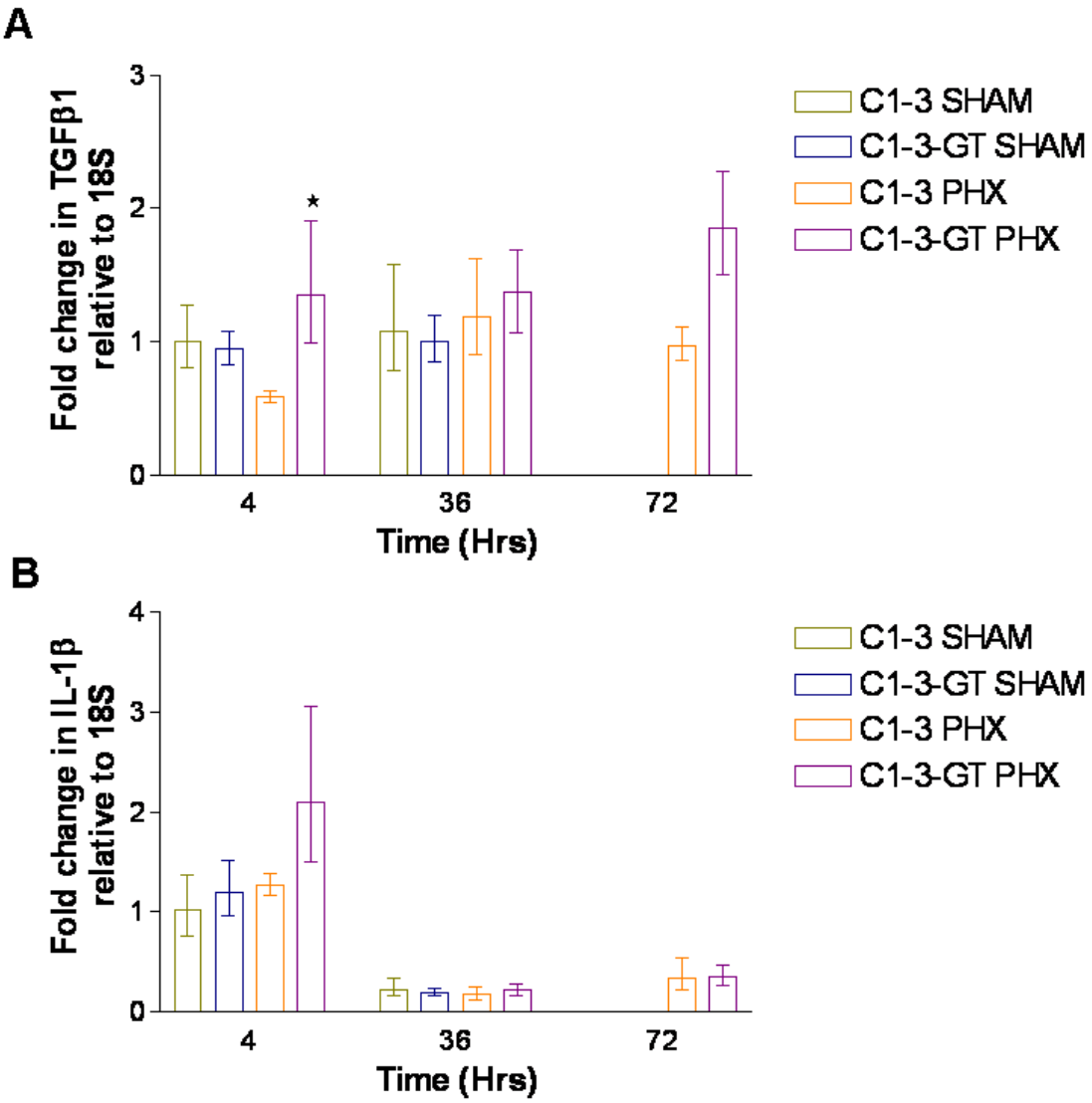

Figure 5-29. Relative gene expression levels of TGFβ1 and IL-1β in sham and PHx mice. RNA was isolated from each mouse liver using Trizol, quantified and reverse transcribed using oligo dT. RT-PCR was carried out for 40 cycles and analysed using Applied Biosystems TaqMan software. Data are the mean and SD of the fold change of TGFβ (A) and IL-1β (B) relative to 18S standard and normalised to expression levels in C1-3 SHAM operated mice at 4hrs. Data tested for statistical significance using Student's two tailed T test, A/C: * represents significance between C1-3-GT PHX vs. C1-3 PHX ($p<0.05$). Animal group numbers: C1-3 4hr n=5; 36hr n=6; 72hr n=4. C1-3-GT 4hr n=4; 36hr n=3; 72hr n=4. Sham n=3 per treatment group and time point. All samples performed in duplicate.

It was predicted that the gene expression levels of these two cytokines would peak around 72hrs after PHx surgery since cellular proliferation would be almost completed and liver mass almost returned to normal. The data in figure 5-29A shows a significant increase in TGFβ gene expression in C1-3-GT mice at 4hrs in comparison to C1-3 controls. This may account for the decrease in cellular proliferation, as measured by BrDU incorporation, observed in the C1-3-GT mice at 36hrs (figures 5-25 and 5-26). However, PHx surgery did not affect the relative gene expression levels of both cytokines since expression remained relatively constant between all treatment groups at both 36 and 72hr time points. This does not necessarily mean that these cytokines are not involved in the inhibition of proliferation, for example IL-1β is intracellularly stored, thus it can be readily released without the need for gene transcription.

5.3 Discussion

The liver has the remarkable ability to regenerate following injury or even when up to 75% of the tissue is lost, and it is this response which may be critical in determining the outcome of chronic disease. Typically, liver mass is restored by the proliferation of existing hepatocytes however oval cell proliferation can be induced if hepatocyte proliferation has been inhibited.

The pathways governing liver regeneration have been under investigation for many years with the two thirds partial hepatectomy model, first proposed by Higgins and Anderson in 1931 [128], providing a useful paradigm for studying organ growth [180]. Although this model was slightly modified for use with mice, it has identified key components in the initiation, proliferation and termination of liver regenerative pathways. More importantly, however, this model has shown that the liver has many redundant pathways governing each phase of regeneration which are capable of compensating if key components are inhibited/removed and tend to only delay regeneration rather than preventing it altogether.

The activation and transdifferentiation of the hepatic stellate cell into a hepatic myofibroblast has been shown to be a key event in fibrosis, furthermore its lifespan is thought to dictate the course of fibrosis leading to either cirrhosis or regression [36, 91, 100, 253]. Their role in liver regeneration is somewhat complex, since they produce key factors responsible for the priming and proliferation of hepatocytes e.g. IL-6, HGF and serotonin [131, 138, 146] yet also secrete factors responsible for the termination of liver regeneration e.g. TGFβ [259].

Few studies have actually investigated the outcome of hepatic myofibroblast depletion during liver regeneration yet many researchers are proposing that their depletion during fibrosis is crucial for disease reversal [100-102, 126, 249] which may have severe consequences for liver function and patient well being. C1-3-GT has been shown to specifically target and deplete synaptophysin positive hepatic myofibroblasts during CCl_4 induced liver injury in mice, with 60% depletion of total myofibroblasts significantly reducing fibrosis severity [126]. This chapter utilises the targeted apoptotic effects of C1-3-GT to investigate the role of hepatic myofibroblasts during the regenerative process initiated by two thirds PHx.

After successful conjugation and functional testing *in vitro*, C1-3-GT was injected into the intraperitoneal cavity of mice at crucial time points during liver regeneration, as determined by the current scientific literature. The remaining liver weight was used as a measure of liver regeneration between the treatment groups since there were no significant differences observed in the average liver weight removed during surgery.

Initial experiments set out to prove that C1-3-GT had specifically targeted and depleted synaptophysin positive hepatic myofibroblasts. Quantification of αSMA IHC staining showed a significant increase in the number of αSMA positive cells surrounding the PT at 36 and 72hrs in the PHx mice treated with C1-3-GT. This result was unexpected since previous studies have shown that C1-3-GT treatment resulted in a significant decrease in the number of αSMA positive cells [126, 249]. Interestingly, synaptophysin IHC revealed no significant differences in the number of synaptophysin cells in the first 36hrs after surgery for all treatment groups. The data suggest that the C1-3-GT has not worked *in vivo* since both the IHC and RT-PCR reveal no differences in the number of synaptophysin positive cells or any changes in gene expression at both 4 and 36hr. Furthermore, a significant increase in both αSMA and synaptophysin positive cells at 72hr would suggest that C1-3-GT treatment stimulated cellular proliferation.

The inclusion of αSMA and synaptophysin counts from untreated and 4wk CCl_4 mice revealed that the number of hepatic myofibroblasts proliferating in response to the PHx stimulus is significantly lower than CCl_4 treatment suggesting that hepatic myofibroblasts do not play a major role in liver regeneration. Furthermore, only a few synaptophysin positive cells were present in the liver tissue of the sham and PHx mice, which was similar to CCl_4 treatment, thus if any cells had in fact been depleted it may be difficult to show this.

Animal studies using knockout mice have implicated IL-6 and TNFα as the principal cytokines involved in the initiation of the regenerative process and are important in priming the resident hepatocytes to be responsive to growth factors [132, 136]. This process is believed to be instigated by TNFα, which upon binding to its receptor on non parenchymal cells in the liver stimulates the activation of the NFκB pathway and the subsequent production of IL-6. Hepatic myofibroblasts are a known source of IL-6 [131] thus it was predicted that their removal would reduce hepatocyte priming and subsequent proliferation. In this study, cytokine

levels were quantified by RT-PCR and once normalised, fold change in gene expression was calculated with respect to expression in sham C1-3 mice at 4hrs. As anticipated, the data showed a significant increase in TNFα gene expression in C1-3-GT PHx mice with respect to C1-3 PHx controls. This trend has been previously observed by our group when C1-3-GT has been administered to mice with acute CCl_4 induced liver injury (unpublished observations). Whilst a similar trend was observed with IL-6 gene expression this difference was not significant. However when IL-6 was quantified using IHC staining a significant increase in the number of IL-6 positive cells around both PT and CLV was observed in C1-3-GT PHx and sham mice at 4hrs following surgery.

RT-PCR analysis of the two growth factors essential in stimulating hepatocyte proliferation, HGF and EGF, showed that hepatic myofibroblast depletion resulted in a significant increase in EGF gene expression in C1-3-GT PHx mice at 4hrs in comparison to C1-3 PHx control. EGF has been shown to be essential in liver regeneration since removal of the salivary gland prior to PHx prevented subsequent liver regrowth [160] however the relationship between EGF and hepatic myofibroblasts is unknown. No differences were observed in HGF expression between the treatment groups at any of the time points analysed, however research groups have shown that HGF is capable of binding matrix proteins thus the initial sources of HGF may be released by matrix remodelling rather than active secretion by hepatic myofibroblasts [154, 155].

Whilst no differences in liver regeneration were observed at 4hrs, as determined by liver weight, BrDU incorporation was shown to be significantly higher at 4hrs in parenchymal cells surrounding both PT and CLV in C1-3-GT PHx mice suggesting that the increase in priming cytokines accelerated the proliferative response in response to the elevated EGF levels. This also correlated with a significant increase in the cellular markers of proliferation (cyclin D1, E1 and CDK2) in C1-3-GT PHx mice at 4hrs post surgery. Cyclin E1 binds CDK2, a component essential for the transition from G1 phase to S phase. This complex also binds cyclin A1 which is necessary for the completion of S phase. Cyclin D1, which forms a complex with and is a regulatory subunit of CDK4 or CDK6 is also required for the passage of the cell from the G1 phase of the cell cycle to the S phase.

Taken together, the data suggest that the depletion of hepatic myofibroblasts using C1-3-GT stimulates an increase in TNFα and IL-6 expression which could result in accelerated liver regeneration. However, analysis of cellular proliferation at 36hrs revealed that hepatic myofibroblast depletion resulted in a significant decrease in BrDU incorporation in parenchymal and non parenchymal cells surrounding both PT and CLV in C1-3-GT PHx mice. Whilst relative expression levels of cyclin D1, E1 and CDK2 were significantly higher in the PHx mice at 36hr in comparison to the sham controls, there were no significant differences between the treatment groups of the PHx at 36 and 72hrs. It is possible that the decrease in BrDU incorporation at 36hrs is associated with the increase in αSMA positive myofibroblasts and suggests a possible regulatory role for hepatic myofibroblasts. To confirm this theory, it would be necessary to a dual label IHC stain for BrDU and αSMA to reveal any cellular proximity relationships.

Analysis of TGFβ and IL-1β, two cytokines implicated in the termination of liver regeneration, revealed a significant increase in TGFβ expression in C1-3-GT PHx mice at 4hrs only with no differences in IL-1β observed between the treatment groups at any of the time points. It is therefore possible that the increase in TGFβ may account for the decreased proliferative response at 36hr since addition of TGFβ to hepatocytes in culture inhibited their proliferative response [167, 168]. *In* vivo inhibition of TGFβ signalling prior to PHx surgery resulted in an early peak in DNA proliferation and was associated with accelerated entry into the S phase of the cell cycle, as determined by an increase in cyclin D1 and E [171]. More importantly, the study showed that hepatocyte proliferation halted when the correct liver mass was reached suggesting that TGFβ signalling is not essential for the termination of liver regeneration. To investigate whether hepatic myofibroblast depletion affected the termination of proliferation, it would be interesting to extend the time course beyond 5 days, the normal time taken for liver regeneration to occur.

At 72hrs, there were no differences in cellular proliferation markers between the treatment groups. Intriguingly, quantification of synaptophysin staining revealed a significant increase in the number of synaptophysin positive cells surrounding both PT and CLV at this time point in C1-3-GT treated mice. Whilst synaptophysin is a marker of quiescent HSCs and hepatic myofibroblasts, it is also expressed by oval cells which reside in the canals of herring and can

transdifferentiate into hepatocytes and biliary epithelial cells when required [260]. Therefore it is possible that the decrease in parenchymal and non parenchymal cell proliferation at 36hrs may be compensated for by the activation of the oval cell response. To investigate this possibility it would be necessary to do a dual label IHC stain of synaptophysin and another oval cell marker e.g. OV-6.

The data generated by this study propose a complex role for hepatic myofibroblasts in liver regeneration. Following PHx, the data suggest that hepatic myofibroblasts exert a suppressive effect on kupffer cells restricting the expression of the priming cytokines and in turn controlling the number of hepatocytes undergoing cellular proliferation. In conjunction with this, hepatic myofibroblasts are known sources of hepatocyte growth factors, HGF and serotonin [146, 149], therefore are essential in ensuring that hepatocytes enter the cell cycle (Figure 5-30A). Depletion of hepatic myofibroblasts using C1-3-GT removes the inhibitory effect on the kupffer cells which leads to an increase in TNFα and IL-6 gene expression and stimulates accelerated entry into the cell cycle. However a reduction in parenchymal cell proliferation is also observed, and whilst the data show no significant changes in HGF expression between the treatment groups, this would suggest that hepatic myofibroblasts produce and express a key component involved in modulating hepatocyte proliferation, for example serotonin (Figure 5-30B). In conclusion, the data reveal that hepatic myofibroblasts have distinct, opposing roles during liver regeneration and further work is necessary to determine if hepatic myofibroblast depletion is a viable option during disease.

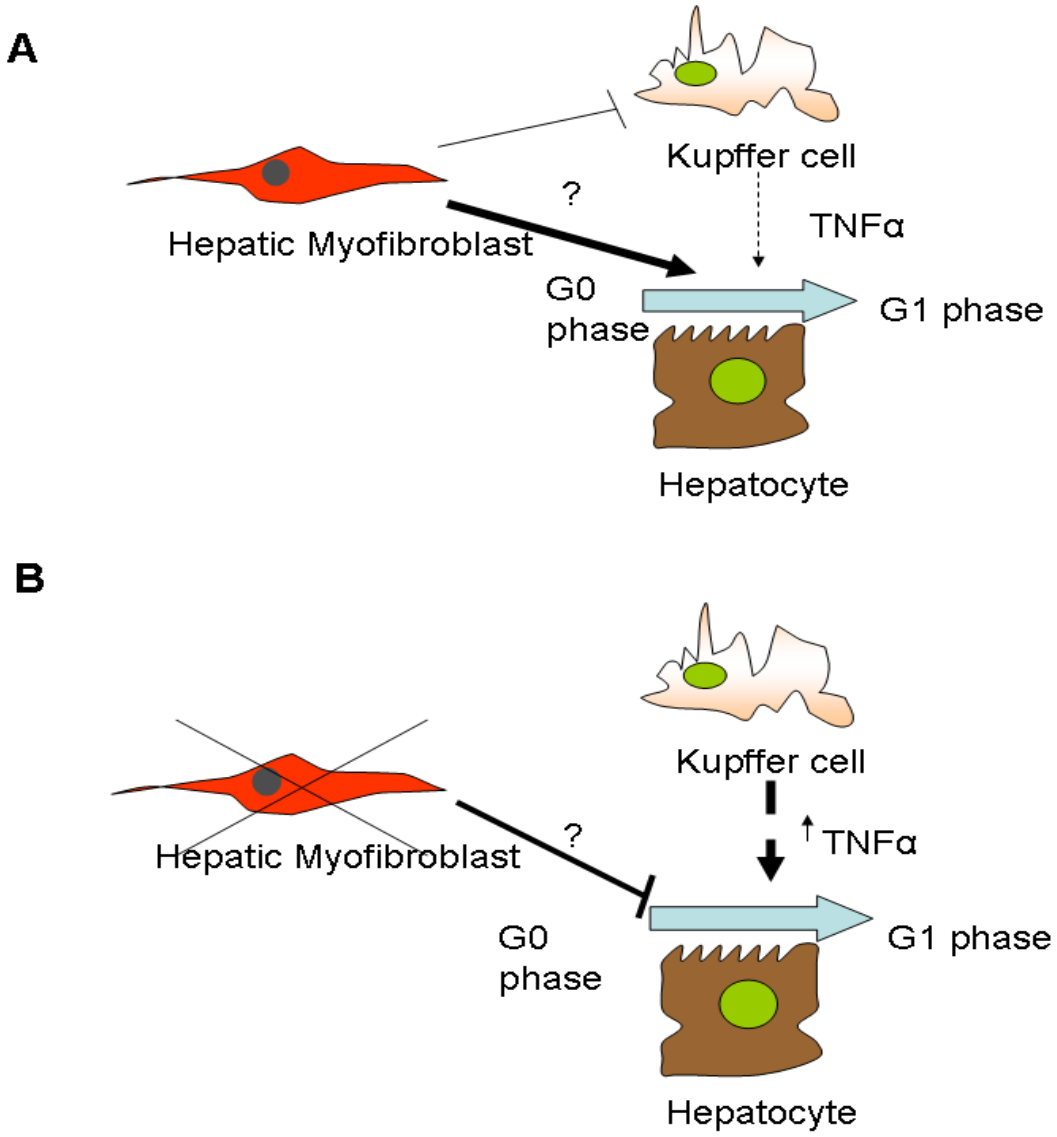

Figure 5-30 Proposed roles of hepatic myofibroblast during liver regeneration. A: Hepatic myofibroblasts exert a suppressive effect on kupffer cells and thus controls the release of TNFα. They also produce an unknown component which stimulates passage of hepatocytes into the G1 phase of the cell cycle. B: Depletion of HM increases TNFα production by kupffer cells but decreases hepatocyte proliferation.

Chapter 6. Use of C1-3-GT to investigate the effect of hepatic myofibroblast depletion during sustained liver injury

6.1 Introduction

Hepatic fibrosis is a wound healing response to liver injury caused by a wide range of aetiologies. In the UK alone, liver disease is the 5th biggest killer (source British Liver Trust) and with a surge in alcohol consumption and obesity the incidence can only increase. With no treatments currently available, a vast majority of research is dedicated to the cells involved in the disease progression to try and discover new therapeutic options.

The literature to date has provided convincing evidence that hepatic myofibroblasts are the key cell involved in fibrosis [102, 253]. More importantly, emerging evidence has shown that removal of hepatic myofibroblasts can stimulate the reversal of fibrosis in recovery models [126, 249]. However this is not a perfect clinical representation since it is not always possible to remove the damaging insult. This chapter aims to investigate the effect of C1-3-GT mediated hepatic myofibroblast depletion during sustained CCl_4 induced liver injury.

6.2 Results

It was decided to use C1-3-FITC as a conjugated antibody control, successful conjugation to FITC was confirmed by an increase in molecular weight on a 9% polyacrylamide gel (Figure 6-1A).

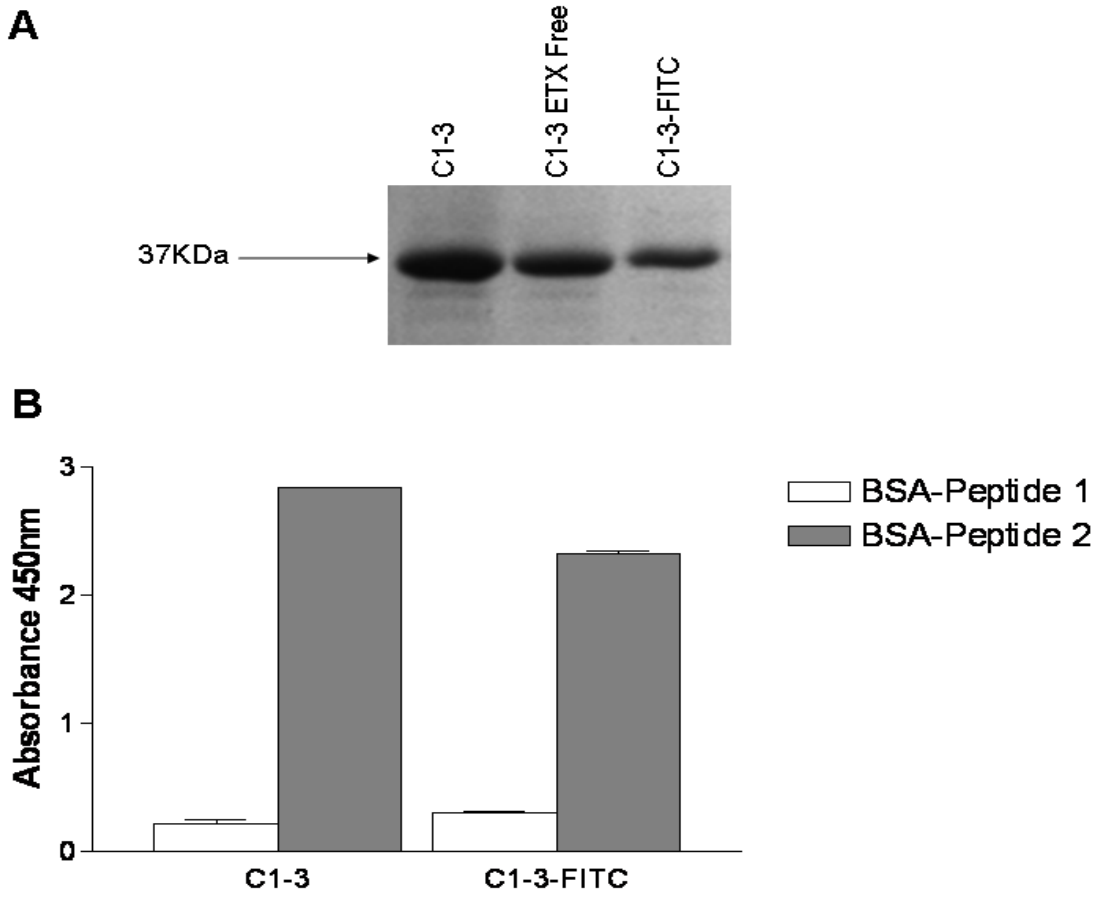

Figure 6-1 SDS-PAGE and peptide a/2 binding ELISA to confirm C1-3-FITC conjugation and function A: Samples of C1-3, C1-3 endotoxin (ETX) free and C1-3-FITC were diluted 1:1 with reducing loading buffer and 10µl of each sample was loaded onto a SDS-PAGE gel. Results are typical of 3 separate conjugation reactions. B: 96 well plates were coated with BSA-conjugated peptide 1 or peptide 2. Antibody samples of unknown concentrations were initially diluted 1:10 with PBS then serially diluted across the plate. Bound antibody was detected using a secondary HRP conjugated goat-anti human Cκ light chain antibody and quantified by measuring a colorimetric reaction by the addition of TMB and the absorbance at 450nm noted. All experiments were performed in triplicate and the mean absorbance and SD at dilution 5 (1/160) plotted. Results are typical of 3 experimental repeats.

To check antibody binding ability, a binding ELISA was also carried out. Figure 6-1B demonstrates that C1-3-FITC is capable of binding to its antigen peptide 2. C1-3 binding was measured at the same time as a positive control and although C1-3 has a slightly higher absorbance at dilution 5 this is likely due to slight differences in antibody concentration and not antibody affinity. C1-3-GT

functionality was tested as previously described in the methods section 2.4.3 and 2.7.9 and was shown in figures 5-1 to 5-3.

To test the effect of myofibroblast depletion during sustained liver injury a CCl_4 model of livery injury was set up (figure 6-2).

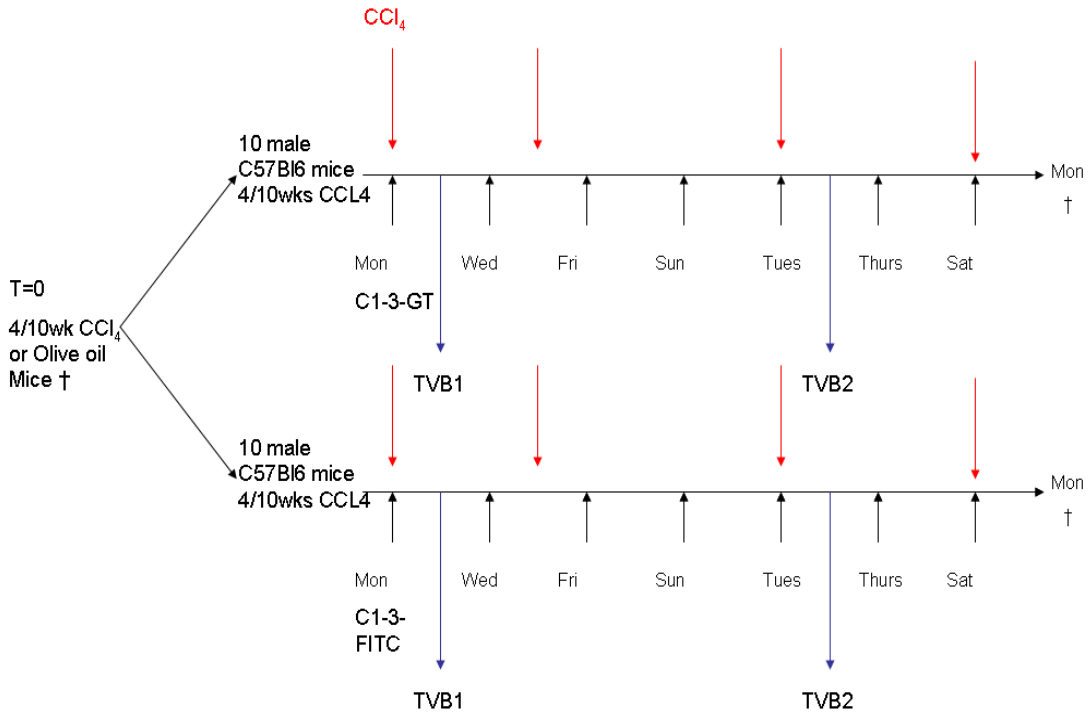

Figure 6-2 Overview of animal study indicating C1-3 and CCl_4 dosing times. Male C57Bl6 mice were dosed for 4,6,10 or 12wks with CCl_4 or with olive oil for 4 or 10wks. CCl_4 and olive oil T=0 mice were schedule 1 killed following 4 and 10wks of treatment. The remaining mice received CCl_4 treatment for a further 2 weeks with either C1-3-FITC/GT dosing every other day. Tail vein bleeds were taken at strategic time points during the final two weeks of treatment and serum sent for analysis of liver damage. Whole blood was extracted following schedule 1 killing and serum sent for analysis of liver damage markers. Animal group numbers: Olive oil 4/10wk n=3. CCl_4 4wk n=6; 10wk n=5. C1-3-FITC 6wk n=7; 12wk n=8. C1-3-GT 6/12wk n=8.

Two time points of 6 and 12 weeks of CCl_4 treatment were chosen since they represent chronic injury and end stage cirrhosis. Although most liver disease is diagnosed at its end stages it is clinically relevant to know if therapeutic treatments would be effective at both the early and end stage time points. Tail bleeds were carried out at two strategic time points throughout the final two weeks of therapy to determine if the treatments were having any effect on the serum marker of liver fibrosis, ALT. 48hrs following the final dose of CCl_4 and C1-3, mice were killed and livers harvested. CCl_4 and olive oil mice were also harvested at 4/10wks to serve as baseline controls for injury. Serum from each treatment group and time point was sent for ALT/ALP analysis as an indicator of liver injury (figure 6-3).

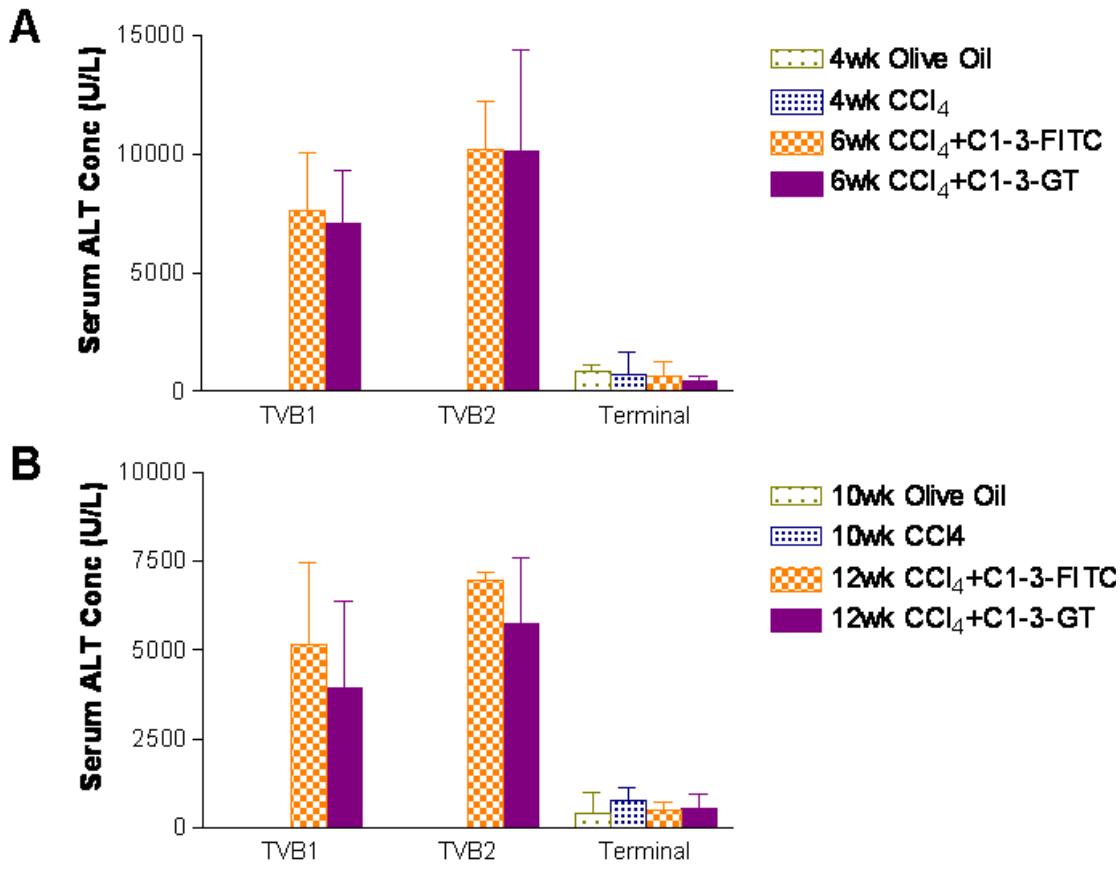

Figure 6-3 Assessment of liver damage using the serum marker ALT. Whole blood was extracted following either tail vein bleed or schedule 1 killing. Whole blood was allowed to clot at room temperature for 1hr. Serum was removed following centrifugation and diluted in 0.9% (w/v) sodium chloride. All serum samples were analysed by Newcastle Clinical Biochemistry Department. Data are the mean and SD for each treatment group. Animal group numbers: Olive oil 4/10wk n=3. CCl_4 4wk n=6; 10wk n=5. C1-3-FITC 6wk n=7; 12wk n=8. C1-3-GT 6/12wk n=8.

Figure 6-3 shows that there are no significant differences in ALT serum concentration after both tail bleeds and the final terminal bleeds. Serum ALT concentrations from the terminal bleeds are substantially lower than the tail vein bleeds however this is most likely due to the dosing of CCl_4 two days before termination. Whilst the data would suggest that C1-3-GT is not having an affect on liver fibrosis, it is unlikely that serum ALT quantification would be sensitive enough to distinguish between the later stages of fibrosis. Since ALP is an enzyme released during cholestasis, levels were typically below an accurate threshold measurement thus have not been presented.

To determine if C1-3-GT was successfully depleting hepatic myofibroblasts *in vivo* paraffin embedded liver tissue sections were stained for the presence of αSMA and the number of cells surrounding each CLV quantified using Leica

software analysis of the percentage area stained. Representative images and quantification are illustrated in figures 6-4 and 6-5.

Quantification revealed that there is a significantly higher percentage of αSMA staining present in the CCl_4 treated animals compared to the olive oil controls for both treatment times of CCl_4 (figure 6-4B and 6-5B). However the number of hepatic myofibroblasts, as determined by the percentage of area stained since it is very difficult to accurately quantify cell number, remained relatively constant between 4-10wks of CCl_4 (figure 6-4B and 6-5B) treatment suggesting that increased treatment time does not necessarily correlate with increased hepatic myofibroblast number. Ideally, hepatic myofibroblast number would be determined by counting the number of positive cells with clear nuclear staining however the dense staining pattern observed makes this task very difficult and error prone. Nevertheless, treatment with C1-3-GT for an additional 2 wks after 4wks of CCl_4 did not reduce αSMA stainig in comparison with the C1-3-FITC control (figure 6-4B). Interestingly, figure 6-5B shows a 12% significant reduction in αSMA staining (as determined by subtracting the percentage area of αSMA staining of C1-3-GT mice from those treated with C-1-3-FITC) in mice treated for 12wks CCl_4 plus two weeks of C1-3-GT in comparison to its C1-3-FITC control.

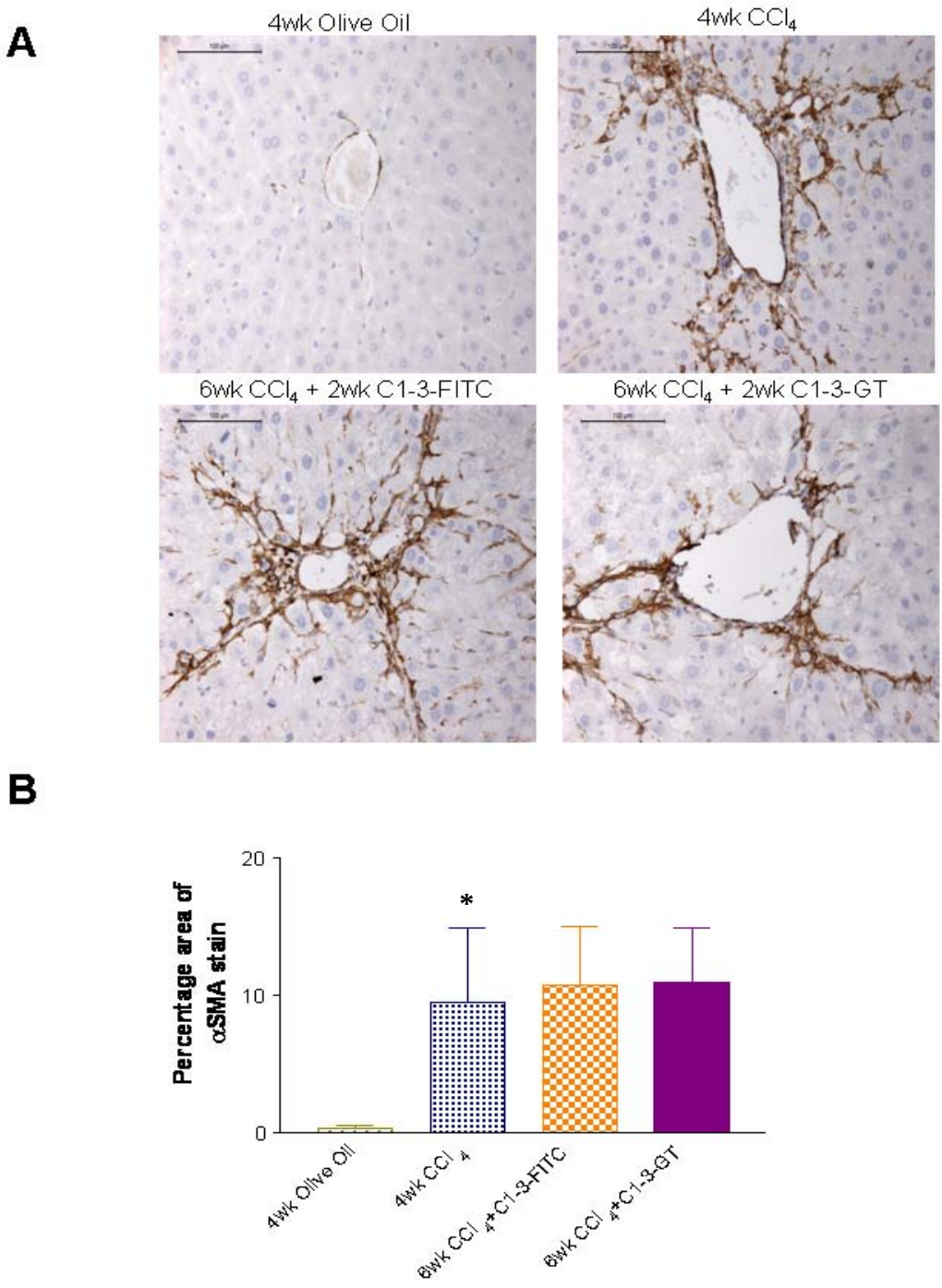

Figure 6-4 αSMA staining and quantification following 4-6wks of CCl_4 treatment. A: Formalin fixed paraffin embedded tissue samples from each animal were stained with mouse anti αSMA antibody. All images taken at x200 magnification. B: For quantification, pictures were taken around 10 random CLV at x200 magnification and subjected to analysis using Leica software to determine the percentage area of the αSMA stain. Data are the mean and SD of percentage area of the αSMA stain for each treatment group. Data tested for statistical significance using the Student's two tailed T test; * represents significance between CCl_4 and olive oil ($p<0.0001$). Animal group numbers: Olive oil 4wk n=3. CCl_4 4wk n=6. C1-3-FITC 6wk n=7. C1-3-GT 6 n=8. Scale bar=100μm.

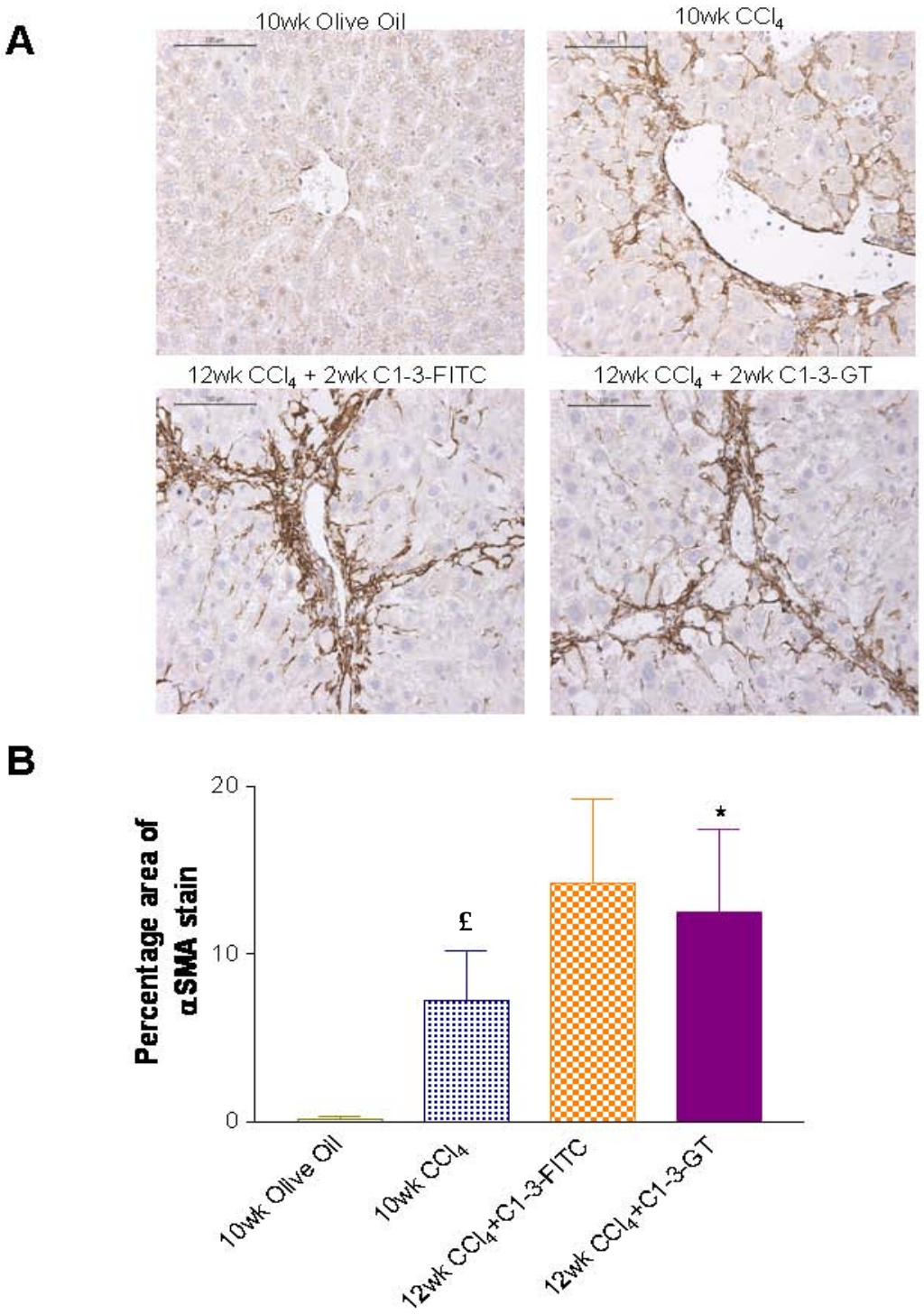

Figure 6-5 αSMA staining and quantification following 10-12wks of CCl_4 treatment. A: Formalin fixed paraffin embedded tissue samples from each animal were stained with mouse anti αSMA antibody. All images taken at x200 magnification. B: For quantification, pictures were taken around 10 random CLV at x200 magnification and subjected to analysis using Leica software to determine the percentage area of the αSMA stain. Data are the mean and SD of percentage area of the αSMA stain for each treatment group. Animal group numbers: Olive oil 10wk n=3. CCl_4 10wk n=5. C1-3- 12wk n=8. C1-3-GT 12wk n=8. Data tested for statistical significance using the student's two tailed T test, * represents significance between C1-3-GT vs. C1-3-FITC ($p<0.01$); £ represents significance between CCl4 and olive oil ($p<0.0001$). Scale bar=100μm.

Sustained CCl_4 injury during the final 2 weeks of C1-3 therapy provides a continuous stimulus for the proliferation of hepatic myofibroblasts thus it is possible that whilst there is little difference in αSMA IHC staining due to the dense staining patterns observed, C1-3-GT may be having a greater effect on the reduction of αSMA gene levels. To determine if this was the case, whole liver samples were analysed for αSMA gene expression by RT-PCR. As expected, following 4-6wks CCl_4 treatment there is a significant increase in αSMA gene expression in both C1-3-FITC and C1-3-GT compared to the olive oil control however no significant differences were observed between the C1-3-GT and C1-3-FITC treatment groups (Figure 6-6A). This agrees with the immunohistochemical data in figure 6-4. Intriguingly the data observed in figure 6-6B is somewhat different from figure 6-5. Whilst a significant increase in αSMA gene expression is observed in mice treated for 12wks with CCl_4, there appears to be no difference in αSMA gene expression between the 10wk CCl_4 and olive oil mice. Interestingly, 2wks of C1-3-GT treatment resulted in a significant increase in expression of the αSMA gene compared to the C1-3-FITC control. This is the opposite of what would be expected as C1-3-GT would be expected to reduce αSMA gene expression and furthermore this does not correlate with the IHC quantification. However, αSMA is expressed by other myofibroblasts which are not derived from HSCs and this could account for the difference.

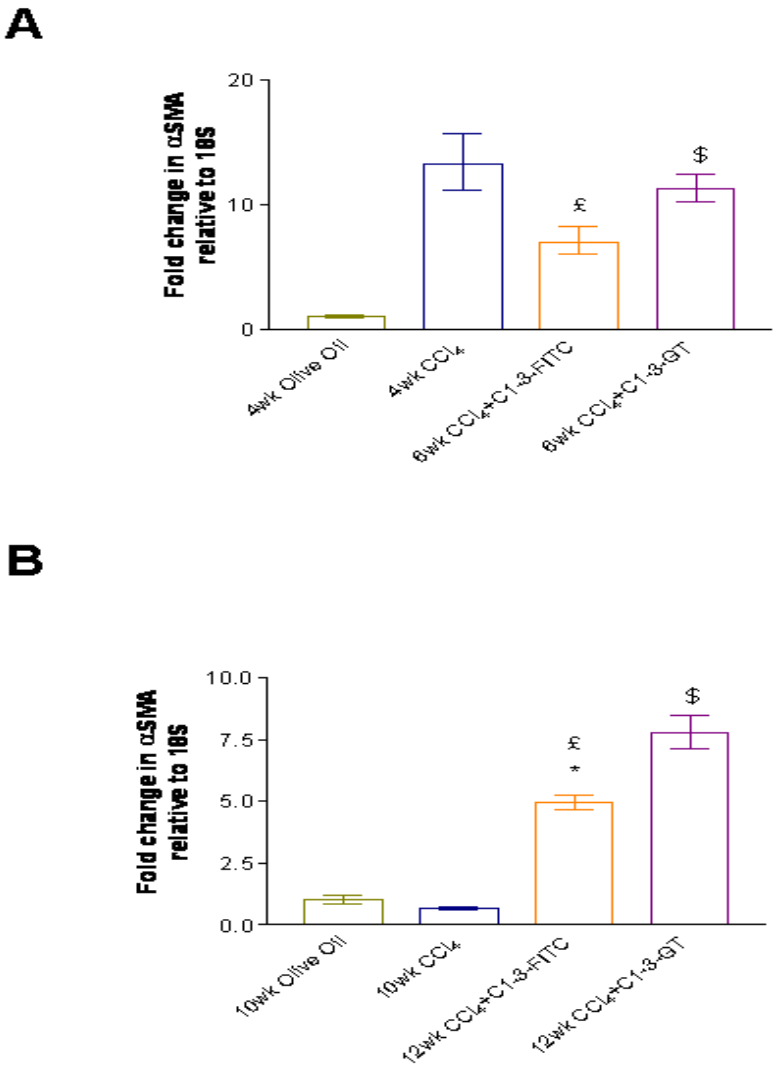

Figure 6-6 Relative gene expression levels of αSMA in CCl_4 and olive oil treatment groups. RNA was isolated from each mouse liver using Trizol, quantified and reverse transcribed using oligo dTRT-PCR was carried out for 40 cycles and analysed using Applied Biosystems TaqMan software. All experiments were performed in duplicate and data are the mean and SD of the fold change relative to 18S and normalised to expression levels in the relative olive oil controls. Animal group numbers: Olive oil 4/10wk n=3. CCl_4 4wk n=6; 10wk n=5. C1-3-FITC 6wk n=7; 12wk n=8. C1-3-GT 6/12wk n=8. Data tested for statistical significance using the Student's two tailed T test. * represents significance between C1-3-GT and C1-3-FITC (A: $p<0.05$); £ represents significance between C1-3-FITC and olive oil (A: $p<0.01$; B: $p<0.05$); $ represents significance between C1-3-GT and olive oil (A:$p<0.01$; B: $p<0.0001$).

Since C1-3-GT only targets hepatic myofibroblasts expressing synaptophysin, it was necessary to determine if the αSMA protein and gene levels reflected the presence of synaptophysin positive hepatic myofibroblasts. Paraffin embedded liver tissue sections were stained for the presence of synaptophysin as detailed in the materials and methods sections. Analysis of the synaptophysin staining revealed populations of positive cells surrounding both PT and CLV thus images were taken around 10 random PT and CLV and the number of positive cells quantified. Figures 6-7 to 6-10 are typical representations of staining patterns observed for each time point and treatment group.

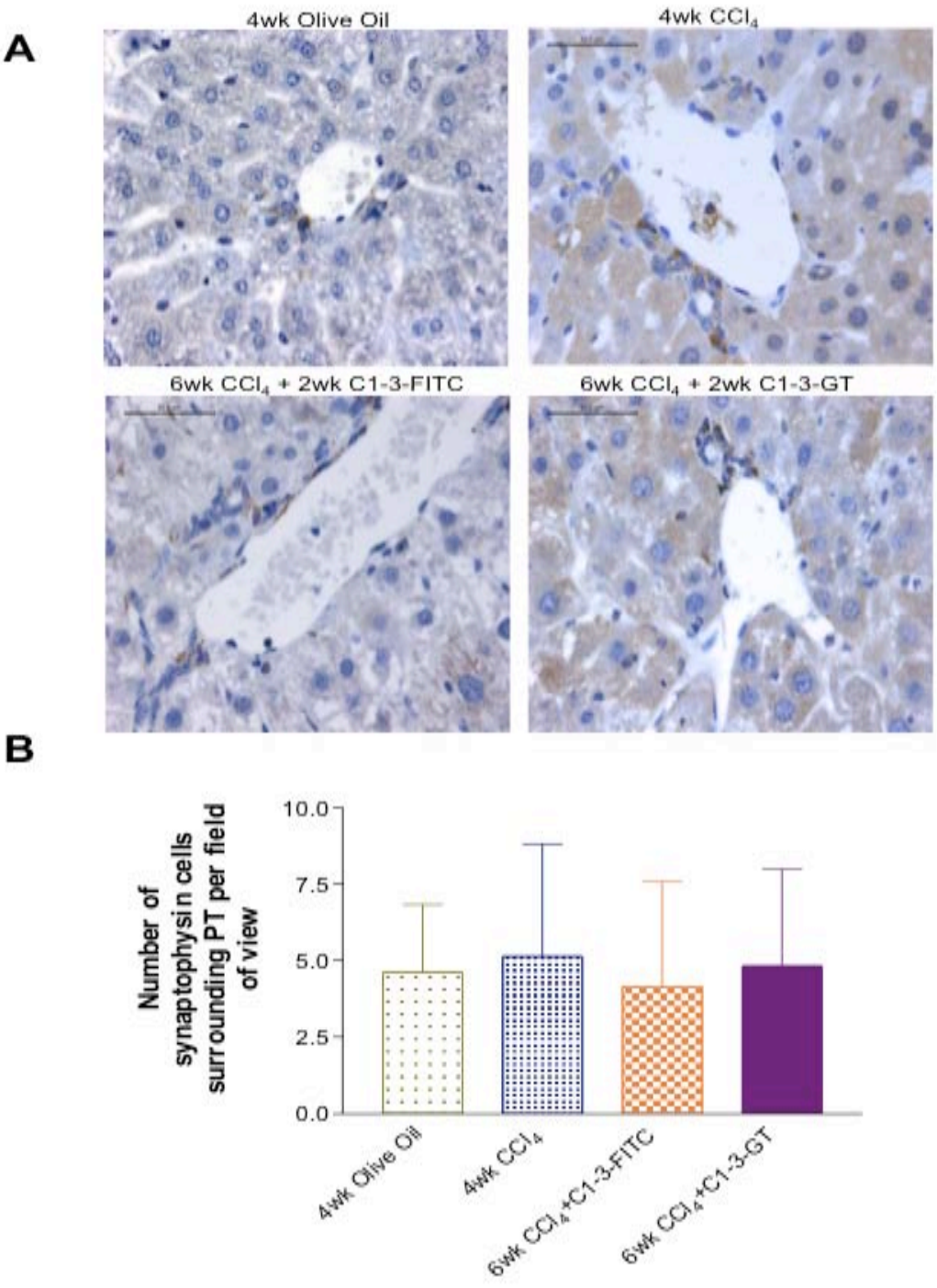

Figure 6-7 Synaptophysin IHC staining and quantification around PT following 4-6wks of CCl_4/olive oil treatment. A: 4µm sections were incubated with rabbit anti synaptophysin antibody. Images were taken at x400 magnification and are representative of each treatment group. Scale bar=50µm. B: For quantification, pictures were taken around 10 random PT at x400 magnification and the number of positive cells with clear nuclear staining counted. Data presented are the mean and SD of the number of cells per treatment group. Animal group numbers: Olive oil 4wk n=3. CCl_4 4wk n=6. C1-3-FITC 6wk n=7. C1-3-GT 6 n=8.

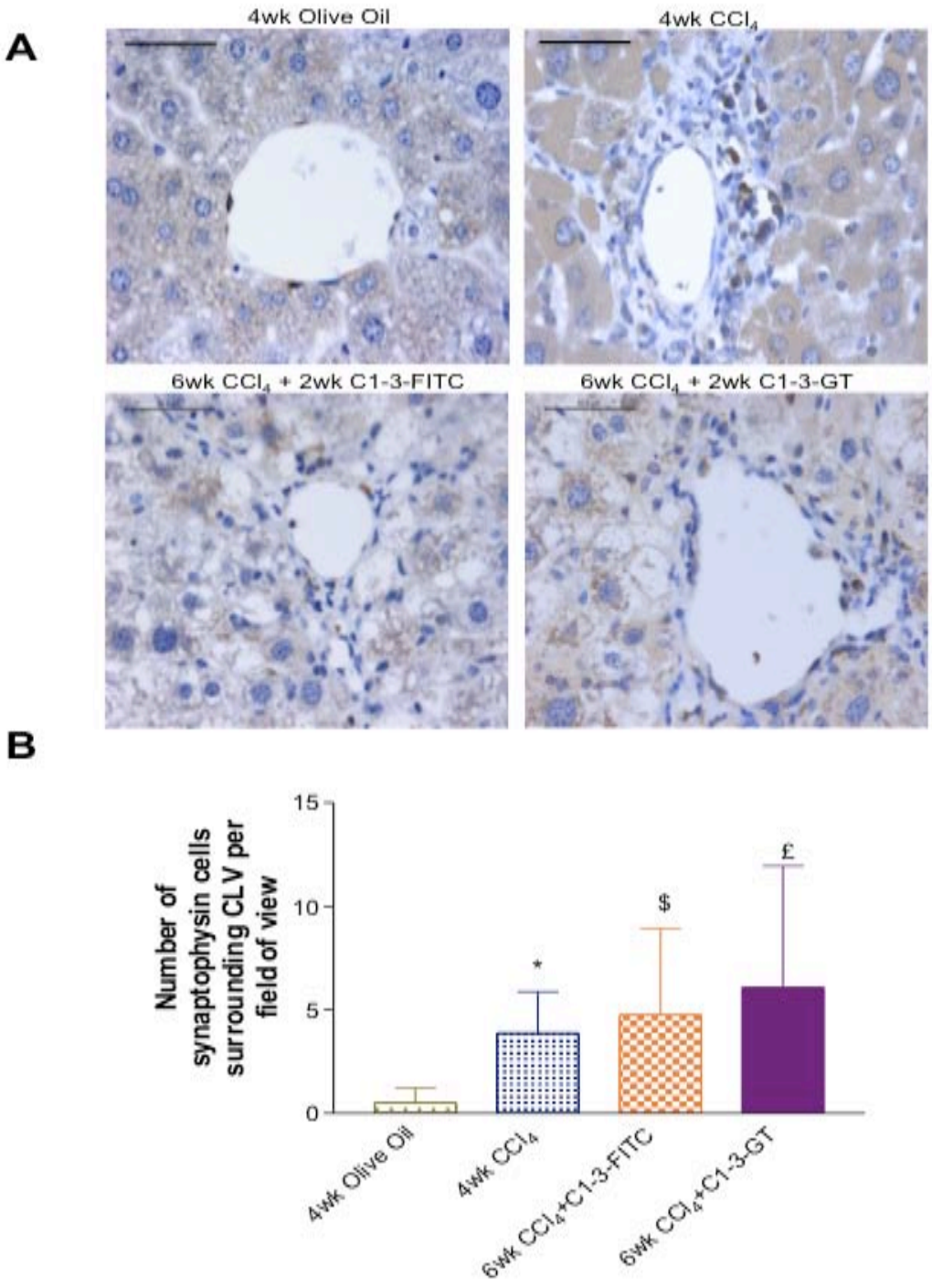

Figure 6-8 Synaptophysin IHC staining and quantification around CLV following 4-6wks of CCl_4/olive oil treatment. A: 4µm sections were incubated with rabbit anti synaptophysin antibody. Images were taken at x400 magnification and are representative of each treatment group. Scale bar=50µm.B: For quantification, pictures were taken around 10 random PT at x400 magnification and the number of positive cells with clear nuclear staining counted. Data presented are the mean and SD of the number of cells per treatment group. Animal group numbers: Olive oil 4wk n=3. CCl_4 4wk n=6. C1-3-FITC 6wk n=7. C1-3-GT 6 n=8. Data tested for statistical significance using Student's two tailed T test; * represents significance between 4wk CCl_4 and 4 wk olive oil ($p<0.0001$); $ represents significance between C1-3-FITC and 4wk olive oil ($p<0.005$); £ represents significance between C1-3-GT and 4wk olive oil ($p<0.005$).

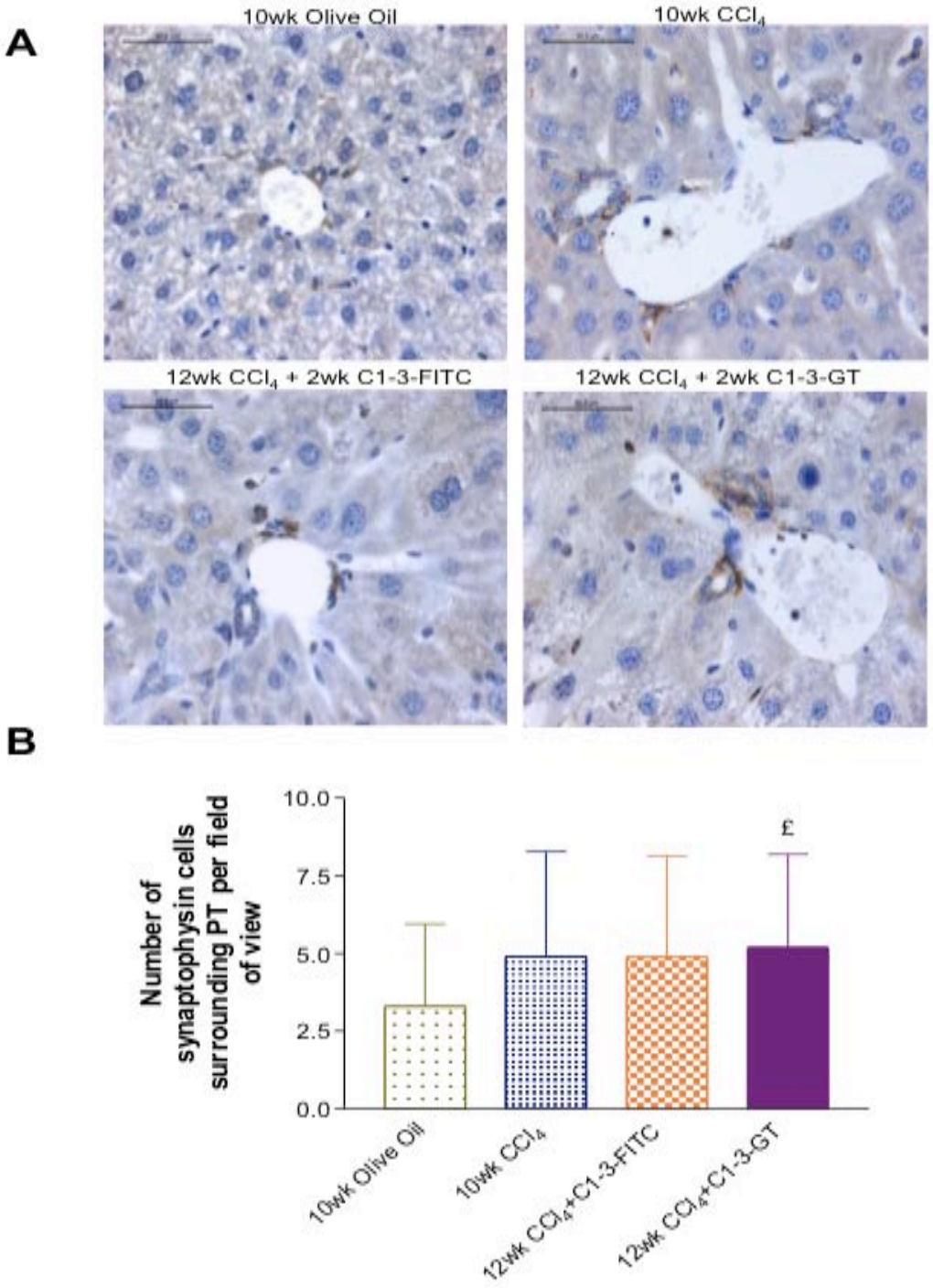

Figure 6-9 Synaptophysin IHC staining and quantification around PT following 10-12wks of CCl_4/olive oil treatment. A: 4µm sections were incubated with rabbit anti synaptophysin antibody. Images were taken at x400 magnification and are representative of each treatment group. Scale bar=50µm. B: For quantification, pictures were taken around 10 random PT at x400 magnification and the number of positive cells with clear nuclear staining counted. Data presented are the mean and SD of the number of cells per treatment group. Animal group numbers: Olive oil 10wk n=3. CCl_4 10wk n=5. C1-3-FITC 12wk n=8. C1-3-GT 12wk n=8. Data tested for statistical significance using Student's two tailed T test; £ represents significance between C1-3-GT and 10wk olive oil ($p<0.05$).

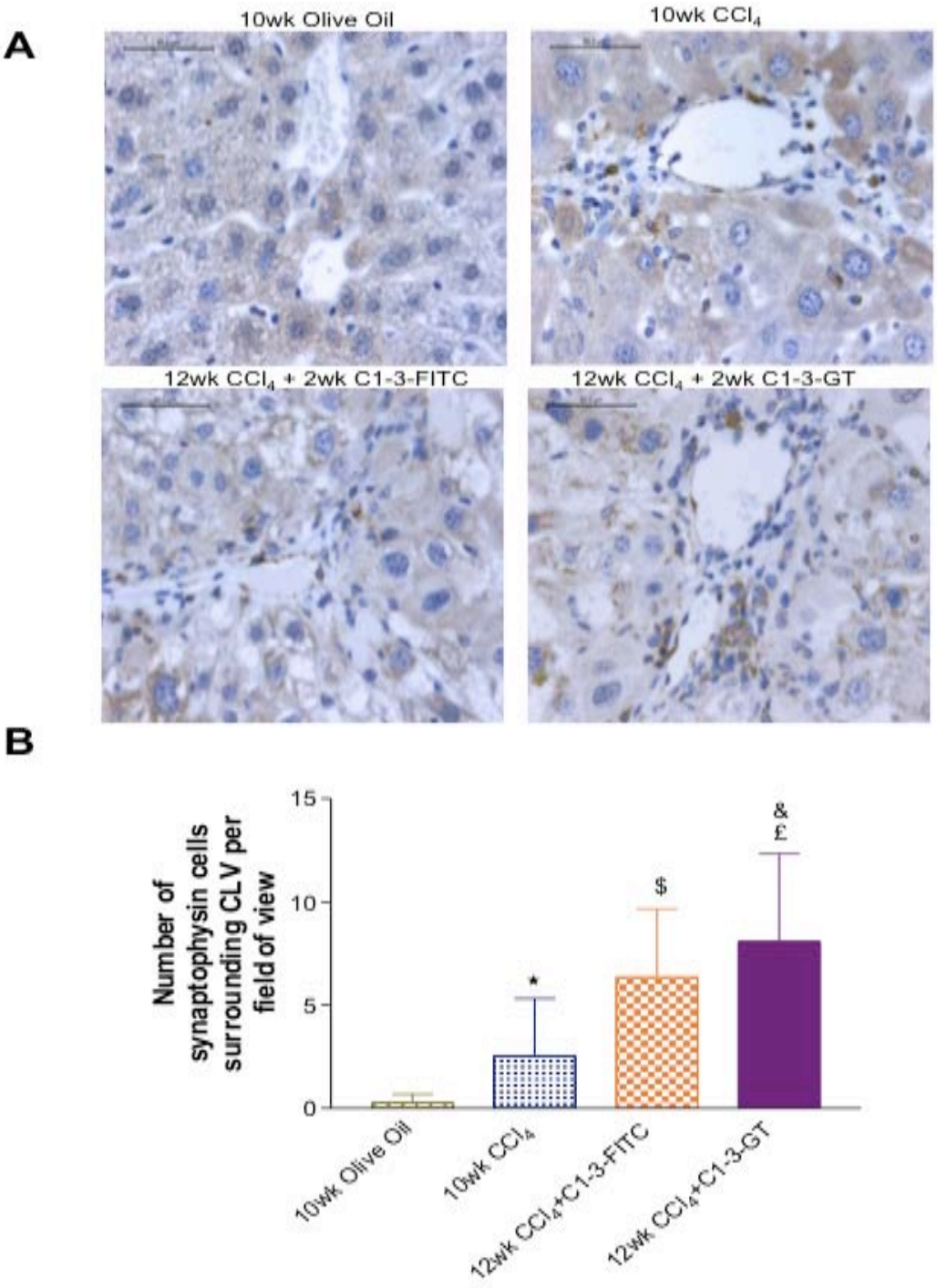

Figure 6-10 Synaptophysin IHC staining and quantification around CLV following 10-12wks of CCl_4/olive oil treatment. A: 4µm sections were incubated with rabbit anti synaptophysin antibody. Images were taken at x400 magnification and are representative of each treatment group. Scale bar=50µm. B: For quantification, pictures were taken around 10 random PT at x400 magnification and the number of positive cells with clear nuclear staining counted. Data presented are the mean and SD of the number of cells per treatment group. Animal group numbers: Olive oil 10wk n=3. CCl_4 10wk n=5. C1-3-FITC 12wk n=8. C1-3-GT 12wk n=8.Data tested for statistical significance using Student's two tailed T test; * represents significance between 10wk CCl_4 and 10wk olive oil ($p<0.0001$); $ represents significance between C1-3-FITC and 10wk olive oil ($p<0.0001$); £ represents significance between C1-3-GT and 10wk olive oil ($p<0.0001$). & represent significance between C1-3-GT vs. C1-3-FITC ($p<0.01$).

The data in figures 6-7B and 6-9B show that the number of synaptophysin positive cells surrounding PT are relatively similar in all treatment groups at both time points. However centrilobular induced damage by CCl_4 resulted in a significant increase in the number of synaptophysin positive cells surrounding CLV in all CCl_4 treatment groups compared to olive oil controls at both time points (figures 6-8B and 6-10B). Furthermore, treatment of mice with C1-3-GT for a further 2 weeks following 10wks of CCl_4 resulted in a 20% significant increase in synaptophysin positive cells compared to the C1-3-FITC controls (figure 6-10B). No significant differences in synaptophysin cell number were observed in 6wk CCl_4 mice treated with C1-3-GT compared to the C1-3-FITC control.

To determine if the synaptophysin cell counts were reflective of gene expression, synaptophysin was quantified by RT-PCR. Quantification revealed that synaptophysin gene expression remained relatively constant between all the treatment groups for both of the injury time points (figure 6-11). This would suggest that there is little proliferation of synaptophysin positive hepatic myofibroblasts following CCl_4 induced centrilobular liver injury, however this would disagree with the IHC staining observed in figures 6-7 and 6-10.

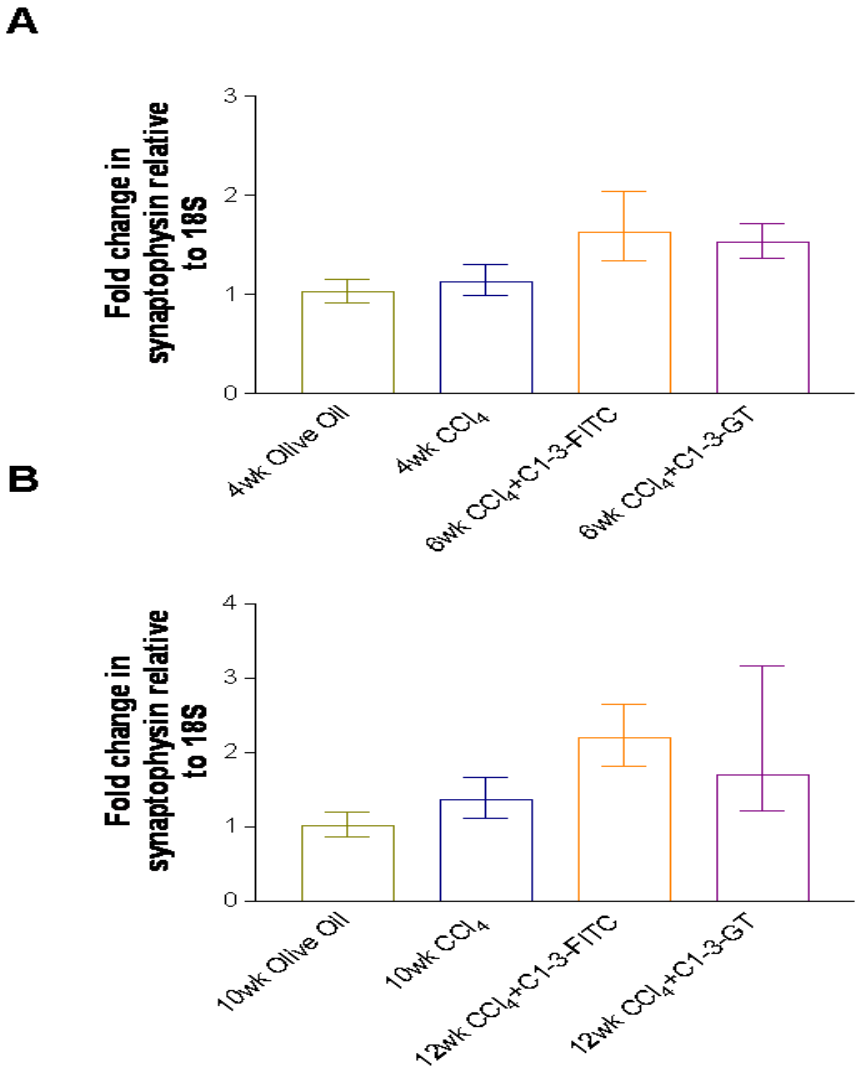

Figure 6-11 Relative gene expression levels of synaptophysin in CCl_4 and olive oil treatment groups. RNA was isolated from each mouse liver using Trizol, quantified and reverse transcribed using oligo dT. RT-PCR was carried out for 40 cycles and analysed using Applied Biosystems TaqMan software All experiments were performed in duplicate and data are the mean and SD of the fold change relative to 18S and normalised to expression levels in the relative olive oil controls. Animal group numbers: Olive oil 4/10wk n=3. CCl_4 4wk n=6; 10wk n=5. C1-3-FITC 6wk n=7; 12wk n=8. C1-3-GT 6/12wk n=8.

Depletion of hepatic myofibroblasts during sustained injury may stimulate recruitment of myofibroblasts from other sources, e.g. bone marrow, and may account for the lack of difference between the C1-3-GT and C1-3-FITC treatment groups. Whilst research has shown that a significant proportion of myofibroblasts are derived from the bone marrow in human liver fibrosis [24], the contribution of these cells to matrix deposition is somewhat debated [261]. To determine if C1-3-GT treatment had an effect on liver fibrosis, picro-sirius red staining was used to assess collagen deposition and quantified using Leica software analysis (figures 6-12 and 13).

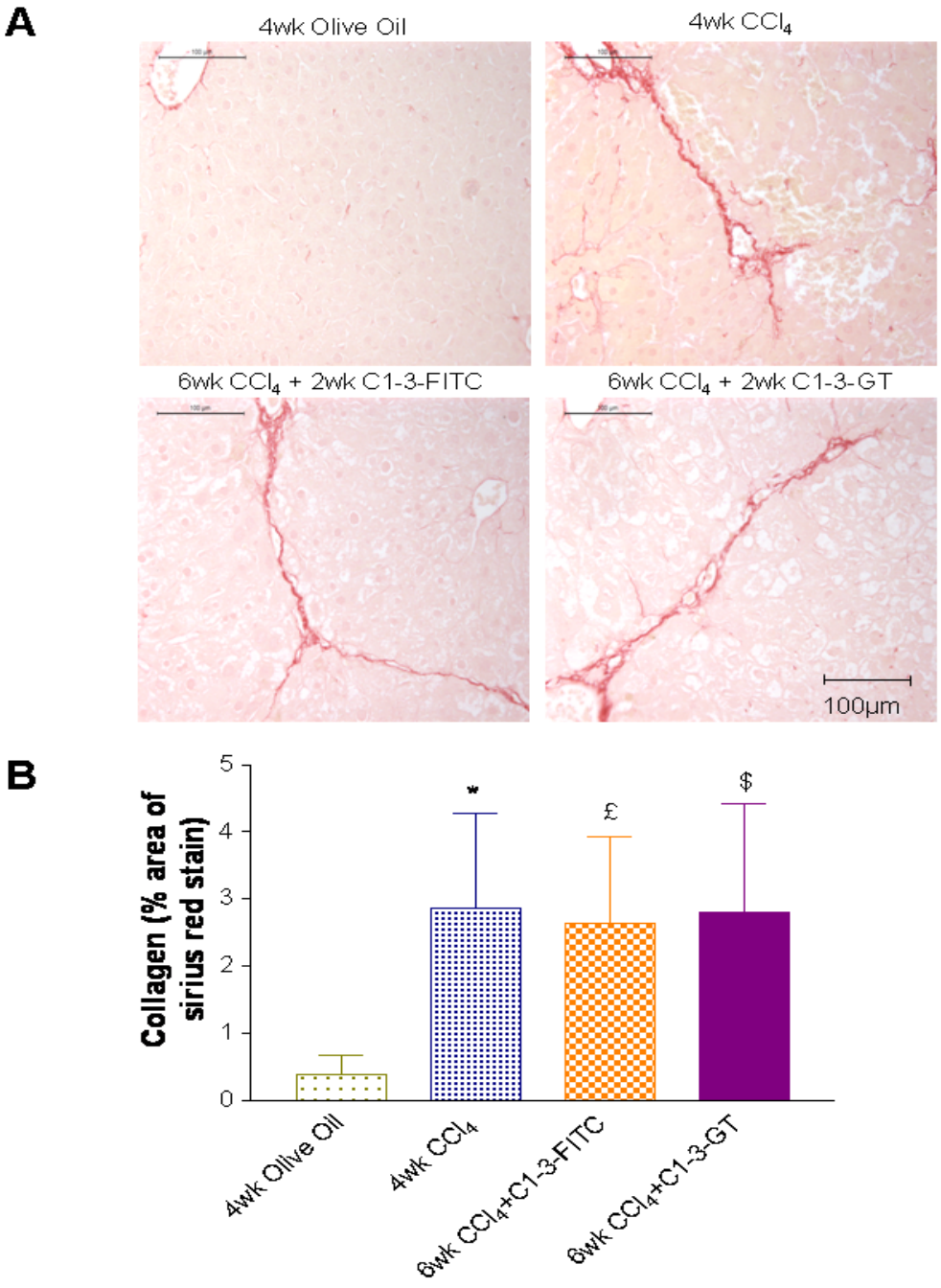

Figure 6-12 Picro-Sirius red staining and quantification following 4-6wks of CCl_4 or olive oil treatment. A: 4µm sections were incubated in picro-sirius red stain. Images were taken at x200 magnification and are representative of each treatment group. Scale bar=100µm. B: For quantification 10 random CLV were located and moved to the corner of the field of view to allow quantification of the band of collagen by Leica software analysis. Data are mean and SD of percentage area of picro-sirius red stain. Animal group numbers: Olive oil 4wk n=3. CCl_4 4wk n=6. C1-3-FITC 6wk n=7. C1-3-GT 6 n=8. Data tested for statistical significance using the Student's two tailed T test. * represents significance between 4wk olive oil and 4wk CCl_4 ($p<0.0001$); £ represents significance between C1-3-FITC and 4wk olive oil ($p<0.0001$); $ represents significance between C1-3-GT and 4wk olive oil ($p<0.0001$).

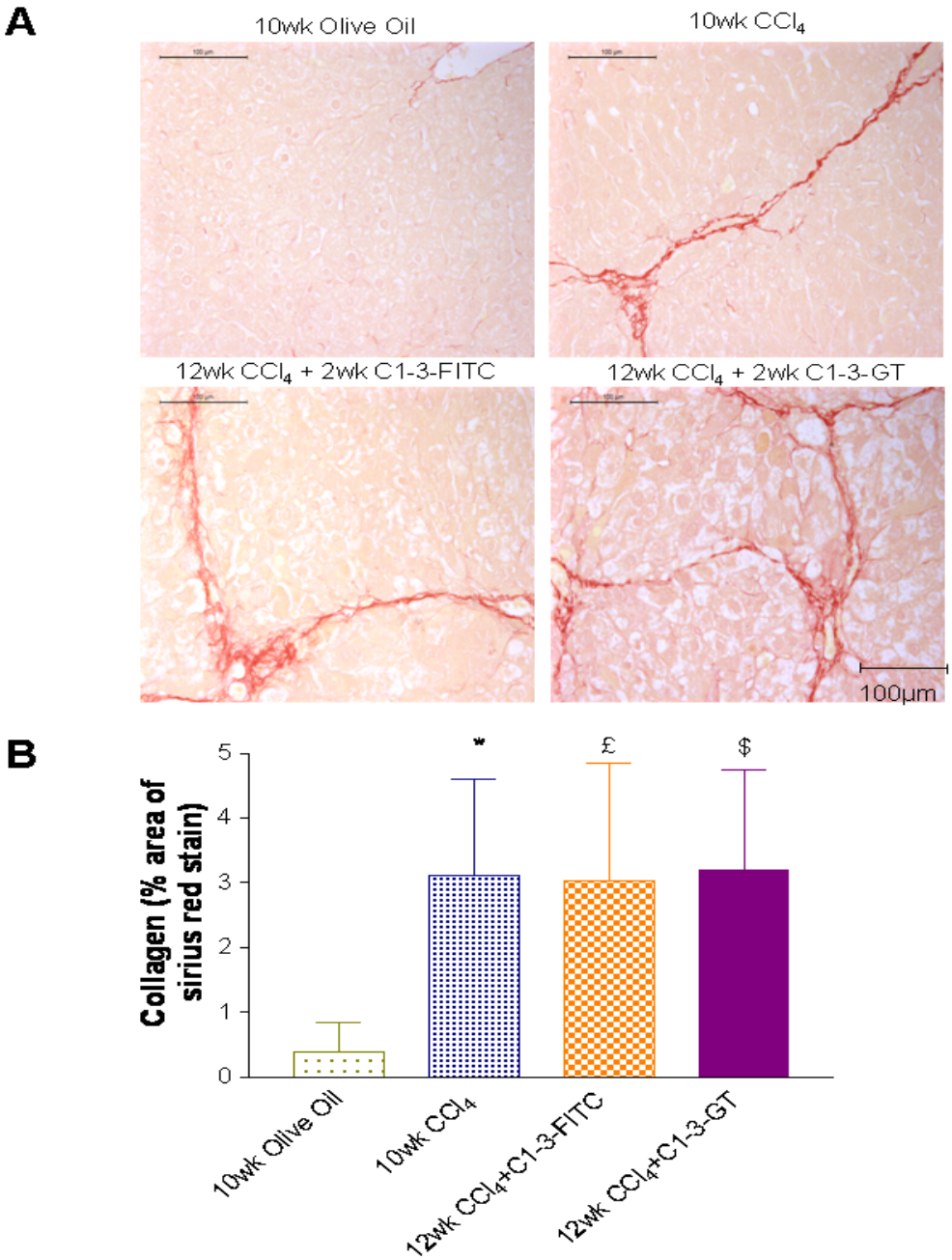

Figure 6-13 Picro-Sirius red staining and quantification following 10-12wks of CCl_4 or olive oil treatment. A: 4µm sections were incubated in picro-sirius red stain. Images were taken at x200 magnification and are representative of each treatment group. Scale bar=100µm. B: For quantification 10 random CLV were located and moved to the corner of the field of view to allow quantification of the band of collagen by Leica software analysis. Data are mean and SD of percentage area of picro-sirius red stain. Animal group numbers: Olive oil 10wk n=3. CCl_4 10wk n=5. C1-3-FITC 12wk n=8. C1-3-GT 12wk n=8. Data tested for statistical significance using the Student's two tailed T test. * represents significance between 10wk olive oil and 10wk CCl_4 ($p<0.0001$); £ represents significance between C1-3-FITC and 10wk olive oil ($p<0.0001$); $ represents significance between C1-3-GT and 10wk olive oil ($p<0.0001$).

The data show that treatment with CCl_4 results in a significant amount of collagen deposition in comparison to the olive oil controls (figure 6-12 and 13). Even after 4 wks of CCl_4 treatment the collagen deposition extends outwards from the centrilobular vein and after 10-12wks of CCl_4 treatment these bands of scar connect together, termed bridging fibrosis. More importantly however, the

quantification data show that treatment with C1-3-GT did not affect the amount of collagen deposited when compared to the C1-3-FITC control mice at either of the two injury time points (figures 6-12B and 6-13B). RT-PCR was used to confirm that these data were reflective of the expression of the col1a1 gene (figure 6-14).

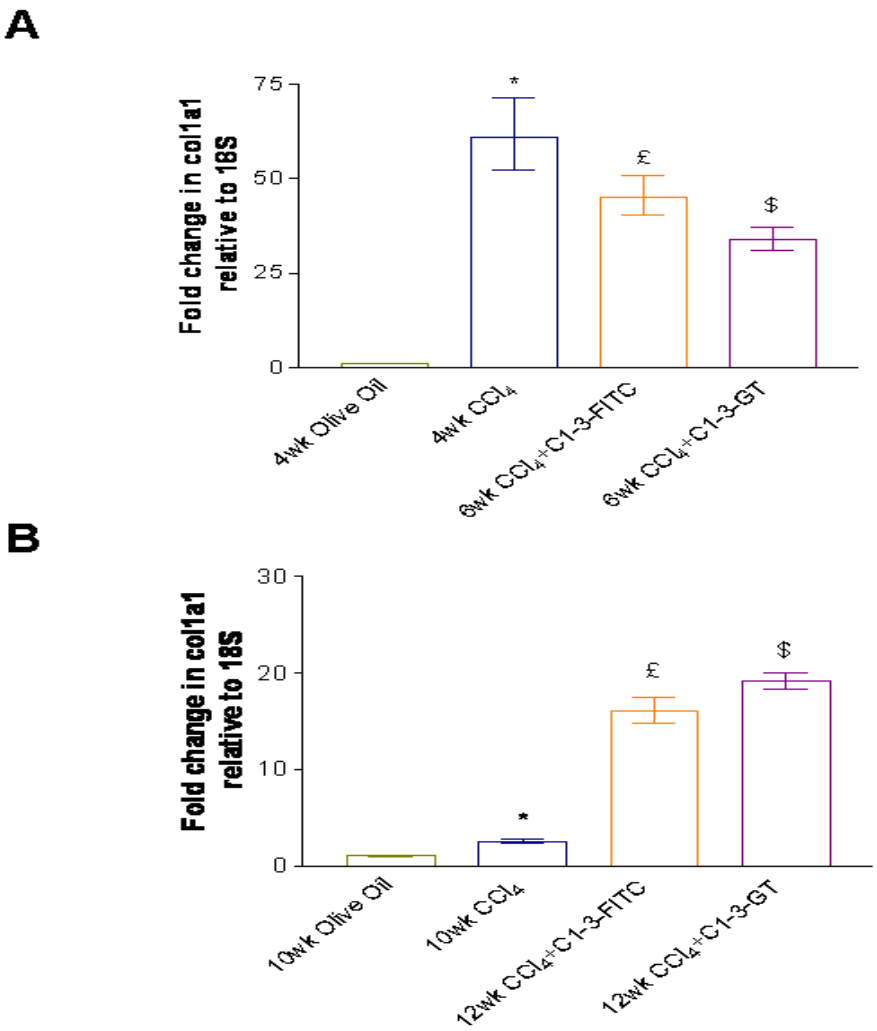

Figure 6-14 Relative gene expression levels of collagen 1a1 in CCl_4 and olive oil treatment groups. RNA was isolated from each mouse liver using Trizol, quantified and reverse transcribed using oligo dT. RT-PCR was carried out for 40 cycles and analysed using Applied Biosystems TaqMan software. All experiments were performed in duplicate and data are the mean and SD of the fold change relative to 18S and normalised to expression levels in the relative olive oil controls. Data tested for statistical significance using the Student's two tailed T test. * represents significance between olive oil and CCl_4 (A:$p<0.05$; B:$p<0.01$); £ represents significance between C1-3-FITC and olive oil (A:$p<0.0001$; B:$p<0.005$)); $ represents significance between C1-3-GT and olive oil (A/B:$p<0.0001$). Animal group numbers: Olive oil 4/10wk n=3. CCl_4 4wk n=6; 10wk n=5. C1-3-FITC 6wk n=7; 12wk n=8. C1-3-GT 6/12wk n=8.

Figure 6-14A and B show that treatment with CCl_4 results in a significant increase in collagen 1a1 gene expression relative to the olive oil controls. This correlates with the picro-sirius red staining and quantification in figures 6-12 and 6-13. Whilst the data in figure 6-14B show that collagen 1a1 expression in mice treated with CCl_4 for 10wk was significantly higher than the 10wk olive oil, the fold

change in expression for the 10wk CCl_4 group is not as high as that observed in figure 6-14A. This disagrees with the picro-sirius red quantification data which showed a substantial significant increase in collagen deposition in CCl_4 treated mice compared to the olive oil controls (figure 6-13B). Nevertheless, collagen 1a1 expression in both 6 and 12wk CCl_4 treatment groups was unaffected by C1-3-GT treatment.

Regression of fibrosis is an event regulated by the delicate balance of matrix metalloproteinases (MMPs), which are responsible for the degradation of ECM, and tissue inhibitors of metalloproteinases (TIMPs), which inhibit MMP mediated degradation. Hepatic myofibroblasts are a known source of MMPs and TIMPs, both of which are significantly upregulated during activation. Research has shown that TIMP-1 can be used as a serum marker of fibrosis [193] and over expression results in increased scarring during liver fibrosis [262]. Therefore TIMP-1 gene expression was investigated for all treatment groups at both injury time points by RT-PCR.

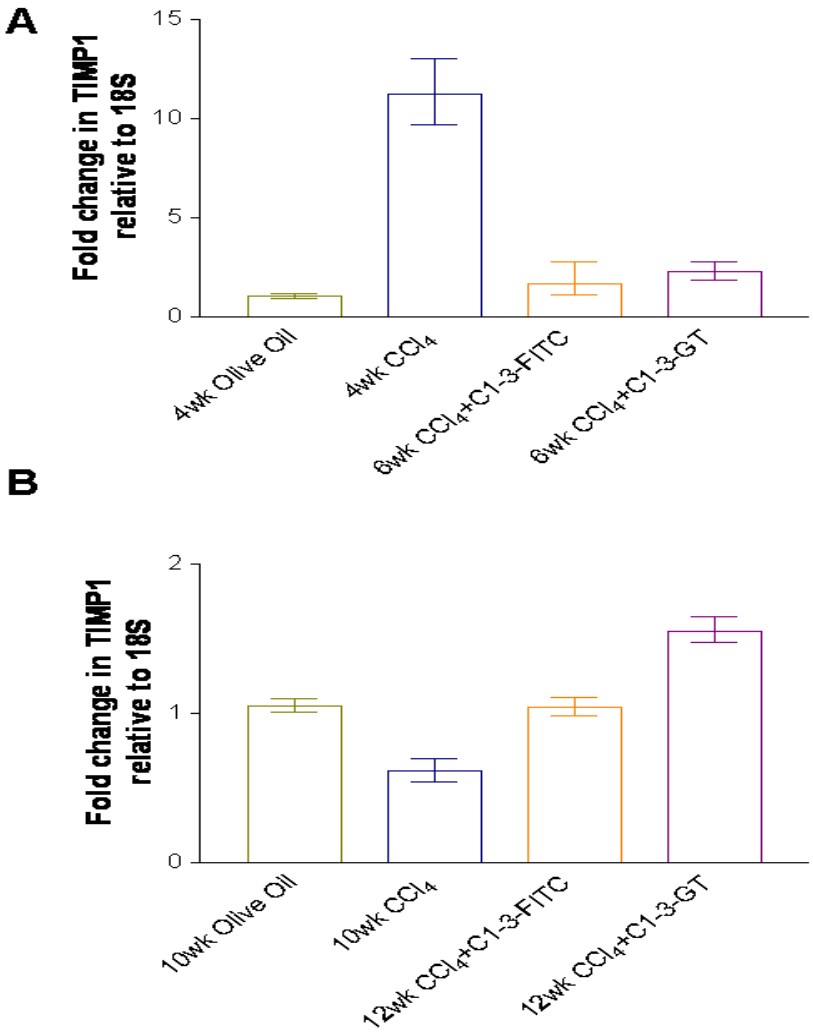

Figure 6-15 Relative gene expression levels of TIMP1 in CCl_4 and olive oil treatment groups. RNA was isolated from each mouse liver using Trizol, quantified and reverse transcribed using oligo dT. RNA was isolated from each mouse liver using Trizol, quantified and reverse transcribed using oligo dT. RT-PCR was carried out for 40 cycles and analysed using Applied Biosystems TaqMan software. All experiments were performed in duplicate and data are the mean and SD of the fold change relative to 18S and normalised to expression levels in the relative olive oil controls. Animal group numbers: Olive oil 4/10wk n=3. CCl_4 4wk n=6; 10wk n=5. C1-3-FITC 6wk n=7; 12wk n=8. C1-3-GT 6/12wk n=8.

Whilst the data in figure 6-15A shows a substantial increase in TIMP expression in mice treated for 4wks with CCl_4, due to huge differences in TIMP-1 gene expression between the animals this difference is not statistically significantly in comparison to the olive oil controls or the C1-3 treatment groups. No further differences in TIMP-1 expression are seen between the treatment groups and time points (figure 6-15).

TGFβ plays a prominent role in liver fibrogenesis inducing the net accumulation of ECM by the following mechanisms [263]:

1. Increasing synthesis of ECM components e.g. α2(I) procollagen
2. Preventing collagen degradation through inhibition of tissue collagenase
3. Stimulating production of inhibitors of ECM degrading enzymes e.g. TIMP-1

Hepatic myofibroblasts are a major source of TGFβ-1 during liver fibrogenesis, with expression levels directly associated with cellular activation status. Persistence of TGFβ signalling during fibrosis is thought to directly relate to disease progression since it has been shown to inhibit both proliferation and apoptosis of rat hepatic myofibroblasts [98]. Therefore expression levels of TGFβ-1 were analysed by RT-PCR to determine if C1-3-GT treatment had any effect on the signalling pathway. The results summarised in figure 6-16 show that TGFβ-1 gene expression remained relatively constant throughout the experiment with no significant differences observed between the C1-3-GT treatment groups in comparison to the C1-3-FITC control.

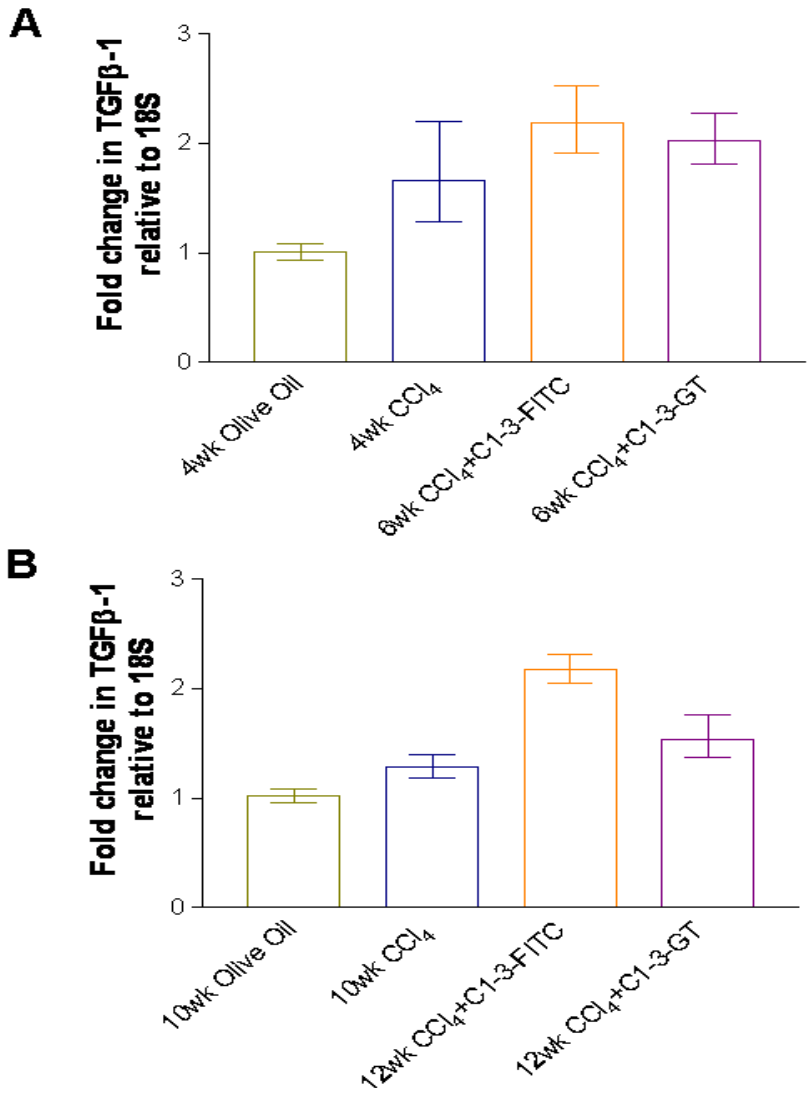

Figure 6-16 Relative gene expression levels of TGFβ-1 in CCl_4 and olive oil treatment groups. RNA was isolated from each mouse liver using Trizol, quantified and reverse transcribed using oligo dT. RNA was isolated from each mouse liver using Trizol, quantified and reverse transcribed using oligo dT. RT-PCR was carried out for 40 cycles and analysed using Applied Biosystems TaqMan software. All experiments were performed in duplicate and data are the mean and SD of the fold change relative to 18S and normalised to expression levels in the relative olive oil controls. Animal group numbers: Olive oil 4/10wk n=3. CCl_4 4wk n=6; 10wk n=5. C1-3-FITC 6wk n=7; 12wk n=8. C1-3-GT 6/12wk n=8.

Neutrophils form a vital part of the innate immune response to tissue injury and microbial infections. Their recruitment during injury or infection is thought to be aided by hepatic myofibroblast secretion of chemokines and cytokines [68]. Neutrophils were quantified by IHC staining to determine if C1-3-GT affected the number of neutrophils recruited in response to the CCl_4 injury (figure 6-17 and 18).

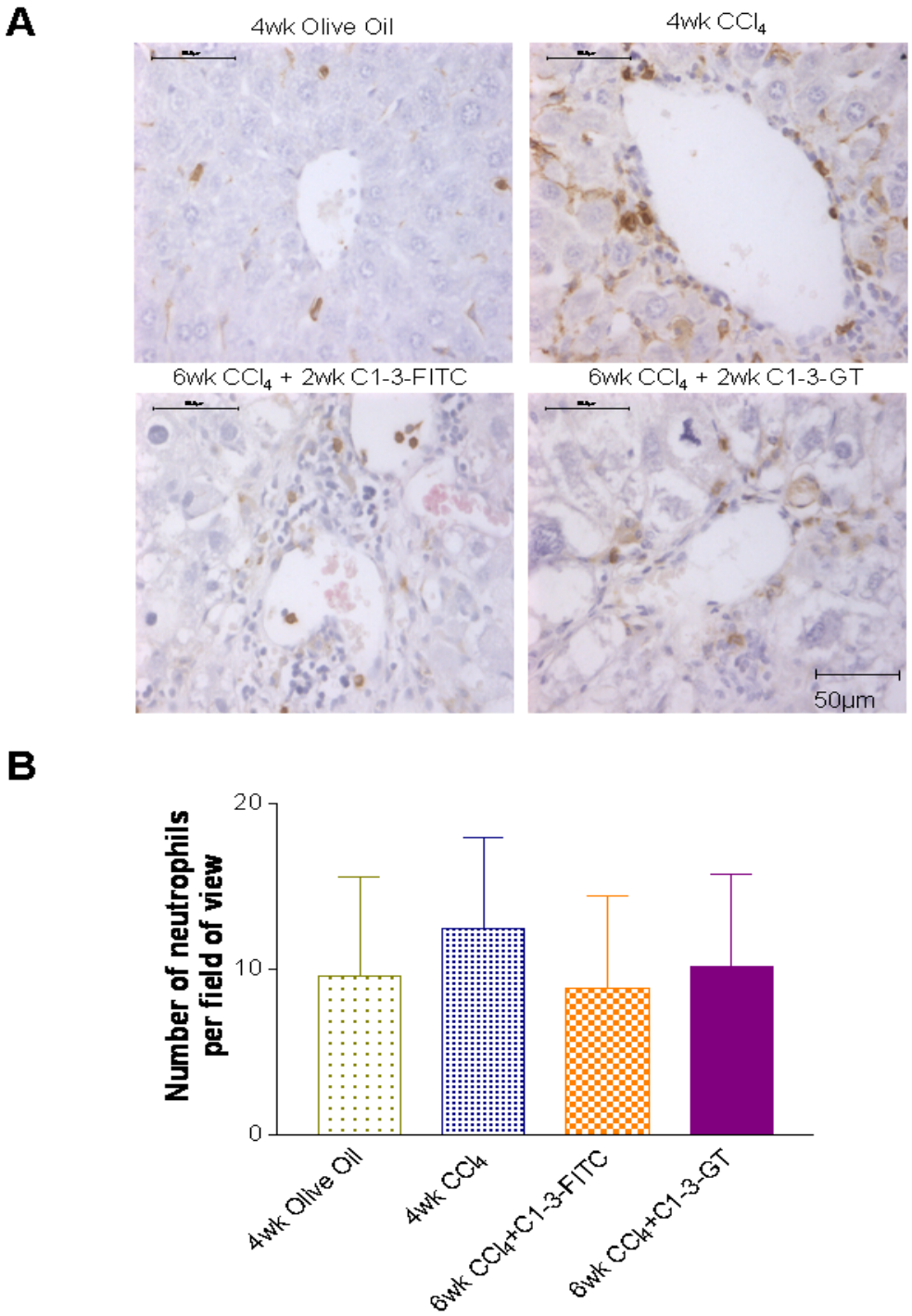

Figure 6-17 Neutrophil IHC staining and quantification in mice following 4-6wks treatment with CCl_4 or olive oil. A: Formalin fixed paraffin embedded tissue samples from each animal were cut into 4µm sections. Sections were dewaxed, subjected to proteinase K antigen retrieval, blocked and rat anti neutrophil primary antibody. Images were taken at x400 magnification and are representative of each treatment group. Scale bar=50µm. B: For quantification, pictures of 10 random CLV were taken at x400 magnification and the number of positive cells with clear nuclear staining counted. Data are the mean and SD of neutrophils per treatment group.

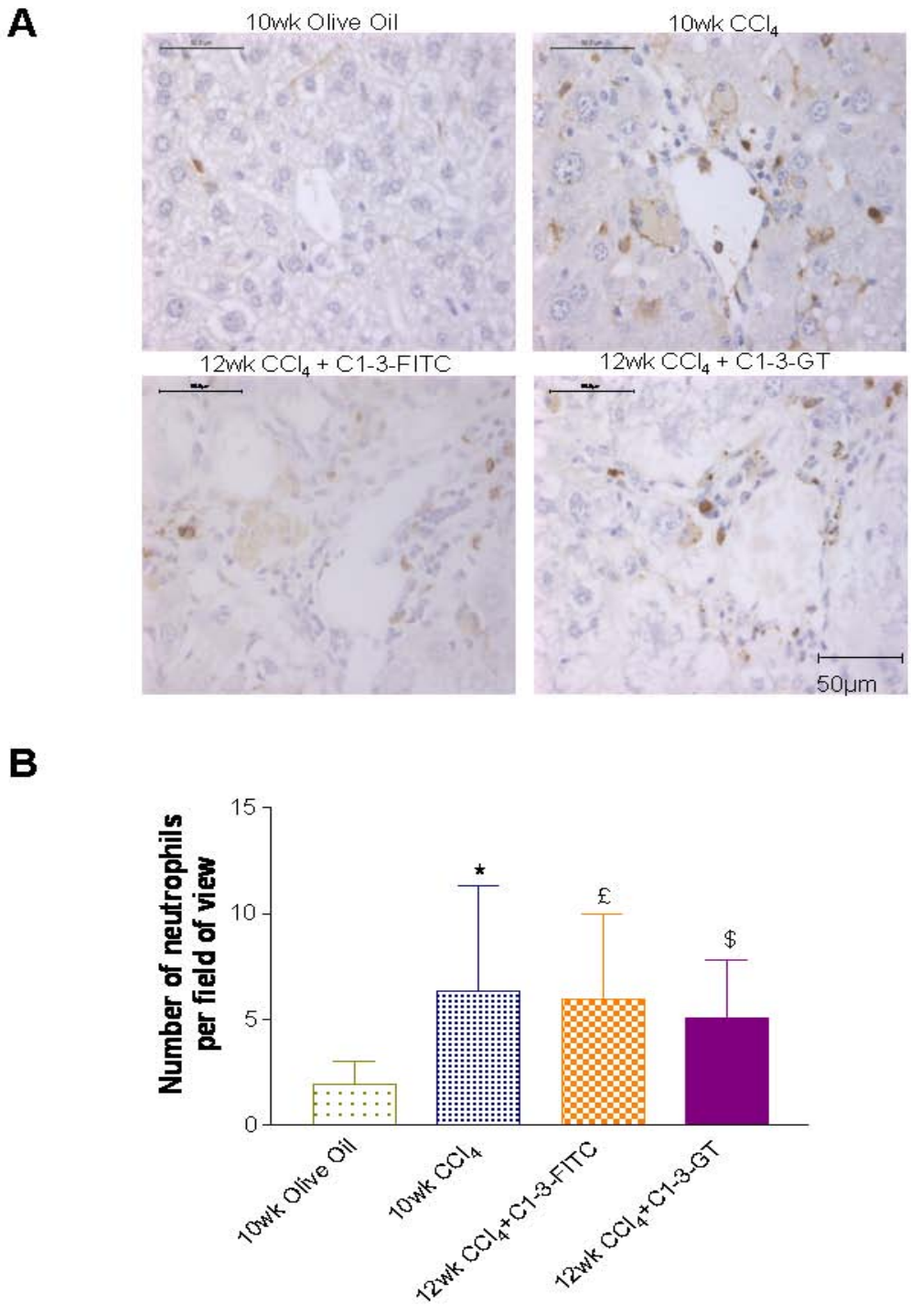

Figure 6-18 Neutrophil IHC staining and quantification in mice following 10-12wks treatment with CCl_4 or olive oil A: Formalin fixed paraffin embedded tissue samples from each animal were cut into 4µm sections. Sections were dewaxed, subjected to proteinase K antigen retrieval, blocked and rat anti neutrophil primary antibody. Images were taken at x400 magnification and are representative of each treatment group. Scale bar=50µm. B: For quantification, pictures of 10 random CLV were taken at x400 magnification and the number of positive cells with clear nuclear staining counted. Data are the mean and SD of neutrophils per treatment group. Data tested for statistical significance using the Student's two tailed T test. * represents significance between 10wk olive oil and 10wk CCl_4 ($p<0.0001$); £ represents significance between C1-3-FITC and 10wk olive oil ($p<0.0001$); $ represents significance between C1-3-GT and 10wk olive oil ($p<0.0001$).

The data in figure 6-17 show that there are no differences in the number of neutrophils surrounding CLV between the treatment groups. The numbers of

neutrophils present in the olive oil controls after 4 weeks of treatment was relatively similar to the CCl_4 mice at the same time point (figure 6-17B). After 10 to 12 weeks of CCl_4 treatment, neutrophil numbers were significantly higher than the olive oil controls (figure 6-18B) yet no differences were observed between the C1-3-FITC and C1-3-GT treatment groups. However, neutrophil numbers were significant reduced in the 10 week CCl_4 mice comparison to the 4 week CCl_4 mice (figure 6-19) suggesting that the inflammatory infiltrate is dependent upon injury progression.

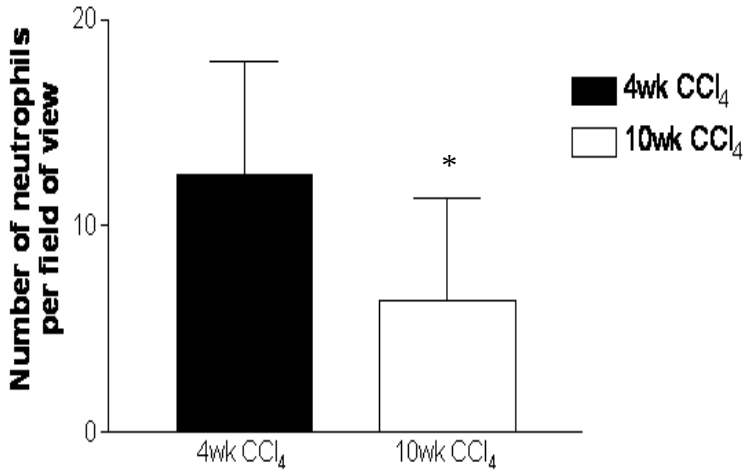

Figure 6-19 Neutrophil quantification following 4/10wk CCl_4 treatment. Data represent the average number (from 10 fields of view) of neutrophils surrounding CLV in 4/10wk CCl_4 treatment groups. Data tested for statistical significance using the Student's two tailed T test. * represents a significant reduction in neutrophils following 10wk CCl_4 vs 4wk CCl_4 ($p<0.0001$).

There is a vast amount of evidence suggesting that depletion of hepatic myofibroblasts during liver injury is essential for promoting repair and regeneration [100, 126] however myofibroblasts also secrete cytokines and growth factors that prime and stimulate proliferation of hepatocytes. To investigate cellular proliferation in this study, BrDU incorporation into newly synthesised DNA was quantified by IHC staining. Representative images of the staining are shown in figures 6-20 and 6-21.

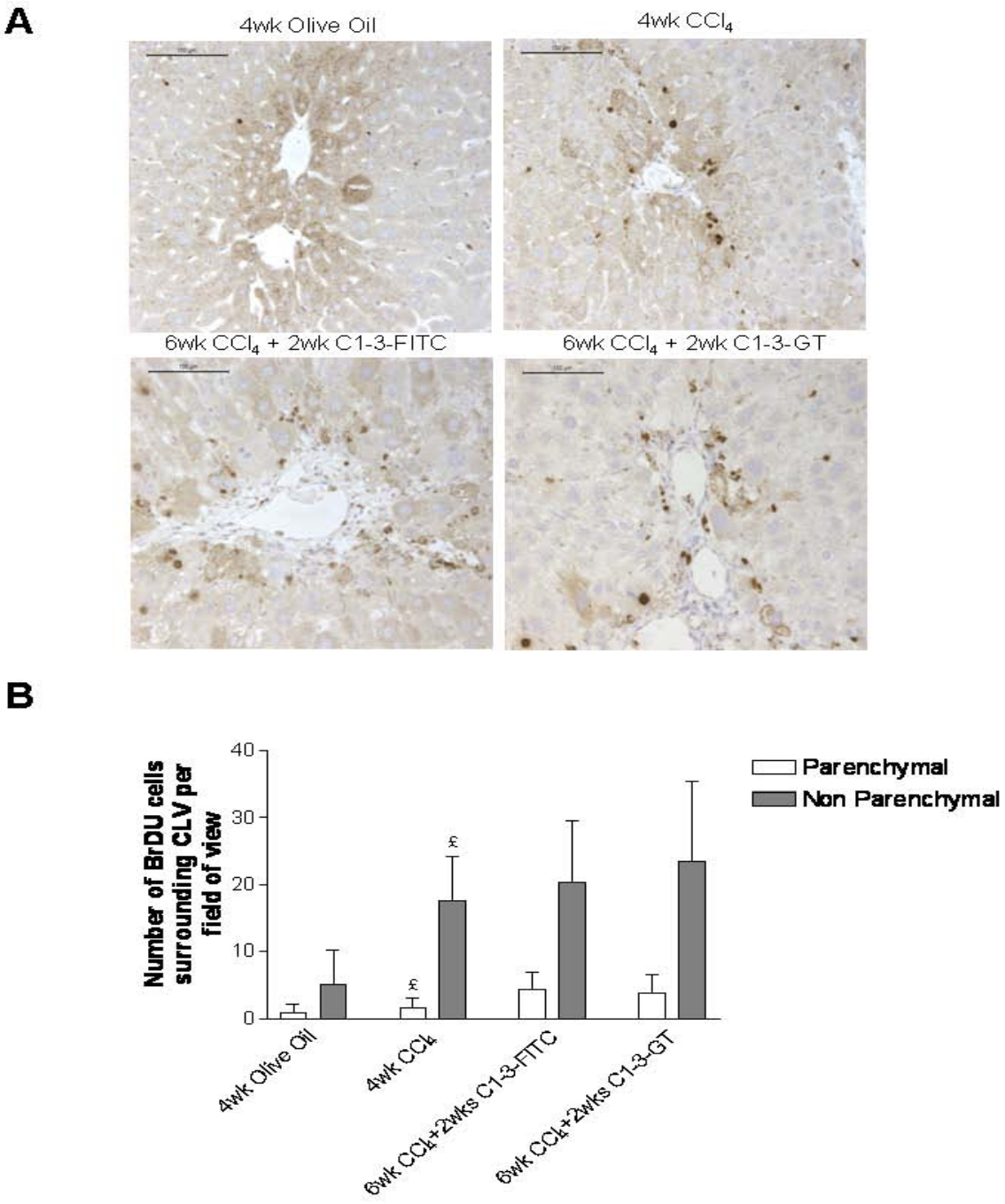

Figure 6-20 BrDU IHC staining and quantification of parenchymal and non parenchymal cells surrounding CLV in mice following 4-6 wks of treatment with CCl_4 or olive oil. A: 4µm were incubated with mouse anti BrDU primary antibody. All images taken at x200 magnification and are representative of each treatment group. Scale bar=100µm. B: For quantification, the number of parenchymal and non parenchymal cells (as determined by cellular morphology) with clear BrDU nuclear staining surrounding 10 random CLV regions were counted at x200 magnification. Data presented are the mean and SD of the average number of cells for each treatment group at each time point. Statistical significance was tested using Student's two tailed T test, % represents significance of parenchymal cells between 4wk CCl_4 vs. 4wk olive oil ($p<0.05$) £ represent significance of non parenchymal cells between 4wk CCl_4 vs. 4wk olive oil.

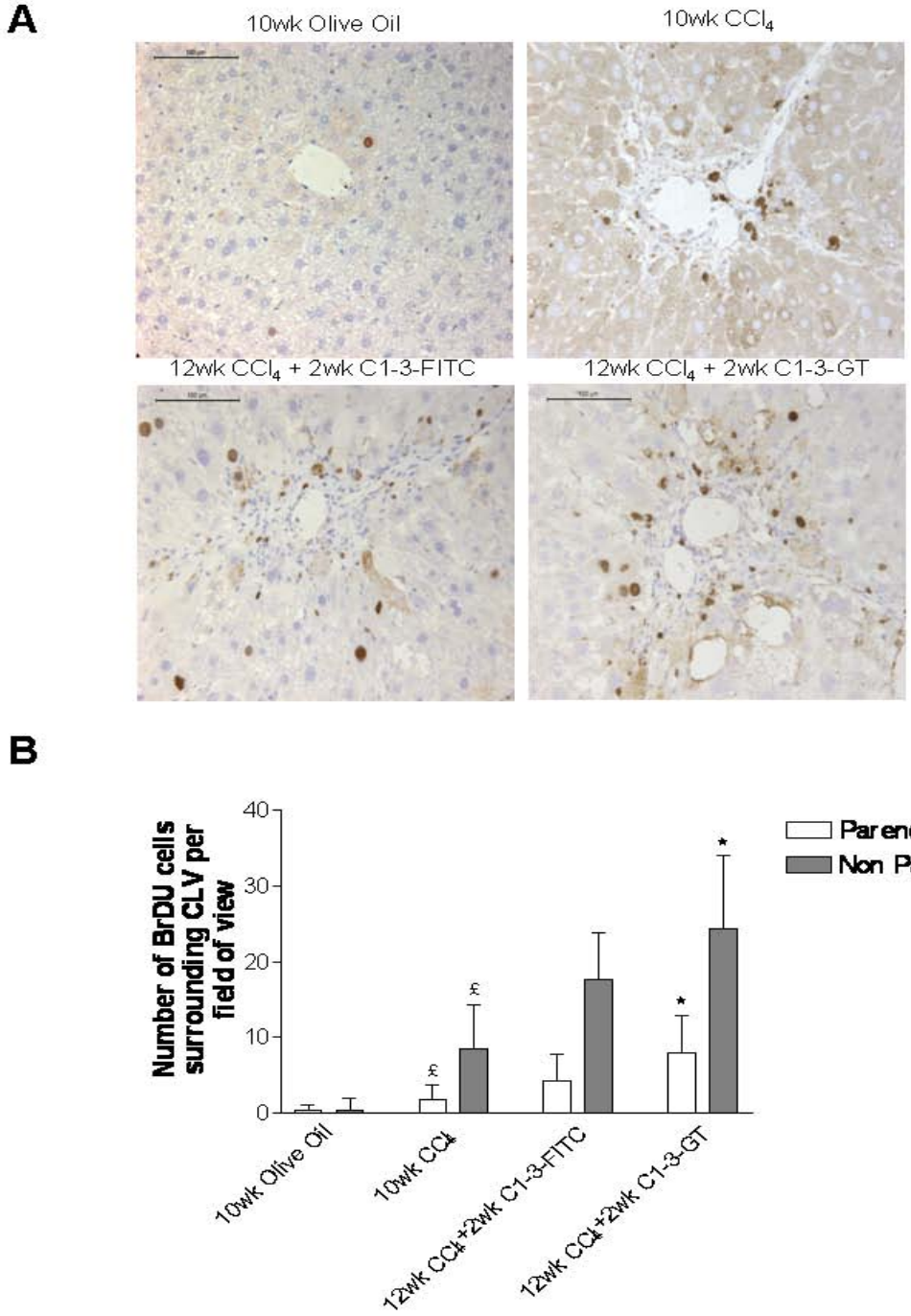

al cells surrounding CLV in mice following 10-12 wks of treatment with CCl_4 or olive oil. . A: 4µm were incubated with mouse anti BrDU primary antibody. All images taken at x200 magnification and are representative of each treatment group. Scale bar=100µm. B: For quantification, the number of parenchymal and non parenchymal cells (as determined by cellular morphology) with clear BrDU nuclear staining surrounding 10 random CLV regions were counted at x200 magnification. Data presented are the mean and SD of the average number of cells for each treatment group at each time point. Statistical significance was tested using Student's two tailed T test, % represents significance of parenchymal cells between 10wk CCl_4 vs. 12wk olive oil ($p<0.00001$) £ represent significance of non parenchymal cells between 10wk CCl_4 vs. 10wk olive oil ($p<0.0001$) * represents significance of parenchymal cells between C1-3-GT vs. C1-3-FITC ($p<0.0001$) £ non parenchymal C1-3-GT vs. C1-3-FITC ($P<0.0001$).

The data show that BrDU incorporation was significantly higher in mice treated for 4wks with CCl_4 in comparison to the olive oil controls yet no significant differences were observed between the C1-3 treatment groups (Figure 6-20). A similar trend was observed in the 10wk CCl_4 mice, furthermore C1-3-GT mice had a significantly higher number of BrDU positive parenchymal and non parenchymal cells when compared to the C1-3-FITC controls (Figure 6-21).

6.3 Discussion

The current paradigm of hepatic stellate cell activation into ECM secreting hepatic myofibroblasts remains the foundation for defining events in hepatic fibrosis [253] and continued elucidation of their mechanistic actions have made them attractive targets in the development of novel anti-fibrogenic therapies.

There is a growing body of evidence which implicates hepatic myofibroblast survival in the progression of hepatic fibrosis, with numerous animal studies concluding that reversal of liver fibrosis was associated with apoptosis of αSMA positive myofibroblasts [100-102, 126, 249] or eradication of the injurious agent [205]. A fundamental discovery by Wright *et al* [102] provided proof of concept data which showed that induction of hepatic myofibroblast apoptosis by gliotoxin was essential for reducing collagen deposition and improving liver function in a rat recovery model of liver fibrosis. Gliotoxin, a fungal metabolite, is a potent NFκB inhibitor [102] and is capable of inhibiting TNFα inducible NFκB DNA binding activity in hepatic myofibroblasts as well as stimulating their apoptosis through a specific thiol redox-dependent interaction with the adenine nucleotide transporter [105]. Furthermore, when conjugated to C1-3, a scAb which specifically binds synaptophysin expressing hepatic myofibroblasts, the apoptotic effect of gliotoxin could be specifically targeted providing a novel approach for depleting ECM secreting myofibroblasts during injury [126, 249] without removing cells essential in liver regeneration [264]. The major limitation with these and other fibrosis studies is that the anti-fibrogenic agents are tested in recovery models of fibrosis, i.e. where the injurious agents have been removed. Recent publications have demonstrated that hepatic myofibroblasts secrete key factors involved in liver regeneration [144, 146, 265]. Therefore it is essential to determine if depletion of myofibroblasts during sustained injury would promote or hinder liver regeneration. This chapter set out to investigate whether depletion of hepatic myofibroblasts during two different stages of liver fibrosis would promote reversal and regeneration during sustained injury.

For this study, two liver injury time points were chosen to represent two different grades of fibrosis. Previous work investigating spontaneous resolution of liver fibrosis in rats has shown that following 4wks of CCl_4 injury complete resolution of normal tissue architecture can be achieved following cessation of injury [100]. However after 12wks of treatment, remodelling of the ECM took substantially

longer and was incomplete with extensive collagen cross linking only allowing the mirconodular cirrhosis to be remodelled to macronodules [266].

Mice were divided into treatment groups to either receive 4 or 10wks of CCl_4 or olive oil treatment with further subgroups receiving C1-3-FITC or C1-3-GT for a following 2 weeks in combination with CCl_4 treatment. This would allow for changes in fibrosis to be directly compared between C1-3 treatment groups as well as monitoring changes in collagen deposition in reference to baseline controls, i.e. 4 and 10wks of CCl_4 or olive oil treatment.

Initial experiments set out to confirm that the C1-3-GT had depleted hepatic myofibroblasts by quantifying myofibroblast number through IHC staining and RT-PCR. Interestingly, no differences in αSMA/synaptophysin IHC staining or gene expression were observed in mice treated for 6wks with CCl_4 with 2 weeks of C1-3-GT in comparison to the C1-3-FITC control. This would suggest that the study had not worked, with mice not receiving an effective therapeutic dose of C1-3-GT since previous studies have shown that C1-3-GT depleted approximately 60% of hepatic myofibroblasts in a recovery model of liver injury [126]. Hepatic myofibroblasts derived from quiescent HSCs are not the only source of αSMA positive cells during liver injury, with portal myofibroblasts [55], biliary epithelial cells undergoing EMT [25, 62] and circulating bone marrow derived myofibroblasts [24, 60] also contributing to this population (Figure 6-23). It is important to note that the contribution of bone marrow myofibroblasts and myofibroblasts derived from EMT is still debated. Recent publications have shown that hepatocytes do not undergo EMT [267] and genetic labelling failed to detect EMT in murine cholangiocytes [268]. Yet, there is convincing evidence in the literature that they sources do exist [24, 26, 60, 61, 269] thus, it is possible that depletion of hepatic myofibroblasts may stimulate the recruitment of other myofibroblast populations. Whilst the synaptophysin RT-PCR and IHC data may discredit this idea somewhat, it is important to note that the number of synaptophysin positive cells was substantially lower than the number of αSMA positive cells suggesting that the commercial antibodies available may not detect all synaptophysin positive cells. This is possibly due to a splice variant of the protein, and thus is not an accurate reflection of synaptophysin expressing hepatic myofibroblasts. Ideally, synaptophysin expressing hepatic myofibroblasts would be quantified using the C1-3 antibody itself, however since C1-3 does not

work in fixed tissue further optimisation of IHC staining protocols are required. To determine if αSMA myofibroblasts are derived from other cellular sources, it would be necessary to carry out a dual antibody stain combining αSMA with markers of portal myofibroblasts, e.g. elastin or markers of the EMT process e.g. S100A4 [26].

Mice treated for 12wks with CCl_4 with the addition of C1-3-GT for a final 2 weeks had a significant 12% reduction in αSMA staining in comparison to the C1-3-FITC controls. However synaptophysin staining revealed that this decrease was associated with a 21% significant increase in synaptophysin positive cells around CLV. Synaptophysin is also expressed by oval cells, a progenitor cell population which contribute to liver regeneration by differentiation into hepatocytes and biliary epithelial cells. Since the number of synaptophysin positive cells quantified suggests that not all cells are being stained with the commercial antibody, it is possible that hepatic myofibroblast depletion, as determined by a decrease in αSMA staining, promotes liver regeneration through increased oval cell proliferation. To confirm if this is the case it would be necessary to do a dual label for synaptophysin and an oval cell marker, e.g. OV6.

Hepatic myofibroblasts have been identified as the principal producer of the major component of the hepatic scar, collagen I [32, 270], which disrupts tissue architecture and function. Collagen deposition increases with continued injurious stimulus which correlates with an increasing number of αSMA expressing hepatic myofibroblasts [251]. Upon cessation of injury, regression of fibrosis is associated with a significant decrease in collagen 1a1 gene expression due to ECM remodelling. In this study, collagen deposition was quantified by picro-sirius red IHC staining and RT-PCR analysis. Both quantification methods showed that there were no significant differences in collagen deposition between the C1-3-GT and C1-3-FITC treatment groups. Whilst no difference in collagen levels in the 6 week treatment groups can be explained by a failure of hepatic myofibroblast depletion, a significant decrease in αSMA staining typically correlates with decreases in collagen, as shown by previous animal models of fibrosis [100, 126]. This may be the result of extensive collagen cross-linking making the scar degradation resistant [266] or a longer recovery time required to allow for tissue remodelling. Furthermore recent reports have suggested that hepatic myofibroblasts are not the only source of ECM components during fibrosis, with

studies implicating bone marrow myofibroblasts [24], portal fibroblast [22, 23] and fibroblasts derived by EMT [25] contributing to ECM deposition.

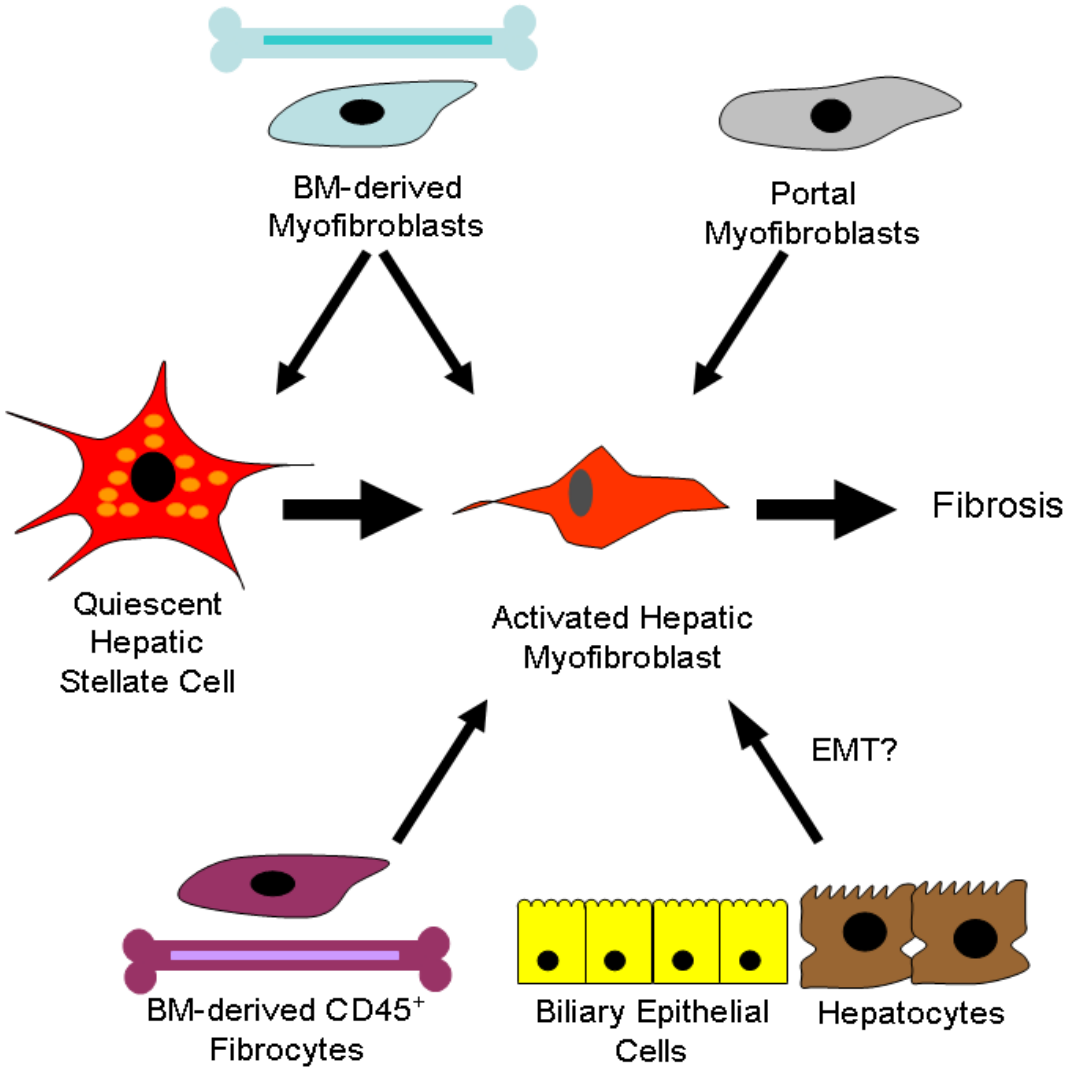

Figure 6-22 Sources of myofibroblasts during liver injury. Adapted from [80], this diagram illustrates all potential sources of activated myofibroblasts involved in liver fibrosis.

TGFβ1 is secreted in a latent form by hepatic myofibroblasts in response to liver injury [37]. Once activated, this cytokine exerts its potent fibrogenic effects on cells in both an autocrine and paracrine manner promoting the net accumulation of ECM components during liver fibrosis [263]. TGFβ1 gene levels in human hepatic fibrosis have been found to closely correlate with serum type III procollagen peptide suggesting that TGFβ1 has an important role in the pathogenesis of liver fibrosis [271]. Interestingly, TGFβ1 gene expression remained relatively constant between the CCl_4 and olive oil treatment groups for both injury time points which would suggest that this cytokine was not important in liver disease. However, TGFβ can be stored in an inactive form within the extracellular matrix thus it is possible that the extracellular stores may be being

used to drive fibrosis [272]. To confirm RT-PCR results, TGFβ1 protein expression could be investigated by immunohistochemical methods in the mouse liver tissue.

Regression of fibrosis is dependent upon the delicate balance of MMPs and their inhibitors, TIMPs. High expression levels of TIMP-1, which are produced by hepatic myofibroblasts during liver injury [50], correlate with advanced fibrosis and prevent fibrosis regression through inhibition of the degradation of the scar matrix and inhibition of myofibroblast apoptosis [273]. Furthermore, spontaneous resolution of liver fibrosis was associated with a decrease in TIMP-1 expression [100] whilst over expression of TIMP-1 enhanced experimental fibrosis [262]. It was predicted that TIMP-1 gene expression would be significantly higher in CCl_4 treated mice in comparison to the olive oil controls however this was not the case in either treatment groups. Instead TIMP-1 gene expression remained relatively constant when fold change was calculated with respect to the olive oil controls indicating no difference in TIMP-1 gene expression. This result may reflect actual levels of TIMP-1 gene expression in the liver however only a small proportion of the tissue is used for RNA extraction thus this may not be reflective of the whole tissue levels. Analysis of key MMPs, e.g. MMP2, MMP13 [274], would be of interest since MMP catabolism of the ECM is an important feature of recovery.

The neutrophil chemotactic response following liver injury is thought to be partially mediated by hepatic myofibroblast secretion of platelet activating factor [270] thus C1-3-GT mediated hepatic myofibroblast depletion may affect the inflammatory response during injury. Quantification of neutrophil IHC revealed that there were no differences in the number of neutrophils surrounding CLV following 4-6wks of olive oil or CCl_4 treatment. The presence of neutrophils in the olive oil controls may reflect an inflammatory reaction in response to the regular dosing of ‘fat’. This is commonly seen in clinical practice in patients that consume excess amounts of fats and is termed non alcoholic steatohepatitis (NASH). As fibrosis progresses the number of neutrophils surrounding CLV decreased, particularly in the olive oil controls since neutrophils are an important part of the innate immune response to tissue injury and infection and only persist in the tissue in certain disease pathologies, e.g. alcoholic hepatitis [275] and ischemia reperfusion injury [276, 277]. Hepatic myofibroblasts are known to secrete cytokines and chemokines chemotactic for immune cells, thus it would be of

interest to investigate kupffer cell numbers following C1-3-GT treatment as they play an important role in modulating the inflammatory response and fibrosis progression/regression [5, 278].

The current scientific literature implicates hepatic myofibroblast apoptosis as a significant event in the stasis or reversal of liver fibrosis [100, 101, 126, 266], however there is emerging evidence that hepatic myofibroblasts provide essential factors which promote hepatocyte proliferation [144, 146, 265] thus their depletion may have unprecedented effects on subsequent liver regeneration. The data in this chapter show that hepatic myofibroblast depletion in mice treated for 12wks with CCl_4 significantly increased cellular proliferation, as determined by parenchymal and non parenchymal cellular BrDU incorporation. This correlated with a significant increase in synaptophysin cell number which may be indicative of an oval cell response. To confirm this dual IHC staining with both synaptophysin and OV6 would be required. However no change in collagen deposition was observed suggesting that either hepatic myofibroblast depletion promoted recruitment of other myofibroblasts to the liver or extensive collagen cross linking made the scar resistant to degradation. Taken together the data suggest that hepatic myofibroblast depletion during sustained injury does not promote reversal of liver fibrosis and previous results obtained in recovery models imply that the removal/treatment of the injurious agent is critical for regeneration [205, 279, 280].

Chapter 7. Final Discussion

7.1 Results Summary

Liver fibrosis refers to the accumulation of tough, fibrous scar tissue within the liver. It is a natural wound healing response to an injurious agent to encapsulate the damage and once the injurious agent is removed the distorted architecture is remodelled and the liver regenerates damaged hepatocytes by stimulating their proliferation. However if the injurious agent is not removed, the liver becomes overwhelmed with the continued stimulation causing prolonged activation of hepatic myofibroblasts with excessive deposition of ECM distorting normal liver architecture and ultimately affecting liver function. Historically end staged liver disease, cirrhosis, was deemed to be irreversible with a liver transplant being the only viable treatment option. However further elucidation of the cellular and molecular fibrogenic wound healing pathways have identified new therapeutic targets [281] which are desperately needed. A recent report highlighted that approximately 1-2% of the US population suffer from HBV and HCV infection, which are leading causes of both cirrhosis and hepatocellular carcinoma resulting in the preventable deaths of approximately 15,000 US citizens each year [282].

Despite the recent advances there are still no anti fibrotic therapies available which have been proven to slow fibrosis progression or even stimulate the fibrosis regression. Nevertheless even if a major breakthrough did occur, the poor diagnostic tools currently available prevent the accurate monitoring of disease progression, an essential criterion for any new treatment regime. Furthermore, the development of a highly sensitive, reproducible non invasive test to aid in the distinction between the stages of liver disease will allow the implementation of appropriate therapeutics that may slow/prevent further progression of fibrosis and favour liver regeneration. The data presented in this thesis show that the number of hepatic myofibroblasts within the liver, as determined by αSMA staining, is representative of the stage of fibrosis, with increasing cell number correlating with advanced fibrosis and collagen deposition. Interestingly, *i.p.* injection of C1-3-AF, which binds to synaptophysin positive hepatic myofibroblasts only, demonstrated a significant increase in total flux in CCl_4 treated animals in comparison to the olive oil controls at selected time points during the live animal imaging and in the 12wk CCl_4 livers only. However, total flux did not increase proportionally with

CCl_4 treatment time suggesting that C1-3-AF would not be a useful tool in the diagnosis of liver disease since it cannot clearly distinguish between the different stages of liver fibrosis.

Previous work by the Wright group, as well as many others, have demonstrated that hepatic myofibroblast depletion (due to induced or spontaneous apoptosis) following cessation of liver injury enhances liver regeneration in comparison to controls [100-102, 126, 249, 266]. However, this is not representative of the clinical situation since the underlying injurious agent cannot always be removed. Furthermore, recent studies have identified that hepatic myofibroblasts produce factors that are critical in the regenerative response, such as IL-6, HGF and serotonin [131, 138, 146] thus further investigation of the effects of myofibroblast depletion are urgently required. In an attempt to answer this question, hepatic myofibroblasts were depleted in two different animal models; chronic injury and liver regeneration

C1-3-GT or C1-3-FITC was administered during the final two weeks of CCl_4 treatment to determine if depletion during sustained injury promoted fibrosis reversal. Hepatic myofibroblast depletion was only successful in the 12wk CCl_4 model of end stage cirrhosis, as confirmed by a reduction in the percentage of αSMA staining. However, no significant differences in collagen deposition were observed suggesting that the collagen may be resistant to degradation. This result correlates with a previous report which has shown that remodelling of extensively crossed-linked collagen scar tissue was incomplete even after 366 days following removal of the fibrosis causing agent [266]. To investigate if C1-3-GT mediated depletion would enhance the resolution of fibrosis following the cessation of CCl_4 injury, it would be necessary to extend the study and sacrifice the animals at a later time point, e.g. 6 months post injury.

To investigate the role of hepatic myofibroblasts during liver regeneration, C1-3-GT was administered at critical time points before and after PHx. The data obtained from this study were quite conflicting with synaptophysin and αSMA quantification failing to confirm successful depletion of hepatic myofibroblasts. Nevertheless, C1-3-GT treatment suggested that hepatic myofibroblasts have opposing roles in liver regeneration, both enhancing and inhibiting cellular proliferation. Since there is no evidence within the literature which can support

these findings, it would be necessary to confirm these results using another method of hepatic myofibroblast depletion.

7.2 Project Limitations

C1-3 has been shown to bind to synaptophysin positive hepatic myofibroblasts *in vivo* providing a novel method for targeting therapeutics [125, 126, 249], yet its use in the animal studies described above is subject to limitations. Historically hepatic myofibroblasts have been considered the principal cell type involved in the perpetuation of liver fibrosis due to excessive ECM deposition and resistance to apoptosis [37, 270]. However, there is now emerging evidence that other cellular sources contribute to the population of myofibroblasts present during liver disease [17, 22-26, 283] with a large proportion of them expressing the classical myofibroblast marker, αSMA. This means that C1-3-GT mediated depletion needs to be confirmed by both αSMA and synaptophysin quantification, a task which has proved difficult. Synaptophysin IHC staining was optimised with mouse pancreatic tissue however the number of cells staining positive for synaptophysin in the liver was substantially lower than expected, especially for CCl_4 treatment groups. An example of this is the PHx study, whilst the data suggest that C1-3-GT depletion has delayed subsequent liver regeneration, as demonstrated by BrDU incorporation, synaptophysin IHC and RT-PCR would suggest that only a small percentage of the αSMA myofibroblasts express synaptophysin. It is possible that other myofibroblast/liver cell populations regulate the pathways governing liver regeneration, for example C1-3-GT resulted in a significant increase in the proliferation of αSMA myofibroblasts surrounding PT with no significant differences observed in those surrounding CLV. The location of these cells would suggest that they are either portal myofibroblasts or derived from cholangiocytes by EMT or a combination of both. Whilst EMT is still debated in the literature, its contribution could be easily tested using markers of the EMT process: S100A4, vimentin and MMP2. These markers have been validated by groups investigating EMT [26, 66] and when used in combination with elastin, a marker of portal myofibroblasts, they would be sufficient to distinguish the populations of αSMA myofibroblasts within both animal models. However, it is still important to confirm myofibroblast depletion in order to validate the results generated in both animal models. To date, there are no unique hepatic myofibroblast markers making it very difficult to confirm C1-3-GT mediated

depletion by other methods and even if any were identified, it would be necessary to confirm that they were expressed by synaptophysin positive hepatic myofibroblasts thus further optimisation of synaptophysin detection methods are required. Since C1-3 does not work in fixed tissue, it would be necessary to develop a polyclonal antibody which detects the peptide 2 region of the synaptophysin protein in case a splice variant of the protein exists.

RT-PCR, using commercially available TaqMan probes, has been extensively used in this project to confirm hepatic myofibroblast depletion and its subsequent effect on cytokines/growth factors associated with the cell type. On many occasions the data failed to show differences in cytokine/growth factor expression between the treatment groups, a result that was somewhat unexpected. Whilst some cytokines/growth factors, e.g. HGF and TGFβ, are stored in an inactive form within the ECM thus production is not required, it is possible that RT-PCR was not functioning under optimal conditions. In order to validate the RT-PCR data it would be necessary to perform a serial dilution of the cDNA template, plotting the log concentration vs. C_T value. If the reaction is 100% efficient, the R^2 value should be 1. If the value is less than this, it would suggest problems with cDNA quantitation or quality. Furthermore, a range of endogenous controls, e.g. GAPDH; actin, should be evaluated to ensure that the absolute quantification values are accurate since any slight variations in the endogenous control will reflect in the fold change of gene expression recorded.

The imaging data acquired using IVIS provides proof of concept that myofibroblasts can be used to distinguish between fibrotic and non fibrotic liver with data from the excised liver showing a significant increase in liver flux in 12wk CCl_4 liver in comparison to the olive oil controls. However, the quenching of the fluorescent signal by the liver and other tissues means that the total flux obtained during the live animal imaging is not reflective of the actual value. To overcome this, a fluorophore which emits near the end of the infra red spectrum could be used since non specific absorption by the bodily fluids and tissue is substantially lower. Furthermore, the expression of synaptophysin by cells within the pancreas limits the use of C1-3 as a diagnostic tool as it would not be liver specific. To overcome this, a 3D scan could be used to map the fluorescence to a specific area within the body however this is not feasibly possible at the moment. Finally, C1-3-AF was only trialled as an imaging agent in liver disease caused by

centrilobular injury. Since research has implicated the portal fibroblast as the principal cell type in obstructive cholestasis [52, 53] further testing in different animals models of liver disease, e.g. obstructive cholestasis, are required.

Whilst the animal studies described in this thesis provide useful pilot data, the group numbers used are too low to provide a statistically significant result, particularly in the RT-PCR data due to the large variations in gene expression between animals. Future studies need to take into account death from surgical/procedural complications and should be calculated using the power analysis method to estimate the minimum number of animal required to achieve statistically significant differences.

7.3 Future Directions

In order to understand the implications of the animal studies described in this thesis it is necessary to establish that C1-3-GT therapy has successfully depleted hepatic myofibroblasts *in vivo*. It is possible that problems associated with the conjugation process, excess PMPI:Gliotoxin addition favours protein precipitation, resulted in mice receiving a sub-optimal dose of C1-3-GT making it difficult to interpret the results. One way to confirm this would be to use C1-3 itself or a polyclonal antibody reactive with the peptide 2 region of the synaptophysin protein (in case a synaptophysin splice variant exists) in Western blotting and IHC analysis. Since C1-3 binds to synaptophysin under native conditions, i.e. unfixed cells, IHC needs to be carried out in frozen tissue where the synaptophysin protein will not have been affected by formalin fixation. However frozen tissue has poor morphology and results in diffuse staining patterns making it difficult to interpret results. In the final animal study C1-3-FITC was used as a conjugated scAb control in an attempt to quantify the number of synaptophysin positive cells in the CCl_4 tissue since, in theory, it could be either visualised directly in the tissue by fluorescence or using an antibody that is directed against FITC and is directly conjugated to HRP (mouse anti FITC-HRP). However further optimisation of staining protocols are required since no fluorescence was visible when the tissue was excited at the appropriate wavelength and amplification of the fluorescent signal using a mouse anti FITC-HRP antibody resulted in high background staining making identification of individual cells difficult.

An independent method to confirm the results obtained by the sustained injury and PHx animal studies would be to use a genetic model of hepatic myofibroblast depletion. Studies have shown that the prolonged survival of hepatic myofibroblasts which favours progression of liver fibrosis is associated with constitutive NFκB signalling and prevents cellular apoptosis [106]. Administration of sulfasalazine resulted in the selective blocking of NFκB dependent gene transcription and promoted hepatic myofibroblast apoptosis *in vivo*. NFκB is an important signalling pathway in many biological processes, thus targeted inactivation in hepatic myofibroblasts can be achieved using transgenic mice in which the super repressor human IκB transgene is expressed under the control of glial fibrillary acidic protein (GFAP) promoter. Inactivation of NFκB signalling in astroglial cells has been shown to have a protective effect following spinal cord injury and was associated with a reduced inflammatory response [284]. GFAP expression correlates with activation of HSC into hepatic myofibroblasts thus the effect of myofibroblast depletion during sustained injury and liver regeneration could be investigated without the concern about therapeutic doses of C1-3-GT.

A recent study has shown that hepatic myofibroblasts co-express $p75^{NTR}$ (p75 neurotrophin receptor) and sortillin which allows the cells to respond to the pro apoptotic mature nerve growth factor (NGF) and the anti apoptotic pro NGF [285]. The group demonstrated that levels of pro NGF correlate with fibrosis progression, with the highest levels present at peak fibrosis and subsequently fall during recovery which is accompanied by a decrease in hepatic myofibroblast number. Furthermore $p75^{NTR-/-}$ mice subjected to CCl_4 induced fibrosis had a reduced regenerative response due to a reduction in hepatic myofibroblast, hepatocyte and oval cell proliferation suggesting that hepatic myofibroblasts play an essential role in recovery. Whilst this data suggest that hepatic myofibroblasts promote recovery in a recovery fibrosis model, it would be interesting to subject these mice to PHx to investigate whether hepatic myofibroblasts are important in liver regeneration in the absence of inflammation. Not only would this be an independent method to confirm the C1-3-GT PHx study, if used in combination with 2-acetylaminofluorene [286] or retrosine [287] which inhibit hepatocyte proliferation, the model would investigate the effect of hepatic myofibroblast depletion on the oval cell regenerative response.

To investigate the potential clinical use of C1-3 as an imaging agent, the contribution of hepatic myofibroblasts to portal fibrosis resulting from obstructive cholestasis, hepatitis and NAFLD/NASH needs to be evaluated. Ideally C1-3 conjugated to a near infra red fluorophore would be used in these animal models with fluorescence being 'mapped' to specific organs using 3D scans. This would overcome the limitation associated with synaptophysin expression in the pancreas allowing for accurate quantification. To improve resolution, C1-3 could be conjugated to a radioactive label, e.g. ^{18}F SFB, with images generated by PET scans overlaid on CT images to provide accurate quantification.

7.4 General Conclusions

Since its initial discovery by von Kupffer in 1876, the hepatic myofibroblast has been shown to be the principal cell type involved in the initiation, perpetuation and termination of liver fibrosis caused by a vast array of aetiological agents. Whilst the continued elucidation of hepatic fibrogenesis has identified potential therapeutic targets to stimulate fibrosis stasis or regression, the lack of diagnostic tools to accurately grade and stage fibrosis would make it difficult to implement the therapeutics when they are most beneficial.

The data presented in this thesis provide proof of concept that the hepatic myofibroblast can be as a non invasive measure of liver fibrosis, with cell number increasing with disease progression (as determined by αSMA quantification). However, the use of C1-3 as an imaging agent is somewhat limited since the total flux of C1-3-AF from both the live animal imaging and the excised liver failed to accurately distinguish between the different stages of fibrosis. Furthermore, the role of hepatic myofibroblasts in liver regeneration seems to be more complex, with further elucidation of their mechanistic actions required before hepatic myofibroblast depletion can be recommended as an effective therapy for liver fibrosis. Whilst expression of synaptophysin by beta cells within the pancreas limits it clinical use as both an imaging agent and a method for targeting therapeutic drugs, C1-3 is still the only method to date which can selectively target hepatic myofibroblasts without the need for genetic knockouts. Moreover, continued development of the antibody by the Wright group, through the conjugation of liposomes to C1-3, ensures that it will be a great scientific tool in the investigation of hepatic myofibroblasts in future studies.

Chapter 8. References

1. Jungermann, K. and T. Kietzmann, *Zonation of parenchymal and nonparenchymal metabolism in liver.* Annu Rev Nutr, 1996. **16**: p. 179-203.
2. Lamers, W.H., W.J. Geerts, A. Jonker, F.J. Verbeek, G.T. Wagenaar, and A.F. Moorman, *Quantitative graphical description of portocentral gradients in hepatic gene expression by image analysis.* Hepatology, 1997. **26**(2): p. 398-406.
3. Haussinger, D., W.H. Lamers, and A.F. Moorman, *Hepatocyte heterogeneity in the metabolism of amino acids and ammonia.* Enzyme, 1992. **46**(1-3): p. 72-93.
4. Braet, F. and E. Wisse, *Structural and functional aspects of liver sinusoidal endothelial cell fenestrae: a review.* Comp Hepatol, 2002. **1**(1): p. 1.
5. Duffield, J.S., S.J. Forbes, C.M. Constandinou, S. Clay, M. Partolina, S. Vuthoori, S. Wu, R. Lang, and J.P. Iredale, *Selective depletion of macrophages reveals distinct, opposing roles during liver injury and repair.* J Clin Invest, 2005. **115**(1): p. 56-65.
6. Melton, A.C. and H.F. Yee, *Hepatic stellate cell protrusions couple platelet-derived growth factor-BB to chemotaxis.* Hepatology, 2007. **45**(6): p. 1446-53.
7. Shepard, C.W., L. Finelli, and M.J. Alter, *Global epidemiology of hepatitis C virus infection.* Lancet Infect Dis, 2005. **5**(9): p. 558-67.
8. Czaja, A.J., *Autoimmune liver disease.* Curr Opin Gastroenterol, 2007. **23**(3): p. 255-62.
9. Jones, D.E., *Pathogenesis of primary biliary cirrhosis.* Gut, 2007. **56**(11): p. 1615-24.
10. Feder, J.N., A. Gnirke, W. Thomas, Z. Tsuchihashi, D.A. Ruddy, A. Basava, F. Dormishian, R. Domingo, Jr., M.C. Ellis, A. Fullan, L.M. Hinton, N.L. Jones, B.E. Kimmel, G.S. Kronmal, P. Lauer, V.K. Lee, D.B. Loeb, F.A. Mapa, E. McClelland, N.C. Meyer, G.A. Mintier, N. Moeller, T. Moore, E. Morikang, C.E. Prass, L. Quintana, S.M. Starnes, R.C. Schatzman, K.J. Brunke, D.T. Drayna, N.J. Risch, B.R. Bacon, and R.K. Wolff, *A novel*

MHC class I-like gene is mutated in patients with hereditary haemochromatosis. Nat Genet, 1996. **13**(4): p. 399-408.

11. Ferenci, P., *Wilson's Disease.* Clin Gastroenterol Hepatol, 2005. **3**(8): p. 726-33.
12. LaRusso, N.F., B.L. Shneider, D. Black, G.J. Gores, S.P. James, E. Doo, and J.H. Hoofnagle, *Primary sclerosing cholangitis: summary of a workshop.* Hepatology, 2006. **44**(3): p. 746-64.
13. Reeves, H.L. and S.L. Friedman, *Activation of hepatic stellate cells--a key issue in liver fibrosis.* Front Biosci, 2002. **7**: p. d808-26.
14. Li, D. and S.L. Friedman, *Liver fibrogenesis and the role of hepatic stellate cells: new insights and prospects for therapy.* J Gastroenterol Hepatol, 1999. **14**(7): p. 618-33.
15. Friedman, S.L. and M.J. Arthur, *Reversing Hepatic Fibrosis.* Science and Medicine, 2002. **8**(4): p. 194-205.
16. Bedossa, P. and V. Paradis, *Liver extracellular matrix in health and disease.* J Pathol, 2003. **200**(4): p. 504-15.
17. Wells, R.G., *Cellular sources of extracellular matrix in hepatic fibrosis.* Clin Liver Dis, 2008. **12**(4): p. 759-68, viii.
18. McGuire, R.F., D.M. Bissell, J. Boyles, and F.J. Roll, *Role of extracellular matrix in regulating fenestrations of sinusoidal endothelial cells isolated from normal rat liver.* Hepatology, 1992. **15**(6): p. 989-97.
19. Bissell, D.M. and M.O. Choun, *The role of extracellular matrix in normal liver.* Scand J Gastroenterol Suppl, 1988. **151**: p. 1-7.
20. Gaca, M.D., X. Zhou, R. Issa, K. Kiriella, J.P. Iredale, and R.C. Benyon, *Basement membrane-like matrix inhibits proliferation and collagen synthesis by activated rat hepatic stellate cells: evidence for matrix-dependent deactivation of stellate cells.* Matrix Biol, 2003. **22**(3): p. 229-39.
21. Zhou, X., F.R. Murphy, N. Gehdu, J. Zhang, J.P. Iredale, and R.C. Benyon, *Engagement of alphavbeta3 integrin regulates proliferation and apoptosis of hepatic stellate cells.* J Biol Chem, 2004. **279**(23): p. 23996-4006.
22. Kinnman, N. and C. Housset, *Peribiliary myofibroblasts in biliary type liver fibrosis.* Front Biosci, 2002. **7**: p. d496-503.

23. Wells, R.G., E. Kruglov, and J.A. Dranoff, *Autocrine release of TGF-beta by portal fibroblasts regulates cell growth.* FEBS Lett, 2004. **559**(1-3): p. 107-10.
24. Forbes, S.J., F.P. Russo, V. Rey, P. Burra, M. Rugge, N.A. Wright, and M.R. Alison, *A significant proportion of myofibroblasts are of bone marrow origin in human liver fibrosis.* Gastroenterology, 2004. **126**(4): p. 955-63.
25. Kalluri, R. and E.G. Neilson, *Epithelial-mesenchymal transition and its implications for fibrosis.* J Clin Invest, 2003. **112**(12): p. 1776-84.
26. Rygiel, K.A., H. Robertson, H.L. Marshall, M. Pekalski, L. Zhao, T.A. Booth, D.E. Jones, A.D. Burt, and J.A. Kirby, *Epithelial-mesenchymal transition contributes to portal tract fibrogenesis during human chronic liver disease.* Lab Invest, 2008. **88**(2): p. 112-23.
27. Guyot, C., S. Lepreux, C. Combe, E. Doudnikoff, P. Bioulac-Sage, C. Balabaud, and A. Desmouliere, *Hepatic fibrosis and cirrhosis: the (myo)fibroblastic cell subpopulations involved.* Int J Biochem Cell Biol, 2006. **38**(2): p. 135-51.
28. Rockey, D.C., J.K. Boyles, G. Gabbiani, and S.L. Friedman, *Rat hepatic lipocytes express smooth muscle actin upon activation in vivo and in culture.* J Submicrosc Cytol Pathol, 1992. **24**(2): p. 193-203.
29. Wake, K., *Perisinusoidal stellate cells (fat-storing cells, interstitial cells, lipocytes), their related structure in and around the liver sinusoids, and vitamin A-storing cells in extrahepatic organs.* Int Rev Cytol, 1980. **66**: p. 303-53.
30. Kent, G., S. Gay, T. Inouye, R. Bahu, O.T. Minick, and H. Popper, *Vitamin A-containing lipocytes and formation of type III collagen in liver injury.* Proc Natl Acad Sci U S A, 1976. **73**(10): p. 3719-22.
31. Friedman, S.L., F.J. Roll, J. Boyles, and D.M. Bissell, *Hepatic lipocytes: the principal collagen-producing cells of normal rat liver.* Proc Natl Acad Sci U S A, 1985. **82**(24): p. 8681-5.
32. Maher, J.J., D.M. Bissell, S.L. Friedman, and F.J. Roll, *Collagen measured in primary cultures of normal rat hepatocytes derives from lipocytes within the monolayer.* J Clin Invest, 1988. **82**(2): p. 450-9.
33. Friedman, S.L. and F.J. Roll, *Isolation and culture of hepatic lipocytes, Kupffer cells, and sinusoidal endothelial cells by density gradient*

centrifugation with Stractan. Analytical Biochemistry, 1987. **161**(1): p. 207-218.

34. Friedman, S.L., D.C. Rockey, R.F. McGuire, J.J. Maher, J.K. Boyles, and G. Yamasaki, *Isolated hepatic lipocytes and Kupffer cells from normal human liver: morphological and functional characteristics in primary culture.* Hepatology, 1992. **15**(2): p. 234-43.
35. Friedman, S.L., *Seminars in medicine of the Beth Israel Hospital, Boston. The cellular basis of hepatic fibrosis. Mechanisms and treatment strategies.* N Engl J Med, 1993. **328**(25): p. 1828-35.
36. Friedman, S.L., *Mechanisms of Hepatic Fibrogenesis.* Gastroenterology, 2008. **134**(6): p. 1655-1669.
37. Friedman, S.L., *Hepatic stellate cells: protean, multifunctional, and enigmatic cells of the liver.* Physiol Rev, 2008. **88**(1): p. 125-72.
38. Canbay, A., P. Taimr, N. Torok, H. Higuchi, S. Friedman, and G.J. Gores, *Apoptotic body engulfment by a human stellate cell line is profibrogenic.* Lab Invest, 2003. **83**(5): p. 655-63.
39. Canbay, A., A.E. Feldstein, H. Higuchi, N. Werneburg, A. Grambihler, S.F. Bronk, and G.J. Gores, *Kupffer cell engulfment of apoptotic bodies stimulates death ligand and cytokine expression.* Hepatology, 2003. **38**(5): p. 1188-98.
40. Bachem, M.G., R. Melchior, and A.M. Gressner, *The role of thrombocytes in liver fibrogenesis: effects of platelet lysate and thrombocyte-derived growth factors on the mitogenic activity and glycosaminoglycan synthesis of cultured rat liver fat storing cells.* J Clin Chem Clin Biochem, 1989. **27**(9): p. 555-65.
41. Deleve, L.D., X. Wang, and Y. Guo, *Sinusoidal endothelial cells prevent rat stellate cell activation and promote reversion to quiescence.* Hepatology, 2008. **48**(3): p. 920-30.
42. Jarnagin, W.R., D.C. Rockey, V.E. Koteliansky, S.S. Wang, and D.M. Bissell, *Expression of variant fibronectins in wound healing: cellular source and biological activity of the EIIIA segment in rat hepatic fibrogenesis.* J Cell Biol, 1994. **127**(6 Pt 2): p. 2037-48.
43. Wong, L., G. Yamasaki, R.J. Johnson, and S.L. Friedman, *Induction of beta-platelet-derived growth factor receptor in rat hepatic lipocytes during*

cellular activation in vivo and in culture. J Clin Invest, 1994. **94**(4): p. 1563-9.

44. Pinzani, M., *PDGF and signal transduction in hepatic stellate cells.* Front Biosci, 2002. **7**: p. d1720-6.
45. Pinzani, M. and F. Marra, *Cytokine receptors and signaling in hepatic stellate cells.* Semin Liver Dis, 2001. **21**(3): p. 397-416.
46. Kinnman, N., R. Hultcrantz, V. Barbu, C. Rey, D. Wendum, R. Poupon, and C. Housset, *PDGF-mediated chemoattraction of hepatic stellate cells by bile duct segments in cholestatic liver injury.* Lab Invest, 2000. **80**(5): p. 697-707.
47. Marra, F., R.G. Romanelli, C. Giannini, P. Failli, S. Pastacaldi, M.C. Arrighi, M. Pinzani, G. Laffi, P. Montalto, and P. Gentilini, *Monocyte chemotactic protein-1 as a chemoattractant for human hepatic stellate cells.* Hepatology, 1999. **29**(1): p. 140-8.
48. Bonacchi, A., P. Romagnani, R.G. Romanelli, E. Efsen, F. Annunziato, L. Lasagni, M. Francalanci, M. Serio, G. Laffi, M. Pinzani, P. Gentilini, and F. Marra, *Signal transduction by the chemokine receptor CXCR3: activation of Ras/ERK, Src, and phosphatidylinositol 3-kinase/Akt controls cell migration and proliferation in human vascular pericytes.* J Biol Chem, 2001. **276**(13): p. 9945-54.
49. Stefanovic, B., L. Stefanovic, B. Schnabl, R. Bataller, and D.A. Brenner, *TRAM2 protein interacts with endoplasmic reticulum Ca2+ pump Serca2b and is necessary for collagen type I synthesis.* Mol Cell Biol, 2004. **24**(4): p. 1758-68.
50. Arthur, M.J., *Fibrogenesis II. Metalloproteinases and their inhibitors in liver fibrosis.* Am J Physiol Gastrointest Liver Physiol, 2000. **279**(2): p. G245-9.
51. Lee, T.F., K.M. Mak, O. Rackovsky, Y.L. Lin, A.J. Kwong, J.C. Loke, and S.L. Friedman, *Downregulation of hepatic stellate cell activation by retinol and palmitate mediated by adipose differentiation-related protein (ADRP).* J Cell Physiol, 2010. **223**(3): p. 648-57.
52. Knittel, T., D. Kobold, B. Saile, A. Grundmann, K. Neubauer, F. Piscaglia, and G. Ramadori, *Rat liver myofibroblasts and hepatic stellate cells: different cell populations of the fibroblast lineage with fibrogenic potential.* Gastroenterology, 1999. **117**(5): p. 1205-21.

53. Ramadori, G. and B. Saile, *Portal tract fibrogenesis in the liver.* Lab Invest, 2004. **84**(2): p. 153-9.
54. Cassiman, D., L. Libbrecht, V. Desmet, C. Denef, and T. Roskams, *Hepatic stellate cell/myofibroblast subpopulations in fibrotic human and rat livers.* Journal of Hepatology, 2002. **36**(2): p. 200-209.
55. Tang, L., Y. Tanaka, F. Marumo, and C. Sato, *Phenotypic change in portal fibroblasts in biliary fibrosis.* Liver, 1994. **14**(2): p. 76-82.
56. Beaussier, M., D. Wendum, E. Schiffer, S. Dumont, C. Rey, A. Lienhart, and C. Housset, *Prominent contribution of portal mesenchymal cells to liver fibrosis in ischemic and obstructive cholestatic injuries.* Lab Invest, 2007. **87**(3): p. 292-303.
57. Li, Z., J.A. Dranoff, E.P. Chan, M. Uemura, J. Sevigny, and R.G. Wells, *Transforming growth factor-beta and substrate stiffness regulate portal fibroblast activation in culture.* Hepatology, 2007. **46**(4): p. 1246-56.
58. Milani, S., H. Herbst, D. Schuppan, H. Stein, and C. Surrenti, *Transforming growth factors beta 1 and beta 2 are differentially expressed in fibrotic liver disease.* Am J Pathol, 1991. **139**(6): p. 1221-9.
59. Forbes, S.R., F.P. Rey, V. Burra, P. Rugge, M. Wright, N.A. Alison, M.R., *A Significant Proportion of Myofibroblasts are of Bone Marrow Origin in Human LIver Fibrosis.* Gastroenterology, 2004. **126**: p. 955-963.
60. Russo, F.P., M.R. Alison, B.W. Bigger, E. Amofah, A. Florou, F. Amin, G. Bou-Gharios, R. Jeffery, J.P. Iredale, and S.J. Forbes, *The Bone Marrow Functionally Contributes to Liver Fibrosis.* Gastroenterology, 2006. **130**(6): p. 1807-1821.
61. Kisseleva, T., H. Uchinami, N. Feirt, O. Quintana-Bustamante, J.C. Segovia, R.F. Schwabe, and D.A. Brenner, *Bone marrow-derived fibrocytes participate in pathogenesis of liver fibrosis.* J Hepatol, 2006. **45**(3): p. 429-38.
62. Iwano, M., D. Plieth, T.M. Danoff, C. Xue, H. Okada, and E.G. Neilson, *Evidence that fibroblasts derive from epithelium during tissue fibrosis.* J Clin Invest, 2002. **110**(3): p. 341-50.
63. Kalluri, R. and E.G. Neilson, *Epithelial-mesenchymal transition and its implications for fibrosis.* J Clin Invest, 2003. **112**: p. 1776-1784.

64. Okada, H., T.M. Danoff, R. Kalluri, and E.G. Neilson, *Early role of Fsp1 in epithelial-mesenchymal transformation.* Am J Physiol, 1997. **273**(4 Pt 2): p. F563-74.
65. Robertson, H., S. Ali, B.J. McDonnell, A.D. Burt, and J.A. Kirby, *Chronic renal allograft dysfunction: the role of T cell-mediated tubular epithelial to mesenchymal cell transition.* J Am Soc Nephrol, 2004. **15**: p. 390-397.
66. Kirby, J.A., H. Robertson, H.L. Marshall, K.A. Rygiel, M. Hudson, D.E. Jones, and A.D. Burt, *Epithelial to mesenchymal transition in primary sclerosing cholangitis.* Liver Int, 2008. **28**(8): p. 1176-7.
67. Robertson, H., J.A. Kirby, W.W. Yip, D.E. Jones, and A.D. Burt, *Biliary epithelial-mesenchymal transition in posttransplantation recurrence of primary biliary cirrhosis.* Hepatology, 2007. **45**(4): p. 977-81.
68. Holt, A.P., M. Salmon, C.D. Buckley, and D.H. Adams, *Immune interactions in hepatic fibrosis.* Clin Liver Dis, 2008. **12**(4): p. 861-82.
69. Pinzani, M., V. Carloni, F. Marra, D. Riccardi, G. Laffi, and P. Gentilini, *Biosynthesis of platelet-activating factor and its 1O-acyl analogue by liver fat-storing cells.* Gastroenterology, 1994. **106**(5): p. 1301-11.
70. Marra, F., A.J. Valente, M. Pinzani, and H.E. Abboud, *Cultured human liver fat-storing cells produce monocyte chemotactic protein-1. Regulation by proinflammatory cytokines.* J Clin Invest, 1993. **92**(4): p. 1674-80.
71. Marra, F., *Hepatic stellate cells and the regulation of liver inflammation.* J Hepatol, 1999. **31**(6): p. 1106-1119.
72. Winau, F., G. Hegasy, R. Weiskirchen, S. Weber, C. Cassan, P.A. Sieling, R.L. Modlin, R.S. Liblau, A.M. Gressner, and S.H. Kaufmann, *Ito cells are liver-resident antigen-presenting cells for activating T cell responses.* Immunity, 2007. **26**(1): p. 117-29.
73. Vinas, O., R. Bataller, P. Sancho-Bru, P. Gines, C. Berenguer, C. Enrich, J.M. Nicolas, G. Ercilla, T. Gallart, J. Vives, V. Arroyo, and J. Rodes, *Human hepatic stellate cells show features of antigen-presenting cells and stimulate lymphocyte proliferation.* Hepatology, 2003. **38**(4): p. 919-29.
74. Muhanna, N., S. Doron, O. Wald, A. Horani, A. Eid, O. Pappo, S.L. Friedman, and R. Safadi, *Activation of hepatic stellate cells after phagocytosis of lymphocytes: A novel pathway of fibrogenesis.* Hepatology, 2008. **48**(3): p. 963-77.

75. Dunn, C., M. Brunetto, G. Reynolds, T. Christophides, P.T. Kennedy, P. Lampertico, A. Das, A.R. Lopes, P. Borrow, K. Williams, E. Humphreys, S. Afford, D.H. Adams, A. Bertoletti, and M.K. Maini, *Cytokines induced during chronic hepatitis B virus infection promote a pathway for NK cell-mediated liver damage.* J Exp Med, 2007. **204**(3): p. 667-80.
76. Melhem, A., N. Muhanna, A. Bishara, C.E. Alvarez, Y. Ilan, T. Bishara, A. Horani, M. Nassar, S.L. Friedman, and R. Safadi, *Anti-fibrotic activity of NK cells in experimental liver injury through killing of activated HSC.* J Hepatol, 2006. **45**(1): p. 60-71.
77. Radaeva, S., R. Sun, B. Jaruga, V.T. Nguyen, Z. Tian, and B. Gao, *Natural killer cells ameliorate liver fibrosis by killing activated stellate cells in NKG2D-dependent and tumor necrosis factor-related apoptosis-inducing ligand-dependent manners.* Gastroenterology, 2006. **130**(2): p. 435-52.
78. Muhanna, N., A. Horani, S. Doron, and R. Safadi, *Lymphocyte-hepatic stellate cell proximity suggests a direct interaction.* Clin Exp Immunol, 2007. **148**(2): p. 338-47.
79. Holt, A.P., E.L. Haughton, P.F. Lalor, A. Filer, C.D. Buckley, and D.H. Adams, *Liver myofibroblasts regulate infiltration and positioning of lymphocytes in human liver.* Gastroenterology, 2009. **136**(2): p. 705-14.
80. Iredale, J.P., *Models of liver fibrosis: exploring the dynamic nature of inflammation and repair in a solid organ.* J Clin Invest, 2007. **117**(3): p. 539-48.
81. Janakat, S. and H. Al-Merie, *Optimization of the dose and route of injection, and characterisation of the time course of carbon tetrachloride-induced hepatotoxicity in the rat.* J Pharmacol Toxicol Methods, 2002. **48**(1): p. 41-4.
82. Gadgoli, C. and S.H. Mishra, *Antihepatotoxic activity of p-methoxy benzoic acid from Capparis spinosa.* J Ethnopharmacol, 1999. **66**(2): p. 187-92.
83. Ferrali, M. and M. Comporti, *On the mechanisms of the CCl4-induced inhibition of liver cytochrome P-450.* Res Commun Chem Pathol Pharmacol, 1987. **56**(3): p. 375-86.
84. Wong, F.W., W.Y. Chan, and S.S. Lee, *Resistance to carbon tetrachloride-induced hepatotoxicity in mice which lack CYP2E1 expression.* Toxicol Appl Pharmacol, 1998. **153**(1): p. 109-18.

85. Weber, L.W., M. Boll, and A. Stampfl, *Hepatotoxicity and mechanism of action of haloalkanes: carbon tetrachloride as a toxicological model.* Crit Rev Toxicol, 2003. **33**(2): p. 105-36.
86. Clawson, G.A., J.R. MacDonald, and C.H. Woo, *Early hypomethylation of 2'-O-ribose moieties in hepatocyte cytoplasmic ribosomal RNA underlies the protein synthetic defect produced by CCl4.* J Cell Biol, 1987. **105**(2): p. 705-11.
87. Poli, G., E. Chiarpotto, E. Albano, D. Cottalasso, G. Nanni, U.M. Marinari, A.M. Bassi, and M.U. Dianzani, *Carbon tetrachloride-induced inhibition of hepatocyte lipoprotein secretion: functional impairment of Golgi apparatus in the early phases of such injury.* Life Sci, 1985. **36**(6): p. 533-9.
88. Poli, G., D. Cottalasso, M.A. Pronzato, E. Chiarpotto, F. Biasi, F.P. Corongiu, U.M. Marinari, G. Nanni, and M.U. Dianzani, *Lipid peroxidation and covalent binding in the early functional impairment of liver Golgi apparatus by carbon tetrachloride.* Cell Biochem Funct, 1990. **8**(1): p. 1-10.
89. Ueda, K., S. Kobayashi, J. Morita, and T. Komano, *Site-specific DNA damage caused by lipid peroxidation products.* Biochim Biophys Acta, 1985. **824**(4): p. 341-8.
90. Srivastava, S.P., N.Q. Chen, and J.L. Holtzman, *The in vitro NADPH-dependent inhibition by CCl4 of the ATP-dependent calcium uptake of hepatic microsomes from male rats. Studies on the mechanism of the inactivation of the hepatic microsomal calcium pump by the CCl3.radical.* J Biol Chem, 1990. **265**(15): p. 8392-9.
91. Elsharkawy, A.M., F. Oakley, and D.A. Mann, *The role and regulation of hepatic stellate cell apoptosis in reversal of liver fibrosis.* Apoptosis, 2005. **10**(5): p. 927-39.
92. George, J., D. Roulot, V.E. Koteliansky, and D.M. Bissell, *In vivo inhibition of rat stellate cell activation by soluble transforming growth factor beta type II receptor: a potential new therapy for hepatic fibrosis.* Proc Natl Acad Sci U S A, 1999. **96**(22): p. 12719-24.
93. Popov, Y. and D. Schuppan, *Targeting liver fibrosis: strategies for development and validation of antifibrotic therapies.* Hepatology, 2009. **50**(4): p. 1294-306.

94. Roderfeld, M., R. Weiskirchen, S. Wagner, M.L. Berres, C. Henkel, J. Grotzinger, A.M. Gressner, S. Matern, and E. Roeb, *Inhibition of hepatic fibrogenesis by matrix metalloproteinase-9 mutants in mice.* Faseb J, 2006. **20**(3): p. 444-54.

95. Wang, B., B.M. Dolinski, N. Kikuchi, D.R. Leone, M.G. Peters, P.H. Weinreb, S.M. Violette, and D.M. Bissell, *Role of alphavbeta6 integrin in acute biliary fibrosis.* Hepatology, 2007. **46**(5): p. 1404-12.

96. Saile, B., T. Knittel, N. Matthes, P. Schott, and G. Ramadori, *CD95/CD95L-mediated apoptosis of the hepatic stellate cell. A mechanism terminating uncontrolled hepatic stellate cell proliferation during hepatic tissue repair.* Am J Pathol, 1997. **151**(5): p. 1265-72.

97. Taimr, P., H. Higuchi, E. Kocova, R.A. Rippe, S. Friedman, and G.J. Gores, *Activated stellate cells express the TRAIL receptor-2/death receptor-5 and undergo TRAIL-mediated apoptosis.* Hepatology, 2003. **37**(1): p. 87-95.

98. Saile, B., N. Matthes, T. Knittel, and G. Ramadori, *Transforming growth factor beta and tumor necrosis factor alpha inhibit both apoptosis and proliferation of activated rat hepatic stellate cells.* Hepatology, 1999. **30**(1): p. 196-202.

99. Saile, B., C. Eisenbach, J. Dudas, H. El-Armouche, and G. Ramadori, *Interferon-gamma acts proapoptotic on hepatic stellate cells (HSC) and abrogates the antiapoptotic effect of interferon-alpha by an HSP70-dependant pathway.* Eur J Cell Biol, 2004. **83**(9): p. 469-76.

100. Iredale, J.P., R.C. Benyon, J. Pickering, M. McCullen, M. Northrop, S. Pawley, C. Hovell, and M.J. Arthur, *Mechanisms of spontaneous resolution of rat liver fibrosis. Hepatic stellate cell apoptosis and reduced hepatic expression of metalloproteinase inhibitors.* J Clin Invest, 1998. **102**(3): p. 538-49.

101. Issa, R., E. Williams, N. Trim, T. Kendall, M.J.P. Arthur, J. Reichen, R.C. Benyon, and J.P. Iredale, *Apoptosis of hepatic stellate cells: involvement in resolution of biliary fibrosis and regulation by soluble growth factors.* Gut, 2001. **48**(4): p. 548-557.

102. Wright, M.C., R. Issa, D.E. Smart, N. Trim, G.I. Murray, J.N. Primrose, M.J. Arthur, J.P. Iredale, and D.A. Mann, *Gliotoxin stimulates the apoptosis of human and rat hepatic stellate cells and enhances the*

resolution of liver fibrosis in rats. Gastroenterology, 2001. **121**(3): p. 685-98.

103. Ward, C., E.R. Chilvers, M.F. Lawson, J.G. Pryde, S. Fujihara, S.N. Farrow, C. Haslett, and A.G. Rossi, *NF-kappaB activation is a critical regulator of human granulocyte apoptosis in vitro.* J Biol Chem, 1999. **274**(7): p. 4309-18.
104. Pahl, H.L., B. Krauss, K. Schulze-Osthoff, T. Decker, E.B. Traenckner, M. Vogt, C. Myers, T. Parks, P. Warring, A. Muhlbacher, A.P. Czernilofsky, and P.A. Baeuerle, *The immunosuppressive fungal metabolite gliotoxin specifically inhibits transcription factor NF-kappaB.* J Exp Med, 1996. **183**(4): p. 1829-40.
105. Orr, J.G., V. Leel, G.A. Cameron, C.J. Marek, E.L. Haughton, L.J. Elrick, J.E. Trim, G.M. Hawksworth, A.P. Halestrap, and M.C. Wright, *Mechanism of action of the antifibrogenic compound gliotoxin in rat liver cells.* Hepatology, 2004. **40**(1): p. 232-42.
106. Oakley, F., M. Meso, J.P. Iredale, K. Green, C.J. Marek, X. Zhou, M.J. May, H. Millward-Sadler, M.C. Wright, and D.A. Mann, *Inhibition of inhibitor of kappaB kinases stimulates hepatic stellate cell apoptosis and accelerated recovery from rat liver fibrosis.* Gastroenterology, 2005. **128**(1): p. 108-20.
107. Sutton, P., N.R. Newcombe, P. Waring, and A. Mullbacher, *In vivo immunosuppressive activity of gliotoxin, a metabolite produced by human pathogenic fungi.* Infect Immun, 1994. **62**(4): p. 1192-8.
108. Waring, P. and J. Beaver, *Gliotoxin and related epipolythiodioxopiperazines.* Gen Pharmacol, 1996. **27**(8): p. 1311-6.
109. Hagens, W.I., P. Olinga, D.K. Meijer, G.M. Groothuis, L. Beljaars, and K. Poelstra, *Gliotoxin non-selectively induces apoptosis in fibrotic and normal livers.* Liver Int, 2006. **26**(2): p. 232-9.
110. Beljaars, L., G. Molema, B. Weert, H. Bonnema, P. Olinga, G.M. Groothuis, D.K. Meijer, and K. Poelstra, *Albumin modified with mannose 6-phosphate: A potential carrier for selective delivery of antifibrotic drugs to rat and human hepatic stellate cells.* Hepatology, 1999. **29**(5): p. 1486-93.
111. de Bleser, P.J., P. Jannes, S.C. van Buul-Offers, C.M. Hoogerbrugge, C.F. van Schravendijk, T. Niki, V. Rogiers, J.L. van den Brande, E. Wisse, and A. Geerts, *Insulinlike growth factor-II/mannose 6-phosphate receptor is*

expressed on CCl4-exposed rat fat-storing cells and facilitates activation of latent transforming growth factor-beta in cocultures with sinusoidal endothelial cells. Hepatology, 1995. **21**(5): p. 1429-37.

112. Hagens, W.I., L. Beljaars, D.A. Mann, M.C. Wright, B. Julien, S. Lotersztajn, C. Reker-Smit, and K. Poelstra, *Cellular targeting of the apoptosis-inducing compound gliotoxin to fibrotic rat livers.* J Pharmacol Exp Ther, 2008. **324**(3): p. 902-10.
113. Ashburn, T.T. and K.B. Thor, *Drug repositioning: identifying and developing new uses for existing drugs.* Nat Rev Drug Discov, 2004. **3**(8): p. 673-83.
114. Ramachandran, P. and J.P. Iredale, *Reversibility of liver fibrosis.* Ann Hepatol, 2009. **8**(4): p. 283-91.
115. Williams, E.J., R.C. Benyon, N. Trim, R. Hadwin, B.H. Grove, M.J. Arthur, E.N. Unemori, and J.P. Iredale, *Relaxin inhibits effective collagen deposition by cultured hepatic stellate cells and decreases rat liver fibrosis in vivo.* Gut, 2001. **49**(4): p. 577-83.
116. Zhao, C., W. Chen, L. Yang, L. Chen, S.A. Stimpson, and A.M. Diehl, *PPARgamma agonists prevent TGFbeta1/Smad3-signaling in human hepatic stellate cells.* Biochem Biophys Res Commun, 2006. **350**(2): p. 385-91.
117. Belfort, R., S.A. Harrison, K. Brown, C. Darland, J. Finch, J. Hardies, B. Balas, A. Gastaldelli, F. Tio, J. Pulcini, R. Berria, J.Z. Ma, S. Dwivedi, R. Havranek, C. Fincke, R. DeFronzo, G.A. Bannayan, S. Schenker, and K. Cusi, *A placebo-controlled trial of pioglitazone in subjects with nonalcoholic steatohepatitis.* N Engl J Med, 2006. **355**(22): p. 2297-307.
118. Ratziu, V., P. Giral, S. Jacqueminet, F. Charlotte, A. Hartemann-Heurtier, L. Serfaty, P. Podevin, J.M. Lacorte, C. Bernhardt, E. Bruckert, A. Grimaldi, and T. Poynard, *Rosiglitazone for nonalcoholic steatohepatitis: one-year results of the randomized placebo-controlled Fatty Liver Improvement with Rosiglitazone Therapy (FLIRT) Trial.* Gastroenterology, 2008. **135**(1): p. 100-10.
119. Aithal, G.P., J.A. Thomas, P.V. Kaye, A. Lawson, S.D. Ryder, I. Spendlove, A.S. Austin, J.G. Freeman, L. Morgan, and J. Webber, *Randomized, placebo-controlled trial of pioglitazone in nondiabetic*

subjects with nonalcoholic steatohepatitis. Gastroenterology, 2008. **135**(4): p. 1176-84.

120. Wiedenmann, B. and W.W. Franke, *Identification and localization of synaptophysin, an integral membrane glycoprotein of Mr 38,000 characteristic of presynaptic vesicles.* Cell, 1985. **41**(3): p. 1017-1028.
121. Edelmann, L., P.I. Hanson, E.R. Chapman, and R. Jahn, *Synaptobrevin binding to synaptophysin: a potential mechanism for controlling the exocytotic fusion machine.* Embo J, 1995. **14**(2): p. 224-31.
122. Bargou, R.C. and R.E. Leube, *The synaptophysin-encoding gene in rat and man is specifically transcribed in neuroendocrine cells.* Gene, 1991. **99**(2): p. 197-204.
123. Bahler, M., A.M. Cesura, G. Fischer, H. Kuhn, R.L. Klein, and M. Da Prada, *Serotonin organelles of rabbit platelets contain synaptophysin.* Eur J Biochem, 1990. **194**(3): p. 825-9.
124. Cassiman, D., J. van Pelt, R. De Vos, F. Van Lommel, V. Desmet, S.-H. Yap, and T. Roskams, *Synaptophysin: A Novel Marker for Human and Rat Hepatic Stellate Cells.* Am J Pathol, 1999. **155**(6): p. 1831-1839.
125. Elrick, L.J., V. Leel, M.G. Blaylock, L. Duncan, M.R. Drever, G. Strachan, K.A. Charlton, M. Koruth, A.J. Porter, and M.C. Wright, *Generation of a monoclonal human single chain antibody fragment to hepatic stellate cells--a potential mechanism for targeting liver anti-fibrotic therapeutics.* J Hepatol, 2005. **42**(6): p. 888-96.
126. Douglass, A., K. Wallace, R. Parr, J. Park, E. Durward, I. Broadbent, C. Barelle, A.J. Porter, and M.C. Wright, *Antibody-targeted myofibroblast apoptosis reduces fibrosis during sustained liver injury.* J Hepatol, 2008. **49**(1): p. 88-98.
127. Michalopoulos, G.K. and M.C. DeFrances, *Liver regeneration.* Science, 1997. **276**(5309): p. 60-6.
128. Higgins, G.M. and R.M. Anderson, *Experimental pathology of the liver.* Arch Pathol Lab Med, 1931. **12**: p. 186-202.
129. Fausto, N., J.S. Campbell, and K.J. Riehle, *Liver regeneration.* Hepatology, 2006. **43**(2 Suppl 1): p. S45-53.
130. Tumanov, A.V., E.P. Koroleva, P.A. Christiansen, M.A. Khan, M.J. Ruddy, B. Burnette, S. Papa, G. Franzoso, S.A. Nedospasov, Y.X. Fu, and R.A.

Anders, *T cell-derived lymphotoxin regulates liver regeneration.* Gastroenterology, 2009. **136**(2): p. 694-704 e4.

131. Malik, R., C. Selden, and H. Hodgson, *The role of non-parenchymal cells in liver growth.* Semin Cell Dev Biol, 2002. **13**(6): p. 425-31.
132. Cressman, D.E., L.E. Greenbaum, R.A. DeAngelis, G. Ciliberto, E.E. Furth, V. Poli, and R. Taub, *Liver failure and defective hepatocyte regeneration in interleukin-6-deficient mice.* Science, 1996. **274**(5291): p. 1379-83.
133. Yamada, Y., I. Kirillova, J.J. Peschon, and N. Fausto, *Initiation of liver growth by tumor necrosis factor: deficient liver regeneration in mice lacking type I tumor necrosis factor receptor.* Proc Natl Acad Sci U S A, 1997. **94**(4): p. 1441-6.
134. Kovalovich, K., R.A. DeAngelis, W. Li, E.E. Furth, G. Ciliberto, and R. Taub, *Increased toxin-induced liver injury and fibrosis in interleukin-6-deficient mice.* Hepatology, 2000. **31**(1): p. 149-59.
135. Iwai, M., T.X. Cui, H. Kitamura, M. Saito, and T. Shimazu, *Increased secretion of tumour necrosis factor and interleukin 6 from isolated, perfused liver of rats after partial hepatectomy.* Cytokine, 2001. **13**(1): p. 60-64.
136. Akerman, P., P. Cote, S.Q. Yang, C. McClain, S. Nelson, G.J. Bagby, and A.M. Diehl, *Antibodies to tumor necrosis factor-alpha inhibit liver regeneration after partial hepatectomy.* Am J Physiol, 1992. **263**(4 Pt 1): p. G579-85.
137. Campbell, J.S., L. Prichard, F. Schaper, J. Schmitz, A. Stephenson-Famy, M.E. Rosenfeld, G.M. Argast, P.C. Heinrich, and N. Fausto, *Expression of suppressors of cytokine signaling during liver regeneration.* J Clin Invest, 2001. **107**(10): p. 1285-92.
138. Balabaud, C., P. Bioulac-Sage, and A. Desmouliere, *The role of hepatic stellate cells in liver regeneration.* J Hepatol, 2004. **40**(6): p. 1023-6.
139. Sakamoto, T., Z. Liu, N. Murase, T. Ezure, S. Yokomuro, V. Poli, and A.J. Demetris, *Mitosis and apoptosis in the liver of interleukin-6-deficient mice after partial hepatectomy.* Hepatology, 1999. **29**(2): p. 403-11.
140. Wuestefeld, T., C. Klein, K.L. Streetz, U. Betz, J. Lauber, J. Buer, M.P. Manns, W. Muller, and C. Trautwein, *Interleukin-6/glycoprotein 130-*

dependent pathways are protective during liver regeneration. J Biol Chem, 2003. **278**(13): p. 11281-8.

141. Yoshida, K., T. Taga, M. Saito, S. Suematsu, A. Kumanogoh, T. Tanaka, H. Fujiwara, M. Hirata, T. Yamagami, T. Nakahata, T. Hirabayashi, Y. Yoneda, K. Tanaka, W.Z. Wang, C. Mori, K. Shiota, N. Yoshida, and T. Kishimoto, *Targeted disruption of gp130, a common signal transducer for the interleukin 6 family of cytokines, leads to myocardial and hematological disorders.* Proc Natl Acad Sci U S A, 1996. **93**(1): p. 407-11.
142. Kuhn, R., F. Schwenk, M. Aguet, and K. Rajewsky, *Inducible gene targeting in mice.* Science, 1995. **269**(5229): p. 1427-9.
143. Veenstra-VanderWeele, J., G.M. Anderson, and E.H. Cook, Jr., *Pharmacogenetics and the serotonin system: initial studies and future directions.* Eur J Pharmacol, 2000. **410**(2-3): p. 165-181.
144. Lesurtel, M., R. Graf, B. Aleil, D.J. Walther, Y. Tian, W. Jochum, C. Gachet, M. Bader, and P.A. Clavien, *Platelet-derived serotonin mediates liver regeneration.* Science, 2006. **312**(5770): p. 104-7.
145. Papadimas, G.K., K.N. Tzirogiannis, G.I. Panoutsopoulos, M.D. Demonakou, S.D. Skaltsas, R.I. Hereti, Z. Papadopoulou-Daifoti, and M.G. Mykoniatis, *Effect of serotonin receptor 2 blockage on liver regeneration after partial hepatectomy in the rat liver.* Liver Int, 2006. **26**(3): p. 352-61.
146. Ruddell, R.G., F. Oakley, Z. Hussain, I. Yeung, L.J. Bryan-Lluka, G.A. Ramm, and D.A. Mann, *A role for serotonin (5-HT) in hepatic stellate cell function and liver fibrosis.* Am J Pathol, 2006. **169**(3): p. 861-76.
147. Webber, E.M., J. Bruix, R.H. Pierce, and N. Fausto, *Tumor necrosis factor primes hepatocytes for DNA replication in the rat.* Hepatology, 1998. **28**(5): p. 1226-34.
148. Michalopoulos, G.K. and Z. Khan, *Liver regeneration, growth factors, and amphiregulin.* Gastroenterology, 2005. **128**(2): p. 503-6.
149. Pediaditakis, P., J.C. Lopez-Talavera, B. Petersen, S.P. Monga, and G.K. Michalopoulos, *The processing and utilization of hepatocyte growth factor/scatter factor following partial hepatectomy in the rat.* Hepatology, 2001. **34**(4 Pt 1): p. 688-93.
150. Naldini, L., L. Tamagnone, E. Vigna, M. Sachs, G. Hartmann, W. Birchmeier, Y. Daikuhara, H. Tsubouchi, F. Blasi, and P.M. Comoglio,

Extracellular proteolytic cleavage by urokinase is required for activation of hepatocyte growth factor/scatter factor. Embo J, 1992. **11**(13): p. 4825-33.

151. Mars, W.M., R. Zarnegar, and G.K. Michalopoulos, *Activation of hepatocyte growth factor by the plasminogen activators uPA and tPA.* Am J Pathol, 1993. **143**(3): p. 949-58.
152. Bladt, F., D. Riethmacher, S. Isenmann, A. Aguzzi, and C. Birchmeier, *Essential role for the c-met receptor in the migration of myogenic precursor cells into the limb bud.* Nature, 1995. **376**(6543): p. 768-71.
153. Schmidt, C., F. Bladt, S. Goedecke, V. Brinkmann, W. Zschiesche, M. Sharpe, E. Gherardi, and C. Birchmeier, *Scatter factor/hepatocyte growth factor is essential for liver development.* Nature, 1995. **373**(6516): p. 699-702.
154. Lindroos, P.M., R. Zarnegar, and G.K. Michalopoulos, *Hepatocyte growth factor (hepatopoietin A) rapidly increases in plasma before DNA synthesis and liver regeneration stimulated by partial hepatectomy and carbon tetrachloride administration.* Hepatology, 1991. **13**(4): p. 743-50.
155. Schuppan, D., M. Schmid, R. Somasundaram, R. Ackermann, M. Ruehl, T. Nakamura, and E.O. Riecken, *Collagens in the liver extracellular matrix bind hepatocyte growth factor.* Gastroenterology, 1998. **114**(1): p. 139-52.
156. Zarnegar, R., M.C. DeFrances, D.P. Kost, P. Lindroos, and G.K. Michalopoulos, *Expression of hepatocyte growth factor mRNA in regenerating rat liver after partial hepatectomy.* Biochem Biophys Res Commun, 1991. **177**(1): p. 559-65.
157. Huh, C.G., V.M. Factor, A. Sanchez, K. Uchida, E.A. Conner, and S.S. Thorgeirsson, *Hepatocyte growth factor/c-met signaling pathway is required for efficient liver regeneration and repair.* Proc Natl Acad Sci U S A, 2004. **101**(13): p. 4477-82.
158. Borowiak, M., A.N. Garratt, T. Wustefeld, M. Strehle, C. Trautwein, and C. Birchmeier, *Met provides essential signals for liver regeneration.* Proc Natl Acad Sci U S A, 2004. **101**(29): p. 10608-13.
159. Paranjpe, S., W.C. Bowen, A.W. Bell, K. Nejak-Bowen, J.H. Luo, and G.K. Michalopoulos, *Cell cycle effects resulting from inhibition of hepatocyte growth factor and its receptor c-Met in regenerating rat livers by RNA interference.* Hepatology, 2007. **45**(6): p. 1471-7.

160. Jones, D.E., Jr., R. Tran-Patterson, D.M. Cui, D. Davin, K.P. Estell, and D.M. Miller, *Epidermal growth factor secreted from the salivary gland is necessary for liver regeneration.* Am J Physiol, 1995. **268**(5 Pt 1): p. G872-8.

161. Berasain, C., E.R. Garcia-Trevijano, J. Castillo, E. Erroba, D.C. Lee, J. Prieto, and M.A. Avila, *Amphiregulin: an early trigger of liver regeneration in mice.* Gastroenterology, 2005. **128**(2): p. 424-32.

162. Paranjpe, S., W.C. Bowen, G.C. Tseng, J.H. Luo, A. Orr, and G.K. Michalopoulos, *RNA interference against hepatic epidermal growth factor receptor has suppressive effects on liver regeneration in rats.* Am J Pathol. **176**(6): p. 2669-81.

163. Bissell, D.M., S.S. Wang, W.R. Jarnagin, and F.J. Roll, *Cell-specific expression of transforming growth factor-beta in rat liver. Evidence for autocrine regulation of hepatocyte proliferation.* J Clin Invest, 1995. **96**(1): p. 447-55.

164. Boulton, R., A. Woodman, D. Calnan, C. Selden, F. Tam, and H. Hodgson, *Nonparenchymal cells from regenerating rat liver generate interleukin-1alpha and -1beta: a mechanism of negative regulation of hepatocyte proliferation.* Hepatology, 1997. **26**(1): p. 49-58.

165. Kogure, K., W. Omata, M. Kanzaki, Y.Q. Zhang, H. Yasuda, T. Mine, and I. Kojima, *A single intraportal administration of follistatin accelerates liver regeneration in partially hepatectomized rats.* Gastroenterology, 1995. **108**(4): p. 1136-42.

166. Kogure, K., Y.Q. Zhang, M. Kanzaki, W. Omata, T. Mine, and I. Kojima, *Intravenous administration of follistatin: delivery to the liver and effect on liver regeneration after partial hepatectomy.* Hepatology, 1996. **24**(2): p. 361-6.

167. Houck, K.A. and G.K. Michalopoulos, *Altered responses of regenerating hepatocytes to norepinephrine and transforming growth factor type beta.* J Cell Physiol, 1989. **141**(3): p. 503-9.

168. Nakamura, T., Y. Tomita, R. Hirai, K. Yamaoka, K. Kaji, and A. Ichihara, *Inhibitory effect of transforming growth factor-beta on DNA synthesis of adult rat hepatocytes in primary culture.* Biochem Biophys Res Commun, 1985. **133**(3): p. 1042-50.

169. Braun, L., J.E. Mead, M. Panzica, R. Mikumo, G.I. Bell, and N. Fausto, *Transforming growth factor beta mRNA increases during liver regeneration: a possible paracrine mechanism of growth regulation.* Proc Natl Acad Sci U S A, 1988. **85**(5): p. 1539-43.
170. Sanderson, N., V. Factor, P. Nagy, J. Kopp, P. Kondaiah, L. Wakefield, A.B. Roberts, M.B. Sporn, and S.S. Thorgeirsson, *Hepatic expression of mature transforming growth factor beta 1 in transgenic mice results in multiple tissue lesions.* Proc Natl Acad Sci U S A, 1995. **92**(7): p. 2572-6.
171. Oe, S., E.R. Lemmer, E.A. Conner, V.M. Factor, P. Leveen, J. Larsson, S. Karlsson, and S.S. Thorgeirsson, *Intact signaling by transforming growth factor beta is not required for termination of liver regeneration in mice.* Hepatology, 2004. **40**(5): p. 1098-105.
172. Russell, W.E., R.J. Coffey, Jr., A.J. Ouellette, and H.L. Moses, *Type beta transforming growth factor reversibly inhibits the early proliferative response to partial hepatectomy in the rat.* Proc Natl Acad Sci U S A, 1988. **85**(14): p. 5126-30.
173. Rana, B., D. Mischoulon, Y. Xie, N.L. Bucher, and S.R. Farmer, *Cell-extracellular matrix interactions can regulate the switch between growth and differentiation in rat hepatocytes: reciprocal expression of C/EBP alpha and immediate-early growth response transcription factors.* Mol Cell Biol, 1994. **14**(9): p. 5858-69.
174. Reid, L.M. and D.M. Jefferson, *Culturing hepatocytes and other differentiated cells.* Hepatology, 1984. **4**(3): p. 548-59.
175. Rojkind, M., Z. Gatmaitan, S. Mackensen, M.A. Giambrone, P. Ponce, and L.M. Reid, *Connective tissue biomatrix: its isolation and utilization for long-term cultures of normal rat hepatocytes.* J Cell Biol, 1980. **87**(1): p. 255-63.
176. Mooney, D., L. Hansen, J. Vacanti, R. Langer, S. Farmer, and D. Ingber, *Switching from differentiation to growth in hepatocytes: control by extracellular matrix.* J Cell Physiol, 1992. **151**(3): p. 497-505.
177. Rudolph, K.L., C. Trautwein, S. Kubicka, T. Rakemann, M.J. Bahr, N. Sedlaczek, D. Schuppan, and M.P. Manns, *Differential regulation of extracellular matrix synthesis during liver regeneration after partial hepatectomy in rats.* Hepatology, 1999. **30**(5): p. 1159-66.

178. Yamamoto, H., Y. Murawaki, and H. Kawasaki, *Hepatic collagen synthesis and degradation during liver regeneration after partial hepatectomy.* Hepatology, 1995. **21**(1): p. 155-61.
179. Mohammed, F.F., C.J. Pennington, Z. Kassiri, J.S. Rubin, P.D. Soloway, U. Ruther, D.R. Edwards, and R. Khokha, *Metalloproteinase inhibitor TIMP-1 affects hepatocyte cell cycle via HGF activation in murine liver regeneration.* Hepatology, 2005. **41**(4): p. 857-67.
180. Michalopoulos, G.K., *Liver regeneration after partial hepatectomy: critical analysis of mechanistic dilemmas.* Am J Pathol, 2010. **176**(1): p. 2-13.
181. Gkretsi, V., U. Apte, W.M. Mars, W.C. Bowen, J.H. Luo, Y. Yang, Y.P. Yu, A. Orr, R. St-Arnaud, S. Dedhar, K.H. Kaestner, C. Wu, and G.K. Michalopoulos, *Liver-specific ablation of integrin-linked kinase in mice results in abnormal histology, enhanced cell proliferation, and hepatomegaly.* Hepatology, 2008. **48**(6): p. 1932-41.
182. Apte, U., V. Gkretsi, W.C. Bowen, W.M. Mars, J.H. Luo, S. Donthamsetty, A. Orr, S.P. Monga, C. Wu, and G.K. Michalopoulos, *Enhanced liver regeneration following changes induced by hepatocyte-specific genetic ablation of integrin-linked kinase.* Hepatology, 2009. **50**(3): p. 844-51.
183. Afdhal, N.H. and D. Nunes, *Evaluation of liver fibrosis: a concise review.* Am J Gastroenterol, 2004. **99**(6): p. 1160-74.
184. Thampanitchawong, P. and T. Piratvisuth, *Liver biopsy:complications and risk factors.* World J Gastroenterol, 1999. **5**(4): p. 301-304.
185. Ishak, K., A. Baptista, L. Bianchi, F. Callea, J. De Groote, F. Gudat, H. Denk, V. Desmet, G. Korb, R.N.M. MacSween, M.J. Phillips, B.G. Portmann, H. Poulsen, P.J. Scheuer, M. Schmid, and H. Thaler, *Histological grading and staging of chronic hepatitis.* Journal of Hepatology, 1995. **22**(6): p. 696-699.
186. Poynard, T., P. Bedossa, and P. Opolon, *Natural history of liver fibrosis progression in patients with chronic hepatitis C. The OBSVIRC, METAVIR, CLINIVIR, and DOSVIRC groups.* Lancet, 1997. **349**(9055): p. 825-32.
187. Desmet, V.J., M. Gerber, J.H. Hoofnagle, M. Manns, and P.J. Scheuer, *Classification of chronic hepatitis: diagnosis, grading and staging.* Hepatology, 1994. **19**(6): p. 1513-20.
188. Knodell, R.G., K.G. Ishak, W.C. Black, T.S. Chen, R. Craig, N. Kaplowitz, T.W. Kiernan, and J. Wollman, *Formulation and application of a numerical*

scoring system for assessing histological activity in asymptomatic chronic active hepatitis. Hepatology, 1981. **1**(5): p. 431-5.

189. Regev, A., M. Berho, L.J. Jeffers, C. Milikowski, E.G. Molina, N.T. Pyrsopoulos, Z.Z. Feng, K.R. Reddy, and E.R. Schiff, *Sampling error and intraobserver variation in liver biopsy in patients with chronic HCV infection.* Am J Gastroenterol, 2002. **97**(10): p. 2614-8.
190. Ramaiah, S.K., *A toxicologist guide to the diagnostic interpretation of hepatic biochemical parameters.* Food Chem Toxicol, 2007. **45**(9): p. 1551-7.
191. Adams, L.A., M. Bulsara, E. Rossi, B. DeBoer, D. Speers, J. George, J. Kench, G. Farrell, G.W. McCaughan, and G.P. Jeffrey, *Hepascore: An Accurate Validated Predictor of Liver Fibrosis in Chronic Hepatitis C Infection.* Clin Chem, 2005. **51**(10): p. 1867-1873.
192. Boeker, K.H., C.I. Haberkorn, D. Michels, P. Flemming, M.P. Manns, and R. Lichtinghagen, *Diagnostic potential of circulating TIMP-1 and MMP-2 as markers of liver fibrosis in patients with chronic hepatitis C.* Clin Chim Acta, 2002. **316**(1-2): p. 71-81.
193. Patel, K., S.C. Gordon, I. Jacobson, C. Hézode, E. Oh, K.M. Smith, J.-M. Pawlotsky, and J.G. McHutchison, *Evaluation of a panel of non-invasive serum markers to differentiate mild from moderate-to-advanced liver fibrosis in chronic hepatitis C patients.* Journal of Hepatology, 2004. **41**(6): p. 935-942.
194. Guechot, J., L. Serfaty, A.M. Bonnand, O. Chazouilleres, R.E. Poupon, and R. Poupon, *Prognostic value of serum hyaluronan in patients with compensated HCV cirrhosis.* J Hepatol, 2000. **32**(3): p. 447-52.
195. Gressner, O.A., R. Weiskirchen, and A.M. Gressner, *Biomarkers of hepatic fibrosis, fibrogenesis and genetic pre-disposition pending between fiction and reality.* J Cell Mol Med, 2007. **11**(5): p. 1031-51.
196. Anderson, F.H., L. Zeng, N.R. Rock, and E.M. Yoshida, *An assessment of the clinical utility of serum ALT and AST in chronic hepatitis C.* Hepatol Res, 2000. **18**(1): p. 63-71.
197. Manning, D.S. and N.H. Afdhal, *Diagnosis and quantitation of fibrosis.* Gastroenterology, 2008. **134**(6): p. 1670-81.
198. Park, G.J., B.P. Lin, M.C. Ngu, D.B. Jones, and P.H. Katelaris, *Aspartate aminotransferase: alanine aminotransferase ratio in chronic hepatitis C*

infection: is it a useful predictor of cirrhosis? J Gastroenterol Hepatol, 2000. **15**(4): p. 386-90.

199. Sheth, S.G., S.L. Flamm, F.D. Gordon, and S. Chopra, *AST/ALT ratio predicts cirrhosis in patients with chronic hepatitis C virus infection.* Am J Gastroenterol, 1998. **93**(1): p. 44-8.
200. Wai, C.T., J.K. Greenson, R.J. Fontana, J.D. Kalbfleisch, J.A. Marrero, H.S. Conjeevaram, and A.S. Lok, *A simple noninvasive index can predict both significant fibrosis and cirrhosis in patients with chronic hepatitis C.* Hepatology, 2003. **38**(2): p. 518-26.
201. Kawasaki, T., A. Takeshita, K. Souda, Y. Kobayashi, M. Kikuyama, F. Suzuki, F. Kageyama, Y. Sasada, E. Shimizu, G. Murohisa, S. Koide, T. Yoshimi, H. Nakamura, and R. Ohno, *Serum thrombopoietin levels in patients with chronic hepatitis and liver cirrhosis.* Am J Gastroenterol, 1999. **94**(7): p. 1918-22.
202. Imbert-Bismut, F., V. Ratziu, L. Pieroni, F. Charlotte, Y. Benhamou, and T. Poynard, *Biochemical markers of liver fibrosis in patients with hepatitis C virus infection: a prospective study.* Lancet, 2001. **357**(9262): p. 1069-75.
203. Rossi, E., L. Adams, A. Prins, M. Bulsara, B. de Boer, G. Garas, G. MacQuillan, D. Speers, and G. Jeffrey, *Validation of the FibroTest biochemical markers score in assessing liver fibrosis in hepatitis C patients.* Clin Chem, 2003. **49**(3): p. 450-4.
204. Poynard, T., F. Imbert-Bismut, M. Munteanu, D. Messous, R.P. Myers, D. Thabut, V. Ratziu, A. Mercadier, Y. Benhamou, and B. Hainque, *Overview of the diagnostic value of biochemical markers of liver fibrosis (FibroTest, HCV FibroSure) and necrosis (ActiTest) in patients with chronic hepatitis C.* Comp Hepatol, 2004. **3**(8): p. 1-12.
205. Poynard, T., J. McHutchison, M. Manns, C. Trepo, K. Lindsay, Z. Goodman, M.H. Ling, and J. Albrecht, *Impact of pegylated interferon alfa-2b and ribavirin on liver fibrosis in patients with chronic hepatitis C.* Gastroenterology, 2002. **122**(5): p. 1303-13.
206. Forns, X., S. Ampurdanes, J.M. Llovet, J. Aponte, L. Quinto, E. Martinez-Bauer, M. Bruguera, J.M. Sanchez-Tapias, and J. Rodes, *Identification of chronic hepatitis C patients without hepatic fibrosis by a simple predictive model.* Hepatology, 2002. **36**(4 Pt 1): p. 986-92.

207. Koda, M., Y. Matunaga, M. Kawakami, Y. Kishimoto, T. Suou, and Y. Murawaki, *FibroIndex, a practical index for predicting significant fibrosis in patients with chronic hepatitis C.* Hepatology, 2007. **45**(2): p. 297-306.
208. Sterling, R.K., E. Lissen, N. Clumeck, R. Sola, M.C. Correa, J. Montaner, S.S. M, F.J. Torriani, D.T. Dieterich, D.L. Thomas, D. Messinger, and M. Nelson, *Development of a simple noninvasive index to predict significant fibrosis in patients with HIV/HCV coinfection.* Hepatology, 2006. **43**(6): p. 1317-25.
209. Vallet-Pichard, A., V. Mallet, B. Nalpas, V. Verkarre, A. Nalpas, V. Dhalluin-Venier, H. Fontaine, and S. Pol, *FIB-4: an inexpensive and accurate marker of fibrosis in HCV infection. comparison with liver biopsy and fibrotest.* Hepatology, 2007. **46**(1): p. 32-6.
210. Becker, L., W. Salameh, A. Sferruzza, K. Zhang, R. Chen, R. Malik, R. Reitz, I. Nasser, and N.H. Afdhal, *Validation of Hepascore, compared to simple indices of fibrosis, in US patients with chronic hepatitis C virus infection.* Clin Gastroenterol Hepatol, 2009. **7**(6): p. 696-701.
211. Naveau, S., T. Poynard, C. Benattar, P. Bedossa, and J.C. Chaput, *Alpha-2-macroglobulin and hepatic fibrosis. Diagnostic interest.* Dig Dis Sci, 1994. **39**(11): p. 2426-32.
212. Rosenberg, W.M., M. Voelker, R. Thiel, M. Becka, A. Burt, D. Schuppan, S. Hubscher, T. Roskams, M. Pinzani, and M.J. Arthur, *Serum markers detect the presence of liver fibrosis: a cohort study.* Gastroenterology, 2004. **127**(6): p. 1704-13.
213. Parkes, J., P. Roderick, S. Harris, C. Day, D. Mutimer, J. Collier, M. Lombard, G. Alexander, J. Ramage, G. Dusheiko, M. Wheatley, C. Gough, A. Burt, and W. Rosenberg, *Enhanced liver fibrosis test can predict clinical outcomes in patients with chronic liver disease.* Gut, 2010. **59**(9): p. 1245-51.
214. Muller, A., B. Krombholz, G. Pott, G. Machnik, R. Vollandt, M. Reinhardt, and D. Jorke, *Collagen peptidase and type III procollagen peptide serum levels in chronic liver diseases.* Clin Chim Acta, 1991. **197**(1): p. 59-66.
215. Teare, J.P., D. Sherman, S.M. Greenfield, J. Simpson, G. Bray, A.P. Catterall, I.M. Murray-Lyon, T.J. Peters, R. Williams, and R.P. Thompson, *Comparison of serum procollagen III peptide concentrations and PGA*

index for assessment of hepatic fibrosis. Lancet, 1993. **342**(8876): p. 895-8.

216. Trinchet, J.C., D.J. Hartmann, D. Pateron, M. Laarif, P. Callard, G. Ville, and M. Beaugrand, *Serum type I collagen and N-terminal peptide of type III procollagen in chronic hepatitis. Relationship to liver histology and conventional liver tests.* J Hepatol, 1991. **12**(2): p. 139-44.
217. Benyon, R.C. and M.J. Arthur, *Extracellular matrix degradation and the role of hepatic stellate cells.* Semin Liver Dis, 2001. **21**(3): p. 373-84.
218. Molleken, C., B. Sitek, C. Henkel, G. Poschmann, B. Sipos, S. Wiese, B. Warscheid, C. Broelsch, M. Reiser, S.L. Friedman, I. Tornoe, A. Schlosser, G. Kloppel, W. Schmiegel, H.E. Meyer, U. Holmskov, and K. Stuhler, *Detection of novel biomarkers of liver cirrhosis by proteomic analysis.* Hepatology, 2009. **49**(4): p. 1257-66.
219. Nelson, D.R., R.P. Gonzalez-Peralta, K. Qian, Y. Xu, C.G. Marousis, G.L. Davis, and J.Y. Lau, *Transforming growth factor-beta 1 in chronic hepatitis C.* J Viral Hepat, 1997. **4**(1): p. 29-35.
220. Walsh, K.M., A. Fletcher, R.N. MacSween, and A.J. Morris, *Basement membrane peptides as markers of liver disease in chronic hepatitis C.* J Hepatol, 2000. **32**(2): p. 325-30.
221. Gressner, A.M. and R. Haarmann, *Hyaluronic acid synthesis and secretion by rat liver fat storing cells (perisinusoidal lipocytes) in culture.* Biochem Biophys Res Commun, 1988. **151**(1): p. 222-9.
222. Guechot, J., A. Laudat, A. Loria, L. Serfaty, R. Poupon, and J. Giboudeau, *Diagnostic accuracy of hyaluronan and type III procollagen amino-terminal peptide serum assays as markers of liver fibrosis in chronic viral hepatitis C evaluated by ROC curve analysis.* Clin Chem, 1996. **42**(4): p. 558-63.
223. Sante´, H.A.d. *Non invasive methods for the evaluation of hepatic fibrosis/cirrhosis: an update.* 2008 [cited; Available from: http://www.has-sante.fr.
224. Castera, L. and M. Pinzani, *Biopsy and non-invasive methods for the diagnosis of liver fibrosis: does it take two to tango?* Gut, 2010. **59**(7): p. 861-6.
225. Parkes, J., I.N. Guha, P. Roderick, and W. Rosenberg, *Performance of serum marker panels for liver fibrosis in chronic hepatitis C.* J Hepatol, 2006. **44**(3): p. 462-74.

226. Maïté Lewin, A.P.-R., Pierre-Yves Boëlle, Dominique Wendum, Elisabeth Lasnier, Magalie Viallon, Jérôme Guéchot, Christine Hoeffel, Lionel Arrivé, Jean-Michel Tubiana, Raoul Poupon,, *Diffusion-weighted magnetic resonance imaging for the assessment of fibrosis in chronic hepatitis C.* Hepatology, 2007. **46**(3): p. 658-665.
227. Hirata, M., S.M. Akbar, N. Horiike, and M. Onji, *Noninvasive diagnosis of the degree of hepatic fibrosis using ultrasonography in patients with chronic liver disease due to hepatitis C virus.* Eur J Clin Invest, 2001. **31**(6): p. 528-35.
228. Sandrin, L., B. Fourquet, J.-M. Hasquenoph, S. Yon, C. Fournier, F. Mal, C. Christidis, M. Ziol, B. Poulet, F. Kazemi, M. Beaugrand, and R. Palau, *Transient elastography: a new noninvasive method for assessment of hepatic fibrosis.* Ultrasound in Medicine & Biology, 2003. **29**(12): p. 1705-1713.
229. Rockey, D.C., *Noninvasive assessment of liver fibrosis and portal hypertension with transient elastography.* Gastroenterology, 2008. **134**(1): p. 8-14.
230. Foucher, J., E. Chanteloup, J. Vergniol, L. Castera, B. Le Bail, X. Adhoute, J. Bertet, P. Couzigou, and V. de Ledinghen, *Diagnosis of cirrhosis by transient elastography (FibroScan): a prospective study.* Gut, 2006. **55**(3): p. 403-8.
231. Friedrich-Rust, M., K. Wunder, S. Kriener, F. Sotoudeh, S. Richter, J. Bojunga, E. Herrmann, T. Poynard, C.F. Dietrich, J. Vermehren, S. Zeuzem, and C. Sarrazin, *Liver fibrosis in viral hepatitis: noninvasive assessment with acoustic radiation force impulse imaging versus transient elastography.* Radiology, 2009. **252**(2): p. 595-604.
232. Lupsor, M., R. Badea, H. Stefanescu, Z. Sparchez, H. Branda, A. Serban, and A. Maniu, *Performance of a new elastographic method (ARFI technology) compared to unidimensional transient elastography in the noninvasive assessment of chronic hepatitis C. Preliminary results.* J Gastrointestin Liver Dis, 2009. **18**(3): p. 303-10.
233. Takahashi, H., N. Ono, Y. Eguchi, T. Eguchi, Y. Kitajima, Y. Kawaguchi, S. Nakashita, I. Ozaki, T. Mizuta, S. Toda, S. Kudo, A. Miyoshi, K. Miyazaki, and K. Fujimoto, *Evaluation of acoustic radiation force impulse*

elastography for fibrosis staging of chronic liver disease: a pilot study. Liver Int. **30**(4): p. 538-45.

234. Boursier, J., Y. Bacq, P. Halfon, V. Leroy, V. de Ledinghen, A. de Muret, M. Bourliere, N. Sturm, J. Foucher, F. Oberti, M.C. Rousselet, and P. Cales, *Improved diagnostic accuracy of blood tests for severe fibrosis and cirrhosis in chronic hepatitis C.* Eur J Gastroenterol Hepatol, 2009. **21**(1): p. 28-38.
235. Pinzani, M., F. Vizzutti, U. Arena, and F. Marra, *Technology Insight: noninvasive assessment of liver fibrosis by biochemical scores and elastography.* Nat Clin Pract Gastroenterol Hepatol, 2008. **5**(2): p. 95-106.
236. Poynard, T., P. Ingiliz, L. Elkrief, M. Munteanu, P. Lebray, R. Morra, D. Messous, F.I. Bismut, D. Roulot, Y. Benhamou, D. Thabut, and V. Ratziu, *Concordance in a world without a gold standard: a new non-invasive methodology for improving accuracy of fibrosis markers.* PLoS One, 2008. **3**(12): p. e3857.
237. Yang, C., M. Zeisberg, B. Mosterman, A. Sudhakar, U. Yerramalla, K. Holthaus, L. Xu, F. Eng, N. Afdhal, and R. Kalluri, *Liver fibrosis: Insights into migration of hepatic stellate cells in response to extracellular matrix and growth factors.* Gastroenterology, 2003. **124**(1): p. 147-159.
238. McElhiney, J., M. Drever, L.A. Lawton, and A.J. Porter, *Rapid isolation of a single-chain antibody against the cyanobacterial toxin microcystin-LR by phage display and its use in the immunoaffinity concentration of microcystins from water.* Appl Environ Microbiol, 2002. **68**(11): p. 5288-95.
239. Fox, M., G. Gray, K. Kavanagh, C. Lewis, and S. Doyle, *Detection of Aspergillus fumigatus mycotoxins: immunogen synthesis and immunoassay development.* Journal of Microbiological Methods, 2004. **56**(2): p. 221-230.
240. Lowry, O.H., N.J. Rosebrough, A.L. Farr, and R.J. Randall, *Protein measurement with the Folin phenol reagent.* J Biol Chem, 1951. **193**(1): p. 265-75.
241. Laemmli, U.K., *Cleavage of structural proteins during the assembly of the head of bacteriophage T4.* Nature, 1970. **227**(5259): p. 680-5.
242. Junqueira, L.C., G. Bignolas, and R.R. Brentani, *Picrosirius staining plus polarization microscopy, a specific method for collagen detection in tissue sections.* Histochem J, 1979. **11**(4): p. 447-55.

243. Puchtler, H., F.S. Waldrop, and L.S. Valentine, *Polarization microscopic studies of connective tissue stained with picro-sirius red FBA.* Beitr Pathol, 1973. **150**(2): p. 174-87.

244. Yuan, J.S., A. Reed, F. Chen, and C.N. Stewart, Jr., *Statistical analysis of real-time PCR data.* BMC Bioinformatics, 2006. **7**(85).

245. Edsjo, A., B. Hallberg, S. Fagerstrom, C. Larsson, H. Axelson, and S. Pahlman, *Differences in early and late responses between neurotrophin-stimulated trkA- and trkC-transfected SH-SY5Y neuroblastoma cells.* Cell Growth Differ, 2001. **12**(1): p. 39-50.

246. Elsasser-Beile, U., G. Reischl, S. Wiehr, P. Buhler, P. Wolf, K. Alt, J. Shively, M.S. Judenhofer, H.J. Machulla, and B.J. Pichler, *PET imaging of prostate cancer xenografts with a highly specific antibody against the prostate-specific membrane antigen.* J Nucl Med, 2009. **50**(4): p. 606-11.

247. Thurber, G.M. and K.D. Wittrup, *Quantitative spatiotemporal analysis of antibody fragment diffusion and endocytic consumption in tumor spheroids.* Cancer Res, 2008. **68**(9): p. 3334-41.

248. Krebs, B., H. Griffin, G. Winter, and S. Rose-John, *Recombinant human single chain Fv antibodies recognizing human interleukin-6. Specific targeting of cytokine-secreting cells.* J Biol Chem, 1998. **273**(5): p. 2858-65.

249. Douglass, A., K. Wallace, M. Koruth, C. Barelle, A.J. Porter, and M.C. Wright, *Targeting liver myofibroblasts: a novel approach in anti-fibrogenic therapy.* Hepatol Int, 2008. **2**(4): p. 405-15.

250. Kotlyar, D.S., W. Blonski, and V.K. Rustgi, *Noninvasive monitoring of hepatitis C fibrosis progression.* Clin Liver Dis, 2008. **12**(3): p. 557-71, viii.

251. Carpino, G., S. Morini, S. Ginanni Corradini, A. Franchitto, M. Merli, M. Siciliano, F. Gentili, A. Onetti Muda, P. Berloco, M. Rossi, A.F. Attili, and E. Gaudio, *Alpha-SMA expression in hepatic stellate cells and quantitative analysis of hepatic fibrosis in cirrhosis and in recurrent chronic hepatitis after liver transplantation.* Dig Liver Dis, 2005. **37**(5): p. 349-56.

252. Wallace, K., P.A. Flecknell, A.D. Burt, and M.C. Wright, *Disrupted pancreatic exocrine differentiation and malabsorption in response to chronic elevated systemic glucocorticoid.* Am J Pathol, 2010. **177**(3): p. 1225-32.

253. Friedman, S.L. and M.B. Bansal, *Reversal of hepatic fibrosis -- fact or fantasy?* Hepatology, 2006. **43**(2 Suppl 1): p. S82-8.
254. Kerwin, J., M. Scott, J. Sharpe, L. Puelles, S.C. Robson, M. Martinez-de-la-Torre, J.L. Ferran, G. Feng, R. Baldock, T. Strachan, D. Davidson, and S. Lindsay, *3 dimensional modelling of early human brain development using optical projection tomography.* BMC Neurosci, 2004. **5**(27).
255. Wiedenmann, B., W.W. Franke, C. Kuhn, R. Moll, and V.E. Gould, *Synaptophysin: a marker protein for neuroendocrine cells and neoplasms.* Proc Natl Acad Sci U S A, 1986. **83**(10): p. 3500-4.
256. Duysen, E.G. and O. Lockridge, *Whole body and tissue imaging of the butyrylcholinesterase knockout mouse injected with near infrared dye labeled butyrylcholinesterase.* Chem Biol Interact, 2008. **175**(1-3): p. 119-24.
257. Nguyen, L.N., M.H. Furuya, L.A. Wolfraim, A.P. Nguyen, M.S. Holdren, J.S. Campbell, B. Knight, G.C. Yeoh, N. Fausto, and W.T. Parks, *Transforming growth factor-beta differentially regulates oval cell and hepatocyte proliferation.* Hepatology, 2007. **45**(1): p. 31-41.
258. Burr, A.W., K. Toole, C. Chapman, J.E. Hines, and A.D. Burt, *Anti-hepatocyte growth factor antibody inhibits hepatocyte proliferation during liver regeneration.* J Pathol, 1998. **185**(3): p. 298-302.
259. Bissell, D.M., D. Roulot, and J. George, *Transforming growth factor beta and the liver.* Hepatology, 2001. **34**(5): p. 859-67.
260. Fausto, N. and J.S. Campbell, *The role of hepatocytes and oval cells in liver regeneration and repopulation.* Mech Dev, 2003. **120**(1): p. 117-30.
261. Mannheimer, E.G., L.F. Quintanilha, A.B. Carvalho, B.D. Paredes, F. Goncalves de Carvalho, C.M. Takyia, C.M. Resende, G. Ferreira da Motta Rezende, A. Carlos Campos de Carvalho, A. Schanaider, and R. Coeli Dos Santos Goldenberg, *Bone marrow cells obtained from cirrhotic rats do not improve function or reduce fibrosis in a chronic liver disease model.* Clin Transplant, 2009. **25**(1): p. 54-60.
262. Yoshiji, H., S. Kuriyama, Y. Miyamoto, U.P. Thorgeirsson, D.E. Gomez, M. Kawata, J. Yoshii, Y. Ikenaka, R. Noguchi, H. Tsujinoue, T. Nakatani, S.S. Thorgeirsson, and H. Fukui, *Tissue inhibitor of metalloproteinases-1 promotes liver fibrosis development in a transgenic mouse model.* Hepatology, 2000. **32**(6): p. 1248-54.

263. Tahashi, Y., K. Matsuzaki, M. Date, K. Yoshida, F. Furukawa, Y. Sugano, M. Matsushita, Y. Himeno, Y. Inagaki, and K. Inoue, *Differential regulation of TGF-beta signal in hepatic stellate cells between acute and chronic rat liver injury.* Hepatology, 2002. **35**(1): p. 49-61.
264. Anselmi, K., D.B. Stolz, M. Nalesnik, S.C. Watkins, R. Kamath, and C.R. Gandhi, *Gliotoxin causes apoptosis and necrosis of rat Kupffer cells in vitro and in vivo in the absence of oxidative stress: exacerbation by caspase and serine protease inhibition.* J Hepatol, 2007. **47**(1): p. 103-13.
265. Passino, M.A., R.A. Adams, S.L. Sikorski, and K. Akassoglou, *Regulation of hepatic stellate cell differentiation by the neurotrophin receptor p75NTR.* Science, 2007. **315**(5820): p. 1853-6.
266. Issa, R., X. Zhou, C.M. Constandinou, J. Fallowfield, H. Millward-Sadler, M.D. Gaca, E. Sands, I. Suliman, N. Trim, A. Knorr, M.J. Arthur, R.C. Benyon, and J.P. Iredale, *Spontaneous recovery from micronodular cirrhosis: evidence for incomplete resolution associated with matrix cross-linking.* Gastroenterology, 2004. **126**(7): p. 1795-808.
267. Taura, K., K. Miura, K. Iwaisako, C.H. Osterreicher, Y. Kodama, M. Penz-Osterreicher, and D.A. Brenner, *Hepatocytes do not undergo epithelial-mesenchymal transition in liver fibrosis in mice.* Hepatology. **51**(3): p. 1027-36.
268. Scholten, D., C.H. Osterreicher, A. Scholten, K. Iwaisako, G. Gu, D.A. Brenner, and T. Kisseleva, *Genetic labeling does not detect epithelial-to-mesenchymal transition of cholangiocytes in liver fibrosis in mice.* Gastroenterology. **139**(3): p. 987-98.
269. Rygiel, K.A., H. Robertson, J.D. Willet, J.G. Brain, A.D. Burt, D.E. Jones, and J.A. Kirby, *T cell-mediated biliary epithelial-to-mesenchymal transition in liver allograft rejection.* Liver Transpl, 2010. **16**(5): p. 567-76.
270. Friedman, S.L., *Hepatic fibrosis -- overview.* Toxicology, 2008. **254**(3): p. 120-9.
271. Castilla, A., J. Prieto, and N. Fausto, *Transforming growth factors beta 1 and alpha in chronic liver disease. Effects of interferon alfa therapy.* N Engl J Med, 1991. **324**(14): p. 933-40.
272. Taipale, J., K. Miyazono, C.H. Heldin, and J. Keski-Oja, *Latent transforming growth factor-beta 1 associates to fibroblast extracellular*

matrix via latent TGF-beta binding protein. J Cell Biol, 1994. **124**(1-2): p. 171-81.

273. Murphy, F.R., R. Issa, X. Zhou, S. Ratnarajah, H. Nagase, M.J. Arthur, C. Benyon, and J.P. Iredale, *Inhibition of apoptosis of activated hepatic stellate cells by tissue inhibitor of metalloproteinase-1 is mediated via effects on matrix metalloproteinase inhibition: implications for reversibility of liver fibrosis.* J Biol Chem, 2002. **277**(13): p. 11069-76.
274. Fallowfield, J.A., M. Mizuno, T.J. Kendall, C.M. Constandinou, R.C. Benyon, J.S. Duffield, and J.P. Iredale, *Scar-associated macrophages are a major source of hepatic matrix metalloproteinase-13 and facilitate the resolution of murine hepatic fibrosis.* J Immunol, 2007. **178**(8): p. 5288-95.
275. Bautista, A.P., *Neutrophilic infiltration in alcoholic hepatitis.* Alcohol, 2002. **27**(1): p. 17-21.
276. Jaeschke, H., *Molecular mechanisms of hepatic ischemia-reperfusion injury and preconditioning.* Am J Physiol Gastrointest Liver Physiol, 2003. **284**(1): p. G15-26.
277. Jaeschke, H. and T. Hasegawa, *Role of neutrophils in acute inflammatory liver injury.* Liver Int, 2006. **26**(8): p. 912-9.
278. Kolios, G., V. Valatas, and E. Kouroumalis, *Role of Kupffer cells in the pathogenesis of liver disease.* World J Gastroenterol, 2006. **12**(46): p. 7413-20.
279. Dufour, J.F., R. DeLellis, and M.M. Kaplan, *Reversibility of hepatic fibrosis in autoimmune hepatitis.* Ann Intern Med, 1997. **127**(11): p. 981-5.
280. Wanless, I.R., E. Nakashima, and M. Sherman, *Regression of human cirrhosis. Morphologic features and the genesis of incomplete septal cirrhosis.* Arch Pathol Lab Med, 2000. **124**(11): p. 1599-607.
281. Friedman, S.L., *Evolving challenges in hepatic fibrosis.* Nat Rev Gastroenterol Hepatol, 2010. **7**(8): p. 425-36.
282. Mitchell, A.E., H.M. Colvin, and R. Palmer Beasley, *Institute of Medicine recommendations for the prevention and control of hepatitis B and C.* Hepatology. **51**(3): p. 729-33.
283. Fujita, J., M.W. Marino, H. Wada, A.A. Jungbluth, P.J. Mackrell, D.E. Rivadeneira, P.P. Stapleton, and J.M. Daly, *Effect of TNF gene depletion on liver regeneration after partial hepatectomy in mice.* Surgery, 2001. **129**(1): p. 48-54.

284. Brambilla, R., V. Bracchi-Ricard, W.H. Hu, B. Frydel, A. Bramwell, S. Karmally, E.J. Green, and J.R. Bethea, *Inhibition of astroglial nuclear factor kappaB reduces inflammation and improves functional recovery after spinal cord injury.* J Exp Med, 2005. **202**(1): p. 145-56.

285. Kendall, T.J., S. Hennedige, R.L. Aucott, S.N. Hartland, M.A. Vernon, R.C. Benyon, and J.P. Iredale, *p75 Neurotrophin receptor signaling regulates hepatic myofibroblast proliferation and apoptosis in recovery from rodent liver fibrosis.* Hepatology, 2009. **49**(3): p. 901-10.

286. Tatematsu, M., R.H. Ho, T. Kaku, J.K. Ekem, and E. Farber, *Studies on the proliferation and fate of oval cells in the liver of rats treated with 2-acetylaminofluorene and partial hepatectomy.* Am J Pathol, 1984. **114**(3): p. 418-30.

287. Laconi, S., F. Curreli, S. Diana, D. Pasciu, G. De Filippo, D.S. Sarma, P. Pani, and E. Laconi, *Liver regeneration in response to partial hepatectomy in rats treated with retrorsine: a kinetic study.* J Hepatol, 1999. **31**(6): p. 1069-74.